

Distribution Agreement

In presenting this dissertation/thesis as a partial fulfillment of the requirements for an advanced degree from Emory University, I agree that the Library of the University shall make it available for inspection and circulation in accordance with its regulations governing materials of this type. I agree that permission to copy from, or to publish, this thesis/dissertation may be granted by the professor under whose direction it was written when such copying or publication is solely for scholarly purposes and does not involve potential financial gain. In the absence of the professor, the dean of the Graduate School may grant permission. It is understood that any copying from, or publication of, this thesis/dissertation which involves potential financial gain will not be allowed without written permission.

Gregory Richard Bluemling

Part I: Synthesis of Cyclobutyl Nucleoside Analogs That Mimic AZT for Inhibition of the K65R HIV-1 Reverse Transcriptase Mutant

Part II: Synthesis and Evaluation of Truncated Triptolide Analogs to Suppress Chronic Inflammation

By

Gregory Richard Bluemling
Doctor of Philosophy

Department of Chemistry

Dennis C. Liotta, Ph.D.
Advisor

David G. Lynn, Ph.D.
Committee Member

Frank E. McDonald, Ph.D.

Accepted

Lisa A. Tedesco, Ph.D.
Dean of the Graduate School

Date

Part I: Synthesis of Cyclobutyl Nucleoside Analogs That Mimic AZT for Inhibition of the K65R HIV-1 Reverse Transcriptase Mutant

Part II: Synthesis and Evaluation of Truncated Triptolide Analogs to Suppress Chronic Inflammation

By

Gregory Richard Bluemling

B.S., Berry College, 2003

Advisor: Dennis C. Liotta, Ph.D.

An abstract of
A dissertation submitted to the Faculty of the
James T. Laney School of Graduate Studies of Emory University
in partial fulfillment of the requirements for the degree of
Doctor of Philosophy

Department of Chemistry

2011

Abstract

Part I: Synthesis of Cyclobutyl Nucleoside Analogs That Mimic AZT for Inhibition of the K65R HIV-1 Reverse Transcriptase Mutant

Part II: Synthesis and Evaluation of Truncated Triptolide Analogs to Suppress Chronic Inflammation

By Gregory Richard Bluemling

Part I of this dissertation describes the synthesis and biological activity of novel 3'-azido cyclobutyl nucleoside analogs. These analogs were developed for inhibition of both the WT HIV RT and the K65R HIV RT mutant. The nucleoside analogs were prepared from cyclobutenones which were generated via a [2+2] cycloaddition reaction. The azide was installed through a Michael reaction, and both thymine and adenine were coupled to the cyclobutyl ring through a S_N2 reaction via a brosylate. The nucleosides **GB119**, **GB120**, **GB123**, and **GB124** did not show any anti-HIV activity in human PBM cells and were not toxic to PBM, CEM, and Vero cells up to 100 μM.

Part II of this dissertation describes the synthesis and biological activity of truncated analogs of the diterpenoid triepoxide natural product triptolide. Triptolide possesses potent anti-inflammatory activity but is highly cytotoxic. In an effort to retain the desired anti-inflammatory properties of triptolide while reducing cytotoxicity, a series of truncated analogs were synthesized from phenols. Triptolide showed cytotoxicity at 50 nM in Jurkat cells. None of the analogs tested showed cytotoxicity in PMBCs or Jurkat cells up to 1000 nM. The analogs **GB67B**, **GB97**, and **GB187D** were screened in a carrageenan edema model in mice. **GB67B** was found to reduce TNF-α levels and reduce paw inflammation. To further study this compound, **GB67B** at 10 mg/kg and 30 mg/kg was given orally to rats once daily for 28 consecutive days in an adjuvant arthritis model. **GB67B** was found to give a dose-dependent reduction of paw volume and arthritic score. A luciferase reporter gene assay showed that unlike triptolide, **GB67B** did not inhibit NF-κB activation. However, **GB67B** was found to inhibit TNF-α levels from LPS stimulated mouse splenocytes in a dose-dependent manner supporting the carrageenan edema model results. Triptolide is known to be lethal to mice and rats at a single dose of 1 mg/kg. In order to observe toxicity of the truncated analogs, **GB67B** was dosed at 30, 90, and 180 mg/kg in rats for 7 days. While no animals died during the study there were signs of clinical intolerance for **GB67B** in the 180 mg/kg group.

Part I: Synthesis of Cyclobutyl Nucleoside Analogs That Mimic AZT for Inhibition of the K65R HIV-1 Reverse Transcriptase Mutant

Part II: Synthesis and Evaluation of Truncated Triptolide Analogs to Suppress Chronic Inflammation

By

Gregory Richard Bluemling

B.S., Berry College, 2003

Advisor: Dennis C. Liotta, Ph.D.

A dissertation submitted to the Faculty of the
James T. Laney School of Graduate Studies of Emory University
in partial fulfillment of the requirements for the degree of
Doctor of Philosophy

Department of Chemistry

2011

Acknowledgements

My career at Emory University began the summer after my sophomore year of college. After some unusual turn of events I ended up with a summer job in Dr. Raymond F. Schinazi's laboratory at the VA Medical Center. At first I was just looking for a summer job in the sciences, but what I ended up with was a life changing experience. After my summer job with Dr. Schinazi I knew I wanted to pursue a career in medicinal chemistry.

The following summer Dr. Schinazi helped me secure a summer position with his friend and collaborator Dr. Dennis C. Liotta who eventually became my graduate school advisor and mentor. I would like to thank Dr. Liotta for giving me the tremendous opportunity of working in his lab. I would also like to thank Dr. Liotta for being supportive and open to me exploring my scientific interests throughout my graduate career. Dr. Liotta provided me with a wealth of life and scientific knowledge and helped me through some challenging times.

I would also like to thank my committee members Drs. David Lynn and Frank McDonald for their support and constructive criticisms over the years. Their advice, suggestions, and thought provoking questions helped develop me as a chemist. In addition, I would also like to thank Dr. Liebeskind for being on my proposal committee.

Graduate life would be much different without the help and support of other group members. I would like to thank both past and present Liotta group members for providing a friendly atmosphere to live and work in. Being able to share ideas with other group members really helped to develop me as a scientist. I would also like to thank the members of the Emory Institute for Drug Discovery for providing data for my projects as

well as guidance for my career development. I would like to thank Drs. Wu and Wang of the NMR center, Dr. Strobel of the mass spectrometry center, and Dr. Hardcastle of the X-ray crystallography center for providing amazing facilities to work in as well as for providing critical data for my projects.

Most importantly, I would like to thank my family and friends for their support during my years in graduate school. I counted on them greatly when times got tough and graduate school seemed unbearable. I would like to thank my mom most of all for her love and support over the years, not only during graduate school, but for my entire life. She always challenged me to set goals for myself and to work hard to achieve them, yet she let me find my own path in life. She has always been and will always be my biggest hero.

**Dedicated to my mother Patricia Bluemling and good friends
Israel Tyree (R.I.P.) and Stephen Wust (R.I.P.)**

“All mankind is divided into three classes: those that are immovable, those that are movable, and those that move.”

-Benjamin Franklin

Table of Contents

Part I: Synthesis of Cyclobutyl Nucleoside Analogs That Mimic AZT for Inhibition of the K65R HIV-1 Reverse Transcriptase Mutant

1.1	Statement of purpose	1
1.2	Introduction	4
1.2.1	Current status of the HIV/AIDS pandemic	4
1.2.2	The HIV replication cycle	6
1.2.3	FDA approved anti-HIV therapeutics	10
1.2.4	Drugs currently in clinical trials	15
1.2.5	Additional classes of anti-viral therapies	19
1.2.6	HIV RT	22
1.2.7	NRTI mechanism of action	26
1.2.8	HIV RT NRTI resistance mechanisms	28
1.3	Background	33
1.3.1	3'-Azido-2',3'-dideoxynucleoside analogues	33
1.3.2	Syntheses of AZT and AZA	34
1.3.3	Anti-viral natural product oxetanocin	34
1.3.4	Syntheses of oxetanocin A and cyclobut-A	36
1.3.5	Synthesis of cyclobutenones	38
1.3.6	Methods for the Michael addition of azide	41
1.3.7	Methods for coupling nucleoside bases to a cyclobutyl ring	46
1.3.8	Methods for synthesizing nucleoside triphosphates	50
1.3.9	Synthesis and anti-HIV activity of 3'-hydroxymethyl cyclobutyl nucleosides	53
1.4	Results and discussion	56
1.4.1	Design and synthesis of 3'-azido-3'-hydroxyethyl cyclobutyl adenine	57
1.4.2	Design and synthesis of 3'-azido-3'-hydroxyethyl cyclobutyl thymine.....	60
1.4.3	Anti-viral activity.....	62
1.5	Conclusion	63
1.6	Experimental	64
1.7	References	96

Part II: Synthesis and Evaluation of Truncated Triptolide Analogs to Suppress Chronic Inflammation

2.1	Statement of purpose	103
2.2	Introduction	106
2.2.1	Current status of autoimmune and inflammatory diseases ...	106
2.2.2	Overview of the immune system	107
2.2.3	Autoimmunity	121
2.2.4	Inflammation	124

2.2.5	Drugs used to treat autoimmune/inflammatory diseases	128
2.3	Background	136
2.3.1	Triptolide as a potent immunosuppressant	136
2.3.2	Inhibition of the NF- κ B signaling pathway by triptolide	136
2.3.3	Synthesis of triptolide	140
2.3.4	Design and synthesis of monocyclic truncated triptolide analogs.....	143
2.3.5	Methods for <i>o</i> -formylation of phenols	144
2.3.6	Methods for oxidative dearomatization	146
2.3.7	Epoxidation of electron deficient olefins	148
2.4	Results and discussion	150
2.4.1	Synthesis of 2,5-substituted phenols	150
2.4.2	Synthesis of salicylic alcohols	152
2.4.3	Oxidative dearomatization of salicylic alcohols	153
2.4.4	Synthesis of diepoxide analogs	154
2.4.5	Triepoxide formation	156
2.4.6	Deprotection of the triisopropylsilyl protected analogs	158
2.4.7	Design and synthesis of bicyclic truncated triptolide analogs	158
2.4.8	Minimization of reactive functional groups	162
2.4.9	Synthesis of deuterated analogs for use as biological standards	169
2.4.10	Biological evaluation of truncated triptolide analogs	171
2.5	Conclusion	206
2.6	Experimental	208
2.7	References	368
3.1	Appendix	376

List of Figures

Part I: Synthesis of Cyclobutyl Nucleoside Analogs That Mimic AZT for Inhibition of the K65R HIV-1 Reverse Transcriptase Mutant

Figure 1	Structures of tenofovir, AZT, and d4T	2
Figure 2	2007 estimates for adults and children living with HIV/AIDS	5
Figure 3	The number of people living with HIV globally from 1990 to 2007	5
Figure 4	The number of new AIDS cases and AIDS related deaths from 1981 to 2007	6
Figure 5	The HIV replication cycle	6
Figure 6	FDA approved entry inhibitors	10
Figure 7	FDA approved NRTIs	11
Figure 8	FDA approved NNRTIs	11
Figure 9	FDA approved integrase inhibitor	12
Figure 10	FDA approved protease inhibitors	12
Figure 11	FDA approved foscarnet and hydroxyurea	15
Figure 12	NRTIs in clinical trials	15
Figure 13	Investigational NNRTIs in clinical trials	16
Figure 14	Structure of vicriviroc	16
Figure 15	Structure of elvitegravir	17
Figure 16	Maturation inhibitor bevirimat	17
Figure 17	Structures of KP-1461 and KP-1212	18
Figure 18	Examples of HIV RT RNase H inhibitors	19
Figure 19	Carbohydrate-binding agents	20
Figure 20	Inhibitors of HIV capsid protein assembly	20
Figure 21	Small molecule Vif inhibitors	21
Figure 22	Structure of HIV RT and corresponding amino acid map	22
Figure 23	HIV RT polymerase active site	23
Figure 24	HIV RT bound dNTP	24
Figure 25	Incorporated dNTP	24
Figure 26	Translocation and pyrophosphate release	25
Figure 27	Conversion of AZT into AZTTP by cellular kinases	27
Figure 28	DNA chain termination by AZT and D.E.C. formation	27
Figure 29	Mechanism of NRTI-MP excision	30
Figure 30	3'-Azido-2',3'-dideoxynucleoside analogues	33
Figure 31	Oxetanocin A and analogues	35
Figure 32	Mechanism of azidation of α,β -unsaturated ketones in the presence of Amberlite IRA900F	46
Figure 33	Reported purine and pyrimidine cyclobutyl analogues	53
Figure 34	Desired targets	56
Figure 35	X-ray structure of compound 117	59
Figure 36	X-ray structure of compound 118	61
Figure 37	Nucleoside analogs screened for cytotoxicity and anti-HIV activity	62

Part II: Synthesis and Evaluation of Truncated Triptolide Analogs to Suppress Chronic Inflammation

Figure 1	Structure of (-)-triptolide	105
Figure 2	Incidence of common autoimmune diseases by sex	107
Figure 3	Epithelial barriers to infection	109
Figure 4	Migration of monocytes to sites of infection by chemokine receptors	111
Figure 5	Mannose-binding lectin	112
Figure 6	Activation of the complement system	113
Figure 7	Lymphocyte activation by mature dendritic cells	116
Figure 8	Generation of Lymphocytes Each Bearing a Distinct Antigen receptor	117
Figure 9	Co-stimulation of T and B cells	118
Figure 10	Antibody structure	120
Figure 11	NF- κ B signaling pathway	124
Figure 12	Important cytokines secreted by macrophages	127
Figure 13	Commonly used analgesics	129
Figure 14	Structures of commonly used NSAIDS	130
Figure 15	Structure of prednisone and dexamethasone	131
Figure 16	Structures of DMARDs	133
Figure 17	Structure of (-)-triptolide	136
Figure 18	Inhibition of secreted IL-2 from Jurkat T cells	138
Figure 19	Inhibition of IL-2 luciferase activity by triptolide and cyclosporin A	138
Figure 20	Triptolide inhibits NF- κ B at a step after DNA binding	139
Figure 21	Triptolide's affect on NF- κ B transactivation	140
Figure 22	Truncated triptolide analogs	144
Figure 23	Proposed mechanism for the asymmetric epoxidation of enones utilizing the alkyl-tartrate magnesium system	149
Figure 24	X-ray structures of compounds 60a and 60b	158
Figure 25	X-ray structures of compounds 80 and 81	163
Figure 26	Relative stereochemistry of compound 82	164
Figure 27	X-ray structure of compound 83	165
Figure 28	X-ray structures of compounds 85 and 86	166
Figure 29	X-ray structure of compound 87	167
Figure 30	X-ray structure of compound 88	168
Figure 31	X-ray structure of compound 90	169
Figure 32	Conversion of XTT into formazan dye	171
Figure 33	Compounds screened in XTT assay	172
Figure 34	LPS stimulated PBMC proliferation results	173
Figure 35	Cell proliferation assay in Jurkat cells with PMA and PHA	174
Figure 36	Mouse splenocyte XTT assay results	175
Figure 37	Analogs screened in carrageenan edema model	175
Figure 38	Pictures of paw edema	176
Figure 39	RNA levels of pro-inflammatory cytokines from livers of	177

	mice challenged with carrageenan	
Figure 40	Structure of GB67B (58d)	178
Figure 41	Body weights of animals during study	178
Figure 42	Changes in paw volume	179
Figure 43	Arthritis score for GB67B and dexamethasone	180
Figure 44	Compounds screened in NF- κ B activation assay	180
Figure 45	NF- κ B luciferase reporter gene assay six hour results	181
Figure 46	Compounds screened in cytokine release assays	182
Figure 47	IL-1 cytokine levels from LPS stimulated PBMCs	183
Figure 48	Inhibition of IL-2 from PBMCs stimulated with anti-CD3	184
Figure 49	Inhibition of IL-2 from PBMCs stimulated with anti-CD3 and CD28	184
Figure 50	Inhibition of TNF- α from PBMCs stimulated with anti-CD3	185
Figure 51	Inhibition of TNF- α from PBMCs stimulated with anti-CD3 and CD28	185
Figure 52	Compounds screened for inhibition of TNF- α	186
Figure 53	Inhibition of TNF- α levels from LPS stimulated mouse splenocytes	186
Figure 54	Truncated triptolide analogs evaluated in TNF- α release assay for which the results are shown in figure 55	187
Figure 55	TNF- α levels from PMA/I stimulated Jurkat cells treated with truncated triptolide analogs	187
Figure 56	Truncated analogs screened in TNF- α release assay	188
Figure 57	Affect of truncated triptolide analogs on TNF- α levels from PMA/I stimulated Jurkat cells	188
Figure 58	Additional truncated triptolide analogs screened in TNF- α release assay	189
Figure 59	Results for TNF- α production from PMA/I stimulated Jurkat cells incubated with truncated triptolide analogs	189
Figure 60	Final selection of triptolide analogs tested in TNF- α release assay	190
Figure 61	Results for TNF- α production from PMA/I stimulated Jurkat cells incubated with truncated triptolide analogs	190
Figure 62	Compounds screened in AMES II and Greenscreen assay	191
Figure 63	Structures of triptonide and GB67B	196
Figure 64	Number of genes perturbed by triptonide and GB67B at 16 and 24 hours	196
Figure 65	Compounds evaluated in the pharmacokinetic study	197
Figure 66	GB67B mouse plasma concentration	198
Figure 67	GB97 mouse plasma concentration	199
Figure 68	GB594 mouse plasma concentration	200

List of Schemes

Part I: Synthesis of Cyclobutyl Nucleoside Analogs That Mimic AZT for Inhibition of the K65R HIV-1 Reverse Transcriptase Mutant

Scheme 1	Synthesis of AZT	34
Scheme 2	Synthesis of AZA	34
Scheme 3	Synthesis of oxetanocin A from adenosine	36
Scheme 4	Synthesis of (±)-cyclobut-A	37
Scheme 5	Synthesis of diol (+)- 15a	38
Scheme 6	Dechlorination of gem-dichlorocyclobutenone	40
Scheme 7	Synthesis of 3-silyloxycyclobutenones from ketene	40
Scheme 8	Stille cross-coupling with 3-(tri- <i>n</i> -butylstannyl)-2-cyclobuten-1-one	41
Scheme 9	Addition of azide into an α,β -unsaturated ketone	42
Scheme 10	Azide addition to an α,β -unsaturated lactone	42
Scheme 11	Addition of hydrazoic acid to enoates	43
Scheme 12	Displacement of a mesylate by adenine	47
Scheme 13	Epoxide opening by a guanosine analogue	47
Scheme 14	Mitsunobu coupling of pyrimidine and purine bases to cyclobutanols	48
Scheme 15	Michael addition of nucleoside bases	48
Scheme 16	Construction of thymine base	49
Scheme 17	Construction of purine bases	50
Scheme 18	One-Pot triphosphate synthesis	51
Scheme 19	Triphosphate synthesis using phosphoramidate intermediate	51
Scheme 20	Triphosphate synthesis utilizing an activated phosphite	52
Scheme 21	Synthesis of 5-fluoro-1-[<i>cis</i> -3'-(hydroxymethyl)-cyclobutyl]-cytosine 102	54
Scheme 22	Synthesis of DLS183-TP	55
Scheme 23	Synthesis and reduction of cyclobutenone 23c	57
Scheme 24	Synthesis of cyclobutenone 111	57
Scheme 25	Azide addition to compound 108	58
Scheme 26	Synthesis of activated cyclobutanols 115 and 116	58
Scheme 27	Synthesis of compounds 117 and 118	59
Scheme 28	Deprotection of compounds 117 and 118	60
Scheme 29	Synthesis of compounds 121 and 122	60
Scheme 30	Deprotection of compounds 121 and 122	61

Part II: Synthesis and Evaluation of Truncated Triptolide Analogs to Suppress Chronic Inflammation

Scheme 1	Synthesis of the cyclization precursor	141
Scheme 2	Generation of triptolide ring system	142
Scheme 3	Completion of triptolide synthesis	143

Scheme 4	<i>o</i> -Formylation of <i>p</i> -cresol 22 using 23	145
Scheme 5	Lewis acid promoted <i>o</i> -formylation of <i>p</i> -cresol 22	145
Scheme 6	Utilization of a MOM group for the <i>o</i> -formylation of a phenol	146
Scheme 7	Synthesis of 6-acetoxy-2,6-dimethyl-2,4-cyclohexadione	147
Scheme 8	Oxidation of a salicylic alcohol with sodium periodate	147
Scheme 9	Lactone formation via Wessely oxidation	148
Scheme 10	Oxidation of an enone with alkaline hydrogen peroxide	148
Scheme 11	Synthesis of 5-methyl-2-phenylphenol 44 utilizing the Suzuki cross-coupling reaction	150
Scheme 12	One-pot synthesis of compound 44 using a rhodium (I) catalyst	151
Scheme 13	Synthesis of 44 from 2-amino-5-methylphenol 45	151
Scheme 14	Synthesis of compound 50	152
Scheme 15	Synthesis of salicylic alcohols	153
Scheme 16	Sodium periodate oxidation of salicylic alcohols 55a-f	153
Scheme 17	Synthesis of <i>trans</i> - and <i>cis</i> - diepoxides	154
Scheme 18	Oxidation of dienone 56e	155
Scheme 19	Treatment of monoepoxide 56f with <i>m</i> CPBA	156
Scheme 20	Epoxidation of <i>trans</i> -diepoxides	156
Scheme 21	Epoxidation of <i>cis</i> -diepoxides	157
Scheme 22	Deprotection of compound 60f	158
Scheme 23	Attempted synthesis of 7- <i>tert</i> -butyl-tetralone 68	159
Scheme 24	Synthesis of 7- <i>tert</i> -butyl-tetralone 68	160
Scheme 25	Attempted synthesis of 7- <i>tert</i> -butyl-8-hydroxytetralol 70	160
Scheme 26	Synthesis of 7- <i>tert</i> -butyl-8-hydroxytetralol 70	161
Scheme 27	Synthesis of bicyclic diepoxides and triepoxides	162
Scheme 28	Treatment of 58d with L-Selectride [®]	163
Scheme 29	Reduction of the carbonyl in 58d	164
Scheme 30	Reduction of 60d	164
Scheme 31	Synthesis of diol 85	165
Scheme 32	Synthesis of diol 87	166
Scheme 33	Synthesis of diol 88	167
Scheme 34	Corey-Chaykovsky cyclopropanation of 58d	168
Scheme 35	Synthesis of deuterated 2- <i>tert</i> -butyl-5-methylphenol	169
Scheme 36	Synthesis of deuterated analogs	170

List of Tables

Part I: Synthesis of Cyclobutyl Nucleoside Analogs That Mimic AZT for Inhibition of the K65R HIV-1 Reverse Transcriptase Mutant

Table 1	FDA approved fixed dose combinations	14
Table 2	K65R HIV RT mutants and fold resistance to NRTIs	31
Table 3	Examples of [2+2] cycloaddition reactions with dichloroketene	39
Table 4	[2 + 2] Cycloaddition reactions with disubstituted alkynes	39
Table 5	β -Azidation of α,β -unsaturated ketones in the presence	43

	of amine catalyst	
Table 6	Azidation of α,β -unsaturated ketones in the presence of Amberlite IRA900F	45
Table 7	Anti-HIV and cytotoxicity results for nucleosides 119 , 120 , 123 , and 124	62
Table 8	Crystal data and structure refinement for GB957n	73
Table 9	Atomic coordinates ($\times 10^4$) and equivalent isotropic displacement parameters ($\text{\AA}^2 \times 10^3$) for GB957n	74
Table 10	Bond lengths [\AA] and angles [$^\circ$] for GB957n	75
Table 11	Anisotropic displacement parameters ($\text{\AA}^2 \times 10^3$) for GB957n	77
Table 12	Hydrogen coordinates ($\times 10^4$) and isotropic displacement parameters ($\text{\AA}^2 \times 10^3$) for GB957n	78
Table 13	Torsion angles [$^\circ$] for GB957n	79
Table 14	Hydrogen bonds for GB957n [\AA and $^\circ$]	81
Table 15	Crystal data and structure refinement for GB982s	87
Table 16	Atomic coordinates ($\times 10^4$) and equivalent isotropic displacement parameters ($\text{\AA}^2 \times 10^3$) for GB982s	88
Table 17	Bond lengths [\AA] and angles [$^\circ$] for GB982s	89
Table 18	Anisotropic displacement parameters ($\text{\AA}^2 \times 10^3$) for GB982s	92
Table 19	Hydrogen coordinates ($\times 10^4$) and isotropic displacement parameters ($\text{\AA}^2 \times 10^3$) for GB982s	93
Table 20	Torsion angles [$^\circ$] for GB982s	93
Table 21	Hydrogen bonds for GB982s [\AA and $^\circ$]	95

Part II: Synthesis and Evaluation of Truncated Triptolide Analogs to Suppress Chronic Inflammation

Table 1	List of common autoimmune diseases in the United States	107
Table 2	Results for the conversion of phenols into salicylic alcohols	153
Table 3	Results for the sodium periodate oxidation of salicylic alcohols 55a-f	154
Table 4	Results for the synthesis of diepoxides	155
Table 5	Results for the epoxidation of 57a-e	156
Table 6	Results for the epoxidation of <i>cis</i> -diepoxides 58a-f	157
Table 7	Results of the carrageenan paw edema model	176
Table 8	AMES II results for GB67B in TA98 strain	191
Table 9	AMES II results for GB67B in TAMix strain	192
Table 10	AMES II results for GB594 in TA98 strain	192
Table 11	AMES II results for GB594 in TAMix strain	193
Table 12	GreenScreen results for GB67B	194
Table 13	GreenScreen results for GB594	195
Table 14	Toxicology groups	201
Table 15	Toxicology and toxicokinetic groups	202
Table 16	Aqueous solubility of triptolide and triptolide analogs	204

Table 17	Crystal data and structure refinement for GB2s	237
Table 18	Atomic coordinates ($\times 10^4$) and equivalent isotropic displacement parameters ($\text{\AA}^2 \times 10^3$) for GB2s	238
Table 19	Bond lengths [\AA] and angles [$^\circ$] for GB2s	239
Table 20	Anisotropic displacement parameters ($\text{\AA}^2 \times 10^3$) for GB2s	241
Table 21	Hydrogen coordinates ($\times 10^4$) and isotropic displacement parameters ($\text{\AA}^2 \times 10^3$) for GB2s	242
Table 22	Torsion angles [$^\circ$] for GB2s	242
Table 23	Crystal data and structure refinement for GB1	244
Table 24	Atomic coordinates ($\times 10^4$) and equivalent isotropic displacement parameters ($\text{\AA}^2 \times 10^3$) for GB1	245
Table 25	Bond lengths [\AA] and angles [$^\circ$] for GB1	246
Table 26	Anisotropic displacement parameters ($\text{\AA}^2 \times 10^3$) for GB1	249
Table 27	Hydrogen coordinates ($\times 10^4$) and isotropic displacement parameters ($\text{\AA}^2 \times 10^3$) for GB1	249
Table 28	Torsion angles [$^\circ$] for GB1	250
Table 29	Crystal data and structure refinement for gb587_1_0m	268
Table 30	Atomic coordinates ($\times 10^4$) and equivalent isotropic displacement parameters ($\text{\AA}^2 \times 10^3$) for gb587_1_0m	269
Table 31	Bond lengths [\AA] and angles [$^\circ$] for gb587_1_0m	269
Table 32	Anisotropic displacement parameters ($\text{\AA}^2 \times 10^3$) for gb587_1_0m	273
Table 33	Hydrogen coordinates ($\times 10^4$) and isotropic displacement parameters ($\text{\AA}^2 \times 10^3$) for gb587_1_0m	273
Table 34	Torsion angles [$^\circ$] for gb587_1_0m	274
Table 35	Crystal data and structure refinement for GB587_2s	276
Table 36	Atomic coordinates ($\times 10^4$) and equivalent isotropic displacement parameters ($\text{\AA}^2 \times 10^3$) for GB587_2s	278
Table 37	Bond lengths [\AA] and angles [$^\circ$] for GB587_2s	278
Table 38	Anisotropic displacement parameters ($\text{\AA}^2 \times 10^3$) for GB587_2s	281
Table 39	Hydrogen coordinates ($\times 10^4$) and isotropic displacement parameters ($\text{\AA}^2 \times 10^3$) for GB587_2s	283
Table 40	Crystal data and structure refinement for GB649	285
Table 41	Atomic coordinates ($\times 10^4$) and equivalent isotropic displacement parameters ($\text{\AA}^2 \times 10^3$) for GB649	286
Table 42	Bond lengths [\AA] and angles [$^\circ$] for GB649	287
Table 43	Anisotropic displacement parameters ($\text{\AA}^2 \times 10^3$) for GB649	293
Table 44	Hydrogen coordinates ($\times 10^4$) and isotropic displacement parameters ($\text{\AA}^2 \times 10^3$) for GB649	294
Table 45	Torsion angles [$^\circ$] for GB649	295
Table 46	Hydrogen bonds for GB649 [\AA and $^\circ$]	297

Table 47	Crystal data and structure refinement for GB625s	299
Table 48	Atomic coordinates ($\times 10^4$) and equivalent isotropic displacement parameters ($\text{\AA}^2 \times 10^3$) for GB625s	300
Table 49	Bond lengths [\AA] and angles [$^\circ$] for GB625s	300
Table 50	Anisotropic displacement parameters ($\text{\AA}^2 \times 10^3$) for GB625s	303
Table 51	Hydrogen coordinates ($\times 10^4$) and isotropic displacement parameters ($\text{\AA}^2 \times 10^3$) for GB625s	303
Table 52	Torsion angles [$^\circ$] for GB625s	304
Table 53	Hydrogen bonds for GB625s [\AA and $^\circ$]	306
Table 54	Crystal data and structure refinement for gb630bs	308
Table 55	Atomic coordinates ($\times 10^4$) and equivalent isotropic displacement parameters ($\text{\AA}^2 \times 10^3$) for gb630bs	310
Table 56	Bond lengths [\AA] and angles [$^\circ$] for gb630bs	310
Table 57	Anisotropic displacement parameters ($\text{\AA}^2 \times 10^3$) for gb630bs	313
Table 58	Hydrogen coordinates ($\times 10^4$) and isotropic displacement parameters ($\text{\AA}^2 \times 10^3$) for gb630bs	314
Table 59	Torsion angles [$^\circ$] for gb630bs	315
Table 60	Hydrogen bonds for gb630bs [\AA and $^\circ$]	316
Table 61	Crystal data and structure refinement for GB760	318
Table 62	Atomic coordinates ($\times 10^4$) and equivalent isotropic displacement parameters ($\text{\AA}^2 \times 10^3$) for GB760	319
Table 63	Bond lengths [\AA] and angles [$^\circ$] for GB760	319
Table 64	Anisotropic displacement parameters ($\text{\AA}^2 \times 10^3$) for GB760	323
Table 65	Hydrogen coordinates ($\times 10^4$) and isotropic displacement parameters ($\text{\AA}^2 \times 10^3$) for GB760	324
Table 66	Torsion angles [$^\circ$] for GB760	324
Table 67	Hydrogen bonds for GB760 [\AA and $^\circ$]	326
Table 68	Crystal data and structure refinement for gb594_0m	328
Table 69	Atomic coordinates ($\times 10^4$) and equivalent isotropic displacement parameters ($\text{\AA}^2 \times 10^3$) for gb594_0m	329
Table 70	Bond lengths [\AA] and angles [$^\circ$] for gb594_0m	329
Table 71	Anisotropic displacement parameters ($\text{\AA}^2 \times 10^3$) for gb594_0m	333
Table 72	Hydrogen coordinates ($\times 10^4$) and isotropic displacement parameters ($\text{\AA}^2 \times 10^3$) for gb594_0m	333
Table 73	Torsion angles [$^\circ$] for gb594_0m	335
Table 74	Hydrogen bonds for gb594_0m [\AA and $^\circ$]	336
Table 75	Crystal data and structure refinement for GB813s	338
Table 76	Atomic coordinates ($\times 10^4$) and equivalent isotropic displacement parameters ($\text{\AA}^2 \times 10^3$) for GB813s	339
Table 77	Bond lengths [\AA] and angles [$^\circ$] for GB813s	340
Table 78	Anisotropic displacement parameters ($\text{\AA}^2 \times 10^3$) for GB813s	343

Table 79	Hydrogen coordinates ($\times 10^4$) and isotropic displacement parameters ($\text{\AA}^2 \times 10^3$) for GB813s	344
Table 80	Torsion angles [$^\circ$] for GB813s	344
Table 81	Hydrogen bonds for GB813s [\AA and $^\circ$]	346
Table 82	Crystal data and structure refinement for GB595m	348
Table 83	Atomic coordinates ($\times 10^4$) and equivalent isotropic displacement parameters ($\text{\AA}^2 \times 10^3$) for GB595m	349
Table 84	Bond lengths [\AA] and angles [$^\circ$] for GB595m	351
Table 85	Anisotropic displacement parameters ($\text{\AA}^2 \times 10^3$) for GB595m	357
Table 86	Hydrogen coordinates ($\times 10^4$) and isotropic displacement parameters ($\text{\AA}^2 \times 10^3$) for GB595m	358

List of Abbreviations

3TC-TP	2',3'-Dideoxy-3'-thiacytidine triphosphate
Ac	Acetyl
AcOH	Acetic acid
Ac ₂ O	Acetic anhydride
AZT	3'-azido-2',3'-dideoxythymidine
AIBN	2,2'-Azobis(2-methylpropionitrile)
AIDS	Acquired immunodeficiency syndrome
ALDH	Aldehyde dehydrogenase
AP-1	Activator protein 1
APCI	Atmospheric pressure chemical ionization
ATP	Adenosine triphosphate
AZA	3'-azido-2',3'-dideoxyadenosine
AZC	3'-azido-2',3'-dideoxycytidine
AZDDU	3'-Azido-2'3'-dideoxyuridine
AZG	3'-azido-2',3'-dideoxyguanosine
AZTDP	3'-azido-2',3'-dideoxythymidine diphosphate
AZTMP	3'-azido-2',3'-dideoxythymidine monophosphate
AZTTP	3'-azido-2',3'-dideoxythymidine triphosphate
Bcr-Abl	Fusion gene between the "breakpoint cluster region" on chromosome 22 and the Abl gene on chromosome 9
BF ₃ ·OEt ₂	Boron trifluoride diethyl etherate
BH ₃ ·SMe ₂	Borane dimethyl sulfide complex

B(OMe) ₃	Trimethyl borate
Bs	Brosylate
<i>t</i> -BuCl	2-Chloro-2-methylpropane, <i>tert</i> -butyl chloride
<i>n</i> -BuLi	<i>n</i> -Butyllithium
<i>s</i> -BuLi	<i>sec</i> -Butyllithium
<i>t</i> -BuLi	<i>tert</i> -Butyllithium
Bu ₃ N	Tributylamine
Bu ₄ NBr	Tetrabutylammonium bromide
<i>t</i> -BuOH	<i>tert</i> -Butanol
<i>t</i> -BuOOH	<i>tert</i> -Butyl hydroperoxide
Bz	Benzoyl
BzCl	Benzoyl chloride
CBP	cAMP-response element-binding protein
cm	centimeter
C _{max}	Maximum plasma concentration of a drug
COX	Cyclooxygenase
<i>m</i> CPBA	3-Chloroperbenzoic acid
CsA	Cyclosporin A
CTLA	Cytotoxic T-lymphocyte antigen
CYP3A4	Cytochrome P450 3A4
d	Day
d4T	2',3'-Didehydro-2',3'-dideoxythymidine
dATP	Deoxyadenosine triphosphate

DBU	1,8-Diazabicyclo[5.4.0]undec-7-ene
DCC	<i>N,N'</i> -Dicyclohexylcarbodiimide
dCTP	Deoxycytidine triphosphate
DEAD	Diethyl azodicarboxylate
D.E.C.	Dead end complex
dGTP	Deoxyguanosine triphosphate
DHEA	5-Dehydroepiandrosterone
DIAD	Diisopropyl azodicarboxylate
DIBAL-H	Diisobutylaluminum hydride
DMAP	4-(Dimethylamino)pyridine
DMARDs	Disease-modifying antirheumatic drugs
DMF	<i>N,N</i> ,-Dimethylformamide
DMSO	Dimethyl sulfoxide
DNA	Deoxyribonucleic acid
dNTP	Deoxyribonucleotide triphosphate
dr	Diastereomeric ratio
EC ₅₀	Effective concentration of a drug that is required for 50% inhibition in an <i>in vitro</i> assay
EC ₉₀	Effective concentration of a drug that is required for 90% inhibition in an <i>in vitro</i> assay
EDTA	Ethylenediaminetetraacetic acid
e.e.	Enantiomeric excess
ELISA	Enzyme-linked immunosorbent assay

EMSA	Electrophoretic mobility shift assay
Env	Envelope protein of HIV
equiv	equivalents
ESI	Electrospray ionization
ether	Diethyl ether
Et ₃ N	Triethylamine
EtOH	Ethanol
Eu(fod) ₃	Europium(III)-tris(1,1,1,2,2,3,3-heptafluoro-7,7-dimethyl-4,6-octanedionate)
FDA	US Food and Drug Administration
GADD	Growth arrest and DNA-damage-inducible protein
Gag	HIV structural protein
GAL4	Gene encoding the yeast transcription activator protein Gal4
GAL4DB	GAL4 DNA binding domain
GFP	Green fluorescent protein
GI	Gastrointestinal
gp	Glycoprotein
h	hour
HAART	Highly active anti-retroviral therapy
HIV	Human Immunodeficiency Virus
HMPT	Hexamethylphosphorous triamide
HR2	Heptad repeat 2 domain
HRMS	High resolution mass spectrometry

HSF-1	Heat shock factor-1
HSV-tk	Herpes simplex virus thymidine kinase
hv	High voltage
I	Ionomycin
I κ B	Inhibitor of kappa B
IC ₅₀	Concentration of an inhibitor that is required for 50% inhibition of an enzyme in an in vitro assay
IFN- γ	Interferon-gamma
IKK	Inhibitor of kappa B kinase
IL	Interleukin
i.p.	Intraperitoneal
IR	Infrared
K _d	Dissociation constant
KHMDS	Potassium hexamethyldisilazide
k _{pol}	Catalytic rate constant
LAH	Lithium aluminum hydride
LD ₅₀	Lethal dose of a drug that is required to kill half the members of a tested population
LDA	Lithium diisopropylamide
LPS	Lipopolysaccharides
L-Selectride	Lithium tri- <i>sec</i> -butylborohydride
<i>m</i>	<i>meta</i>
μ M	Micromolar

MAP	Mitogen-activated protein
MBL	Mannose binding lectin
Me	Methyl
MeCN	Acetonitrile
MeI	Methyl iodide
MeLi	Methyl lithium
MeNH ₂	Methylamine
MeOH	Methanol
Me ₂ SO ₄	Dimethyl sulfate
MHC	Major histocompatibility complex
MHz	Megahertz
min	Minute
Mn(OAc) ₃ ·2H ₂ O	Manganese(III) acetate dihydrate
MOM	Methoxymethyl
MOMCl	Chloromethyl methyl ether
mp	Melting point
mRNA	Messenger ribonucleic acid
MsCl	Methanesulfonyl chloride
NaOMe	Sodium methoxide
NDP	Nucleotide diphosphate
Nef	Negative regulatory factor
NF90	Nuclear factor 90
NF-κB	Nuclear factor of kappa B

nm	nanometer
nM	Nanomolar
NMO	4-Methylmorpholine <i>N</i> -oxide
NMR	Nuclear magnetic resonance
NNRTI	Non-nucleoside reverse transcriptase inhibitor
Nrf2	Nuclear factor (erythroid-derived 2)-like 2
NRTI	Nucleoside reverse transcriptase inhibitor
NRTI-MP	Nucleoside reverse transcriptase inhibitor monophosphate
NSAIDs	Non-steroidal anti-inflammatory drugs
<i>o</i>	<i>ortho</i>
<i>p</i>	<i>para</i>
PBL	Peripheral blood lymphocytes
PBMCs	Peripheral blood mononuclear cells
Pb(OAc) ₄	Lead(IV) tetraacetate
Pd(OAc) ₂	Palladium(II) acetate
Pd(PPh ₃) ₄	Tetrakis(triphenylphosphine)palladium(0)
Ph	Phenyl
PHA	Phytohemagglutinin
PhNTf ₂	<i>N</i> -Phenyl-bis(trifluoromethanesulfonimide)
Ph ₃ P	Triphenyl phosphine
PI	Protease inhibitor
PK	Pharmacokinetics
PLE	Pig liver esterase

PMA	Phorbol 12-myristate 13 acetate
PPA	Polyphosphoric acid
PPTS	Pyridinium <i>para</i> -toluenesulfonate
RA	Rheumatoid arthritis
Rev	Regulator of Virion
Rf	Retention factor
[RhCl(cod)] ₂	Chloro(1,5-cyclooctadiene)rhodium(I) dimer
RLUs	Relative light units
RNA	Ribonucleic acid
RNase H	Ribonuclease H
r.t.	Room temperature
RT	Reverse transcriptase
SLE	Systemic lupus erythematosus
S _N 2	Bimolecular nucleophilic substitution
SolFC	Solvent free conditions
TA	Transactivation domain
TAMs	Thymidine associated mutations
Tat	Trans-activator of transcription
TBAF	Tetrabutylammonium fluoride
TBDMS	<i>tert</i> -Butyldimethylsilyl
TBDMSOTf	<i>tert</i> -Butyldimethylsilyl trifluoromethanesulfonate
TBSCl	<i>tert</i> -Butyldimethylsilyl chloride
TC ₂₀	Toxic concentration of a drug that is required to cause cytotoxicity

	in 20% of cells in an in vitro assay
TDF	Tenofovir
Tf ₂ O	Trifluoromethanesulfonic anhydride
TGF-β	Transforming growth factor-beta
T _h	T helper cells
Thd	Thymidine
THF	Tetrahydrofuran
TIPS	Triisopropylsilyl
TIPSCI	Triisopropylsilyl chloride
TLC	Thin layer chromatography
TLRs	Toll-like receptors
TMEDA	<i>N,N,N',N'</i> -Tetramethylethylenediamine
TMSCl	Chlorotrimethylsilane
TMP	Thymidine monophosphate
TMSN ₃	Trimethylsilyl azide
TNF-α	Tumor Necrosis Factor-alpha
pTSA	<i>para</i> -Toluenesulfonic acid
TTP	Thymidine triphosphate
Vif	Viral infectivity factor
WT	Wild-type
XTT	2,3-Bis(2-methoxy-4-nitro-5-sulfophenyl)-2H-tetrazolium-5-carboxanilide sodium salt
Yb(OTf) ₃	Ytterbium(III) trifluoromethanesulfonate

Part I: Synthesis of Cyclobutyl Nucleoside Analogs That Mimic AZT for Inhibition of the K65R HIV-1 Reverse Transcriptase Mutant

1.1 Statement of Purpose

The spread of diseases continues to be a major challenge facing a growing human population. One such disease that continues to spread is AIDS (Acquired Immune Deficiency Syndrome), currently a pandemic, which has claimed the lives of over 25 million people worldwide since 1981.¹ Current estimates indicate that over 33 million people worldwide live with AIDS or HIV (Human Immunodeficiency Virus), the causative agent of AIDS.¹ Despite past misconceptions, HIV affects both males and females. Over the last two decades, the number of women infected with HIV has tripled. Thus, women account for 50% of all adult infections worldwide.¹ An alarming new statistic is that young adults under the age of 25 make up nearly half of new infections.¹

Though there is no cure for AIDS, public and private organizations have funded research aimed to treat the spread of HIV. The efforts of these organizations have resulted in a number of FDA (Food and Drug Administration) approved drugs that disrupt vital steps in the HIV replication cycle. Patients receiving treatment undergo HAART (Highly Active Anti-Retroviral Therapy) which is the administration of three or more drugs designed to disrupt viral replication and to delay the onset of drug resistant mutations. Currently accepted first line regimens include two nucleoside reverse transcriptase inhibitors (NRTIs) that, once activated, are incorporated into viral DNA causing chain termination. In addition to the two NRTIs either a protease inhibitor (PI) or a non-nucleoside reverse transcriptase inhibitor (NNRTI) is co-administered.

Over time the effectiveness of drug regimens is determined by toxicity associated with long term usage of the drugs, patient compliance with dosing schedules, the distribution of drugs throughout the body, and the inevitable emergence of drug resistance.² Mutations arising from NRTI treatment occur near the active site of HIV reverse transcriptase (HIV RT), the enzyme responsible for the replication of the viral genome.³ Mutations such as K65R, arising from regimens containing tenofovir disoproxil fumarate (TDF) (Figure 1), allow HIV RT to discriminate against incoming nucleotides causing high level resistance to multiple NRTIs.⁴⁻⁶ In addition, the group of mutations known as thymidine associated mutations (TAMs), represented by M41L, D67N, K70R, L210W, T215Y, and K219Q, are selected for by zidovudine (AZT) and stavudine (d4T) (Figure 1), provide HIV RT with an ability to excise incorporated NRTIs.³⁻⁵ Interestingly, even though the K65R mutant causes resistance to multiple NRTIs, this mutant is still susceptible to AZT. Additionally, there exists a bidirectional antagonism between K65R and TAMs.⁵ While the incidence of K65R is low, <4%, recent trends show K65R is appearing more as tenofovir is widely being used in many HAART regimens.⁵⁻⁷ Furthermore, the K65R mutation has been found in up to 25% of patients failing chemotherapy that exclude AZT.⁵

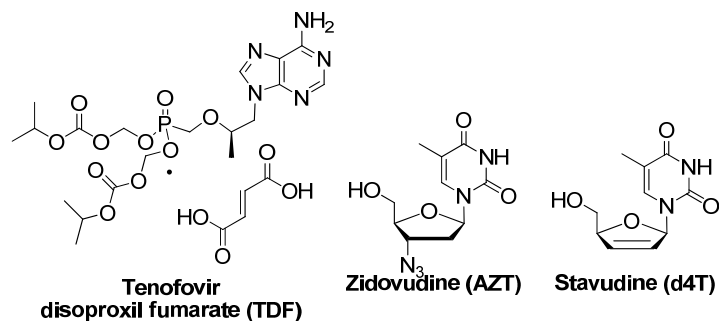


Figure 1. Structures of tenofovir, AZT, and d4T

In an effort to overcome drug resistance due to the K65R mutation, the Liotta group has chosen to focus on the mutant's susceptibility to AZT as inspiration for the development of cyclobutyl nucleoside analogues that mimic AZT. We postulate these analogues will be able to mimic AZT and thus will inhibit the HIV K65R RT mutant while also being resistant to excision promoted by TAMs.

1.2 Introduction

1.2.1 Current Status of the HIV/AIDS Pandemic

The earliest account of HIV infection is thought to have originated from an African tribesman in 1959.⁸ A sample of his blood, which had been preserved by clinical physicians, was identified as containing the HIV-1. The virus has since spread around the world and has been present in the United States since the early 1980's, although new research indicates the virus may have arrived in the United States in 1969 from Haiti.⁹

Since 1981 over 25 million people worldwide have died from AIDS and of these deaths 583,000 have occurred in the United States.¹ Currently an estimated 33 million people worldwide are either carriers of HIV or have developed AIDS (Figure 2) and approximately 2.7 million new infections occur each year.¹ Of the total HIV and AIDS cases worldwide two-thirds are located in sub-Saharan Africa. In addition, Africa also has 11.6 million orphans resulting from AIDS related deaths.¹ Once thought to be a disease affecting only males, HIV now infects 15.5 million women accounting for 50% of all adult cases.¹ Current trends show that of the 2.7 million new infections each year half occur in adults 25 years old or younger.¹ Since 1990 the global trend of people living with HIV has risen from 8 million to 33 million people today and that number is continuing to rise (Figure 3).¹

Even though these figures are overwhelming, the life expectancy for an HIV patient with access to chemotherapy has increased, and the number of global deaths from AIDS has decreased. In the United States, the number of new infections and deaths rose steadily from 1981 peaking in 1993 (Figure 4). With the introduction of combination chemotherapy in 1996, the number of deaths has dropped dramatically. Though some

regions of the world show no increase in new infections, some even showing a decrease, AIDS is still a leading cause of death worldwide and the primary cause of death in sub-Saharan Africa.

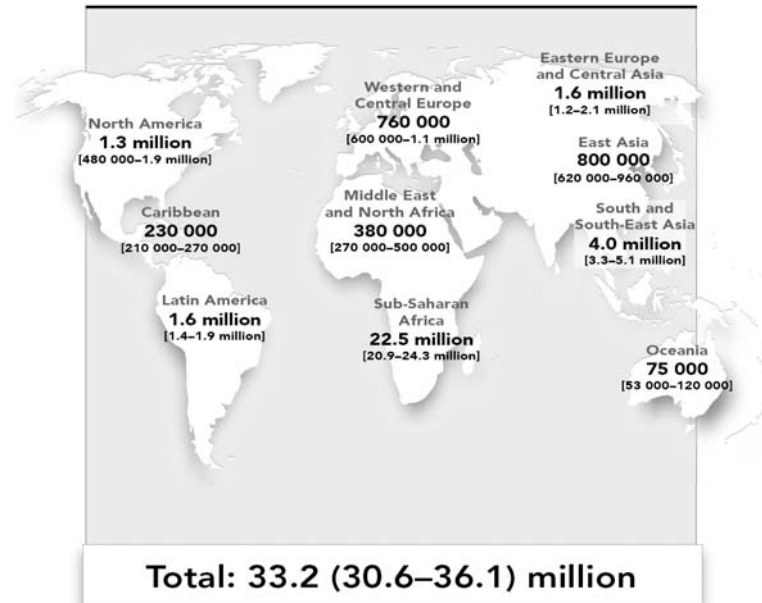


Figure 2. 2007 estimates for adults and children living with HIV/AIDS¹⁰

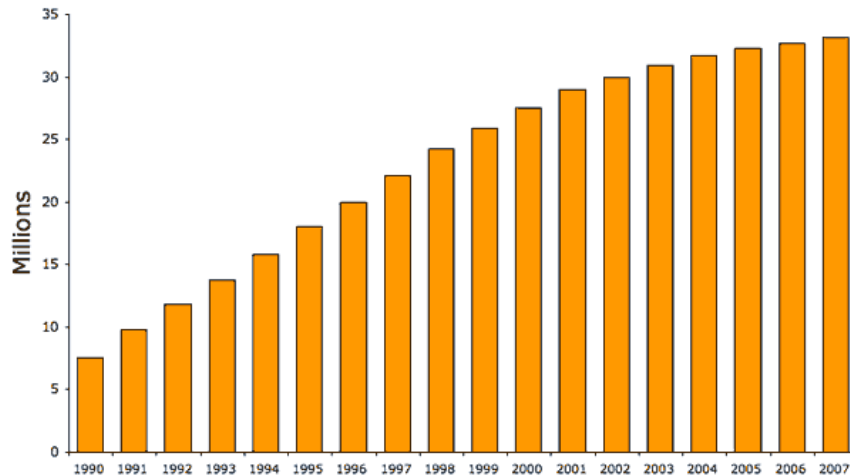


Figure 3. The number of people living with HIV globally from 1990 to 2007¹

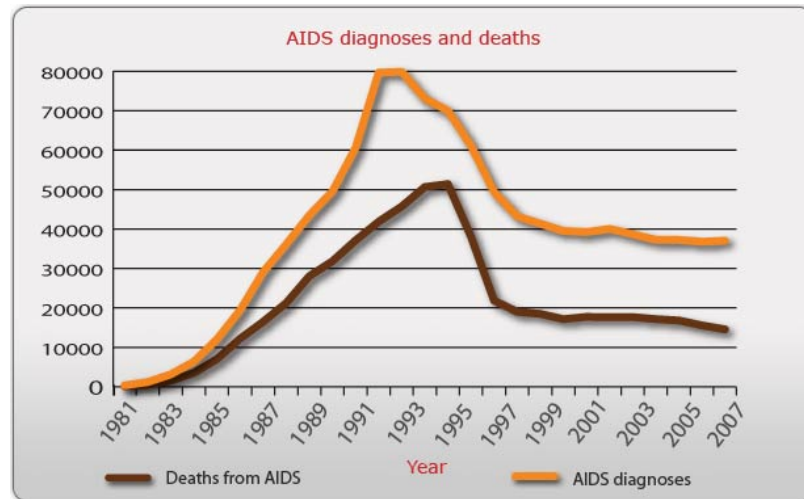


Figure 4. The number of new AIDS cases and AIDS related deaths from 1981 to 2007¹

1.2.2 The HIV Replication Cycle

HIV requires T-helper lymphocytes, macrophages, and dendritic cells to replicate. Viral replication is a multi-step process (Figure 5) consisting of two phases, the early phase and the late phase. During these two phases, the virus invades immune system cells resulting in the production of new virions able to infect other host cells.

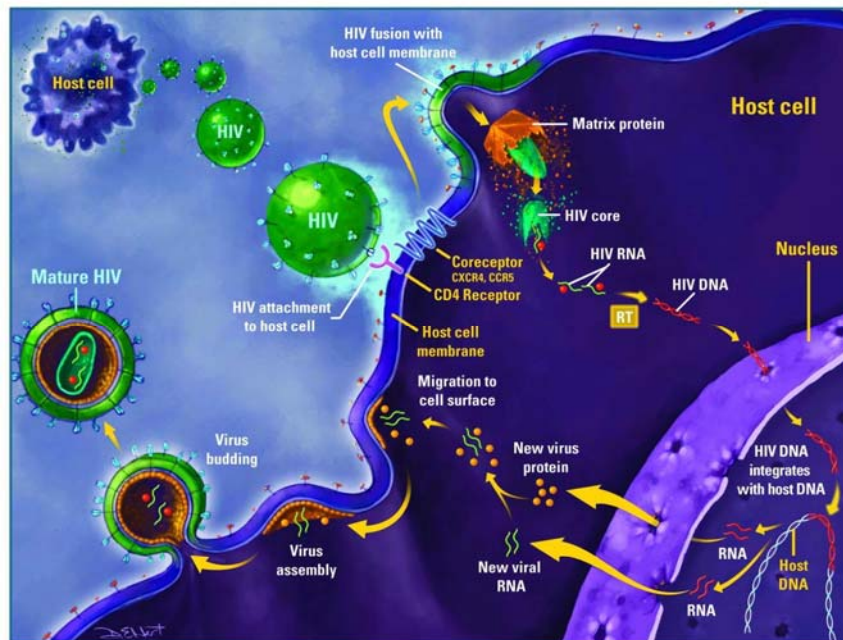


Figure 5. The HIV replication cycle¹¹

1.2.2.1 Early phase

1.2.2.1.1 Attachment/fusion

The invasion of a host cell by HIV commences with the binding of the HIV-1 surface glycoprotein 120 (gp120) to a CD4 receptor of the host cell.^{12,13} The resulting complex is then able to interact with a co-receptor. The co-receptor the virus uses to gain entry into the host cell depends on the virus's tropism.¹⁴ HIV can use the co-receptor CXCR4 to gain entry into T cells, or it can use the co-receptor CCR5 to infect macrophages. The binding of a co-receptor results in a conformational change allowing gp41 to penetrate the cell membrane, enabling fusion of the viral and cellular membranes.^{12,13} The fusion of the membranes results in the release of the viral protein core, including the viral genome, into the host cell.^{12,13}

1.2.2.1.2 Reverse transcription

After entering a host cell, the protein core disintegrates releasing viral proteins and two RNA copies of the viral genome. The HIV RT binds to the viral RNA and converts the single-stranded RNA into double-stranded DNA.¹⁵ The single-stranded viral RNA is used as a template by the RT to synthesize single-stranded DNA.¹⁵ As this polymerization takes place, the RNA template is degraded by HIV RT's second enzymatic active site, the ribonuclease H (RNase H) active site.¹⁶ The newly synthesized single-stranded viral DNA is then used as a template by HIV RT to produce double-stranded viral DNA.¹⁵ The double-stranded DNA is now a substrate for the viral integrase and can now be integrated into the host cell's DNA.¹⁵

1.2.2.1.3 Integration

HIV integrase catalyzes 3'-end processing of the proviral DNA as well as a strand transfer reaction. First, integrase removes two deoxynucleotides from the 3'-end of the proviral DNA.¹⁷ Next, integrase ligates the processed viral DNA into the host cell's DNA.¹⁷ Completion of this process results in the formation of HIV-1 provirus and ends the early phase of the HIV replication cycle.

1.2.2.2 Late phase

1.2.2.2.1 Transcription

After integration of viral DNA into the host cell's DNA is complete, the virus may lay dormant.¹⁵ This stage of HIV infection is known as the latent stage of infection. For the virus to be actively produced, the cell must be activated with certain cellular transcription factors present. The most important of these transcription factors is NF- κ B (NF kappa B).¹⁸ The upregulation of NF- κ B in HIV infected cells allows the mRNA of the provirus to be copied. Early in the transcription process, the provirus mRNA is spliced into smaller units. The smaller pieces of mRNA lead to the production of the regulatory proteins Tat, Rev and Nef.¹⁹ The Tat protein promotes new virus to be produced, and accumulation of the Rev protein inhibits mRNA splicing.¹⁹ Once at this stage, two structural proteins, Gag and Env, are produced from the full-length viral mRNA as well as the Gag-Pol polyprotein. The Gag protein binds to the full-length RNA and helps package it into new viral particles.¹⁹

1.2.2.2.2 Assembly/budding/maturation

The assembly of new HIV-1 virions begins at the plasma membrane of the host cell as the products from Env cleavage, gp41 and gp120, began to accumulate.²⁰ The

gp41 acts as an anchor between gp120 and the cell membrane. In addition, the Gag and Gag-Pol polyproteins also associate with the cell membrane along with viral genomic RNA.²⁰ As these proteins and RNA began to accumulate, the viron begins to bud from the cell surface.²⁰ Lastly, maturation occurs as proteases cleave the polyproteins into functional viral proteins and enzymes.²⁰ Structural proteins then assemble to form a mature HIV viral particle that is able to infect other cells.

1.2.3 FDA Approved Anti-HIV Therapeutics

Currently, there are a number of FDA approved anti-HIV therapeutics that target different stages of the HIV replication cycle.²¹ To date there are two approved fusion/entry inhibitors. These drugs interfere with the virus's ability to interact with host cell surface receptors and co-receptors for gaining entry into the cell. The first entry inhibitor, enfuvirtide (Figure 6), is a 36 amino acid peptide that corresponds to the heptad repeat 2 (HR2) domain of gp41. Enfuvirtide inhibits the conformational change gp41 undergoes to fuse with the cell membrane. The CCR5 co-receptor antagonist maraviroc (Figure 6) prevents entry into the cell of CCR5-tropic HIV.²⁸

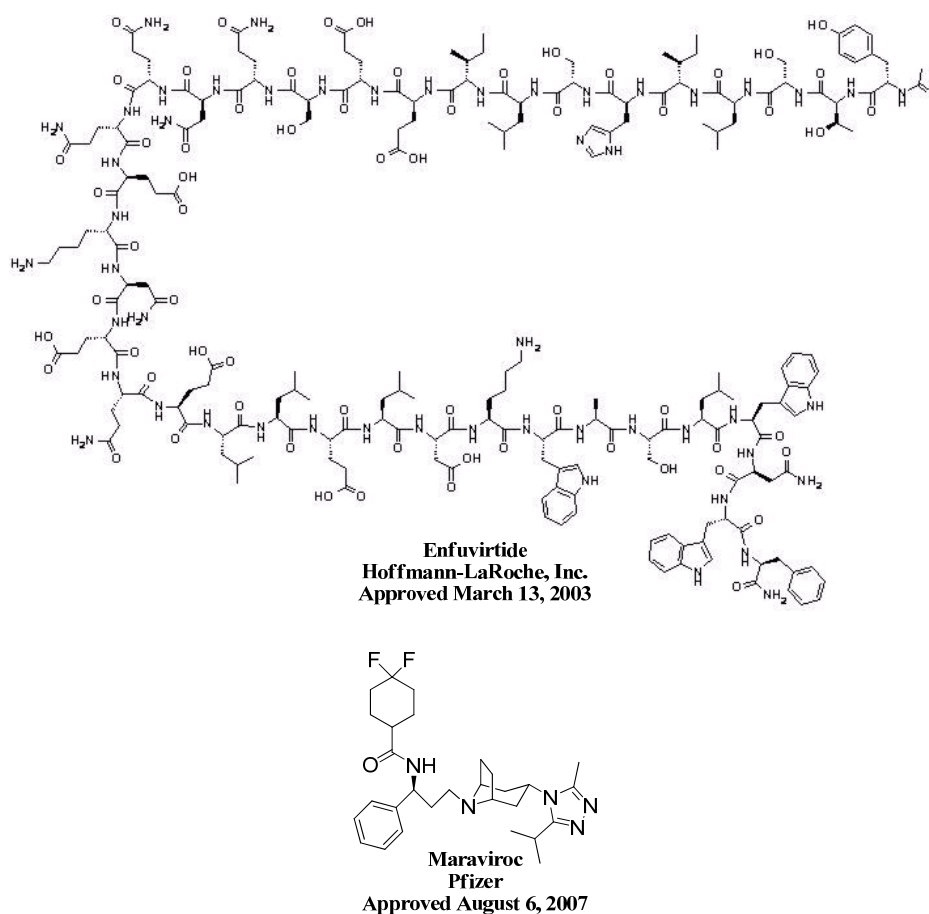


Figure 6. FDA approved entry inhibitors

FDA approved drugs that target HIV RT can be classified as either nucleoside reverse transcriptase inhibitors (NRTIs) or non-nucleoside reverse transcriptase inhibitors (NNRTIs). NRTIs are prodrugs that are activated by cellular kinases. Once converted to their corresponding triphosphate, or diphosphate in the case of tenofovir, NRTIs are able to compete with natural deoxynucleotide triphosphates as substrates for HIV RT. Once incorporated into viral DNA, NRTIs act as chain terminators and DNA synthesis is halted. There are currently eight NRTIs approved by the FDA (Figure 7).

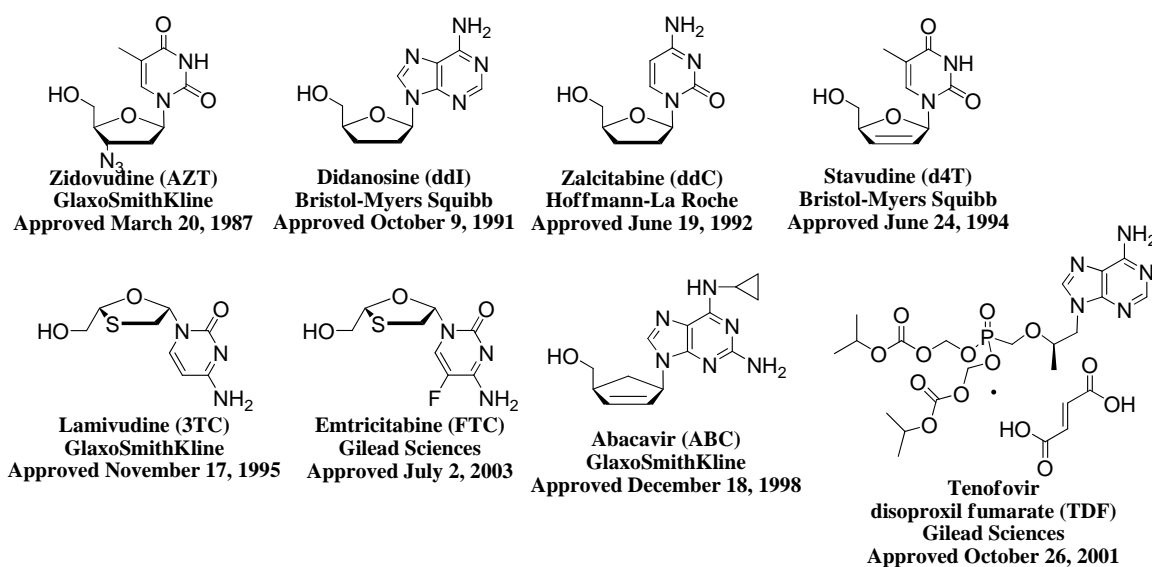


Figure 7. FDA approved NRTIs

NNRTIs (Figure 8) bind to an allosteric site of HIV RT through an induced-fit mechanism creating a stable, open conformation of the RT. By limiting the conformational flexibility of HIV RT, DNA polymerization is impaired.

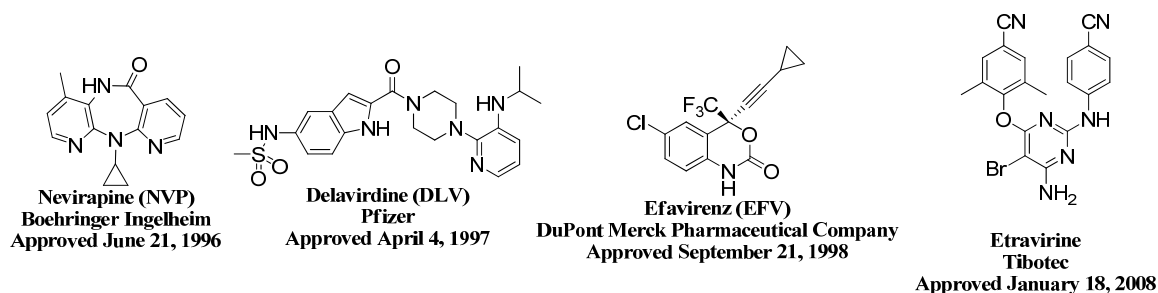


Figure 8. FDA approved NNRTIs

There is currently only one FDA approved integrase inhibitor, raltegravir (Figure 9). Raltegravir inhibits the strand transfer of viral DNA into the host cell genome.

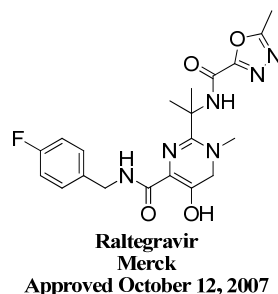
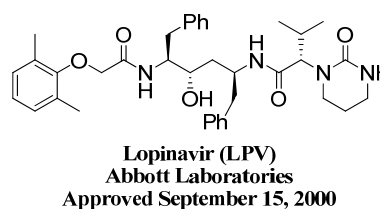
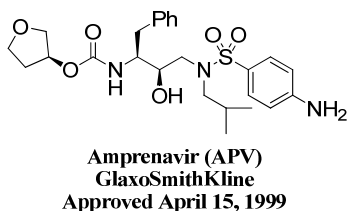
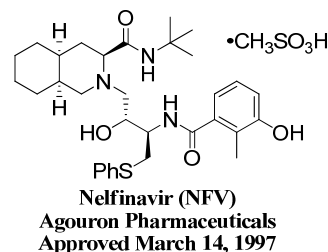
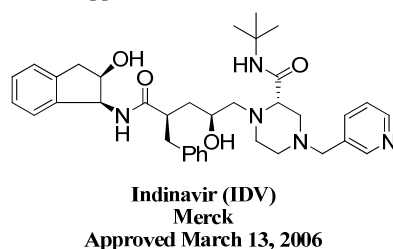
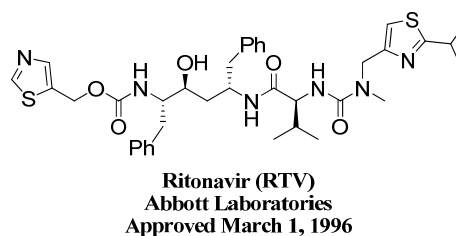
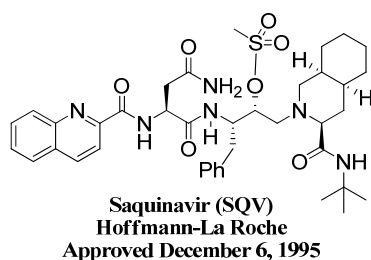


Figure 9. FDA approved integrase inhibitor

HIV protease inhibitors (PIs) (Figure 10) are competitive inhibitors of HIV protease that block cleavage of the Gag-Pol polyprotein during maturation. This results in virions that are unable to infect new cells.



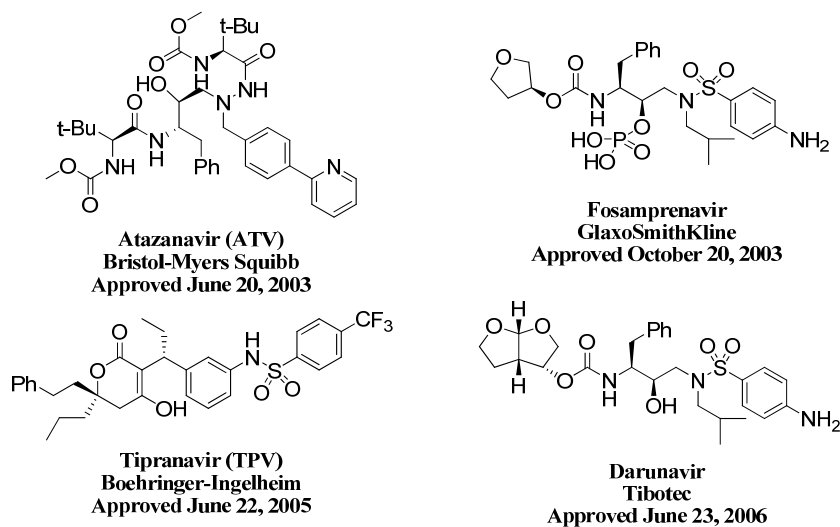


Figure 10. FDA approved protease inhibitors

HAART combines three or more FDA approved drugs in order to lower viral loads below detectable levels. Preferred combinations consist of tenofovir and emtricitabine with either a NNRTI or a PI. Other combinations combine zidovudine and lamivudine with a NNRTI or a PI. HAART is responsible for changing HIV infection from an almost certain death to a chronic but usually manageable condition. In addition, HAART has lowered the number of opportunistic infections that occur in those that are HIV-positive. However, HAART does not work for everyone and is not a cure. Serious side effects can occur especially over the long term. In addition, strict dosing schedules must be followed in order to avoid drug resistance.

Since combination chemotherapy is important in reducing viral loads and delaying drug resistance, a number of fixed dose combinations (Table 1) have been developed that combine two or more FDA approved drugs into one formulation. In addition, by limiting pill burden, patients are more likely to follow their dosing regimens avoiding missed doses that can lead to drug resistance.

Trade Name	Combined Drugs	FDA Approval Date	Company
Combivir	zidovudine + lamivudine	September 26, 1997	GlaxoSmithKline
Kaletra	lopinavir + ritonavir	September 15, 2000	Abbott Laboratories
Trizivir	abacavir + zidovudine + lamivudine	November 15, 2000	GlaxoSmithKline
Epzicom	abacavir + lamivudine	August 2, 2004	GlaxoSmithKline
Truvada	emtricitabine + tenofovir	August 2, 2004	Gilead Sciences
Atripla	efavirenz + emtricitabine + tenofovir	July 12, 2006	Gilead Sciences and Bristol-Myers Squibb

Table 1. FDA approved fixed dose combinations

Unfortunately, even with combination chemotherapy treatment failure occurs and is currently on the rise. Once treatment failure occurs, patients will be switched to second and third line therapies known as salvage therapies. In order to choose a therapy that has a high potential of success a number of factors must be considered such as the patient's CD4 count, the patient's viral load, and the results of viral genotypic and phenotypic assays.²² In some cases mega-HAART may be commenced which includes the administration of six or more anti-HIV drugs to a patient.²³ The FDA approved fusion/entry inhibitors enfuvirtide and maraviroc as well as the approved integrase

inhibitor raltegravir are usually reserved for use in salvage therapies in combination with other drugs. In addition, foscarnet and hydroxyurea (Figure 11) may also be added to salvage therapies. Foscarnet is a pyrophosphate analogue that binds to the pyrophosphate binding site of DNA polymerases and is used mainly to treat herpes simplex virus.²⁴ Hydroxyurea was approved for the treatment of many types of cancers as well as sickle cell disease but was also found to have anti-retroviral properties. It is believed that hydroxyurea inhibits ribonucleotide reductase thereby reducing levels of deoxyribonucleotides.²⁵

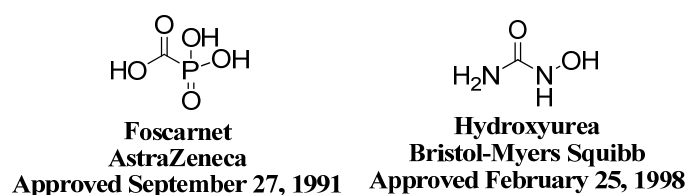


Figure 11. FDA approved foscarnet and hydroxyurea

1.2.4 Drugs Currently in Clinical Trials

New anti-HIV drugs are continually needed as drug resistance mutations make current therapies ineffective in reducing viral loads. There are currently a number of NRTIs (Figure 12) in clinical trials.¹²

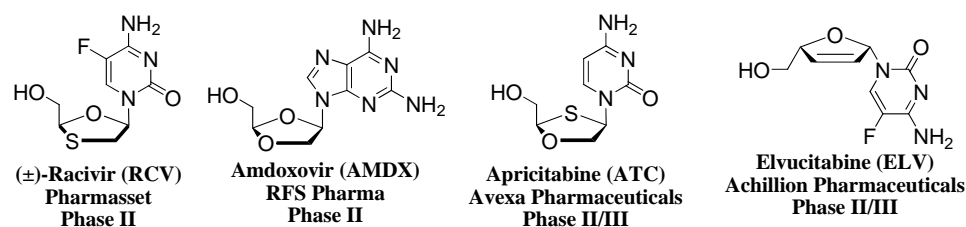


Figure 12. NRTIs in clinical trials

In addition to the NRTIs in clinical trials there are also a number of NNRTIs (Figure 13) being investigated.¹²

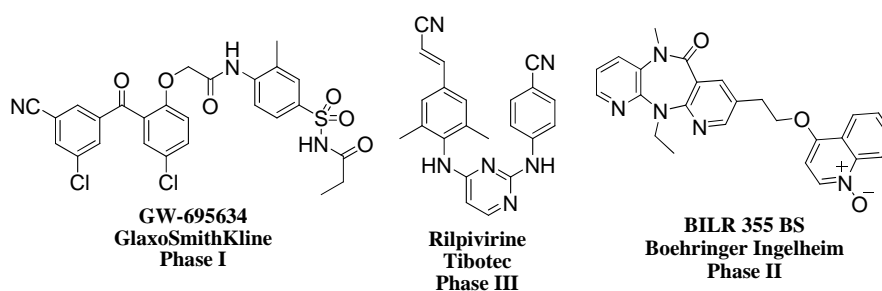


Figure 13. Investigational NNRTIs in clinical trials

There is currently one small molecule entry inhibitor, vicriviroc (Figure 14), in clinical trials.²⁶ Vicriviroc binds to the CCR5 co-receptor on the surface of cells thus preventing CCR5-tropic HIV from infecting healthy cells.²⁷ In addition to this small molecule entry inhibitor, there are two monoclonal antibodies, ibalizumab and PRO 140, being investigated as entry inhibitors. Ibalizumab is currently being developed by Taimed Biologics and is in phase II clinical trials as a non-immunosuppressive monoclonal antibody that binds to CD4. As a result, ibalizumab has the potential for blocking both CCR5- and CXCR4- tropic viruses from entering and infecting cells. Progenics Pharmaceuticals is developing PRO 140, a monoclonal antibody raised against CCR5. PRO 140 is currently in phase II clinical trials.

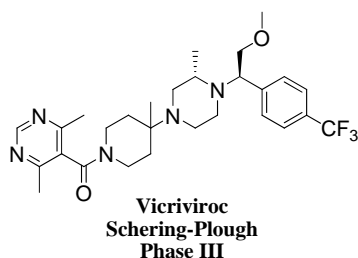


Figure 14. Structure of vicriviroc²⁷

In addition to ritonavir being a PI, it also inhibits cytochrome P450-3A4

(CYP3A4), an enzyme that metabolizes PIs. Because of this inhibitory activity, ritonavir is also known as a pharmacokinetic booster and is used in many HIV regimens to boost the half-life of other anti-HIV drugs. This effectively increases the amount of anti-HIV drugs in circulation. Recently, Gilead Sciences developed another pharmacokinetic booster, GS-9350, that inhibits CYP3A4 but does not have any anti-HIV activity of its own.²⁶ This compound is now moving into phase II clinical trials.

Elvitegravir is an integrase inhibitor being developed by Gilead Sciences that is currently boosted with ritonavir (Figure 15).²⁸

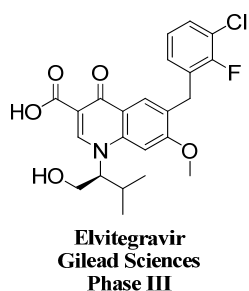


Figure 15. Structure of elvitegravir²⁸

A new class of compounds that is showing promise in the clinic are maturation inhibitors. Like PIs, maturation inhibitors interfere with the processing of the HIV Gag polyprotein. However, unlike PIs, maturation inhibitors bind to the Gag polyprotein blocking a critical cleavage step.²⁹ Currently two maturation inhibitors, bevirimat and vivecon, are being developed by Myriad Genetics (Figure 16).²⁶

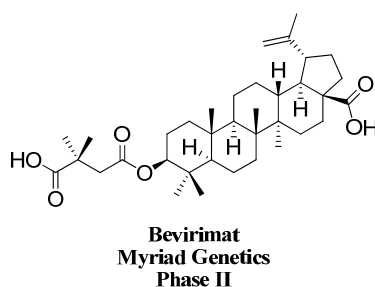


Figure 16. Maturation inhibitor bevirimat

Viral decay acceleration is an interesting area of anti-HIV research that gives yet another opportunity to impair viral replication. While mutations in the targets of approved drugs usually lead to drug resistance, too many mutations throughout the entire viral genome will overcome the threshold of viability for the virus. KP-1461 is a prodrug that is converted into KP-1212 in the liver (Figure 17).³⁰ KP-1212 is a mutagenic nucleoside analogue that has a modified base and does not cause DNA chain termination. Instead KP-1212 incorporation into viral DNA increases the mutation rate of HIV RT by 50-100% resulting in genetic material that codes for inactive viral proteins.³⁰

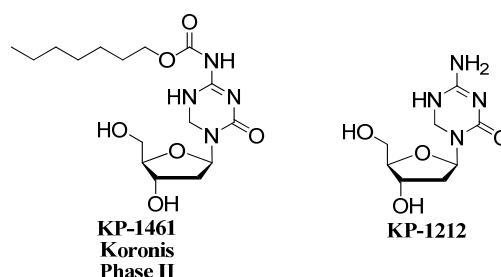


Figure 17. Structures of KP-1461 and KP-1212

There are a number of compounds in clinical trials that constitute immune-based therapies.²⁶ Rather than targeting HIV directly, these therapies are designed to boost the immune system of people infected with HIV. Immunitin is a formulation of alpha-epibromide that is similar to the hormone DHEA. Immunitin is being developed by HollisEden Pharmaceuticals and is currently in phase II clinical trials. Exactly how immunitin works is unknown; however, it does appear to boost key immune system cells. This helps in preventing opportunistic infections and allows better control over HIV. IR 103 is being developed by the Immune Response Corporation and is in phase II clinical trials. IR 103 is a therapeutic vaccine that combines a non-infectious form of HIV with an immune system stimulating adjuvant. This combination is designed to booster the

cells responsible for controlling HIV infection.

1.2.5 Additional Classes of Anti-Viral Therapies

As drug resistant strains of HIV emerge, new drugs in established drug classes as well as drugs for new targets are needed. In addition to the drug classes of approved drugs and drugs in the clinic, there are a few new targets being investigated, though no compounds active against these targets have made it to the clinic.

Viral enzymes are very attractive for drug development since they carry out vital transformation during viral replication. The HIV RT polymerization activity has already been successfully targeted with NRTIs and NNRTIs. However, the HIV RT also possesses RNase H catalytic activity which is vital in the conversion of viral RNA into viral DNA. Cellular RNase H cannot substitute for the viral enzyme.³¹ There have been a number of different compounds identified as inhibitors of HIV RT RNase H activity (Figure 18).³¹⁻³⁵ These compounds in general suffer from poor potency.

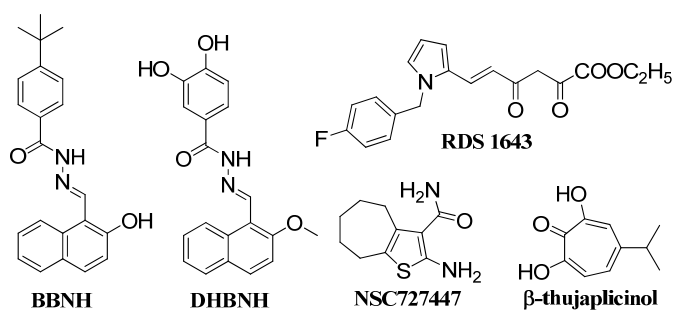


Figure 18. Examples of HIV RT RNase H inhibitors³¹⁻³⁵

The virion surface of HIV is believed to be coated with oligosaccharides containing high levels of mannose residues. Ongoing research has investigated anti-fungal agents that bind to mannose containing oligosaccharides on fungi as potential inhibitors of HIV infection (Figure 19).^{36,37}

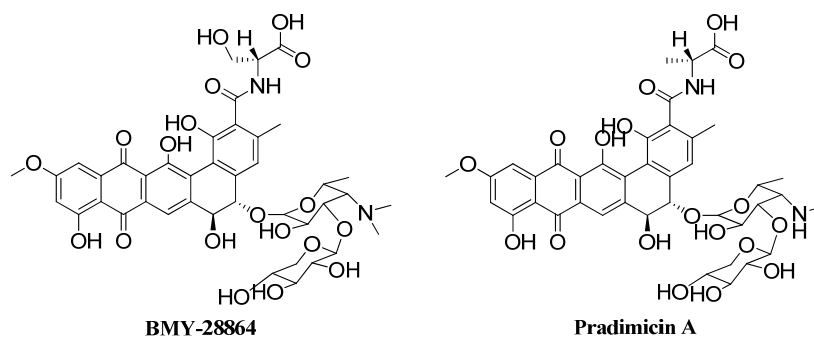


Figure 19. Carbohydrate-binding agents^{36,37}

The HIV capsid protein is being explored as another drug target for the treatment of HIV infection. The assembly of the capsid protein is essential for converting an immature, non-infectious HIV particle into a mature, infectious one. Presently, a collaboration between Achillion Pharmaceuticals and The University of Maryland, Baltimore County have identified two HIV capsid protein assembly inhibitors (Figure 20).³⁸

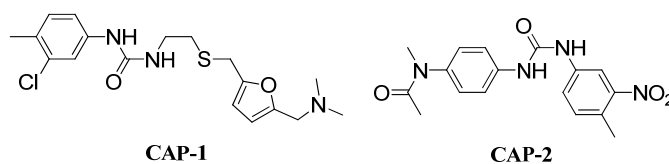


Figure 20. Inhibitors of HIV capsid protein assembly³⁸

There are a number of systems available in the immune system to control and inhibit the spread of viral infections including HIV. However, HIV has many proteins to disable these systems and overwhelm the immune system. One such protein, virion infectivity factor (Vif), disables the cellular anti-viral protein APOBEC3, a cytidine

deaminase, by taking control of the cellular ubiquitin system and targeting APOBEC3 for destruction.³⁹⁻⁴¹ Thus, Vif has become a new drug target in the fight against HIV infection. In addition to a number of peptides exhibiting anti-Vif activity, a recent high-throughput screen at the University of Massachusetts Medical School revealed a number of small molecules inhibiting Vif activity (Figure 21).³⁹

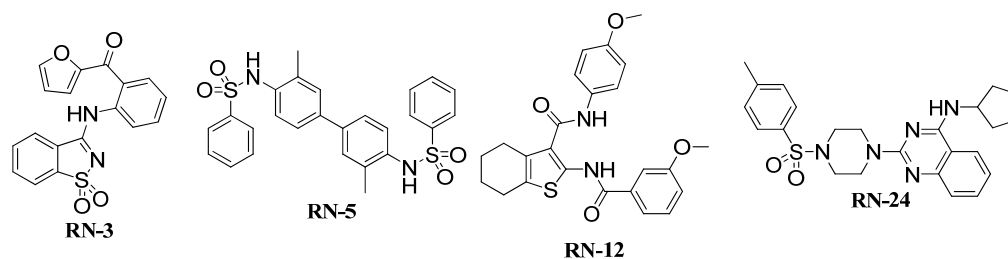


Figure 21. Small molecule Vif inhibitors³⁹

1.2.6 HIV RT

HIV RT (Figure 22) is a heterodimeric enzyme consisting of p51 and p66 subunits.⁴² The p66 subunit is responsible for both the polymerase and RNase H activities of RT. The p66 N-terminal polymerase domain is divided into the thumb, fingers, and palm sub-domains and resembles a human right hand.⁴² The polymerase and the C-terminal RNase H domains are joined by the connection domain. The p51 subunit results from proteolytic cleavage of the p66 subunit and corresponds to the polymerase domain of p66. Except for the RNase H domain, p51 contains all the other domains and sub-domains of p66.⁴² However, due to its more compact structure p51 does not possess any polymerase activity.

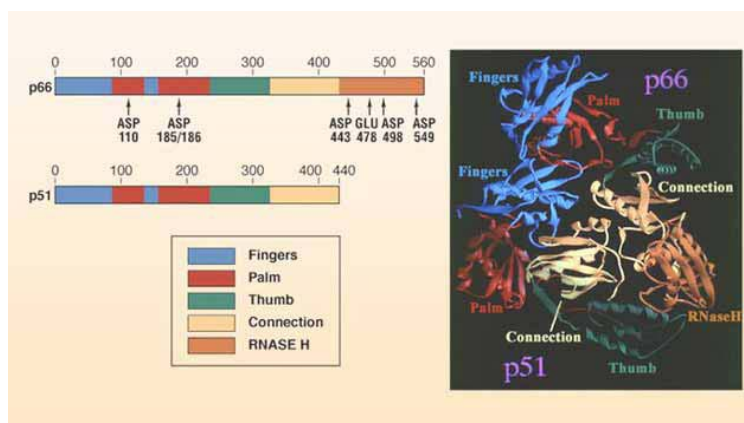


Figure 22. Structure of HIV RT and corresponding amino acid map⁹⁰

In order to obtain double-stranded viral DNA, HIV RT carries out RNA-directed DNA synthesis, RNase H degradation of the RNA template, and DNA-directed DNA synthesis. HIV RT must use tRNA^{Lys-3} as a primer for RNA-directed DNA synthesis.⁴² In order to begin DNA-directed DNA synthesis, HIV RT requires an RNase H-resistant polypurine tract as primer.⁴²

The fingers, thumb, and palm sub-domains of p66 help make up the DNA binding

cleft.⁴² The palm sub-domain lies at the base of the cleft and contains the polymerase active site consisting of three conserved aspartic acid residues (Asp110, Asp185, and Asp186).⁴² The Asp185 and Asp186 residues are part of the YMDD (Tyr-Met-Asp-Asp) motif, a motif that in a general form YXDD (X = Met, Val, Leu, or Ala) is conserved among retroviral RTs. Also present in the palm sub-domain are two conserved magnesium ions that help stabilize the pentavalent transition state that occurs during polymerization.⁴²

Once HIV RT has secured a template 5' to 3' polymerization can occur. The 3'-end of the primer being extended is located in the priming site (post-translocation complex P) and the finger and thumb sub-domains are in an open conformation (Figure 23).⁴²

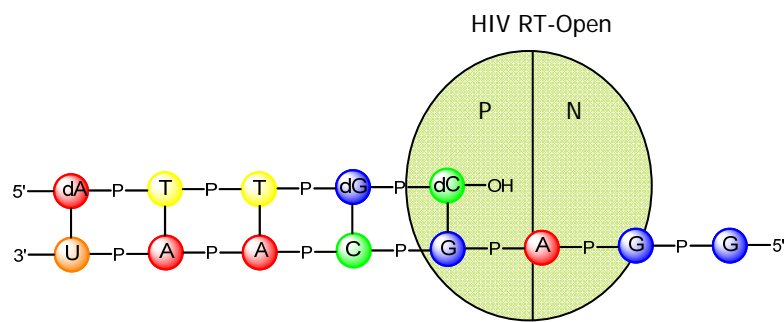


Figure 23. HIV RT polymerase active site

The two conserved magnesium ions assist in the polymerization of incoming deoxynucleotide triphosphates (dNTPs) to extend the primer one nucleotide at a time.⁴² The incoming dNTP binds in the HIV RT's nucleotide-binding site (pre-translocation complex N) and the HIV RT finger and thumb sub-domains transition to a closed conformation (Figure 24).⁴²

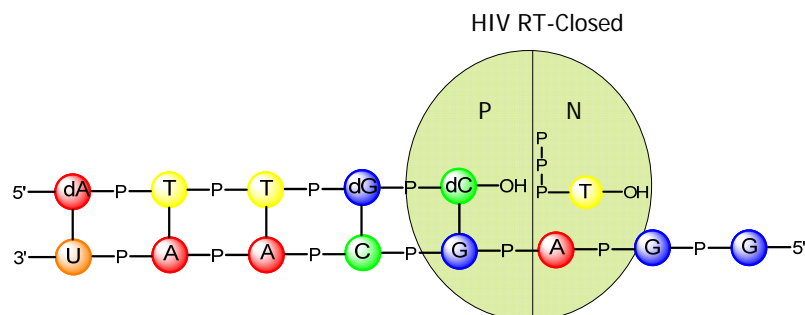


Figure 24. HIV RT bound dNTP

One magnesium ion coordinates with the β - and γ - phosphates of the incoming dNTP while the second magnesium ion coordinates with the 3'-OH group of the growing primer chain.⁴² The primer is extended by one nucleotide when the α -phosphate of the dNTP is attacked by the 3'-OH nucleophile of the primer. This reaction proceeds through a pentavalent transition state that is stabilized by both magnesium ions. In addition to the primer being extended by one nucleotide, pyrophosphate is also produced (Figure 25).

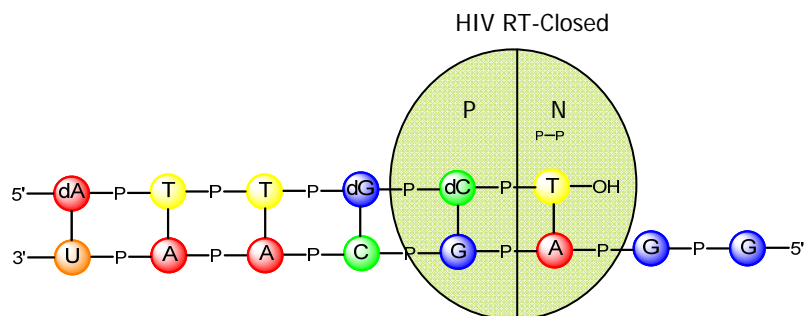


Figure 25. Incorporated dNTP

As the finger and thumb sub-domains of HIV RT transition to an open conformation, the 3'-end of the primer translocates from the N to the P site and pyrophosphate is released (Figure 26).⁴² The entire process continues until the template has been completely transcribed.

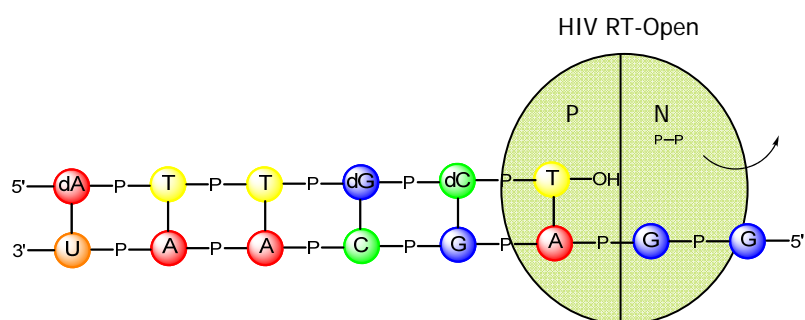


Figure 26. Translocation and pyrophosphate release

The RNase H activity of HIV RT is required to remove the RNA template during and after RNA-directed DNA synthesis. The RNase H active site is located on the C-terminal end of the p66 subunit and possesses both endonuclease and 3'- to 5'-exonuclease activity.⁴³ Two magnesium ions are required for RNase H activity. The polymerization rate is 7-10 times faster than the RNase H rate.⁴⁴ This difference in enzymatic rates leads to the incorporation of many nucleotides into the DNA primer during the time it takes RNase H to cleave the RNA template. Cleavage of RNA by the RT carrying out polymerization is known as the polymerization-dependent mode of cleavage.⁴⁴ When RNA-directed DNA synthesis is complete many RNA template fragments of varying lengths remain annealed to the newly synthesized DNA strand. These fragments are removed before double-stranded DNA synthesis can begin by the 50-100 RTs contained in virions that infect cells.⁴⁴ RNA cleavage by RTs not performing polymerization is known as the polymerization-independent mode of cleavage.⁴⁴

1.2.7 NRTI Mechanism of Action

The understanding of viral replication has led to the identification of many therapeutic targets. The conversion of viral RNA into double-stranded viral DNA is catalyzed by HIV RT and is a major target for drug design. HIV RT has been successfully targeted by two drug classes which inhibit its polymerization activity. NNRTIs inhibit HIV RT by binding to an allosteric site on the enzyme that only exists in the presence of an NNRTI.⁴² The binding of a NNRTI to the allosteric site inhibits the polymerase domain from closing and allowing polymerization to occur.⁴² NRTIs target the polymerase active site and act as DNA chain terminators, thus inhibiting transcription.⁴²

NRTIs are analogues of naturally occurring nucleic acids that lack a 3'-OH group.⁴² NRTIs are prodrugs and must be converted to an active metabolite before they are able to inhibit viral transcription.⁴² All NRTIs, except for tenofovir, are converted to their corresponding triphosphate form by cellular kinases, as exemplified by AZT (Figure 27). Tenofovir is a monophosphonate prodrug and must be converted to its corresponding diphosphate by cellular kinases. The 5'-OH group of the NRTI is converted by cellular kinases to its corresponding triphosphate in three distinct phosphorylation steps. The first step is catalyzed by thymidine kinase (Thd kinase), the second step is catalyzed by thymidylate kinase (TMP kinase), and the third step is catalyzed by nucleoside diphosphate kinase (NDP kinase).

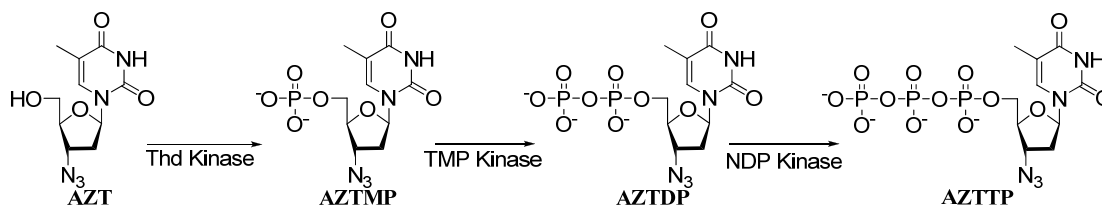


Figure 27. Conversion of AZT into AZTTP by cellular kinases

Once activated, the NRTI triphosphate is able to compete with natural deoxynucleotide substrates such as dATP, dGTP, dCTP, and TTP for incorporation into viral DNA.⁴² Once a NRTI is incorporated into viral DNA, transcription is inhibited since the NRTI lacks the necessary 3'-OH needed to continue DNA elongation.⁴² As the next complementary dNTP binds to HIV RT with a chain terminated primer, polymerization cannot occur and a stable dead-end complex (D.E.C.) is formed (Figure 28).^{42,45} HIV RT either stays in the D.E.C. or, depending on the stability of the complex, may slowly release the chain-terminated primer and dNTP.⁴⁵

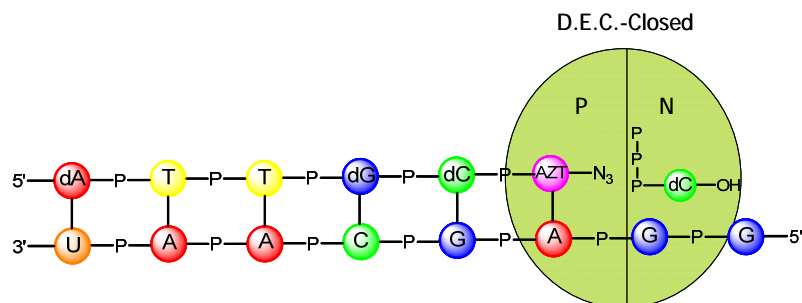


Figure 28. DNA chain termination by AZT and D.E.C. formation

NRTI therapy has been successful because of two characteristics of the HIV RT. First, HIV RT has a natural affinity for dNTPs and can tolerate structural variability more so than cellular DNA polymerases. This leads to the incorporation of NRTIs into viral DNA. Secondly, HIV RT lacks formal proofreading ability leading to low fidelity DNA synthesis as well as an inability to remove NRTIs or mismatched base pairs once they are

incorporated into DNA.

1.2.8 HIV RT NRTI Resistance Mechanisms

Current HAART treatments involve two NRTIs and either a PI or NNRTI in order to improve the efficacy of the drugs being used as well as to delay drug resistance.⁴² However, with the common use of NRTIs, drug resistance eventually develops decreasing the efficacy of these therapeutics for long-term use. Two factors that lead to the emergence of drug resistance are the high replication rate and high mutation rate of HIV. In an untreated patient there are $\sim 10^{10}$ new virions produced each day with 10^7 replication cycles also occurring each day.⁴⁶ In addition, mutations are introduced into the HIV genome by the error-prone HIV RT at a rate of 3×10^{-5} per base per replication cycle.⁴⁷ Coupled with the number of replication cycles that occur each day, a mutation may occur at every nucleotide in the HIV genome each day. These drug resistant variants are thus selected for by incomplete viral suppression resulting from non-compliance to a drug regimen, drug pharmacokinetics, or lack of drug potency.

A number of NRTI resistant mutations have arisen in clinical practice. These mutations confer resistance to NRTIs through either a mechanism of discrimination or excision. Nucleotide discrimination is caused by mutations in the HIV RT active site that lead to recognition of structural differences between inhibitors and natural substrates. Mutations that lead to discrimination usually affect either the affinity of the nucleotide for the RT polymerase active site (K_d) or the catalytic rate constant (k_{pol}).⁷ Mutations that have arisen in the clinic that result in discrimination due to an increase in K_d are the M184V and V75T mutations.⁷ These mutations did not have any significant impact on k_{pol} . On the other hand the mutations K65R, Q151M, L74V, and K70E result in

discrimination due to a decrease in k_{pol} .⁷ It has been reported that K65R also has a small impact on K_d .^{7,49}

The excision mechanism of resistance is a result of thymidine associated mutations (TAMs) that are selected for by AZT and d4T.^{5,42,48-49} TAMs usually emerge in two patterns: M41L/L210W/T215Y and D67N/K70R/T215F/K219Q.⁵ While TAMs are only selected for by thymidine analogues, the excision of any of the NRTIs can take place, though excision of AZT and d4T is most efficient. The outcome of excision is reverse polymerization in which an incorporated NRTI monophosphate (NRTI-MP) is removed from DNA (Figure 29).⁵ This results in a primer shortened by one nucleotide and exposes a 3'-OH group allowing DNA synthesis to continue. The translocation equilibrium for NRTIs in HIV RT containing TAMs lies in favor of the N site where phosphodiester bond formation and cleavage occurs.⁵ HIV RT containing TAMs positions terminated DNA primers in the N site for optimal attack by a polyphosphate donor. HIV RT primarily uses ATP as a polyphosphate donor for excision which, in addition to the unblocked primer, results in a dinucleotide polyphosphate product.⁵

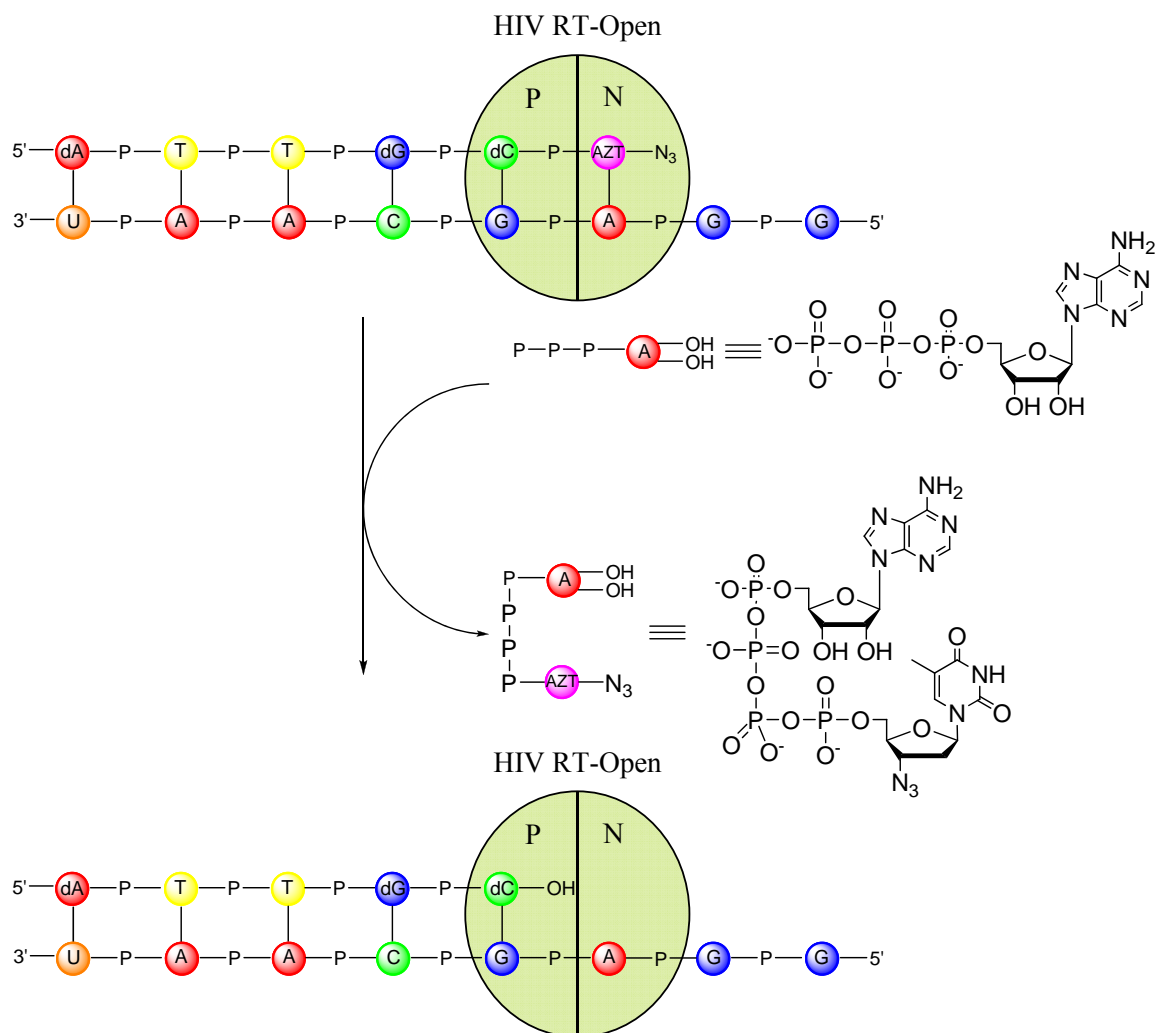


Figure 29. Mechanism of NRTI-MP excision

The K65R mutation is selected for by ddI, abacavir, and tenofovir and causes reduced susceptibility to ddC, ddI, abacavir, tenofovir, 3TC, and FTC.^{6,48} This mutation resides in the fingers sub-domain of the polymerase active site and interacts with the γ -phosphate of the incoming nucleotide.⁵⁰ Even though the γ -phosphate is >7.5 Å away from the 3'-position of the ribose portion of the nucleotide, the K65R mutation leads to discrimination of incoming nucleotides through a decrease in the catalytic rate constant k_{pol} .⁴

The incidence of the K65R mutation still remains low, ~4% currently, but has

risen steadily from 0.8% in 1998.⁶ The increase in the emergence of K65R is attributed to the growing use of tenofovir. Even though the incidence of K65R is low, it is found in up to 25% of patients failing therapies containing dual NRTIs that exclude AZT.⁵ In patients failing therapy containing triple NRTIs that exclude AZT, the frequency of K65R was as high as 92%.⁵ The K65R mutation results in resistance to many 2', 3'-dideoxynucleoside analogues (Table 2); however, it remains susceptible to thymidine analogues like AZT except for in a few rare cases.^{5,51}

Mutation Pattern	Fold Resistance to Indicated NRTI						
	AZT	D4T	TDF	ABC	ddI	ddC	3TC
K65R	0.6	1.6	2	3	2.1	3	9
K65R, M184V	0.3	1	1.1	7.9	3	4.2	200
K65R, Q151M	101	20	4.9	11	22	28	64
K65R, L74V, M184V	0.3	1.2	0.9	12	6.7	4.4	200
K65R, Y115F	0.4	0.9	1.5	6	1.8	1.8	22
K65R, K70R, Y115F, Q151M	2400	20	11	20	28	28	89
K65R, T69D, K70R	0.2	1.6	1.2	3.6	1.5	1.9	8.2

Table 2. K65R HIV RT mutants and fold resistance to NRTIs⁵¹

A bidirectional antagonism exists between the K65R mutation and TAMs which explains why these mutations do not appear together on the same viral genome.⁵ This bidirectional antagonism is supported by clinical and epidemiological observations as well as screening HIV RT mutants with K65R and TAMs against all FDA-approved NRTIs. The K65R mutant reduces the rate of excision conferred by TAMs resulting in

diminished resistance to AZT. TAMs reduced the resistance of abacavir, ddC, and tenofovir conferred by K65R. Since this bidirectional antagonism exists between these mutations, it would be detrimental for HIV to evolve both pathways in combination.

1.3 Background

1.3.1 3'-Azido-2',3'-Dideoxynucleoside Analogues

A resurgence in the interest of 3'-azido-2',3'-dideoxynucleoside analogues as anti-HIV agents occurred with the emergence of the multi-drug resistant HIV RT K65R mutant and its susceptibility to AZT. A number of D- and L- dideoxynucleoside analogues with carbohydrate and base modifications have been screened for activity against the wild-type HIV RT and the K65R mutant of HIV RT.⁵² The nucleoside analogues that have shown the most promise to inhibit the K65R HIV RT mutant are the 3'-azido-2',3'-dideoxynucleoside analogues. AZT and 3'-azido-2',3'-dideoxyadenosine (AZA) are especially potent inhibitors of the K65R HIV RT mutant showing no loss in activity when compared to the wild-type HIV RT.⁵² 3'-azido-2',3'-dideoxycytidine (AZC) and 3'-azido-2',3'-dideoxyguanosine (AZG) though active, showed a greater loss in activity against the K65R HIV RT mutant than AZT or AZA when compared to the wild-type HIV RT.⁵² Additional enzymatic studies with AZT resistant HIV RT have shown that 3'-azido-2',3'-dideoxypurine nucleoside analogues are resistant to excision.⁵³

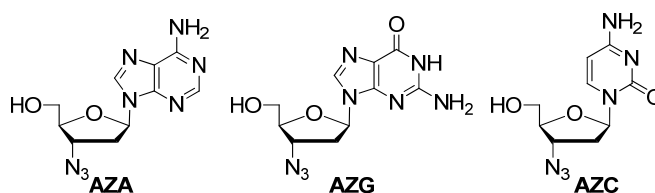
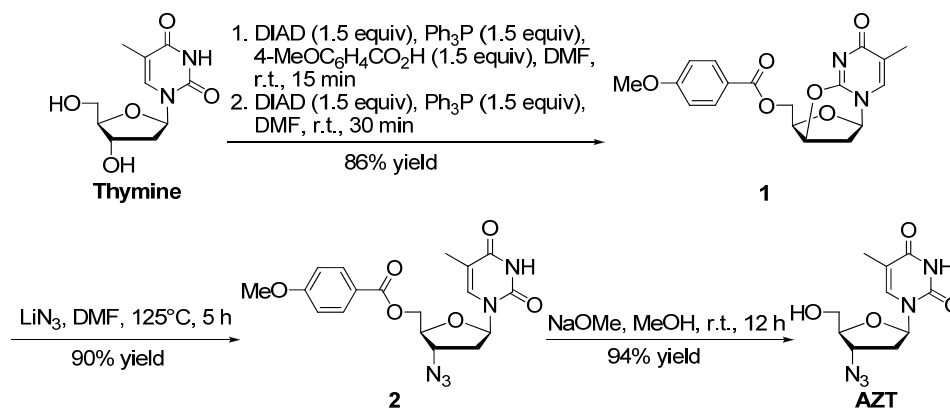


Figure 30. 3'-Azido-2',3'-dideoxynucleoside analogues

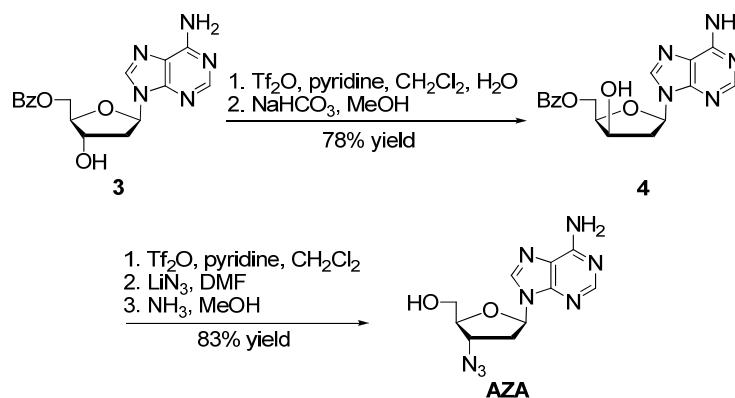
1.3.2 Syntheses of AZT and AZA

Numerous syntheses of AZT have been developed over the years. An efficient synthesis starting from thymidine was published in 1991 (Scheme 1).⁵⁴



Scheme 1. Synthesis of AZT

A synthesis of AZA was published by Herdewijn in 1988 that started with *N*⁶,5'-*O*-dibenzoyl-2'-deoxyadenosine **3** (Scheme 2).⁵⁵



Scheme 2. Synthesis of AZA

1.3.3 Anti-Viral Natural Product Oxetanocin

Oxetanocin A is a natural product from *Bacillus megaterium* that shows good anti-bacterial, anti-cancer, and anti-HIV activity (Figure 33).^{56,57} Oxetanocin A has been the focus of many synthetic studies resulting in numerous analogues (Figure 31).⁵⁶⁻⁵⁹ A

key series of analogues successfully replaced the oxetane ring of oxetanocin A with a cyclobutane ring generating cyclobut-A and its guanine analogue cyclobut-G. These analogues retained promising levels of anti-viral activity. This discovery has led to a surge of interest into cyclobutyl nucleosides and methods for synthesizing these analogues.

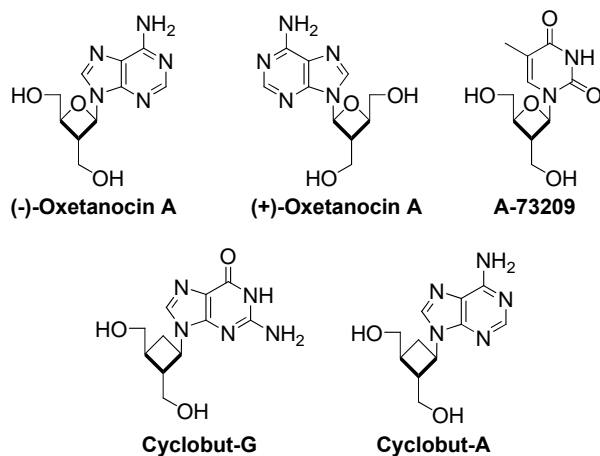
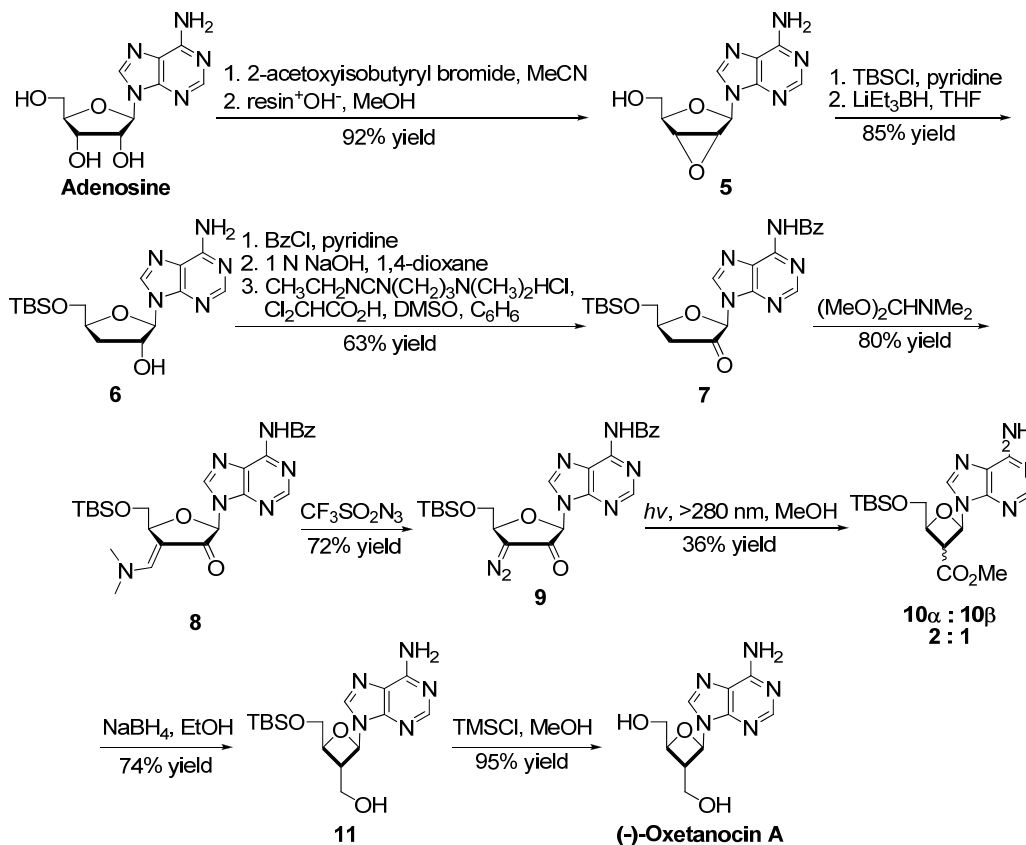


Figure 31. Oxetanocin A and analogues

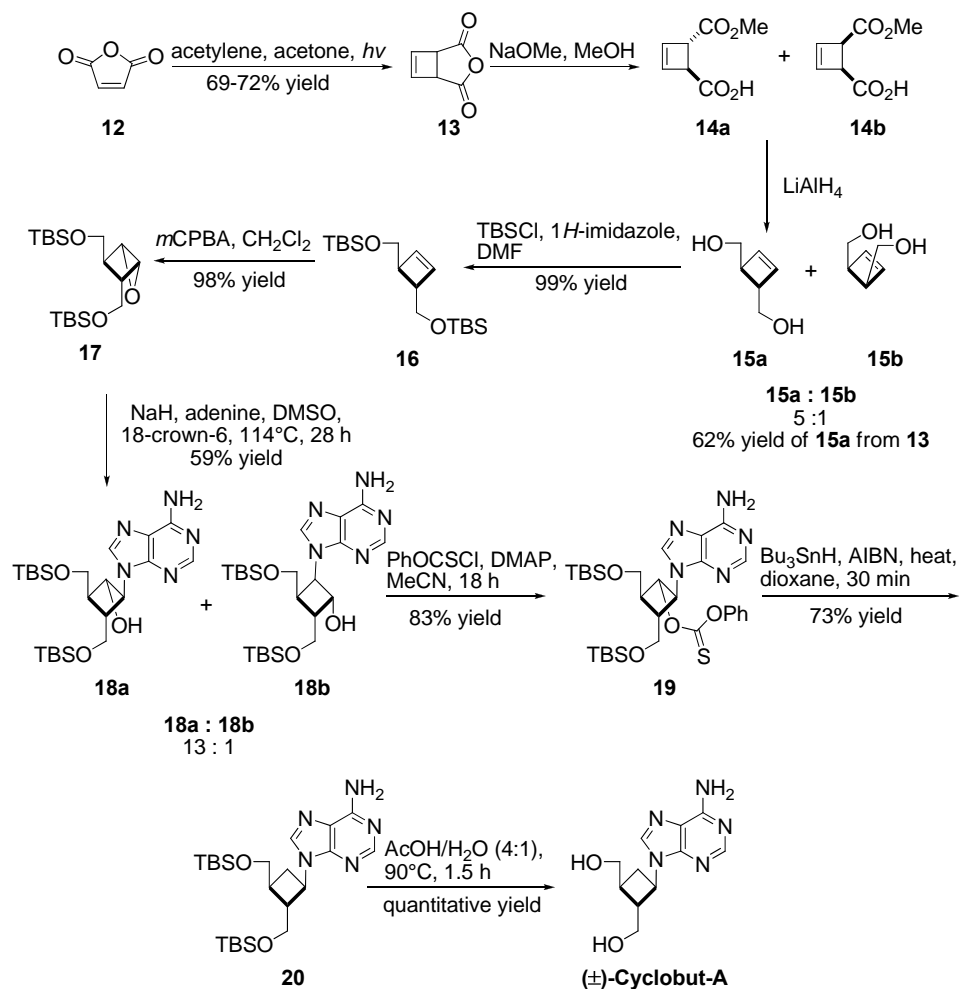
1.3.4 Syntheses of Oxetanocin A and Cyclobut-A

Norbeck and co-workers reported an efficient synthesis of (-)-oxetanocin A in 1988 utilizing a ring contraction strategy starting from adenosine (Scheme 3).⁵⁶ Ring contraction of intermediate compound **9** provided a mixture of diastereomers. Reduction of the major epimer led to (-)-oxetanocin A after deprotection.



Scheme 3. Synthesis of oxetanocin A from adenosine

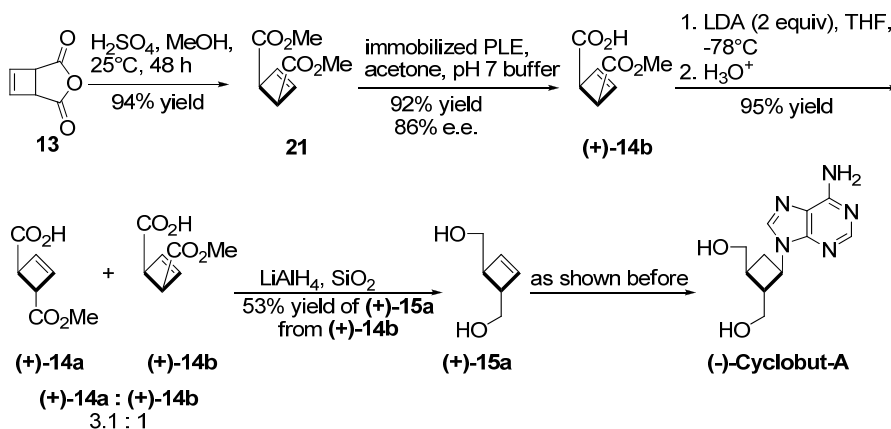
Cyclobut-A was prepared in both a racemic and an optically active form by Jung and co-workers starting from the inexpensive and readily available starting materials maleic anhydride **12** and acetylene.⁶⁰ The photocycloaddition product **13** was hydrolyzed resulting in a mixture of *cis* and *trans* monoesters. Cyclobut-A was obtained from the key intermediate epoxide **17** that resulted from the *trans* diol **15a** (Scheme 4).



Scheme 4. Synthesis of (±)-cyclobut-A

Optically active cyclobut-A was prepared in a similar fashion employing a key enzymatic enantioselective hydrolysis carried out by pig liver esterase (PLE) (Scheme 5). The *cis* diester **21** obtained from acid hydrolysis of **13** was treated with PLE to provide the optically active monoester (+)-**14b** in 92% with an enantiomeric excess (e.e.) of 86%.

Isomerization of monoester **(+)-14b** was accomplished by treatment with lithium diisopropylamide (LDA) to provide **(+)-14a**. Reduction of **(+)-14a** with lithium aluminum hydride (LAH) resulted in the formation of diol **(+)-15a**. Compound **(+)-15a** was converted into (-)-cyclobut-A following the methods described for the racemic synthesis of cyclobut-A.



Scheme 5. Synthesis of diol **(+)-15a**

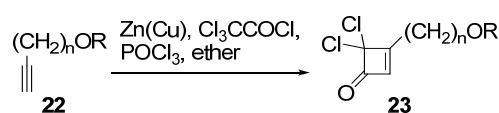
1.3.5 Synthesis of Cyclobutenones

Cyclobutanone, cyclobutamine, and cyclobutanol precursors have been used extensively in the synthesis of cyclobutyl nucleoside analogues. Though cyclobutanones are a common intermediate for a number of cyclobutyl nucleoside analogues, cyclobutenones have seen little use despite their potential for functionalization. The synthetic utility of cyclobutenones can be seen by the vast number of ring expansion and rearrangement reactions they undergo.⁶¹ The two main methods for synthesizing cyclobutenones continue to be [2+2] cycloaddition reactions and modifications of squaric acid esters. In this section, some [2+2] cycloaddition methods for synthesizing cyclobutenones will be described.

The main partners to generate cyclobutenones through [2+2] cycloaddition

reactions are alkynes and ketenes. The electron deficient dichloroketene is often employed in many [2+2] cycloaddition reactions with alkynes. Dichloroketene is often generated in situ from trichloroacetyl chloride and zinc-copper couple. The use of dichloroketene leads to the formation of gem-dichlorocyclobutenones and as a result reductive dechlorination is needed to obtain the desired cyclobutenone.

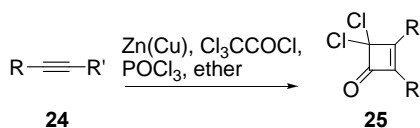
Dillon and co-workers generated gem-dichlorocyclobutenones **23a-d** from dichloroketene and alkynes **22a-d** (Table 3) for use in electrocyclic ring opening reactions to generate lactones.⁶²



22	R	n	% yield, 23
a	Ac	2	62
b	Ac	3	69
c	TBDMS	2	23
d	TBDMS	3	38

Table 3. Examples of [2+2] cycloaddition reactions with dichloroketene

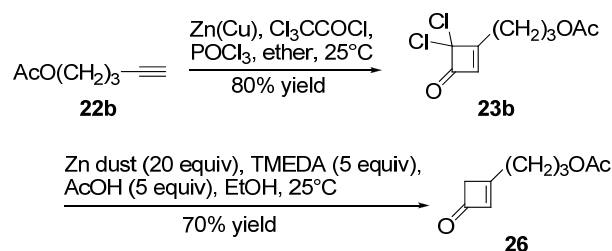
Hassner and Dillon reported on the synthesis of many gem-dichlorocyclobutenones **25a-c** from disubstituted alkynes **24a-c** (Table 4).⁶³



24	R	R'	% yield, 25
a	Me	Me	85
b	Ph	H	75
c	CH ₃ (CH ₂)	H	77

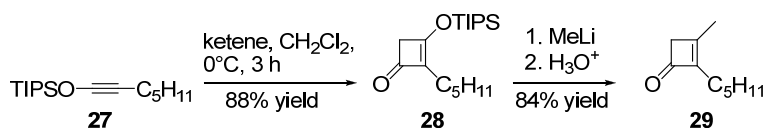
Table 4. [2+2] Cycloaddition reactions with disubstituted alkynes

Danheiser and co-workers synthesized a number of cyclobutenones after reductive dechlorination of gem-dichlorocyclobutenones.⁶⁴ Their method employs the use of excess zinc dust, tetramethylethylenediamine (TMEDA), and acetic acid in ethanol (Scheme 6). The desired cyclobutenones were obtained in moderate to good yield.



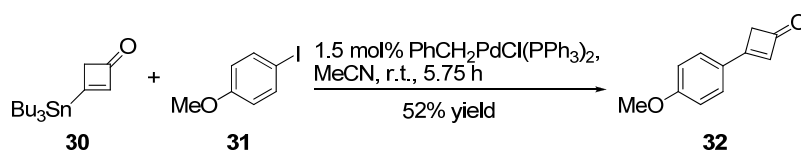
Scheme 6. Dechlorination of gem-dichlorocyclobutenone

Unreactive ketenes such as ketene itself will undergo [2+2] cycloaddition reactions with silyloxyacetylenes to give cyclobutenones directly in good yield (Scheme 7).⁶⁵ Addition of nucleophiles to 3-silyloxycyclobutenones yield 2,3-disubstituted cyclobutenones after acidic workup (Scheme 7).



Scheme 7. Synthesis of 3-silyloxycyclobutenones from ketene

In 1994, Liebeskind and co-workers reported on the synthesis of 3-(tri-*n*-butylstannyl)-2-cyclobuten-1-one **30** as a Stille cross-coupling partner for 3-substituted cyclobutenones (Scheme 8).⁶⁶ 3-(Tri-*n*-butylstannyl)-2-cyclobuten-1-one was prepared from 3-ethoxy-2-cyclobutenone, (tri-*n*-butylstannyl)trimethylsilane, and catalytic tetrabutylammonium cyanide in 71 % yield. 3-(Tri-*n*-butylstannyl)-2-cyclobuten-1-one was subjected to palladium cross-coupling with a variety of unsaturated organic halides to access 3-substituted cyclobutenones.



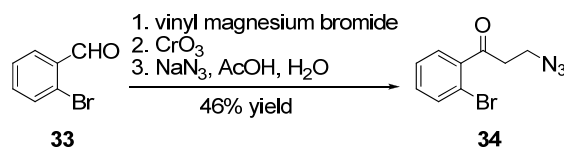
Scheme 8. Stille cross-coupling with 3-(tri-*n*-butylstannyl)-2-cyclobuten-1-one

1.3.6 Methods for the Michael Addition of Azide

Addition of nucleophiles to α,β -unsaturated carbonyl systems, better known as the Michael addition, is a powerful method for functionalizing such systems. Countless methods for the addition of both carbon and heteroatom nucleophiles have been developed. Conjugate addition of nitrogen nucleophiles leads to important classes of compounds such as β -amino acids and ketones, β -lactams, and 1,3-amino alcohols.⁶⁷ A number of methods for the addition of azide into α,β -unsaturated aldehydes, ketones, and esters have been developed and will be described in this section.

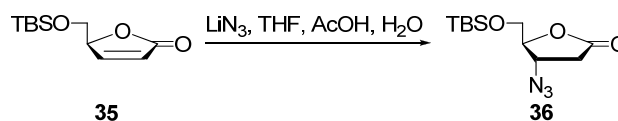
The most common method for the addition of azide into α,β -unsaturated carbonyl systems is to generate hydrazoic acid (HN₃) in situ from sodium azide or trimethylsilyl azide under acetic conditions. In their work investigating allenyl azide cycloaddition reactions, Feldman and co-workers generated an azido propiophenone species from sodium azide and the corresponding α,β -unsaturated ketone under acidic conditions

(Scheme 9).⁶⁸



Scheme 9. Addition of azide into an α,β -unsaturated ketone

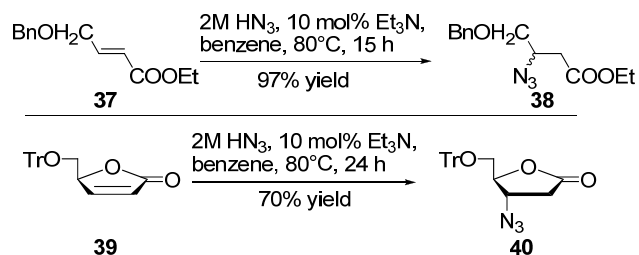
In a similar fashion, Chu and co-workers utilized similar conditions in their synthesis of AZT and 3'-azido-2',3'-dideoxyuridine (AZDDU) from D-mannitol (Scheme 10).⁶⁹ Protection of the 5'-hydroxyl group with a bulky silyl protecting group lead to the formation of only the α -azido product.



Scheme 10. Azide addition to an α,β -unsaturated lactone

There are a number of reports showcasing the addition of azide into α,β -unsaturated carbonyl systems under phase transfer conditions. In most cases tertiary amines, specifically triethylamine, are added to the reaction mixture in catalytic quantities. This modification leads to excellent yields of the desired addition product. Furthermore, phase transfer conditions usually result in good yields of the desired product for reactions that do not yield product under normal acidic conditions.

Lakshmi pathi and co-workers reported on an efficient method for the addition of azide to enoates using preformed hydrazoic acid and triethylamine (Scheme 11).⁷⁰



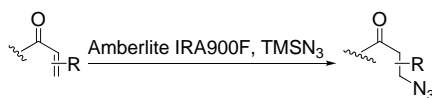
Scheme 11. Addition of hydrazoic acid to enoates

In 1999, Guerin and co-workers showed that generation of hydrazoic acid in situ from acetic acid and trimethylsilyl azide in the presence of tertiary amines lead to efficient azidation of α,β -unsaturated carbonyl compounds (Table 5).⁷¹ They determined that tertiary amines both in solution or bound to a solid support were efficient catalysts.

Entry	Catalyst	Isolated Yield
1	Et ₃ N	77%
2		82%
3		90%
4		26%
5	HMPA	11%
6	none	0%
7		90% after 18 h

Table 5. β -Azidation of α,β -unsaturated ketones in the presence of amine catalyst

Recently, Castrica and co-workers developed a method for the azidation of α,β -unsaturated ketones under solvent-free conditions (SolFC) using Amberlite IRA900F (Table 6).⁷² The mechanism proposed by Castrica and co-workers for the azidation of α,β -unsaturated ketones in the presence of trimethylsilyl azide and Amberlite IRA900F is shown in Figure 32.⁷²



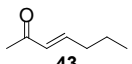
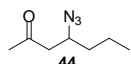
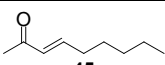
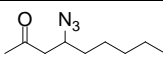
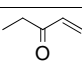
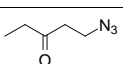
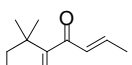
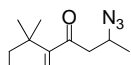
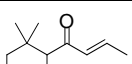
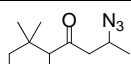
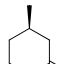
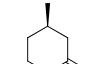
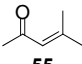
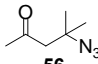
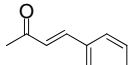
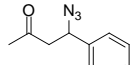
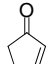
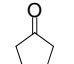
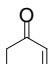
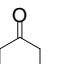
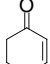
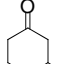
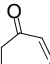
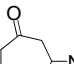
Enone	Amberlite IRA900F (molar equiv)	TMSN ₃ (molar equiv)	T (°C)	t (h)	Adduct	Yield (%)
 43	0.10	1.1	60	2.5	 44	90
 45	0.10	1.1	60	6	 46	95
 47	0.10	1.1	30	5	 48	90
 49	0.50	3.0	60	18	 50	95
 51	0.25	1.5	60	6	 52	95
 53	0.50	1.5	60	24	 54	92
 55	0.25	1.5	60	3	 56	82
 57	0.50	2.0	60	15	 58	70
 59	0.25	3.0	30	4	 60	70
 41	0.25	1.5	30	6	 42	95
 61	0.25	3.0	60	24	 62	75
 63	0.25	3.0	60	18	 64	85

Table 6. Azidation of α,β -unsaturated ketones in the presence of Amberlite IRA900F

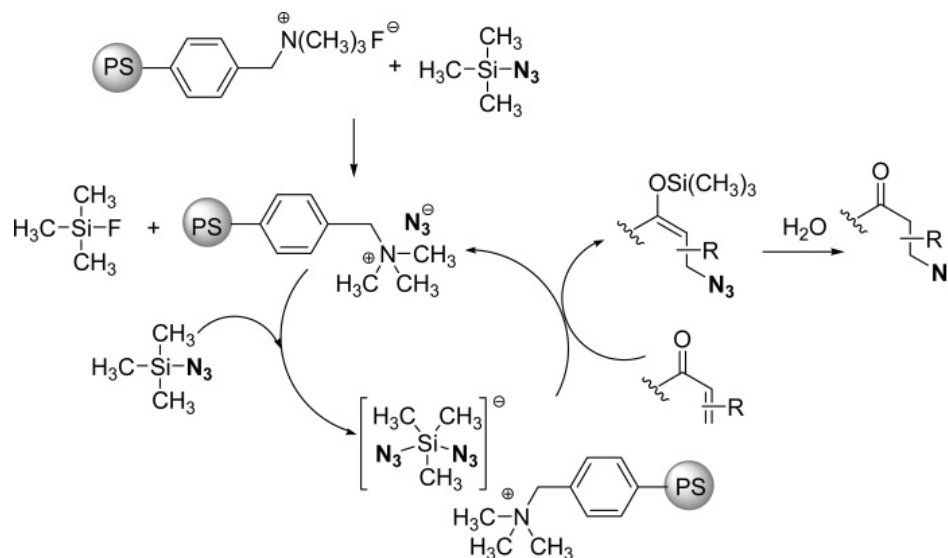


Figure 32. Mechanism of azidation of α,β -unsaturated ketones in the presence of Amberlite IRA900F

1.3.7 Methods for Coupling Nucleoside Bases to a Cyclobutyl Ring

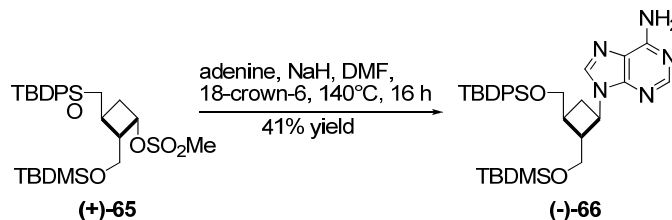
For the synthesis of many nucleoside analogues, glycosylation is typically achieved using the Vorbrüggen ribosylation method. This method is not applicable to the synthesis of cyclobutyl nucleosides since the oxygen atom typically found in most deoxyribose nucleoside analogues is replaced with a carbon atom. Thus, various coupling strategies have been developed and will be described below.

1.3.7.1 Coupling of intact nucleoside bases

A number of methods for coupling nucleoside bases with cyclobutanes have been developed. These coupling strategies involve substitution of activated cyclobutanols, opening of epoxides, and the Michael reaction.

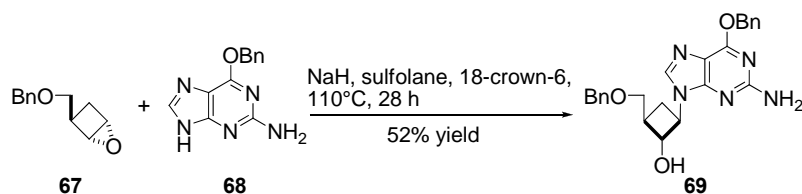
Activation of cyclobutanols can be achieved by converting the desired cyclobutanol into an appropriate leaving group such as a mesylate. Conditions can then be chosen to promote the displacement of the leaving group with a nucleoside base

through an S_N2 reaction. Thus, the nucleoside base is introduced onto the cyclobutane ring while inverting the affected stereocenter. This method typically utilizes harsh conditions that often lead to the elimination of the leaving group as a side reaction. In scheme 12 is shown an example of the displacement of a mesylate leaving group by adenine resulting in the desired regioselective N9 coupled product (-)-**66**.⁷³



Scheme 12. Displacement of a mesylate by adenine

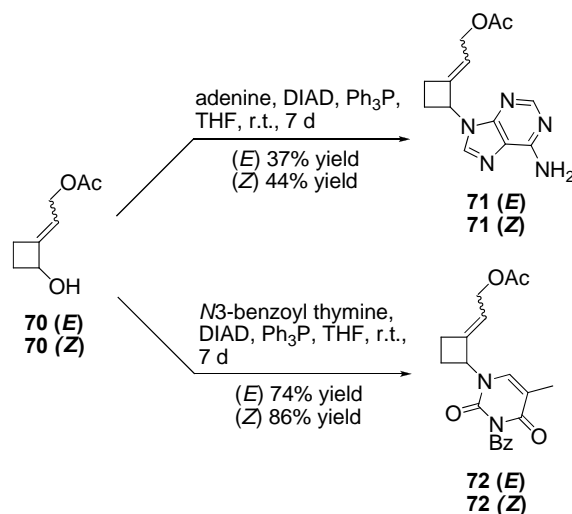
A similar method relies on the opening of an epoxide to introduce the nucleoside base with inversion of stereochemistry of the affected carbon. In this method, it is important when generating the epoxide that the stereochemistry be controlled. Nucleophilic attack of the base can take place at either carbon of the epoxide, thus making control of the regioselectivity critical for obtaining the desired base-coupled product. Scheme 13 shows an example of the opening of epoxide **67** by a protected guanosine analogue **68** to give the desired N9 coupled product **69**.⁷⁴



Scheme 13. Epoxide opening by a guanosine analogue

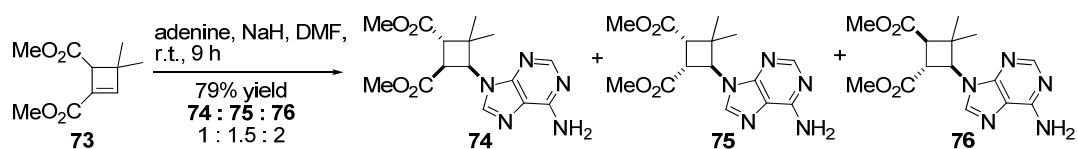
The Mitsunobu reaction has also been used as an alternative method for coupling nucleoside bases to cyclobutanols. This method avoids the harsh reaction conditions seen in the S_N2 and epoxide opening reactions. In most cases protecting groups on the

nucleoside base are needed in order to achieve the correct regioselectivity. Danappe and co-workers utilized the Mitsunobu reaction to generate pyrimidine and purine nucleoside analogues possessing a methylenecyclobutane unit (Scheme 14).⁷⁵



Scheme 14. Mitsunobu coupling of pyrimidine and purine bases to cyclobutanols

The Michael reaction is another commonly used method for introducing intact nucleoside bases onto cyclobutyl rings. A nucleoside base can be added to the β -carbon of an appropriate substrate containing an electron deficient olefin. Johnson and De Jong showed that both adenine and thymine can add to electron deficient olefins to give the desired base-coupled product.⁷⁶ While the overall yields were good, the additions resulted in the formation of isomeric products (Scheme 15).⁷⁶



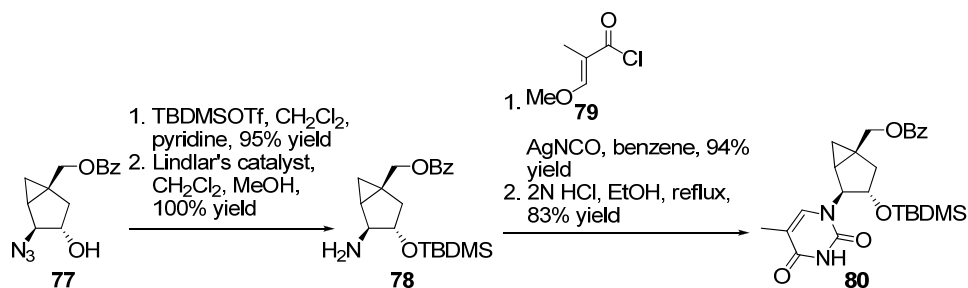
Scheme 15. Michael addition of nucleoside bases

1.3.7.2 Stepwise construction of nucleoside bases from cyclobutamines

Cyclobutamines allow for the stepwise construction of nucleoside bases as an alternative method to the base coupling methods shown in the previous section. Methods for constructing both purine and pyrimidine bases have been developed and examples of each are shown below.

The Shaw and Warrener method is most often used to construct pyrimidines from isocyanates. Isocyanates can be generated in a fashion that will lead to either uracil or thymine. Allowing cyclobutamines and isocyanates to react results in the formation of an acryloylurea intermediate that can be cyclized under acidic or basic conditions to afford the desired pyrimidine product.

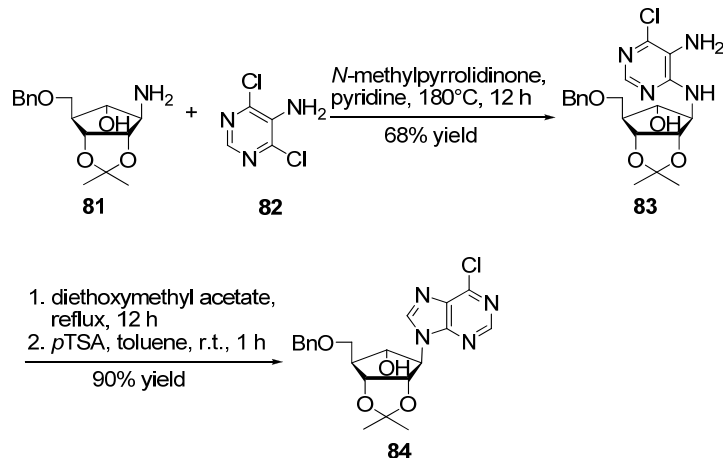
Marques and Comin constructed the thymine base of a novel bicyclo[3.1.0]hexane carbocyclic nucleoside analogue in order to improve binding recognition by herpes thymidine kinase (HSV-tk) (Scheme 16).⁷⁷



Scheme 16. Construction of thymine base

A common method for constructing purine bases utilizes 5-amino-4,6-dichloropyrimidine **82** and amines. Cyclization is then carried out by triethyl orthoformate to produce the 6-chloropurine intermediate. This intermediate can then easily be converted into either adenine or hypoxanthine by treatment with ammonia or hydroxide. Madhavan and Martin utilized this method in their synthesis of (+)- and (-)-

aristeromycin (Scheme 17).⁷⁸



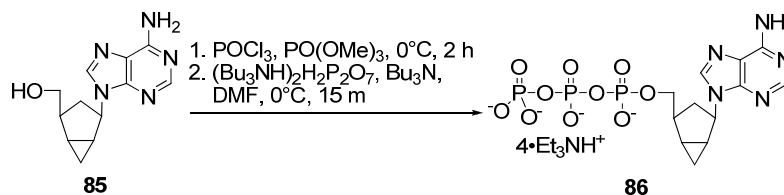
Scheme 17. Construction of purine bases

1.3.8 Methods for Synthesizing Nucleoside Triphosphates

Nucleoside triphosphates are invaluable research tools that are often used to understand biological pathways. Evaluation of triphosphates of nucleoside analogues that are inactive are very useful in helping to determine whether the triphosphate is a poor substrate for polymerases or if there is a problem with conversion of the nucleoside to its corresponding triphosphate. Many challenges exist with preparing nucleoside triphosphates such as finding reaction conditions that cater to both the lipophilic substrate and the highly charged triphosphate product. In addition, triphosphates are known to be unstable decomposing within a matter of days. Triphosphates are also sensitive to hydrolysis under both acidic and basic conditions. However, the current trends in preparing nucleoside triphosphates for optimum stability favor the formation of the corresponding trialkylammonium salt under neutral pH and low temperature. While there is no procedure that is universal for converting all substrates into their corresponding triphosphate forms, many methods have been developed and the most common will be shown below.

1.3.8.1 Utilization of dichlorophosphates in the synthesis of triphosphates

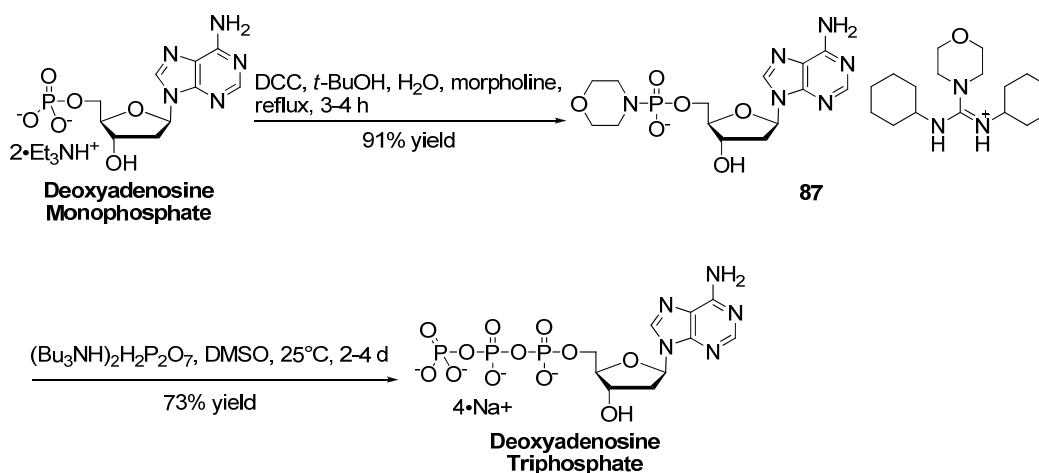
The most common methods for synthesizing nucleoside triphosphates utilize an activated monophosphate or phosphite that can be elaborated on with pyrophosphate. Bhushan and Vince reported the one-pot, three-step synthesis of a nucleoside analogue triphosphate using phosphoryl chloride (Scheme 18).⁷⁹



Scheme 18. One-pot triphosphate synthesis

1.3.8.2 Triphosphate synthesis using phosphoramidates

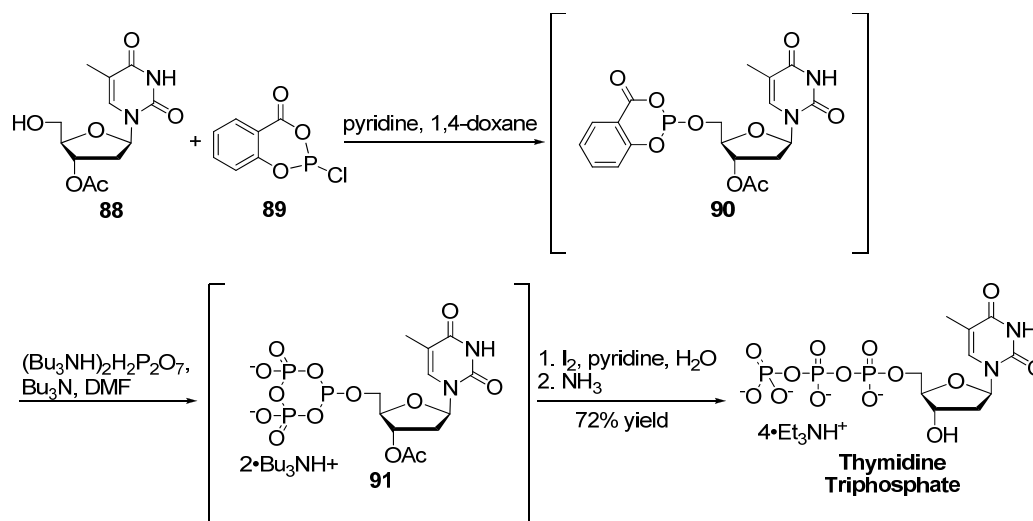
Nucleoside monophosphates can be activated with amines and DCC to generate phosphoramidates using a method developed by Moffatt (Scheme 19).⁸⁰ This method eliminates the generation of mono- and di-phosphates as well as inorganic polyphosphates. In addition these conditions eliminate pyridine from the reaction mixture as this organic base promotes disproportionation of the triphosphate.



Scheme 19. Triphosphate synthesis using phosphoramidate intermediate

1.3.8.3 Triphosphate synthesis using activated phosphites

A method that has been used successfully in recent years is the addition of pyrophosphate to activated phosphites (Scheme 20).⁸¹ The 3'-acetylthymidine **88** was allowed to react with 2-chloro-4H-1,3,2-benzodioxaphosphorin-4-one **89** to form the activated phosphite **90**. Addition of pyrophosphate leads to the formation of the cyclic intermediate **91**. After oxidation and hydrolysis, thymidine triphosphate was obtained.



Scheme 20. Triphosphate synthesis utilizing an activated phosphite

1.3.9 Synthesis and anti-HIV Activity of 3'-Hydroxymethyl Cyclobutyl Nucleosides

Reese and co-workers reported on the synthesis and anti-HIV activity for both purine and pyrimidine 3'-hydroxymethyl cyclobutyl nucleosides (Figure 33).^{82,83} The adenine analogue **92** showed anti-HIV activity with an EC₅₀ of 0.8 μM and no toxicity up to 1000 μM .⁸² The guanine analogue **93** showed weaker anti-HIV activity with an EC₅₀ of 8.0 μM but also showed no toxicity up to 1000 μM .⁸² The pyrimidine analogues showed no anti-HIV activity or toxicity.⁸³

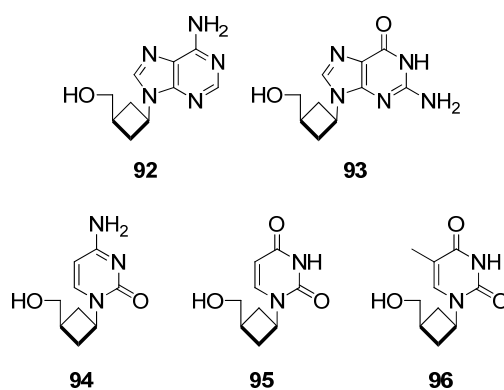
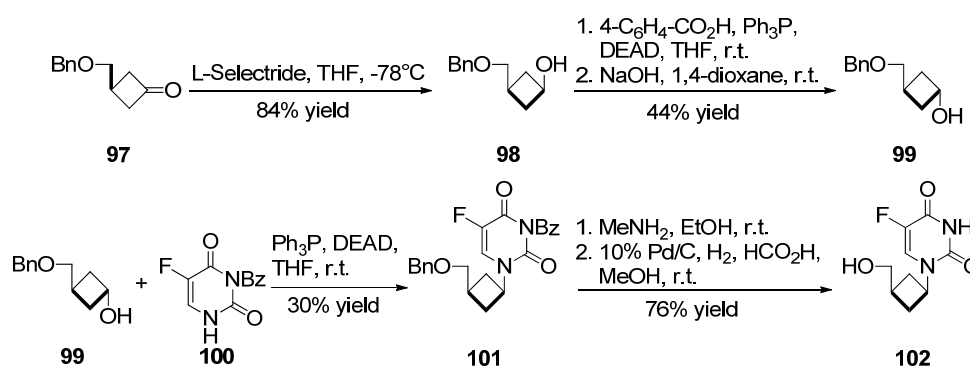


Figure 33. Reported purine and pyrimidine cyclobutyl analogues

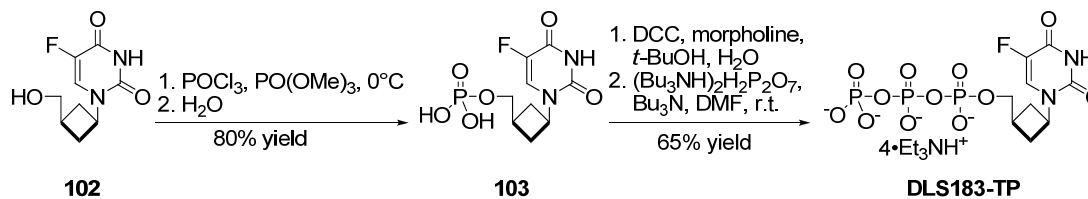
The Liotta group recently reported on the synthesis of 5-fluoro-1-[*cis*-3'-(hydroxymethyl)-cyclobutyl]-cytosine **102** according to the methods reported by Reese (Scheme 21).⁸⁴ The cyclobutanone **97** was constructed using a cycloaddition reaction between dichloroketene and allyl benzyl ether. Further transformations lead to the *trans*-cyclobutanol **99**. Coupling of **99** to the base analogue **100** was accomplished using a Mitsunobu reaction forming **101**. The final analogue **102** was obtained after deprotection and conversion of the 5-fluorouracil base to the 5-fluorocytosine base.



Scheme 21. Synthesis of 5-fluoro-1-[*cis*-3'-(hydroxymethyl)-cyclobutyl]-cytosine **102**

Subsequent work showed that analogue **102** up to 100 μM did not inhibit HIV replication when evaluated in HIV infected primary human lymphocytes.⁸⁵ Thus, the triphosphate **DLS183-TP** was synthesized from an activated morpholine intermediate using Moffatt's procedure (Scheme 22).⁸⁰ The triphosphate was then evaluated in a cell-free assay for DNA incorporation against wild type (WT) HIV RT as well as the 3TC resistant mutants M184I and M184V.⁸⁵ **DLS183-TP** exhibited an $\text{IC}_{50} = 4.7 \mu\text{M}$ against recombinant WT HIV RT which was comparable to the $\text{IC}_{50} = 3.0 \mu\text{M}$ obtained for the triphosphate of 3TC (3TC-TP). When screened against WT HIV RT isolated from HIV infected peripheral blood mononuclear cells (PBMCs), **DLS183-TP** exhibited an $\text{IC}_{50} = 6.9 \mu\text{M}$ while an $\text{IC}_{50} = 6.5 \mu\text{M}$ was obtained for 3TC-TP. When screened up to 10 μM

against the M184I and M184V HIV RT, 3TC-TP showed no inhibition of HIV RT activity. In contrast, **DLS183-TP** showed an $IC_{50} = 6.1 \mu\text{M}$ and an $IC_{50} = 6.9 \mu\text{M}$ against M184I HIV RT and M184V HIV RT, respectively. The inactivity of the nucleoside along with cell-free enzymatic data suggests that the nucleoside **102** is a poor substrate for cellular kinases and is not converted into its active triphosphate form.



Scheme 22. Synthesis of **DLS183-TP**

1.4 Results and Discussion

Current research has indicated that the nucleoside analogues AZT and AZA retain activity against the K65R HIV RT and that AZA is resistant to excision promoted by TAMS.^{52,53} In light of this data and the Liotta's group interest in cyclobutyl nucleoside analogues, 3'-azido-3'-hydroxymethyl cyclobutyl adenine and 3'-azido-3'-hydroxymethyl cyclobutyl thymine was deemed worthy of investigation (Figure 34). Base coupling was envisioned to occur between the nucleobase and an activated cyclobutanol. It was believed that protected 3'-hydroxymethyl cyclobutenones, ultimately arising from a [2+2] cycloaddition reaction, would give rise to the base coupling precursor. A survey of the literature indicated that hydroxymethyl cyclobutenones had not been reported. However, acyl- and silyl- protected hydroxyethyl cyclobutenones had been reported. However, acyl- and silyl- protected hydroxyethyl cyclobutenones **23a-d** had been reported in low yield by Dillion and co-workers.⁶² In order to develop a synthesis for the desired cyclobutenone, the synthesis of **23c** was undertaken to optimize reaction conditions. Furthermore, with **23c** possessing a longer hydroxyethyl chain, analogues derived from it could be better substrates for cellular kinases. Thus, optimization of the synthesis of **23c** and its conversion to nucleoside analogues was undertaken.

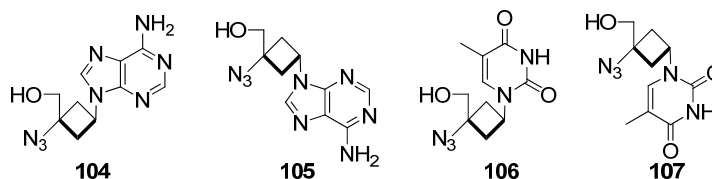
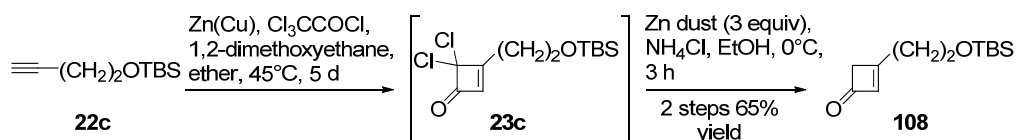


Figure 34. Desired targets

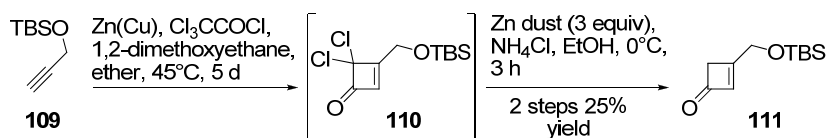
1.4.1 Design and Synthesis of 3'-Azido-3'-Hydroxyethyl Cyclobutyl Adenine

The gem-dichlorocyclobutenone **23c** was synthesized using a modified procedure of Dillon and co-workers (Scheme 23). The phosphorous oxychloride was replaced with 1,2-dimethoxyethane as the additive. After five days at a gentle reflux, the reaction was complete, and the crude material was subjected to dechlorination conditions. The typical dechlorination conditions of excess zinc in warm acetic acid were incompatible with this substrate. The more mild conditions consisting of zinc dust and ammonium chloride in absolute ethanol were chosen which provided the desired product **108** in moderate yield through two steps.



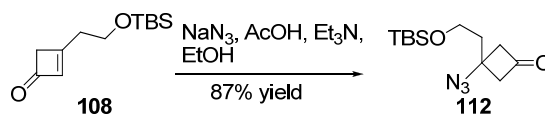
Scheme 23. Synthesis and reduction of cyclobutenone **23c**

With the synthesis of **23c** complete, the same reaction conditions were applied to *tert*-butyldimethyl(2-propynyloxy)silane **109** in order to obtain the protected hydroxymethyl cyclobutenone **111** (Scheme 24). While the desired product was isolated in 25% yield, it decomposed completely within 8 hours.



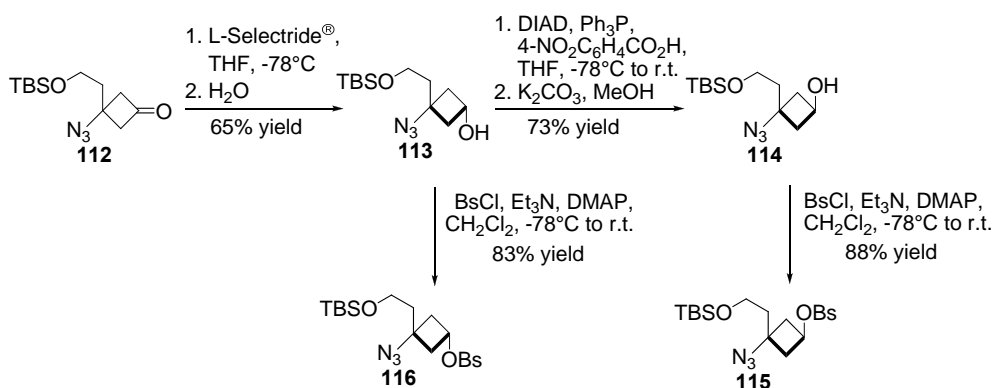
Scheme 24. Synthesis of cyclobutenone **111**

With the observed instability of compound **111**, focus was placed on converting compound **108** into 3'-azido cyclobutyl nucleoside analogs. In order to install the azido group, compound **108** was treated with sodium azide, acetic acid, and triethylamine in ethanol (Scheme 25).



Scheme 25. Azide addition to compound **108**

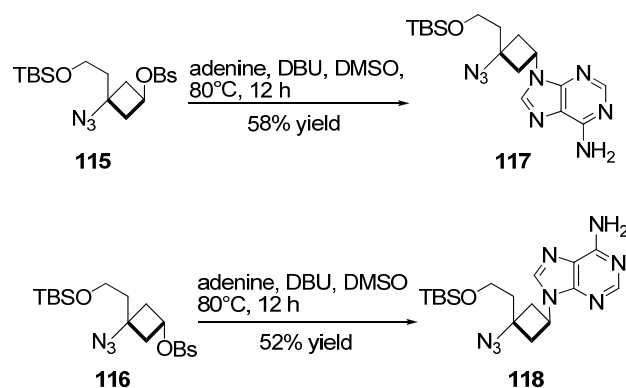
Base coupling was envisioned to occur between a nucleobase and an activated cyclobutanol. To obtain the activated cyclobutanol, compound **112** was reduced with L-Selectride[®] resulting in an inseparable mixture of cyclobutanols **113** and **114** in an 8:1 ratio. A portion of compound **113** was directly treated with 4-bromobenzenesulfonyl chloride (Scheme 26). In addition a portion of compound **113** was subjected to Mitsunobu conditions in order to obtain the isomeric cyclobutanol **114** which was then also treated with 4-bromobenzenesulfonyl chloride.



Scheme 26. Synthesis of activated cyclobutanols **115** and **116**

Upon completing the synthesis of compounds **115** and **116**, each was immediately subjected to base coupling conditions in the presence of adenine to afford the desired protected nucleoside analog (Scheme 27). The base coupling reaction proceeded through

a S_N2 reaction mechanism resulting in inversion of stereochemistry at the carbon atom bearing the brosylate.



The structure of compound **117** (Figure 35) was established through x-ray crystallography and indicates that the protected nucleoside is the α -isomer. Furthermore, the obtained structure indicates that the alcohol compound **117** was derived from was the β -isomer.

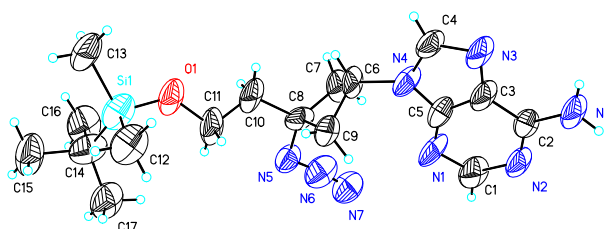
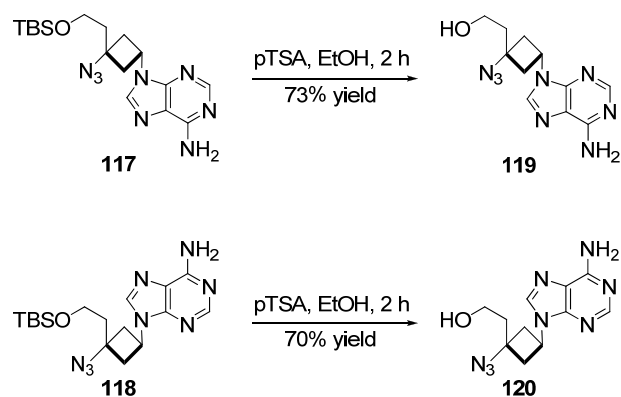


Figure 35. X-ray structure of compound **117**

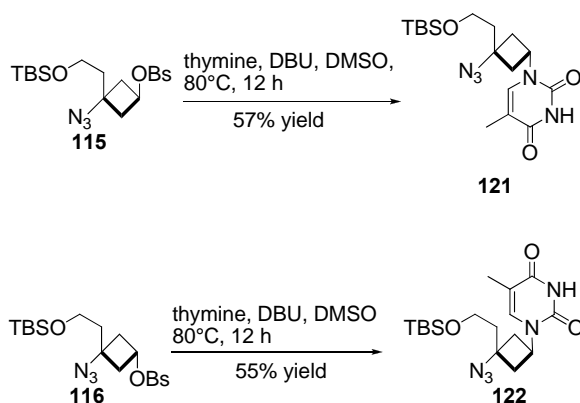
Compounds **117** and **118** were treated with *p*TSA in ethanol to afford the desired nucleoside analogs (Scheme 28).



Scheme 28. Deprotection of compounds **117** and **118**

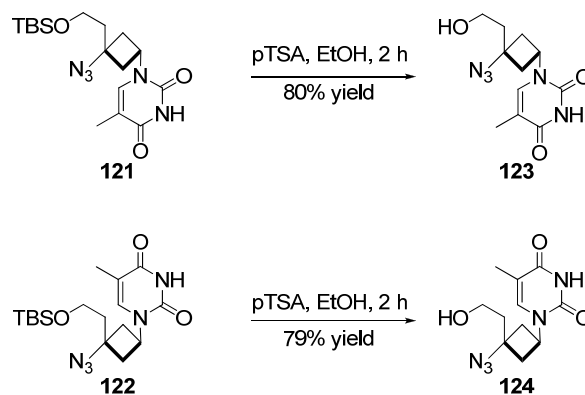
1.4.2 Design and Synthesis of 3'-Azido-3'-Hydroxyethyl Cyclobutyl Thymine

The thymine analogs were synthesized in a fashion similar to that used for compounds **119** and **120**. Alcohols **113** and **114** were each converted into their corresponding brosylate. The brosylates were then subjected to base coupling conditions in the presence of thymine and DBU (Scheme 29).



Scheme 29. Synthesis of compounds **121** and **122**

Compounds **121** and **122** were treated with *p*TSA in ethanol to afford the desired nucleosides **123** and **124** in good yield (Scheme 30).



Scheme 30. Deprotection of compounds **121** and **122**

The structure of compound **124** (Figure 36) was established by x-ray crystallography and indicates that the nucleoside is the β -isomer. In addition, the base coupling reaction proceeded through the desired N1 of thymine.

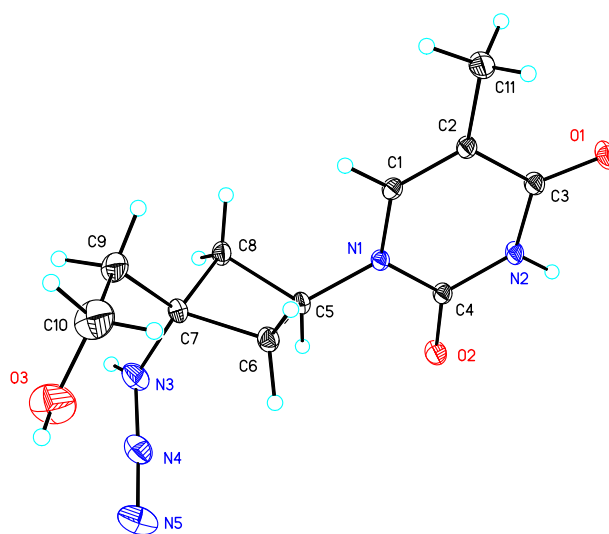


Figure 36. X-ray structure of compound **124**

1.4.3 Anti-Viral Activity

Nucleosides **119**, **120**, **123**, and **124** (Figure 37) were screened for cytotoxicity and for anti-HIV activity following previously reported procedures.

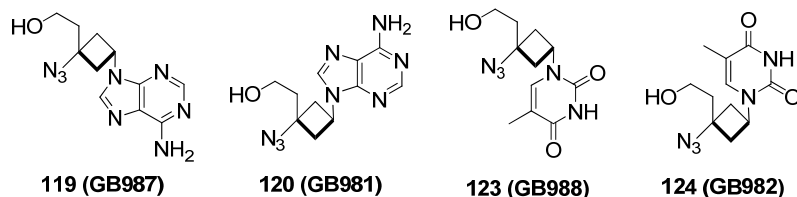


Figure 37. Nucleoside analogs screened for cytotoxicity and anti-HIV activity

Nucleosides **119**, **120**, **123**, and **124** were screened for cytotoxicity in PBM, CEM, and Vero cells.⁸⁸ The nucleosides did not show any toxicity up to 100 μM in any of the cell lines tested (Table 7). In addition, the cyclobutyl nucleoside analogs were screened for anti-HIV activity in HIV infected PBMCs.⁸⁹ The nucleoside analogs did not show anti-HIV activity (Table 7).

Anti-HIV-1 Activity in human PBM cells						Cytotoxicity (IC_{50} , μM) in:		
Code	NBK #	EC_{50} , μM	EC_{90} , μM	Slope	R^2	PBM	CEM	VERO
AZT	AZT	0.0057	0.033	1.3 ± 0.21	0.97	> 100	14.3	56.0
DLS-273	GB-981	>100	>100			>100 (12.4)	>100 (-7.4)	>100 (25.1)
DLS-274	GB-982	>100	>100			>100 (1.6)	>100 (-5.8)	>100 (-13.1)
DLS-275	GB-988	>100	>100			>100 (-11.7)	>100 (-5.7)	>100 (-42.9)
DLS-276	GB-987	56.2	>100	2.7	1.0	>100 (30.0)	>100 (8.0)	>100 (13.1)

Table 7. Anti-HIV and cytotoxicity results for nucleosides **119**, **120**, **123**, and **124**

1.5 Conclusion

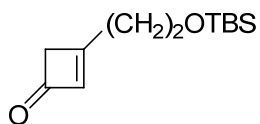
Cyclobutenones **108** and **111** were successfully synthesized using a two-step sequence that involved a [2+2] cycloaddition reaction followed by a dechlorination step. However, cyclobutenone **111** was found to be unstable and only cyclobutenone **108** was used for further transformations. The addition of azide to cyclobutenone **108** in the presence of triethyl amine proceeded smoothly and in high yield to give compound **112**. Cyclobutanol **113** was isolated in moderate yield from the L-Selectride[®] reduction on compound **112**. Additionally, cyclobutanol **114** was isolated by subjecting cyclobutanol **113** to Mitsunobu conditions. The base coupling precursor brosylates **115** and **116** were isolated in high yields from the treatment of cyclobutanols **113** and **114** with 4-bromobenzene sulfonyl chloride in the presence of triethylamine. Base coupling between brosylates **115** and **116** with both adenine and thymine provided the desired protected nucleosides in moderate yield. Base coupling with brosylate **115** provided the α -nucleoside product whereas base coupling with brosylate **116** provided the β -nucleoside product. This indicated the reduction of compound **112** provided the α -cyclobutanol **113**. Treatment of compounds **117**, **118**, **121**, and **122** with *p*TSA in ethanol afforded nucleosides **119**, **120**, **123**, and **124** in good yield. The nucleosides **119**, **120**, **123**, and **124** did not show anti-HIV activity and were not cytotoxicity.

1.6 Experimental

General Notes

Unless otherwise noted, all reagents were obtained from commercial suppliers and used without further purification. All solvents used were anhydrous or kept dry over activated 4Å molecular sieves. Specific reactions were performed in oven-dried glassware under an atmosphere of argon gas. Reaction progress was monitored through thin layer chromatography (TLC) on pre-coated aluminum plates purchased from EM Sciences. Organic extracts were dried over commercially available anhydrous magnesium sulfate, and the solvents were removed at 42°C with a Buchi rotary evaporator. Brine refers to saturated aqueous sodium chloride solution. Flash chromatography was carried out with silica gel 60 (230-400 mesh) from either Sorbent Technologies or Silicycle. ^1H NMR and ^{13}C NMR spectra were recorded on a Mercury 300 or Varian 400 spectrometer (300 or 400 MHz for ^1H and 100 MHz for ^{13}C). Unless otherwise stated, all NMR spectra were recorded in deuterated chloroform (CDCl_3) or methanol (CD_3OD) with residual solvent peaks serving as the internal standards (CDCl_3 : ^1H δ 7.27 and ^{13}C δ 77.23, CD_3OD : ^1H δ 3.31 and ^{13}C δ 49.00). Chemical shifts (δ) are reported in parts per million, and the coupling constants (J) are reported in Hertz. Mass spectra were obtained on either a VG 70-S Nier Johnson or JEOL Mass Spectrometer. Infrared spectra were recorded on a Thermo Nicolet Avatar 370 FT-IR spectrometer as neat films. Elemental analyses were performed by Atlantic Microlab (Norcross, GA).

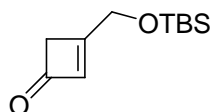
3-(2-(*tert*-Butyldimethylsilyloxy)ethyl)cyclobut-2-enone (108)



Fresh zinc-copper couple was prepared by placing 750 mL of deionized water into a 1 L round bottomed flask. A strong stream of argon gas was bubbled through the deionized water throughout the entire process. After 30 minutes zinc duct (120 g) was placed into the flask and the mixture was stirred vigorously. After a further 30 minutes of stirring, anhydrous cupric sulfate (10 g) was added turning the mixture black. Stirring was continued for another 30 minutes before the zinc-copper couple was filtered under an umbrella of argon gas. The isolated zinc-copper couple was washed with degassed deionized water (500 mL) followed by washing with degassed acetone (500 mL). The zinc-copper couple was transferred to a round bottomed flask and was dried under vacuum overnight. Zinc-copper couple (52 g) was suspended in anhydrous diethyl ether (500 mL) and anhydrous 1,2-dimethoxyethane (90 mL) in a dry 1 L round bottomed flask equipped with a reflux condenser under argon. The suspension was stirred vigorously as 4-(*tert*-butyldimethylsilyloxy)-1-butyne **22c** (56 mL, 271 mmol, 1.0 eq) was added. Finally, trichloroacetyl chloride (80 mL, 716 mmol, 2.64 eq) was added dropwise over the course of 2 hours. The reaction mixture was heated (45°C) to a gentle reflux and stirring was continued for 7 days. The reaction mixture was cooled to room temperature and filtered through Celite. The removed solids were washed with diethyl ether (1.5 L). The filtrate was then concentrated under reduced pressure. The resulting dark residue was diluted with absolute ethanol. The reaction mixture was cooled to 0°C and stirred vigorously as ammonium chloride was added to achieve a saturated solution. Finally zinc

dust was added in 5 g portions every 20-30 minutes until TLC showed no remaining starting material. The reaction mixture was filtered through Celite and the isolated solids were washed with diethyl ether (1.5 L). The filtrate was concentrated under reduced pressure resulting in a thick dark residue. The residue was diluted with diethyl ether (500 mL) and transferred to a separatory funnel. The organic layer was washed with water (4 x 500 mL), dried with MgSO₄, filtered, and concentrated. The resulting residue was purified on silica eluting with 12:1 hexanes/ethyl acetate. The fractions containing product were pooled, concentrated, and purified again on silica eluting with 12:1 hexanes/ethyl acetate resulting in 39.5 g of product (65% yield) as a colorless oil. (Rf: 0.30; 8:1 hexanes/ethyl acetate). ¹H NMR (CDCl₃, 300 MHz): δ: 0.07 (s, 6H), 0.89 (s, 9H), 2.79 (t, 2H, J = 6.0 Hz), 3.22 (s, 2H), 3.89 (t, 2H, J = 6.3 Hz), 5.95 (s, 1H). ¹³C NMR (CDCl₃, 100 MHz): δ: -5.3, 18.3, 25.9, 35.4, 51.3, 59.9, 135.5, 178.8, 188.5. HRMS (APCI): expected for C₁₂H₂₃O₂Si (M+H)⁺ 227.14619. Found 227.14629. IR (neat): ν_{max} 2954, 2929, 2856, 1765, 1099 cm⁻¹. Elemental Analysis for C₁₂H₂₂O₂Si: Found: C, 63.53; H, 9.79. Calculated: C, 63.67; H, 9.79.

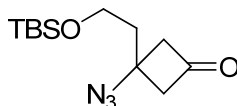
3-((*tert*-Butyldimethylsilyloxy)methyl)cyclobut-2-enone (**111**)



Compound **111** was prepared in an identical manner as compound **108** starting with *tert*-butyldimethyl(2-propynyloxy)silane **109**. 26 g of compound **111** was isolated in 25% yield as a colorless oil. Compound **111** decomposed completely after 8 hours at 0°C. (Rf: 0.17; 8:1 hexanes/ethyl acetate). ¹H NMR (CDCl₃, 400 MHz): δ: 0.07 (s, 6H), 0.88

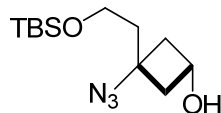
(s, 9H), 3.12 (s, 2H), 4.59 (s, 2H), 6.02 (s, 1H). ^{13}C NMR (CDCl_3 , 100 MHz): δ : -5.4, 18.4, 25.8, 48.8, 62.4, 134.3, 178.4, 186.6. HRMS (ESI): expected for $\text{C}_{11}\text{H}_{21}\text{O}_2\text{Si}$ ($\text{M}+\text{H}$) $^+$ 213.13054. Found 213.13050. IR (neat): ν_{max} 2950, 2925, 2856, 1757 cm^{-1} .

3-Azido-3-(2-(*tert*-butyldimethylsilyloxy)ethyl)cyclobutanone (112)



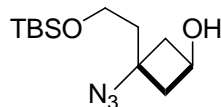
Sodium azide (34.5 g, 530 mmol, 4.0 eq), triethylamine (3.7 mL, 27 mmol, 0.2 eq), and acetic acid (15.1 mL, 265 mmol, 2.0 eq) were dissolved in absolute ethanol (275 mL) in a 500 mL round bottomed flask. This solution was stirred for 30 minutes and then compound **108** (30.0 g, 133 mmol, 1.0 eq) was added. The reaction solution was allowed to stir for 16 hours. The reaction solution was transferred to a separatory funnel and diluted with water (400 mL). The product was extracted with ethyl acetate (3 x 100 mL). The organic layer was washed with water, dried with MgSO_4 , filtered, and concentrated. The resulting residue was purified on silica eluting with 12:1 hexanes/ethyl acetate. The product (31.1 g) was isolated in 87% yield as a colorless oil. (Rf: 0.49; 8:1 hexanes/ethyl acetate). ^1H NMR (CDCl_3 , 300 MHz): δ : 0.07 (s, 6H), 0.90 (s, 9H), 2.14 (t, 2H, $J = 5.7$ Hz), 3.20-3.35 (m, 4H), 3.87 (t, 2H, $J = 5.7$ Hz). ^{13}C NMR (CDCl_3 , 100 MHz): δ : -5.5, 18.2, 25.9, 40.1, 55.5, 58.0, 59.6, 203.2. HRMS (APCI): expected for $\text{C}_{12}\text{H}_{24}\text{NO}_2\text{Si}$ ($\text{M}+\text{H}-\text{N}_2$) $^+$ 242.15708. Found 242.15721. IR (neat): ν_{max} 2958, 2929, 2856, 2108, 1793, 1254, 1095 cm^{-1} . Elemental Analysis for $\text{C}_{12}\text{H}_{23}\text{N}_3\text{O}_2\text{Si}$: Found: C, 54.53; H, 8.91; N, 15.08. Calculated: C, 53.50; H, 8.60; N, 15.60.

3-Azido-3-(2-(*tert*-butyldimethylsilyloxy)ethyl)cyclobutanol (**113**)



Compound **112** (19.2 g, 71.3 mmol, 1.0 eq) was added to a dry round bottomed flask under argon and was dissolved in anhydrous THF (200 mL). The reaction flask was cooled to -78°C and a 1.0 M solution of L-Selectride[®] (86 mL, 86 mmol, 1.2 eq) was added dropwise. The reaction was allowed to stir for 2 hours and was allowed to slowly warm to room temperature. The reaction solution was quenched slowly with water. Once quenched an additional 100 mL of water was added. The reaction mixture was transferred to a separatory funnel and ethyl acetate (100 mL) was added. The organic layer was isolated, dried over MgSO_4 , filtered, and concentrated. The resulting residue was purified on silica eluting with 12:1 hexanes/ethyl acetate providing an inseparable mixture of compounds **113** and **114** (12.6 g) in an inseparable 8:1 ratio as a colorless oil in a 65% yield. (Rf: 0.21; 8:1 hexanes/ethyl acetate). ^1H NMR (CDCl_3 , 300 MHz): δ : 0.07 (s, 6H), 0.90 (s, 9H), 1.79 (t, 2H, $J = 6.3$ Hz), 2.14-2.22 (m, 2H), 2.60-2.68 (m, 2H), 3.73 (t, 2H, $J = 6.6$ Hz), 4.17 (p, 1H, $J = 6.6$ Hz). ^{13}C NMR (CDCl_3 , 100 MHz): δ : -5.3, 18.4, 26.0, 41.2, 43.2, 55.9, 59.6, 60.1. HRMS (APCI): expected for $\text{C}_{12}\text{H}_{26}\text{N}_3\text{O}_2\text{Si}$ ($\text{M}+\text{H}$)⁺ 272.17888. Found 272.17859. IR (neat): ν_{max} 3330, 2954, 2929, 2864, 2100, 1254, 1095 cm^{-1} . Elemental Analysis for $\text{C}_{12}\text{H}_{25}\text{N}_3\text{O}_2\text{Si}$: Found: C, 53.77; H, 9.49; N, 14.56. Calculated: C, 53.10; H, 9.28; N, 15.48.

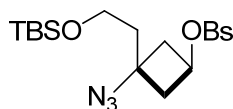
3-Azido-3-(2-(*tert*-butyldimethylsilyloxy)ethyl)cyclobutanol (**114**)



Compound **113** (4.2 g, 15.5 mmol, 1.0 eq) was placed in a dry round bottomed flask under argon and was dissolved with anhydrous THF (300 mL). Next triphenylphosphine (6.1 g, 23.2 mmol, 1.5 eq) and 4-nitrobenzoic acid (3.9 g, 23.2 mmol, 1.5 eq) was added to the reaction solution. The reaction flask was then cooled to -78°C and DIAD (4.3 mL, 23.2 mmol, 1.5 eq) was added dropwise. The reaction solution was then allowed to stir for 16 hours and warm to room temperature. The reaction mixture was then transferred to a separatory funnel and was diluted with water. The organic layer isolated and the aqueous layer was extracted with ethyl acetate (2 x 100 mL). The organic layers were pooled, dried with MgSO_4 , filtered, and concentrated. The resulting residue was purified on silica eluting with 12:1 hexanes/ethyl acetate. The appropriate fractions containing product were pooled and concentrated. The resulting residue was dissolved in methanol (25 mL) and was treated with excess K_2CO_3 . The reaction mixture was stirred for 3 hours and then transferred to a separatory funnel. The reaction mixture was diluted with water (250 mL) and extracted with ethyl acetate (3 x 50 mL). The organic layer was dried with MgSO_4 , filtered, and concentrated. The resulting residue was purified on silica eluting with 12:1 hexanes/ethyl acetate affording compound **114** (3.1 g) as a colorless oil in a 73% yield. (Rf: 0.34; 8:1 hexanes/ethyl acetate). ^1H NMR (CDCl_3 , 300 MHz): δ : 0.07 (s, 6H), 0.90 (s, 9H), 1.95 (t, 2H, $J = 6.3$ Hz), 2.10-2.17 (m, 2H), 2.53-2.61 (m, 2H), 3.75 (t, 2H, $J = 6.6$ Hz), 4.47-4.54 (m, 1H). ^{13}C NMR (CDCl_3 , 100 MHz): δ : -5.4, 18.3, 26.0, 42.5, 43.6, 59.4, 62.9, 63.0. HRMS (APCI): expected for $\text{C}_{12}\text{H}_{26}\text{NO}_2\text{Si}$

(M+H-N₂)⁺ 244.17273. Found 244.17277. IR (neat): ν_{\max} 3330, 2954, 2929, 2852, 2096, 1254, 1107 cm⁻¹. Elemental Analysis for C₁₂H₂₅N₃O₂Si: Found: C, 53.35; H, 9.41; N, 14.78. Calculated: C, 53.10; H, 9.28; N, 15.48.

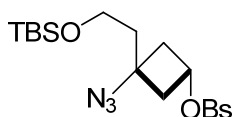
3-Azido-3-(2-(*tert*-butyldimethylsilyloxy)ethyl)cyclobutyl-4-bromobenzenesulfonate
(115)



Compound **114** (2.29 g, 8.5 mmol, 1.0 eq) was placed in a dry round bottomed flask under argon and was dissolved with anhydrous CH₂Cl₂ (50 mL). Next DMAP (0.1 g, 0.8 mmol, 0.1 eq) and 4-bromobenzenesulfonyl chloride (3.2 g, 12.7 mmol, 1.5 eq) were added to the reaction flask. The flask was then cooled to -78°C and triethylamine (1.8 mL, 12.7 mmol, 1.5 eq) was added dropwise. The reaction solution was allowed to stir for 16 hours slowly warming to room temperature. The reaction was quenched with ethanol and then was transferred to a separatory funnel. Water was added to the separatory funnel and the organic layer was isolated. The aqueous layer was then extracted with CH₂Cl₂ (2 x 25 mL). The organic layers were pooled, washed with brine, dried with MgSO₄, filtered, and concentrated. The resulting residue was purified on silica eluting with 12:1 hexanes/ethyl acetate to afford 3.6 g of compound **115** in a 88% yield as a colorless oil. (Rf: 0.47; 8:1 hexanes/ethyl acetate). ¹H NMR (CDCl₃, 400 MHz): δ : 0.02 (s, 6H), 0.86 (s, 9H), 1.90 (t, 2H, J = 5.6 Hz), 2.32-2.37 (m, 2H), 2.46-2.51 (m, 2H), 3.70 (t, 2H, J = 6.0 Hz), 4.95 (p, 1H, J = 7.2 Hz), 7.70 (d, 2H, J = 8.4 Hz), 7.77 (d, 2H, J = 8.4 Hz). ¹³C NMR (CDCl₃, 100 MHz): δ : -5.4, 18.3, 26.0, 41.7, 41.8, 59.1,

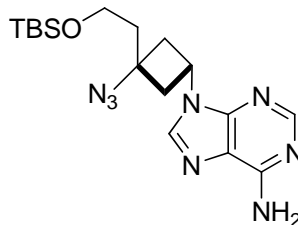
60.0, 71.6, 129.4, 129.5, 132.9, 135.7. HRMS (APCI): expected for $C_{18}H_{29}NO_4SiSBr$ ($M+H-N_2$)⁺ 462.07645. Found 462.07612. IR (neat): ν_{max} 2951, 2923, 2856, 2101, 1187, 842 cm^{-1} . Elemental Analysis for $C_{18}H_{28}N_3O_4SiSBr$: Found: C, 43.81; H, 5.73; N, 8.16. Calculated: C, 44.08; H, 5.75; N, 8.57.

3-Azido-3-(2-(*tert*-butyldimethylsilyloxy)ethyl)cyclobutyl-4-bromobenzenesulfonate (116)



Compound **116** was synthesized in an identical manner as compound **115** starting from compound **113** (6.5 g, 24.0 mmol, 1.0 eq). Compound **116** (9.8 g) was isolated as a colorless oil in 83% yield. (Rf: 0.42; 8:1 hexanes/ethyl acetate). ¹H NMR (CDCl₃, 400 MHz): δ : 0.04 (s, 6H), 0.87 (s, 9H), 1.74 (t, 2H, J = 6.0 Hz), 2.36-2.41 (m, 2H), 2.63-2.68 (m, 2H), 3.69 (t, 2H, J = 6.0 Hz), 4.71 (p, 1H, J = 6.8 Hz), 7.71 (d, 2H, J = 8.4 Hz), 7.78 (d, 2H, J = 8.4 Hz). ¹³C NMR (CDCl₃, 100 MHz): δ : -5.4, 18.2, 26.0, 40.5, 41.0, 56.8, 59.3, 68.5, 129.4, 129.4, 132.8, 135.8. HRMS (APCI): expected for $C_{18}H_{29}NO_4SiSBr$ ($M+H-N_2$)⁺ 462.07645. Found 462.07616. IR (neat): ν_{max} 2951, 2927, 2852, 2101, 1191, 826 cm^{-1} . Elemental Analysis for $C_{18}H_{28}N_3O_4SiSBr$: Found: C, 44.50; H, 5.78; N, 8.32. Calculated: C, 44.08; H, 5.75; N, 8.57.

9-(3-Azido-3-(2-(*tert*-butyldimethylsilyloxy)ethyl)cyclobutyl)-adenine (117)



Compound **115** (1.10 g, 2.24 mmol, 1.0 eq) was dissolved in anhydrous DMSO (3 mL) in a round bottomed flask under argon. Next adenine (0.46 g, 3.36 mmol, 1.5 eq) that had been dried under a high vacuum was added followed by the addition of DBU (0.50 mL, 3.36 mmol, 1.5 eq). The reaction mixture was heated to 80°C and allowed to stir for 12 hours. The reaction mixture was cooled to room temperature and then transferred to a separatory funnel. The reaction mixture was diluted with water (50 mL), and the product was extracted with ethyl acetate (3 x 25 mL). The organic layer was dried with MgSO₄, filtered, and concentrated. The product was purified on silica eluting with 97:3 CH₂Cl₂/MeOH. Compound **117** (0.5 g) was isolated as a white solid in 58% yield. (Rf: 0.45; 9:1 dichloromethane/methanol). mp: 203-207 °C (decomposition). ¹H NMR (CDCl₃, 400 MHz): δ: 0.09 (s, 6H), 0.91 (s, 9H), 2.02 (t, 2H, J = 6.0 Hz), 2.96 (d, 4H, J = 8.4 Hz), 3.83 (t, 2H, J = 6.4 Hz), 4.88 (p, 1H, J = 8.4 Hz), 5.88 (s, 2H), 7.94 (s, 1H), 8.36 (s, 1H). ¹³C NMR (CDCl₃ + 10% CD₃OD, 100 MHz): δ: -5.5, 18.2, 25.9, 39.8, 40.5, 42.2, 57.7, 59.4, 119.4, 138.6, 149.7, 152.7, 155.6. HRMS (APCI): expected for C₁₇H₂₉N₈OSi (M+H)⁺ 389.22391. Found 389.22327. IR (neat): ν_{max} 3330, 3183, 2999, 2946, 2925, 2876, 2848, 2100, 1102 cm⁻¹. Elemental Analysis for C₁₇H₂₈N₈OSi: Found: C, 52.67; H, 7.48; N, 27.12. Calculated: C, 52.55; H, 7.26; N, 28.84. The structure of compound **117** was established by X-ray crystallographic analysis.

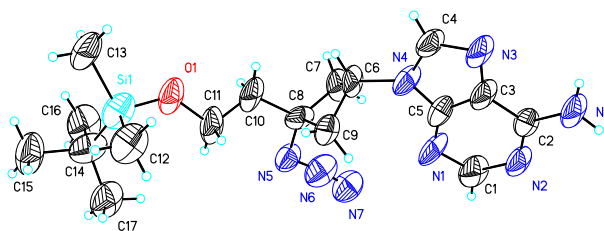


Table 8. Crystal data and structure refinement for GB957n.

Identification code	gb957n	
Empirical formula	C17 H28 N8 O Si	
Formula weight	388.56	
Temperature	173(2) K	
Wavelength	1.54178 Å	
Crystal system	Monoclinic	
Space group	P2(1)/c	
Unit cell dimensions	a = 23.119(16) Å	$\alpha = 90^\circ$.
	b = 7.212(5) Å	$\beta = 100.191(14)^\circ$.
	c = 12.790(8) Å	$\gamma = 90^\circ$.
Volume	2099(2) Å ³	
Z	4	
Density (calculated)	1.230 Mg/m ³	
Absorption coefficient	1.182 mm ⁻¹	
F(000)	832	
Crystal size	0.38 x 0.09 x 0.03 mm ³	
Theta range for data collection	8.38 to 59.99°.	
Index ranges	-24 ≤ h ≤ 23, -7 ≤ k ≤ 7, -14 ≤ l ≤ 13	
Reflections collected	10339	
Independent reflections	2879 [R(int) = 0.2976]	
Completeness to theta = 59.99°	92.1 %	
Absorption correction	Semi-empirical from equivalents	
Max. and min. transmission	0.9654 and 0.6621	
Refinement method	Full-matrix least-squares on F ²	
Data / restraints / parameters	2879 / 0 / 245	
Goodness-of-fit on F ²	1.008	
Final R indices [I > 2σ(I)]	R1 = 0.1078, wR2 = 0.1748	

R indices (all data)	R1 = 0.3217, wR2 = 0.2318
Extinction coefficient	0.0103(9)
Largest diff. peak and hole	0.165 and -0.263 e.Å ⁻³

Table 9. Atomic coordinates ($\times 10^4$) and equivalent isotropic displacement parameters ($\text{\AA}^2 \times 10^3$) for GB957n. $U(\text{eq})$ is defined as one third of the trace of the orthogonalized U_{ij} tensor.

	x	y	z	U(eq)
C(1)	1107(6)	-2130(20)	4480(8)	152(6)
C(2)	433(7)	-210(30)	3452(7)	132(7)
C(3)	547(7)	1050(20)	4295(8)	137(7)
C(4)	565(6)	3460(20)	5340(7)	132(6)
C(5)	933(8)	490(30)	5170(10)	128(7)
C(6)	1374(5)	2456(19)	6867(6)	122(5)
C(7)	1337(6)	803(19)	7725(7)	137(6)
C(8)	2005(9)	1130(20)	8035(8)	115(5)
C(9)	2003(6)	1930(18)	6919(6)	137(6)
C(10)	2217(6)	2453(17)	8958(6)	128(5)
C(11)	2855(6)	3030(20)	9166(7)	169(7)
C(12)	3805(5)	6627(17)	9186(6)	182(7)
C(13)	3273(5)	7732(17)	11055(7)	167(6)
C(14)	4033(7)	4270(20)	11222(10)	146(6)
C(15)	4559(6)	5660(20)	11769(9)	202(8)
C(16)	3779(5)	3322(18)	12120(7)	185(7)
C(17)	4334(6)	2860(20)	10624(9)	174(7)
N(1)	1262(7)	-990(20)	5311(8)	155(7)
N(2)	733(6)	-1805(18)	3549(7)	123(5)
N(3)	293(5)	2800(20)	4392(6)	144(5)
N(4)	977(5)	2065(18)	5801(6)	114(4)
N(5)	2379(11)	-470(30)	8321(12)	146(7)
N(6)	2223(11)	-1850(30)	7891(14)	174(14)
N(7)	2106(12)	-3310(30)	7546(17)	161(9)
N(8)	40(4)	132(11)	2531(5)	134(4)
O(1)	2905(4)	4383(14)	9974(5)	165(4)

Si(1)	3515(2)	5708(8)	10346(2)	160(2)
-------	---------	---------	----------	--------

Table 10. Bond lengths [\AA] and angles [$^\circ$] for GB957n.

C(1)-N(1)	1.340(15)
C(1)-N(2)	1.363(12)
C(2)-N(2)	1.338(14)
C(2)-N(8)	1.378(13)
C(2)-C(3)	1.399(17)
C(3)-C(5)	1.365(18)
C(3)-N(3)	1.404(13)
C(4)-N(3)	1.351(13)
C(4)-N(4)	1.441(13)
C(5)-N(1)	1.303(17)
C(5)-N(4)	1.389(17)
C(6)-C(9)	1.493(12)
C(6)-N(4)	1.528(11)
C(6)-C(7)	1.632(14)
C(7)-C(8)	1.541(15)
C(8)-N(5)	1.45(2)
C(8)-C(10)	1.532(15)
C(8)-C(9)	1.539(13)
C(10)-C(11)	1.511(12)
C(11)-O(1)	1.411(13)
C(12)-Si(1)	1.856(9)
C(13)-Si(1)	1.856(11)
C(14)-C(17)	1.516(14)
C(14)-C(16)	1.540(13)
C(14)-C(15)	1.635(16)
C(14)-Si(1)	1.813(13)
N(5)-N(6)	1.17(2)
N(6)-N(7)	1.15(3)
O(1)-Si(1)	1.701(8)
N(1)-C(1)-N(2)	128.9(14)

N(2)-C(2)-N(8)	119.0(14)
N(2)-C(2)-C(3)	117.7(13)
N(8)-C(2)-C(3)	123.2(14)
C(5)-C(3)-C(2)	116.3(16)
C(5)-C(3)-N(3)	114.8(13)
C(2)-C(3)-N(3)	128.8(14)
N(3)-C(4)-N(4)	106.8(12)
N(1)-C(5)-C(3)	129.8(16)
N(1)-C(5)-N(4)	127.5(17)
C(3)-C(5)-N(4)	101.6(16)
C(9)-C(6)-N(4)	114.8(9)
C(9)-C(6)-C(7)	87.1(9)
N(4)-C(6)-C(7)	111.8(10)
C(8)-C(7)-C(6)	83.9(10)
N(5)-C(8)-C(10)	101.9(14)
N(5)-C(8)-C(9)	115.9(13)
C(10)-C(8)-C(9)	115.4(11)
N(5)-C(8)-C(7)	118.1(17)
C(10)-C(8)-C(7)	117.6(12)
C(9)-C(8)-C(7)	88.9(11)
C(6)-C(9)-C(8)	88.9(10)
C(11)-C(10)-C(8)	118.5(11)
O(1)-C(11)-C(10)	105.6(11)
C(17)-C(14)-C(16)	110.3(13)
C(17)-C(14)-C(15)	104.7(12)
C(16)-C(14)-C(15)	107.9(10)
C(17)-C(14)-Si(1)	112.6(9)
C(16)-C(14)-Si(1)	114.7(10)
C(15)-C(14)-Si(1)	105.9(11)
C(5)-N(1)-C(1)	108.8(15)
C(2)-N(2)-C(1)	117.7(13)
C(4)-N(3)-C(3)	105.2(11)
C(5)-N(4)-C(4)	111.1(12)
C(5)-N(4)-C(6)	129.9(13)
C(4)-N(4)-C(6)	119.0(11)
N(6)-N(5)-C(8)	116(2)

N(7)-N(6)-N(5) 173(3)
 C(11)-O(1)-Si(1) 123.3(8)
 O(1)-Si(1)-C(14) 106.1(8)
 O(1)-Si(1)-C(12) 112.1(4)
 C(14)-Si(1)-C(12) 113.9(6)
 O(1)-Si(1)-C(13) 105.7(5)
 C(14)-Si(1)-C(13) 111.8(6)
 C(12)-Si(1)-C(13) 107.1(6)

Symmetry transformations used to generate equivalent atoms:

Table 11. Anisotropic displacement parameters ($\text{\AA}^2 \times 10^3$) for GB957n. The anisotropic displacement factor exponent takes the form: $-2\pi^2 [h^2 a^{*2} U^{11} + \dots + 2 h k a^* b^* U^{12}]$

	U ¹¹	U ²²	U ³³	U ²³	U ¹³	U ¹²
C(1)	188(15)	216(18)	53(6)	11(9)	30(8)	22(12)
C(2)	160(15)	210(20)	29(6)	-7(9)	18(7)	39(13)
C(3)	205(17)	166(19)	33(6)	8(8)	2(8)	53(14)
C(4)	161(14)	183(19)	54(7)	12(8)	26(8)	32(12)
C(5)	172(19)	160(20)	54(8)	-36(12)	39(10)	-53(15)
C(6)	111(12)	220(17)	30(5)	9(7)	-7(7)	1(11)
C(7)	135(12)	232(18)	38(5)	11(7)	4(7)	-31(12)
C(8)	198(18)	100(16)	52(6)	3(7)	39(9)	18(13)
C(9)	174(14)	206(16)	26(4)	12(6)	6(7)	15(12)
C(10)	188(15)	163(15)	35(5)	-5(6)	25(7)	-28(12)
C(11)	140(15)	300(20)	51(6)	-32(9)	-12(8)	-42(14)
C(12)	255(16)	240(17)	61(6)	27(8)	53(8)	-20(12)
C(13)	185(13)	223(16)	94(7)	-53(10)	27(8)	-18(12)
C(14)	216(18)	150(17)	89(8)	44(10)	78(10)	43(14)
C(15)	193(16)	300(20)	114(10)	-55(11)	20(10)	-102(15)
C(16)	189(14)	300(20)	66(6)	28(9)	12(8)	-23(12)
C(17)	200(16)	215(19)	99(8)	16(10)	3(9)	7(13)
N(1)	258(18)	168(18)	40(5)	-10(7)	28(7)	41(11)
N(2)	169(13)	151(15)	51(5)	-8(7)	24(6)	11(9)

N(3)	188(12)	219(16)	25(4)	28(7)	18(5)	29(11)
N(4)	170(12)	117(12)	59(5)	-7(6)	27(6)	6(9)
N(5)	246(17)	110(20)	91(10)	-5(9)	55(11)	29(15)
N(6)	260(30)	150(40)	120(20)	38(17)	90(20)	80(30)
N(7)	198(15)	170(30)	125(12)	43(13)	67(11)	59(19)
N(8)	194(10)	175(11)	34(3)	-3(5)	22(5)	3(8)
O(1)	189(10)	245(12)	59(4)	-32(5)	21(5)	-50(9)
Si(1)	207(5)	220(6)	57(2)	0(3)	32(3)	9(5)

Table 12. Hydrogen coordinates ($\times 10^4$) and isotropic displacement parameters ($\text{\AA}^2 \times 10^3$) for GB957n.

	x	y	z	U(eq)
H(1A)	1282	-3323	4550	182
H(4)	497	4629	5643	158
H(6A)	1320	3724	7151	147
H(7A)	1109	1118	8286	164
H(7B)	1226	-425	7406	164
H(9A)	2269	3002	6910	164
H(9B)	2066	990	6386	164
H(10A)	1976	3594	8838	154
H(10B)	2131	1870	9615	154
H(11A)	3112	1954	9402	202
H(11B)	2969	3552	8516	202
H(12A)	3945	5596	8797	273
H(12B)	4132	7477	9432	273
H(12C)	3493	7292	8716	273
H(13A)	3118	7301	11679	251
H(13B)	2964	8403	10578	251
H(13C)	3607	8559	11283	251
H(15A)	4862	4947	12232	302
H(15B)	4398	6604	12189	302

H(15C)	4733	6269	11212	302
H(16A)	4081	2528	12532	278
H(16B)	3439	2565	11813	278
H(16C)	3657	4267	12586	278
H(17A)	4606	2113	11130	261
H(17B)	4553	3502	10143	261
H(17C)	4038	2049	10211	261
H(8A)	-12	-694	2017	161
H(8B)	-160	1176	2457	161

Table 13. Torsion angles [$^{\circ}$] for GB957n.

N(2)-C(2)-C(3)-C(5)	-4(2)
N(8)-C(2)-C(3)-C(5)	177.7(13)
N(2)-C(2)-C(3)-N(3)	-179.6(17)
N(8)-C(2)-C(3)-N(3)	2(3)
C(2)-C(3)-C(5)-N(1)	8(3)
N(3)-C(3)-C(5)-N(1)	-176(2)
C(2)-C(3)-C(5)-N(4)	175.9(14)
N(3)-C(3)-C(5)-N(4)	-7.5(19)
C(9)-C(6)-C(7)-C(8)	24.9(9)
N(4)-C(6)-C(7)-C(8)	140.4(11)
C(6)-C(7)-C(8)-N(5)	-143.0(11)
C(6)-C(7)-C(8)-C(10)	94.2(11)
C(6)-C(7)-C(8)-C(9)	-24.0(9)
N(4)-C(6)-C(9)-C(8)	-137.4(11)
C(7)-C(6)-C(9)-C(8)	-24.8(10)
N(5)-C(8)-C(9)-C(6)	147.2(18)
C(10)-C(8)-C(9)-C(6)	-93.9(15)
C(7)-C(8)-C(9)-C(6)	26.3(11)
N(5)-C(8)-C(10)-C(11)	58.8(16)
C(9)-C(8)-C(10)-C(11)	-67.6(19)
C(7)-C(8)-C(10)-C(11)	-170.5(12)

C(8)-C(10)-C(11)-O(1)	173.8(10)
C(3)-C(5)-N(1)-C(1)	-9(3)
N(4)-C(5)-N(1)-C(1)	-174.8(12)
N(2)-C(1)-N(1)-C(5)	9(3)
N(8)-C(2)-N(2)-C(1)	-178.2(10)
C(3)-C(2)-N(2)-C(1)	3(2)
N(1)-C(1)-N(2)-C(2)	-6(2)
N(4)-C(4)-N(3)-C(3)	-0.7(16)
C(5)-C(3)-N(3)-C(4)	5(2)
C(2)-C(3)-N(3)-C(4)	-178.5(15)
N(1)-C(5)-N(4)-C(4)	175.3(18)
C(3)-C(5)-N(4)-C(4)	6.7(15)
N(1)-C(5)-N(4)-C(6)	-6(3)
C(3)-C(5)-N(4)-C(6)	-174.8(12)
N(3)-C(4)-N(4)-C(5)	-3.9(15)
N(3)-C(4)-N(4)-C(6)	177.4(9)
C(9)-C(6)-N(4)-C(5)	46.5(18)
C(7)-C(6)-N(4)-C(5)	-50.6(16)
C(9)-C(6)-N(4)-C(4)	-135.0(12)
C(7)-C(6)-N(4)-C(4)	127.8(12)
C(10)-C(8)-N(5)-N(6)	162.5(17)
C(9)-C(8)-N(5)-N(6)	-71(2)
C(7)-C(8)-N(5)-N(6)	32(2)
C(8)-N(5)-N(6)-N(7)	-161(24)
C(10)-C(11)-O(1)-Si(1)	-169.8(8)
C(11)-O(1)-Si(1)-C(14)	-80.2(10)
C(11)-O(1)-Si(1)-C(12)	44.6(11)
C(11)-O(1)-Si(1)-C(13)	161.0(9)
C(17)-C(14)-Si(1)-O(1)	77.4(12)
C(16)-C(14)-Si(1)-O(1)	-49.8(13)
C(15)-C(14)-Si(1)-O(1)	-168.6(7)
C(17)-C(14)-Si(1)-C(12)	-46.3(15)
C(16)-C(14)-Si(1)-C(12)	-173.6(10)
C(15)-C(14)-Si(1)-C(12)	67.6(9)
C(17)-C(14)-Si(1)-C(13)	-167.8(11)
C(16)-C(14)-Si(1)-C(13)	64.9(14)

C(15)-C(14)-Si(1)-C(13) -53.9(10)

Symmetry transformations used to generate equivalent atoms:

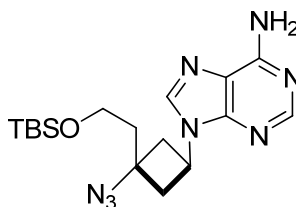
Table 14. Hydrogen bonds for GB957n [\AA and $^\circ$].

D-H...A	d(D-H)	d(H...A)	d(D...A)	$\angle(\text{DHA})$
N(8)-H(8A)...N(3)#1	0.88	2.11	2.966(12)	165.8
N(8)-H(8B)...N(2)#2	0.88	2.22	3.017(15)	150.7

Symmetry transformations used to generate equivalent atoms:

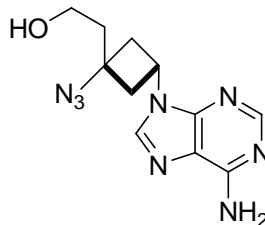
#1 -x,y-1/2,-z+1/2 #2 -x,y+1/2,-z+1/2

9-(3-Azido-3-(2-(*tert*-butyldimethylsilyloxy)ethyl)cyclobutyl)-adenine (118)



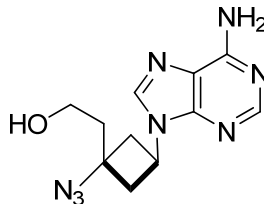
Compound **118** was synthesized in a manner identical to the synthesis of compound **117** from compound **116** (2.00 g, 4.08 mmol, 1.0 eq). Compound **118** (0.8 g) was isolated as white solid in 52% yield. (Rf: 0.47; 9:1 dichloromethane/methanol). mp: 142-144 $^\circ\text{C}$. ^1H NMR (CDCl_3 , 400 MHz): δ : 0.03 (s, 6H), 0.84 (s, 9H), 2.08 (t, 2H, $J = 6.0$ Hz), 2.70-2.75 (m, 2H), 2.96-3.02 (m, 2H), 3.79 (t, 2H, $J = 6.0$ Hz), 5.11 (p, 1H, $J = 8.8$ Hz), 6.63 (s, 2H), 7.81 (s, 1H), 8.28 (s, 1H). ^{13}C NMR (CDCl_3 , 100 MHz): δ : -5.4, 18.3, 26.0, 40.4, 41.6, 46.0, 59.3, 61.0, 120.2, 139.1, 150.2, 152.8, 156.0. HRMS (APCI): expected for $\text{C}_{17}\text{H}_{29}\text{N}_8\text{OSi}$ ($\text{M}+\text{H}$) $^+$ 389.22281. Found 389.22284. IR (neat): ν_{max} 3326, 3170, 2954, 2933, 2856, 2104, 1262, 731 cm^{-1} . Elemental Analysis for $\text{C}_{17}\text{H}_{28}\text{N}_8\text{OSi}$: Found: C, 52.15; H, 7.43; N, 28.42.

2-(3-(6-Amino-9H-purin-9-yl)-1-azidocyclobutyl)ethanol (119**)**



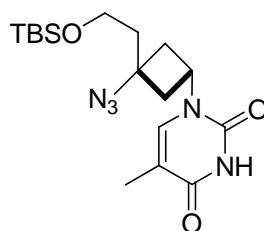
Compound **117** (0.33 g, 0.85 mmol, 1.0 eq) was dissolved in absolute ethanol (4 mL). *p*TSA (0.2 g, 1.87 mmol, 2.2 eq) was dissolved in absolute ethanol (5 mL) and was then added to compound **117** dropwise at room temperature. After stirring for 2 hours, the reaction mixture was concentrated under reduced pressure. The resulting residue was purified on silica eluting with 95:5 CH₂Cl₂/MeOH. The purified material was then dissolved in absolute ethanol and treated with 1M NaOH. After stirring for 10 minutes, the solution was concentrated under reduced pressure. The resulting residue was then purified on silica eluting with 95:5 CH₂Cl₂/MeOH. The product **119** (0.17 g) was isolated as a white solid in 73% yield. (Rf: 0.27; 9:1 dichloromethane/methanol). mp: 155-158 °C. ¹H NMR (CDCl₃, 400 MHz): δ: 2.06 (t, 2H, J = 6.0 Hz), 2.91-2.95 (m, 2H), 3.03-3.08 (m, 2H), 3.88 (m, 2H), 4.85 (p, 1H, J = 8.4 Hz), 5.54 (s, 2H), 7.91 (s, 1H), 8.37 (s, 1H). ¹³C NMR (CD₃OD, 100 MHz): δ: 40.5, 40.8, 43.8, 58.6, 59.0, 120.5, 141.1, 150.8, 153.5, 157.2. HRMS (APCI): expected for C₁₁H₁₅N₈O (M+H)⁺ 275.13633. Found 275.13621. IR (neat): ν_{max} 3317, 3170, 2955, 2923, 2856, 2105, 1255 cm⁻¹. Elemental Analysis for C₁₁H₁₄N₈O: Found: C, 48.33; H, 5.20; N, 39.72. Calculated: C, 48.17; H, 5.14; N, 40.85.

2-(3-(6-Amino-9H-purin-9-yl)-1-azidocyclobutyl)ethanol (120)



Compound **120** was synthesized in an identical manner as compound **119** from compound **118** (0.51 g, 1.32 mmol, 1.0 eq). Compound **120** (0.25 g) was isolated as a white solid in 70% yield. (Rf: 0.31; 9:1 dichloromethane/methanol). mp: 173 °C (decomposition). ¹H NMR (CD₃OD, 400 MHz): δ: 2.14 (t, 2H, J = 6.4 Hz), 2.73-2.78 (m, 2H), 3.01-3.07 (m, 2H), 3.77 (t, 2H, J = 6.4 Hz), 5.20 (p, 1H, J = 8.0 Hz), 8.20 (s, 1H), 8.22 (s, 1H). ¹³C NMR (CD₃OD, 100 MHz): δ: 40.9, 42.3, 47.0, 59.0, 62.2, 120.7, 141.6, 150.9, 153.7, 157.4. HRMS (APCI): expected for C₁₁H₁₅N₈O (M+H)⁺ 275.13634. Found 275.13639. IR (neat): ν_{max} 3333, 3062, 2927, 2852, 2109, 1211 cm⁻¹. Elemental Analysis for C₁₁H₁₄N₈O: Found: C, 48.22; H, 5.19; N, 39.81. Calculated: C, 48.17; H, 5.14; N, 40.85.

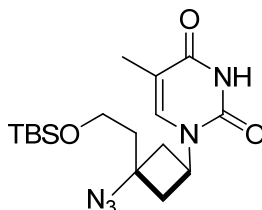
1-(3-Azido-3-(2-(*tert*-butyldimethylsilyloxy)ethyl)cyclobutyl)-5-methylpyrimidine-2,4(1*H*,3*H*)-dione (121)



Compound **121** was synthesized in a similar manner as compound **117** from compound **115** (1.10 g, 2.24 mmol, 1.0 eq) and thymine (0.42 g, 3.36 mmol, 1.5 eq). Compound

121 was purified on silica eluting with 1:1 hexanes/ethyl acetate. The desired product (0.49 g) was isolated as a white solid in 57% yield. (Rf: 0.21; 97:3 dichloromethane/methanol). mp: 142-144 °C. ¹H NMR (CD₃OD, 400 MHz): δ: 0.10 (s, 6H), 0.92 (s, 9H), 1.90 (s, 3H), 1.97 (t, 2H, J = 6.0 Hz), 2.59-2.64 (m, 2H), 2.71-2.76 (m, 2H), 3.83 (t, 2H, J = 6.4 Hz), 4.56 (p, 1H, J = 7.6 Hz), 7.50 (s, 1H). ¹³C NMR (CDCl₃, 100 MHz): δ: -5.5, 12.7, 18.2, 25.9, 39.5, 39.7, 43.5, 57.4, 59.3, 111.3, 136.3, 151.2, 164.3. HRMS (APCI): expected for C₁₇H₃₀N₅O₃Si (M+H)⁺ 380.21125. Found 380.21111. IR (neat): ν_{max} 3174, 3043, 2951, 2927, 2852, 2097, 1680 cm⁻¹. Elemental Analysis for C₁₇H₂₉N₅O₃Si: Found: C, 54.02; H, 7.44; N, 17.89. Calculated: C, 53.80; H, 7.70; N, 18.45.

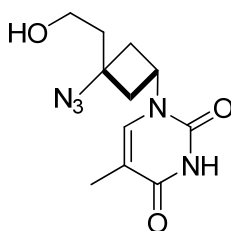
1-(3-Azido-3-(2-(*tert*-butyldimethylsilyloxy)ethyl)cyclobutyl)-5-methylpyrimidine-2,4(1*H*,3*H*)-dione (122)



Compound **122** was synthesized in a similar manner as compound **117** from compound **116** (2.00 g, 4.08 mmol, 1.0 eq) and thymine (0.77 g, 6.12 mmol, 1.5 eq). Compound **122** was purified on silica eluting with 1:1 hexanes/ethyl acetate. The desired product (0.85 g) was isolated as a white solid in 55% yield. (Rf: 0.24; 97:3 dichloromethane/methanol). mp: 123-125 °C. ¹H NMR (CDCl₃, 400 MHz): δ: 0.08 (s, 6H), 0.91 (s, 9H), 1.95 (s, 3H), 1.99 (t, 2H, J = 6.0 Hz), 2.50-2.64 (m, 4H), 3.80 (t, 2H, J = 5.6 Hz), 4.92 (p, 1H, J = 8.4 Hz), 7.02 (s, 1H), 8.06 (s, 1H). ¹³C NMR (CDCl₃, 100

MHz): δ : -5.4, 12.6, 18.2, 25.9, 39.4, 41.4, 48.2, 59.2, 60.4, 110.8, 137.1, 151.1, 164.5. HRMS (APCI): expected for $C_{17}H_{30}N_5O_3Si$ ($M+H$)⁺ 380.21125. Found 380.21117. IR (neat): ν_{max} 3170, 3035, 2951, 2919, 2856, 2097, 1684, 1251, 826 cm^{-1} . Elemental Analysis for $C_{17}H_{29}N_5O_3Si$: Found: C, 54.42; H, 7.85; N, 18.03. Calculated: C, 53.80; H, 7.70; N, 18.45.

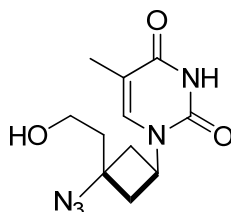
1-(3-Azido-3-(2hydroxyethyl)cyclobutyl)-5-methylpyrimidine-2,4(1*H*,3*H*)-dione
(123)



Compound **121** (0.25 g, 0.66 mmol, 1.0 eq) was dissolved in absolute ethanol (3 mL). *p*TSA (0.14 g, 0.79 mmol, 1.2 eq) was dissolved in absolute ethanol (5 mL) and was then added to compound **121** dropwise at room temperature. After stirring for 2 hours, the reaction mixture was concentrated under reduced pressure. The resulting residue was purified on silica eluting with 95:5 $CH_2Cl_2/MeOH$. The product **123** (0.14 g) was isolated as a white solid in 80% yield. (Rf: 0.08; 97:3 dichloromethane/methanol). mp: 121-123 °C. ¹H NMR (CD_3OD , 400 MHz): δ : 1.86 (s, 3H), 1.94 (t, 2H, $J = 6.8$ Hz), 2.51-2.69 (m, 4H), 3.68 (t, 2H, $J = 6.8$ Hz), 4.51 (p, 1H, $J = 8.4$ Hz), 7.45 (s, 1H). ¹³C NMR (CD_3OD , 100 MHz): δ : 12.4, 39.5, 40.8, 58.3, 59.0, 61.6, 111.2, 139.6, 152.7, 166.4. HRMS (APCI): expected for $C_{11}H_{16}N_5O_3$ ($M+H$)⁺ 266.12477. Found 266.12476. IR (neat): ν_{max} 3428, 3182, 3043, 2951, 2927, 2824, 2097, 1656, 1283, 1255 cm^{-1} . Elemental Analysis for $C_{11}H_{15}N_5O_3$: Found: C, 49.84; H, 5.69; N, 26.12. Calculated: C,

49.81; H, 5.70; N, 26.40.

1-(3-Azido-3-(2-hydroxyethyl)cyclobutyl)-5-methylpyrimidine-2,4(1H,3H)-dione
(124)



Compound **124** was synthesized in an identical manner to compound **123** from compound **122** (0.35 g, 0.91 mmol, 1.0 eq). Compound **124** (0.19 g) was isolated as a white solid in 79% yield. (Rf: 0.06; 97:3 dichloromethane/methanol). mp: 150-152 °C. ¹H NMR (CDCl₃, 400 MHz): δ: 1.81 (t, 1H, J = 4.8 Hz), 1.95 (s, 3H), 2.06 (t, 2H, J = 6.0 Hz), 2.59-2.72 (m, 4H), 3.85-3.89 (m, 2H), 4.83 (p, 1H, J = 8.8 Hz), 7.04 (s, 1H), 8.50 (s, 1H). ¹³C NMR (CD₃OD, 100 MHz): δ: 12.3, 39.8, 42.1, 54.8, 58.8, 61.6, 111.1, 139.8, 152.7, 166.5. HRMS (APCI): expected for C₁₁H₁₆N₅O₃ (M+H)⁺ 266.12477. Found 266.12439. IR (neat): ν_{max} 3448, 3186, 3035, 2951, 2927, 2892, 2816, 2109, 1676, 1287, 1263 cm⁻¹. Elemental Analysis for C₁₁H₁₅N₅O₃: Found: C, 49.77; H, 5.81; N, 26.16. Calculated: C, 49.81; H, 5.70; N, 26.40. The structure of compound **117** was established by X-ray crystallographic analysis.

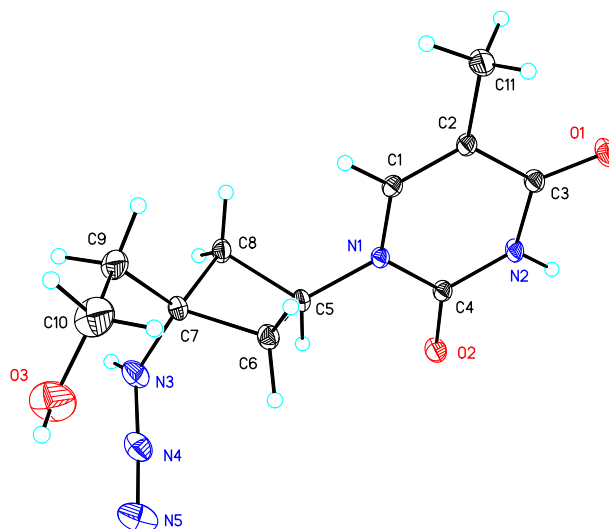


Table 15. Crystal data and structure refinement for GB982s.

Identification code	gb982s	
Empirical formula	C ₁₁ H ₁₆ N ₅ O ₃	
Formula weight	266.29	
Temperature	173(2) K	
Wavelength	0.71073 Å	
Crystal system	Monoclinic	
Space group	P2(1)/c	
Unit cell dimensions	a = 12.9908(16) Å	α = 90°.
	b = 7.7165(9) Å	β = 109.310(2)°.
	c = 13.1611(16) Å	γ = 90°.
Volume	1245.1(3) Å ³	
Z	4	
Density (calculated)	1.421 Mg/m ³	
Absorption coefficient	0.107 mm ⁻¹	
F(000)	564	
Crystal size	0.38 x 0.30 x 0.08 mm ³	
Theta range for data collection	3.11 to 32.46°.	
Index ranges	-19 ≤ h ≤ 19, -11 ≤ k ≤ 11, -19 ≤ l ≤ 19	
Reflections collected	25888	
Independent reflections	4329 [R(int) = 0.0395]	

Completeness to theta = 32.46°	96.3 %
Absorption correction	Semi-empirical from equivalents
Max. and min. transmission	0.9915 and 0.9606
Refinement method	Full-matrix least-squares on F ²
Data / restraints / parameters	4329 / 0 / 172
Goodness-of-fit on F ²	1.034
Final R indices [I > 2sigma(I)]	R1 = 0.0635, wR2 = 0.1817
R indices (all data)	R1 = 0.0759, wR2 = 0.1938
Largest diff. peak and hole	1.450 and -0.787 e.Å ⁻³

Table 16. Atomic coordinates ($\times 10^4$) and equivalent isotropic displacement parameters ($\text{\AA}^2 \times 10^3$) for GB982s. $U(\text{eq})$ is defined as one third of the trace of the orthogonalized U_{ij} tensor.

	x	y	z	U(eq)
C(1)	1776(1)	3216(2)	7991(1)	16(1)
C(2)	1001(1)	4437(2)	7863(1)	17(1)
C(3)	620(1)	4776(2)	8757(1)	17(1)
C(4)	1921(1)	2586(2)	9815(1)	15(1)
C(5)	3017(1)	901(2)	8965(1)	16(1)
C(6)	2592(1)	-633(2)	8185(1)	18(1)
C(7)	3711(1)	-666(2)	7997(1)	17(1)
C(8)	3927(1)	1197(2)	8467(1)	18(1)
C(9)	3732(2)	-899(2)	6857(1)	26(1)
C(10)	3105(2)	-2460(3)	6271(2)	41(1)
C(11)	475(2)	5353(2)	6814(1)	28(1)
N(1)	2244(1)	2306(2)	8933(1)	15(1)
N(2)	1136(1)	3842(2)	9683(1)	17(1)
N(3)	4519(1)	-1836(2)	8778(1)	26(1)
N(4)	4174(1)	-3254(2)	8944(1)	27(1)
N(5)	3948(2)	-4576(2)	9172(2)	42(1)
O(1)	-123(1)	5792(2)	8733(1)	27(1)
O(2)	2284(1)	1791(2)	10667(1)	24(1)
O(3)	3564(2)	-4002(2)	6789(1)	49(1)

Table 17. Bond lengths [Å] and angles [°] for GB982s.

C(1)-C(2)	1.3483(18)
C(1)-N(1)	1.3787(17)
C(1)-H(1A)	0.9500
C(2)-C(3)	1.4422(18)
C(2)-C(11)	1.500(2)
C(3)-O(1)	1.2361(17)
C(3)-N(2)	1.3830(18)
C(4)-O(2)	1.2274(17)
C(4)-N(2)	1.3755(17)
C(4)-N(1)	1.3766(17)
C(5)-N(1)	1.4688(17)
C(5)-C(6)	1.545(2)
C(5)-C(8)	1.5466(19)
C(5)-H(5A)	1.0000
C(6)-C(7)	1.553(2)
C(6)-H(6A)	0.9900
C(6)-H(6B)	0.9900
C(7)-N(3)	1.503(2)
C(7)-C(9)	1.522(2)
C(7)-C(8)	1.5528(19)
C(8)-H(8A)	0.9900
C(8)-H(8B)	0.9900
C(9)-C(10)	1.514(3)
C(9)-H(9A)	0.9900
C(9)-H(9B)	0.9900
C(10)-O(3)	1.403(3)
C(10)-H(10A)	0.9900
C(10)-H(10B)	0.9900
C(11)-H(11A)	0.9800
C(11)-H(11B)	0.9800
C(11)-H(11C)	0.9800
N(2)-H(2A)	0.8800
N(3)-N(4)	1.230(2)

N(3)-H(3A)	0.8800
N(4)-N(5)	1.129(2)
O(3)-H(3B)	0.8400
C(2)-C(1)-N(1)	123.86(12)
C(2)-C(1)-H(1A)	118.1
N(1)-C(1)-H(1A)	118.1
C(1)-C(2)-C(3)	117.92(12)
C(1)-C(2)-C(11)	122.54(12)
C(3)-C(2)-C(11)	119.41(12)
O(1)-C(3)-N(2)	119.97(12)
O(1)-C(3)-C(2)	124.70(13)
N(2)-C(3)-C(2)	115.32(12)
O(2)-C(4)-N(2)	120.86(12)
O(2)-C(4)-N(1)	124.03(12)
N(2)-C(4)-N(1)	115.10(12)
N(1)-C(5)-C(6)	117.11(12)
N(1)-C(5)-C(8)	119.34(11)
C(6)-C(5)-C(8)	89.22(10)
N(1)-C(5)-H(5A)	109.9
C(6)-C(5)-H(5A)	109.9
C(8)-C(5)-H(5A)	109.9
C(5)-C(6)-C(7)	88.30(10)
C(5)-C(6)-H(6A)	113.9
C(7)-C(6)-H(6A)	113.9
C(5)-C(6)-H(6B)	113.9
C(7)-C(6)-H(6B)	113.9
H(6A)-C(6)-H(6B)	111.1
N(3)-C(7)-C(9)	111.53(12)
N(3)-C(7)-C(8)	106.88(12)
C(9)-C(7)-C(8)	116.25(12)
N(3)-C(7)-C(6)	112.35(12)
C(9)-C(7)-C(6)	118.82(13)
C(8)-C(7)-C(6)	88.70(10)
C(5)-C(8)-C(7)	88.24(10)
C(5)-C(8)-H(8A)	113.9
C(7)-C(8)-H(8A)	113.9

C(5)-C(8)-H(8B)	113.9
C(7)-C(8)-H(8B)	113.9
H(8A)-C(8)-H(8B)	111.1
C(10)-C(9)-C(7)	114.45(15)
C(10)-C(9)-H(9A)	108.6
C(7)-C(9)-H(9A)	108.6
C(10)-C(9)-H(9B)	108.6
C(7)-C(9)-H(9B)	108.6
H(9A)-C(9)-H(9B)	107.6
O(3)-C(10)-C(9)	110.87(19)
O(3)-C(10)-H(10A)	109.5
C(9)-C(10)-H(10A)	109.5
O(3)-C(10)-H(10B)	109.5
C(9)-C(10)-H(10B)	109.5
H(10A)-C(10)-H(10B)	108.1
C(2)-C(11)-H(11A)	109.5
C(2)-C(11)-H(11B)	109.5
H(11A)-C(11)-H(11B)	109.5
C(2)-C(11)-H(11C)	109.5
H(11A)-C(11)-H(11C)	109.5
H(11B)-C(11)-H(11C)	109.5
C(4)-N(1)-C(1)	120.77(11)
C(4)-N(1)-C(5)	119.20(11)
C(1)-N(1)-C(5)	119.75(11)
C(4)-N(2)-C(3)	126.95(11)
C(4)-N(2)-H(2A)	116.5
C(3)-N(2)-H(2A)	116.5
N(4)-N(3)-C(7)	116.23(14)
N(4)-N(3)-H(3A)	121.9
C(7)-N(3)-H(3A)	121.9
N(5)-N(4)-N(3)	173.42(19)
C(10)-O(3)-H(3B)	109.5

Symmetry transformations used to generate equivalent atoms:

Table 18. Anisotropic displacement parameters ($\text{\AA}^2 \times 10^3$) for GB982s. The anisotropic displacement factor exponent takes the form: $-2\pi^2 [h^2 a^{*2} U_{11} + \dots + 2 h k a^* b^* U_{12}]$

	U11	U22	U33	U23	U13	U12
C(1)	20(1)	18(1)	13(1)	1(1)	9(1)	3(1)
C(2)	19(1)	20(1)	14(1)	2(1)	8(1)	5(1)
C(3)	20(1)	20(1)	14(1)	1(1)	7(1)	5(1)
C(4)	18(1)	17(1)	13(1)	-1(1)	7(1)	3(1)
C(5)	17(1)	15(1)	17(1)	-1(1)	8(1)	3(1)
C(6)	19(1)	16(1)	22(1)	-4(1)	9(1)	0(1)
C(7)	19(1)	15(1)	19(1)	-2(1)	9(1)	2(1)
C(8)	18(1)	16(1)	23(1)	-4(1)	11(1)	0(1)
C(9)	37(1)	24(1)	22(1)	-5(1)	16(1)	-1(1)
C(10)	58(1)	41(1)	25(1)	-12(1)	16(1)	-9(1)
C(11)	33(1)	37(1)	18(1)	10(1)	13(1)	16(1)
N(1)	18(1)	15(1)	13(1)	0(1)	8(1)	4(1)
N(2)	20(1)	21(1)	13(1)	1(1)	9(1)	7(1)
N(3)	22(1)	21(1)	31(1)	1(1)	5(1)	4(1)
N(4)	29(1)	25(1)	26(1)	1(1)	6(1)	7(1)
N(5)	49(1)	27(1)	46(1)	9(1)	10(1)	3(1)
O(1)	30(1)	35(1)	20(1)	6(1)	13(1)	18(1)
O(2)	29(1)	28(1)	16(1)	6(1)	11(1)	12(1)
O(3)	66(1)	35(1)	43(1)	-14(1)	15(1)	-15(1)

Table 19. Hydrogen coordinates ($\times 10^4$) and isotropic displacement parameters ($\text{\AA}^2 \times 10^3$) for GB982s.

	x	y	z	U(eq)
H(1A)	2013	2968	7397	19
H(5A)	3342	461	9719	19
H(6A)	1970	-334	7535	22
H(6B)	2437	-1691	8535	22
H(8A)	4661	1358	9005	21
H(8B)	3760	2119	7913	21
H(9A)	3427	155	6436	31
H(9B)	4501	-1006	6885	31
H(10A)	2336	-2377	6245	49
H(10B)	3113	-2472	5522	49
H(11A)	823	4986	6293	43
H(11B)	562	6608	6926	43
H(11C)	-303	5065	6539	43
H(2A)	941	4077	10248	21
H(3A)	5202	-1523	9099	31
H(3B)	3193	-4850	6465	73

Table 20. Torsion angles [$^\circ$] for GB982s.

N(1)-C(1)-C(2)-C(3)	-1.7(2)
N(1)-C(1)-C(2)-C(11)	-177.49(15)
C(1)-C(2)-C(3)-O(1)	-176.14(16)
C(11)-C(2)-C(3)-O(1)	-0.2(2)
C(1)-C(2)-C(3)-N(2)	2.6(2)
C(11)-C(2)-C(3)-N(2)	178.57(15)
N(1)-C(5)-C(6)-C(7)	140.63(12)
C(8)-C(5)-C(6)-C(7)	17.71(11)
C(5)-C(6)-C(7)-N(3)	90.10(12)

C(5)-C(6)-C(7)-C(9)	-137.14(13)
C(5)-C(6)-C(7)-C(8)	-17.64(11)
N(1)-C(5)-C(8)-C(7)	-138.71(12)
C(6)-C(5)-C(8)-C(7)	-17.71(11)
N(3)-C(7)-C(8)-C(5)	-95.37(12)
C(9)-C(7)-C(8)-C(5)	139.38(14)
C(6)-C(7)-C(8)-C(5)	17.62(11)
N(3)-C(7)-C(9)-C(10)	80.2(2)
C(8)-C(7)-C(9)-C(10)	-156.98(16)
C(6)-C(7)-C(9)-C(10)	-53.0(2)
C(7)-C(9)-C(10)-O(3)	-63.2(2)
O(2)-C(4)-N(1)-C(1)	178.14(14)
N(2)-C(4)-N(1)-C(1)	-1.54(19)
O(2)-C(4)-N(1)-C(5)	4.3(2)
N(2)-C(4)-N(1)-C(5)	-175.41(12)
C(2)-C(1)-N(1)-C(4)	1.1(2)
C(2)-C(1)-N(1)-C(5)	174.97(14)
C(6)-C(5)-N(1)-C(4)	114.07(15)
C(8)-C(5)-N(1)-C(4)	-140.25(13)
C(6)-C(5)-N(1)-C(1)	-59.87(17)
C(8)-C(5)-N(1)-C(1)	45.81(18)
O(2)-C(4)-N(2)-C(3)	-176.77(15)
N(1)-C(4)-N(2)-C(3)	2.9(2)
O(1)-C(3)-N(2)-C(4)	175.36(15)
C(2)-C(3)-N(2)-C(4)	-3.5(2)
C(9)-C(7)-N(3)-N(4)	-92.33(17)
C(8)-C(7)-N(3)-N(4)	139.61(14)
C(6)-C(7)-N(3)-N(4)	43.92(18)
C(7)-N(3)-N(4)-N(5)	-170.8(17)

Symmetry transformations used to generate equivalent atoms:

Table 21. Hydrogen bonds for GB982s [\AA and $^\circ$].

D-H...A	d(D-H)	d(H...A)	d(D...A)	$\angle(\text{DHA})$
N(2)-H(2A)...O(1)#1	0.88	1.97	2.8234(16)	163.0
O(3)-H(3B)...O(2)#2	0.84	1.98	2.8196(19)	178.0

Symmetry transformations used to generate equivalent atoms:

#1 $-x, -y+1, -z+2$ #2 $x, -y-1/2, z-1/2$

1.7 References

- (1) <http://www.avert.org/worldstats.htm> **2009**. UNAIDS (2009, November). AIDS epidemic update.
- (2) Painter, G. R.; Almond, M. R.; Mao, S.; Liotta, D. C. *Current Topics in Medicinal Chemistry* **2004**, 4, 1035-1044.
- (3) Goldschmidt, V.; Marquet, R. *The International Journal of Biochemistry & Cell Biology* **2004**, 36, 1687-1705.
- (4) Selmi, B.; Boretto, J.; Sarfati, S. R.; Guerreiro, C.; Canard, B. *The Journal of Biological Chemistry* **2001**, 276, 48466-48472.
- (5) Parikh, U. M.; Bachelier, L.; Koontz, D.; Mellors, J. W. *Journal of Virology* **2006**, 80, 4971-4977.
- (6) Feng, J. Y.; Myrick, F. T.; Margot, N. A.; Mulamba, G. B.; Rimsky, L.; Borroto-Esoda, K. *Nucleosides, Nucleotides, and Nucleic Acids* **2006**, 25, 89-107.
- (7) Sluis-Cremer, N.; Sheen, C.; Zelina, S.; Torres, P. S. A.; Parikh, U. M.; Mellors, J. W. *Antimicrobial Agents and Chemotherapy* **2007**, 51, 48-53.
- (8) Zu, T.; Korber, B. T.; Nahmias, A. J.; Hooper, E.; Sharp, P. M.; Ho, D. D. *Nature* **1998**, 391, 594-597.
- (9) Gilbert, M. T. P.; Rambaut, A.; Wlasiuk, G.; Spira, T. J.; Pitchenik, A. E.; Worobey, M. *Proceedings of the National Academy of Sciences* **2007**, 104, 18566-18570.
- (10) http://data.unaids.org/pub/EPISlides/2007/2007_epiupdate_en.pdf **2007**.
- (11) <http://www.nwabr.org/education/hivrequest.html> **2009**. HIV replication image is credited to Dave Ehlert and used with the permission of the HIV Web Study.

- (12) Chan, D. C.; Kim, P. S. *Cell* **1998**, 93, 681-684.
- (13) Wyatt, R.; Sodroski, J. *Science* **1998**, 280, 1884-1889.
- (14) Chan, D. C.; Fass, D.; Berger, J. M.; Kim, P. S. *Cell* **1997**, 89, 263-273.
- (15) Zheng, Y.; Lovsin, N.; Peterlin, B. M. *Immunology Letters* **2005**, 97, 225-234.
- (16) Somasunderam, A.; Ferguson, M. R.; Rojo, D. R.; Thiviyanathan, V.; Li, X.; O'Brien, W. A.; Gorenstein, D. G. *Biochemistry* **2005**, 44, 10388-10395.
- (17) Craigie, R. *The Journal of Biological Chemistry* **2001**, 276, 23213-23216.
- (18) Hiscott, J.; Kwon, H.; Genin, P. *The Journal of Clinical Investigation* **2001**, 107, 143-151.
- (19) Pollard, V. W. *Annual Review of Microbiology* **1998**, 52, 491-532.
- (20) Bukrinskaya, A. G. *Archives of Virology* **2004**, 149, 1067-1082.
- (21) <http://www.fda.gov/oashi/aids/virals.html> **2008**.
- (22) http://www.aidsinfonet.org/fact_sheets/view/408 **2008**.
- (23) <http://www.thebody.com/content/art13630.html> **1999**.
- (24) Marchand, B.; Tchesnokov, E. P.; Gotte, M. *The Journal of Biological Chemistry* **2007**, 282, 3337-3346.
- (25) Lisziewicz, J.; Foli, A.; Wainberg, M.; Lori, F. *Drug Safety* **2003**, 26, 605-624.
- (26) <http://www.aidsmeds.com/list.shtml> **2009**.
- (27) Strizki, J. M.; Tremblay, C.; Xu, S.; Wojcik, L.; Wagner, N.; Gonsiorek, W.; Hipkin, R. W.; Chou, C.; Pugliese-Sivo, C.; Xiao, Y.; Tagat, J. R.; Cox, K.; Priestley, T.; Sorota, S.; Huang, W.; Hirsch, M.; Reyes, G. R.; Baroudy, B. M. *Antimicrobial Agents and Chemotherapy* **2005**, 49, 4911-4919.
- (28) Shimura, K.; Kodama, E.; Sakagami, Y.; Matsuzaki, Y.; Watanabe, W.;

- Yamataka, K.; Watanabe, Y.; Ohata, Y.; Doi, S.; Sato, M.; Kano, M.; Ikeda, S.; Matsuoka, M. *Journal of Virology* **2008**, 82, 764-774.
- (29) Zhou, J.; Huang, L.; Hachey, D. L.; Chen, C. H.; Aiken, C. *The Journal of Biological Chemistry* **2005**, 280, 42149-42155.
- (30) Harris, K. S.; Brabant, W.; Styrchak, S.; Gall, A.; Daifuku, R. *Antiviral Research* **2005**, 67, 1-9.
- (31) Himmel, D. M.; Sarafianos, S. G.; Dharmasena, S.; Hossain, M. M.; McCoy-Simandle, K.; Ilina, T.; Clark, A. D.; Knight, J. L.; Julias, J. G.; Clark, P. K.; Krogh-Jespersen, K.; Levy, R. M.; Hughes, S. H.; Parniak, M. A.; Arnold, E. *ACS Chemical Biology* **2006**, 1, 702-712.
- (32) Tramontano, E.; Esposito, F.; Badas, R.; Di Santo, R.; Costi, R.; La Colla, P. *Antiviral Research* **2005**, 65, 117-124.
- (33) Wendeler, M.; Lee, H.; Bermingham, A.; Miller, J. T.; Chertov, O.; Bona, M. K.; Baichoo, N. S.; Ehteshami, M.; Beutler, J.; O'Keefe, B. R.; Gotte, M.; Kvaratskhelia, M.; Le Grice, S. *ACS Chemical Biology* **2008**, 3, 635-644.
- (34) Budihas, S. R.; Gorshkova, I.; Gaidamakov, S.; Wamiru, A.; Bona, M. K.; Parniak, M. A.; Crouch, R. J.; McMahon, J. B.; Beutler, J. A.; Le Grice, S. F. J. *Nucleic Acids Research* **2005**, 33, 1249-1256.
- (35) Borkow, G.; Fletcher, R. S.; Barnard, J.; Arion, D.; Motakis, D.; Dmitrienko, G. I.; Parniak, M. A. *Biochemistry* **1997**, 36, 3179-3185.
- (36) Mizuochi, T.; Nakata, M. *Journal of Infection Chemotherapy* **1999**, 5, 190-195.
- (37) Kakushima, M.; Masuyoshi, S.; Hirano, M.; Shinoda, M.; Ohta, A.; Kamei, H.; Oki, T. *Antimicrobial Agents and Chemotherapy* **1991**, 35, 2185-2190.

- (38) Tang, C.; Loeliger, E.; Kinde, I.; Kyere, S.; Mayo, K.; Barklis, E.; Sun, Y.; Huang, M.; Summers, M. F. *Journal of Molecular Biology* **2003**, 327, 1013-1020.
- (39) Nathans, R.; Cao, H.; Sharova, N.; Ali, A.; Sharkey, M.; Stranska, R.; Stevenson, M.; Rana, T. M. *Nature Biotechnology* **2008**, 26, 1187-1192.
- (40) Xiao, Z.; Ehrlich, E.; Luo, K.; Xiong, Y.; Yu, X. *The FASEB Journal* **2007**, 21, 217-222.
- (41) Fanf, L.; Landau, N. R. *Virology* **2007**, 359, 162-169.
- (42) Sarafianos, S. G.; Marchand, B.; Das, K.; Himmel, D. M.; Parniak, M. A.; Hughes, S. H.; Arnold, E. *Journal of Molecular Biology* **2009**, 385, 693-713.
- (43) Schatz, O.; Mous, J.; Le Grice, S. F. J. *The EMBO Journal* **1990**, 9, 1171-1176.
- (44) Wisniewski, M.; Balakrishnan, M.; Palaniappan, C.; Fay, P. J.; Bambara, R. A. *Proceedings of the National Academy of Sciences* **2000**, 97, 11978-11983.
- (45) Tong, W.; Lu, C.; Sharma, S. K.; Matsuura, S.; So, A. G.; Scott, W. A. *Biochemistry* **1997**, 36, 5749-5757.
- (46) <http://pathmicro.med.sc.edu/lecture/hiv14a.htm> **2008**.
- (47) Mansky, L. M.; Temin, H. M. *Journal of Virology* **1995**, 69, 5087-5094.
- (48) White, K. L.; Margot, N. A.; Wrin, T.; Petropoulos, C. J.; Miller, M. D.; Naeger, L. K. *Antimicrobial Agents and Chemotherapy* **2002**, 46, 3437-3446.
- (49) Parikh, U. M.; Zelina, S.; Sluis-Cremer, N.; Mellors, J. W. *AIDS* **2007**, 21, 1405-1414.
- (50) Deval, J.; Navarro, J.; Selmi, B.; Courcambeck, J.; Boretto, J.; Halfon, P.; Garrido-Urbani, S.; Sire, J.; Canard, B. *The Journal of Biological Chemistry*

- 2004**, 279, 25489-25496.
- (51) <http://hivdb.stanford.edu/index.html> **2008**.
- (52) Parikh, U. M.; Koontz, D. L.; Chu, C. K.; Schinazi, R. F.; Mellors, J. W. *Antimicrobial Agents and Chemotherapy* **2005**, 49, 1139-1144.
- (53) Sluis-Cremer, N.; Arion, D.; Parikh, U.; Koontz, D.; Schinazi, R. F.; Mellors, J. W.; Parniak, M. A. *The Journal of Biological Chemistry* **2005**, 280, 29047-29052.
- (54) Czernecki, S.; Valery, J. *Synthesis* **1991**, 239-240.
- (55) Herdewijn, P. A. M. *The Journal of Organic Chemistry* **1988**, 53, 5050-5053.
- (56) Norbeck, D. W.; Kramer, J. B. *Journal of the American Chemical Society* **1988**, 110, 7217-7218.
- (57) Gumina, G.; Chu, C. K. *Organic Letters* **2002**, 4, 1147-1149.
- (58) Slusarchyk, W. A.; Young, M. G.; Bisacchi, G. S.; Hockstein, D. R.; Zahler, R. *Tetrahedron Letters* **1989**, 30, 6453-6456.
- (59) Gharbaoui, T.; Legraverend, M.; Ludwig, O.; Bisagni, E.; Aubertin, A.; Chertanova, L. *Tetrahedron* **1995**, 51, 1641-1652.
- (60) Jung, M. E.; Sledeski, A. W. *Journal of the Chemical Society, Chemical Communications* **1993**, 589-591.
- (61) Moore, H. W.; Yerxa, B. R. *Advances in Strain in Organic Chemistry* **1995**, 4, 81-162.
- (62) Dillon, J. L.; Gao, Q.; Dillon, E. A.; Adams, N. *Tetrahedron Letters* **1997**, 38, 2231-2234.
- (63) Hassner, A.; Dillon, J. L. *Journal of Organic Chemistry* **1983**, 48, 3382-3386.

- (64) Danheiser, R. L.; Savariar, S. *Tetrahedron Letters* **1987**, 28, 3299-3302.
- (65) Kowalski, C. J.; Lal, G. S. *Journal of the American Chemical Society* **1988**, 110, 3693-3695.
- (66) Liebeskind, L. S.; Stone, G. B.; Zhang, S. *Journal of Organic Chemistry* **1994**, 59, 7917-7920.
- (67) Adamo, I.; Benedetti, F.; Berti, F.; Campaner, P. *Organic Letters* **2006**, 8, 51-54.
- (68) Feldman, K. S.; Iyer, M. R.; Lopez, C. S.; Faza, O. N. *Journal of Organic Chemistry* **2008**, 73, 5090-5999.
- (69) Chu, C. K.; Beach, J. W.; Ullas, G. V.; Kosugi, Y. *Tetrahedron Letters* **1988**, 5349-5352.
- (70) Lakshmipathi, P.; Rao, A. V. R. *Tetrahedron Letters* **1997**, 2551-2552.
- (71) Guerin, D. J.; Hortsmann, T. E.; Miller, S. J. *Organic Letters* **1999**, 1, 1107-1109.
- (72) Castrica, L.; Fringuelli, F.; Gregoli, L.; Pizzo, F.; Vaccaro, L. *Journal of Organic Chemistry* **2006**, 71, 9536-9539.
- (73) Cotterill, I. C.; Roberts, S. M. *Journal of the Chemical Society Perkin Transactions I* **1992**, 2585-2586.
- (74) Jacobs, G. A.; Tino, J. A.; Zahler, R. *Tetrahedron Letters* **1989**, 30, 6955-6958.
- (75) Danappe, S.; Pal, A.; Alexandre, C.; Aubertin, A.; Bourgougnon, N.; Huet, F. *Tetrahedron* **2005**, 61, 5782-5787.
- (76) Johnson, C. R.; De Jong, R. L. *Journal of Organic Chemistry* 1992, 57, 594-599.
- (77) Marquez, V. E.; Comin, M. J. *Nucleosides, Nucleotides, and Nucleic Acids* **2007**, 26, 585-588.
- (78) Madhavan, G. V. B.; Martn, J. C. *Journal of Organic Chemistry* **1986**, 51, 1287-

- 1293.
- (79) Bhushan, R. G.; Vince, R. *Bioorganic and Medicinal Chemistry* **2002**, 10, 2325-2333.
- (80) Moffatt, J. G. *Canadian Journal of Chemistry* **1964**, 42, 599-604.
- (81) Gaur, R. K.; Sproat, B. S.; Krupp, G. *Tetrahedron Letters* **1992**, 33, 3301-3304.
- (82) Kaiwar, V.; Reese, C. B.; Gray, E. J.; Neidle, S. *Journal of the Chemical Society, Perkin Transactions I* **1995**, 2281-2287.
- (83) Frieden, M.; Giraud, M.; Reese, C. B.; Song, Q. L. *Journal of the Chemical Society, Perkin Transactions I* **1998**, 2827-2832.
- (84) Liotta, D. C.; Mao, S.; Hager, M. **2006**, WO2006063281.
- (85) Li, Y.; Mao, S.; Hager, M. W.; Becnel, K. D.; Schinazi, R. F.; Liotta, D. C. *Bioorganic and Medicinal Chemistry Letters* **2007**, 17, 3398-3401.
- (86) Henlin, J.; Jaekel, K.; Moser, P.; Rink, H.; Spieser, E.; Baschang, G. *Angewandte Chemie International Edition* **1992**, 31, 482-484.
- (87) Prakash, C.; Saleh, S.; Blair, I.A. *Tetrahedron Letters* **1989**, 30, 19-22.
- (88) Schinazi, R. F.; Sommadossi, J.; Saalman, V.; Cannon, D. L.; Xie, M.; Hart, G. C.; Smith, G. A.; Hahn, E. F. *Antimicrobial Agents and Chemotherapy* **1990**, 34, 1061-1067.
- (89) Stuyver, L. J.; Lostia, S.; Adams, M.; Mathew, J. S.; Pai, B. S.; Grier, J.; Tharnish, P. M.; Choi, Y.; Chong, Y.; Choo, H.; Chu, C. K.; Otto, M. J.; Schinazi, R. F. *Antimicrobial Agents and Chemotherapy* **2002**, 46, 3854-3860.
- (90) <http://home.ncifcrf.gov/hivdrp/rt/overview.html>

Part II: Synthesis and Evaluation of Truncated Triptolide Analogs to Suppress Chronic Inflammation

2.1 Statement of Purpose

A healthy immune system is necessary in identifying and eliminating pathogens and tumor cells; however, an overactive immune system that is unable to recognize its “self” constituents, called autoimmunity, can lead to disease. In humans, autoimmunity can form against many cell types and tissues leading to chronic inflammation. If untreated, the autoimmune response and the resulting inflammation can damage tissues resulting in severe functional disabilities.

Autoimmune and inflammatory diseases are among the most common illnesses in the United States along with heart disease and cancer.¹ Collectively, autoimmune and inflammatory diseases affect between 14 and 23 million Americans but may be as high 50 million.^{2,3} Women are 2.7 times more likely than men to acquire an autoimmune disease, thus accounting for approximately 75% of all cases.³ Current trends indicate that the number of autoimmune and chronic inflammatory diseases is increasing as one million new cases are diagnosed each year.⁴

There are currently between 80 and 100 known autoimmune diseases that usually result in chronic inflammation.¹ Autoimmune diseases can be classified as either being systemic or localized.⁵ Examples of systemic autoimmune diseases are rheumatoid arthritis (RA), lupus, and scleroderma. Localized autoimmune diseases include type 1 diabetes, Graves’ disease, and Crohn’s disease.

The United States is the largest market for autoimmune diseases as Americans spend between \$87 and \$100 billion on total health costs associated with autoimmune

diseases each year.^{4,6} This figure is expected to continue to grow and could reach \$400 billion in the near future.⁴ The global market for therapeutics used in the treatment of autoimmune diseases is approximately \$18 billion.⁶ This figure is also expected to continue to grow and could reach \$50 billion by 2015.⁷ Nearly half (48%) of the current costs for therapeutics is spent on the treatment for rheumatoid arthritis.⁶

The current drug treatments for autoimmune diseases can be divided into five major classes.^{8,9,10} Non-steroidal anti-inflammatory drugs (NSAIDs) can be used to treat the inflammation associated with autoimmune diseases. NSAIDs can help reduce swelling, stiffness, and pain but are unable to alter the progression of the disease.^{10,35} Analgesics can be used to help manage the pain associated with inflammation but are unable to reduce inflammation and tissue damage.³¹ Steroids possess potent anti-inflammatory properties but cause serious side effects with long term usage.³⁶ Small molecule disease modifying drugs such as azathioprine, cyclosporin, gold salts, methotrexate, and anti-malaria drugs have been used extensively in the treatment of autoimmune diseases.¹⁰ These drugs were approved for other indications but have been shown to be useful in treating autoimmune diseases. These drugs interfere with the immune system and can thus prevent tissue damage and inflammation. Drugs in this class can take weeks before a clinical affect can be seen and can increase the risk of infection. In addition, drugs in this class have been known to also suffer from poor tolerability. Finally, biologics, a new class of drugs, are antibody/receptor fusion proteins that target specific components of the immune system responsible for the overactive immune response and inflammation.¹⁰ Biologics may also require weeks before a clinical response is seen and are usually given in combination with disease modifying drugs and

NSAIDS. Biologics are administered by injection, increase the risk of infection, and may stay in circulation for weeks.⁹ In addition, biologics can cost a patient \$15,000 to \$20,000 per year.⁵¹

While targeting specific components of the immune system responsible for the autoimmune response and inflammation have made biologics successful, the drawbacks and limitations associated with these drugs bring to light many unmet needs in the drug market. In order to address these unmet needs, the Liotta group has used the potent anti-inflammatory natural product triptolide, isolated from *Tripterygium wilfordii*, as inspiration for developing orally bioavailable small molecule immunosuppressants (Figure 1).⁵³ We believe the truncated triptolide analogues will avoid the high toxicity associated with triptolide while retaining immunosuppressive capabilities.

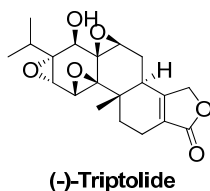


Figure 1. Structure of (-)-triptolide

2.2 Introduction

2.2.1 Current Status of Autoimmune and Inflammatory Diseases

The first traces of modern autoimmune and inflammatory diseases date back to as early as 4500 BC.¹¹ There are many written accounts from ancient and biblical times describing diseases that bare resemblance to current diseases such as psoriasis and arthritis. It was not until the second half of the 20th century that autoimmune and inflammatory diseases began to be understood. However, even today questions remain about the underlying causes of these diseases.¹²

A healthy immune system is necessary for preventing disease by identifying and eliminating pathogens.¹² It is important for the immune system to be able to distinguish between foreign and self components.¹² When the immune system is unable to do this, autoantibodies are developed, and the immune system attacks self components.¹² While a low level of autoimmunity in humans is important for eliminating tumor cells, an overactive autoimmune response leads to diseases such as type 1 diabetes, lupus, Graves' disease, and rheumatoid arthritis.¹² As a result of an overactive immune response, many downstream signaling molecules such as tumor necrosis factor- α (TNF- α) and interleukin-1 (IL-1) are produced.¹³ The combination of autoimmunity and pro-inflammatory signaling molecules results in the inflammation and destruction of the targeted tissue.¹²

Autoimmune diseases can form in many different types of cells and tissues and can be classified as either systemic or localized. Autoimmune and inflammatory diseases along with heart disease and cancer are the most common illnesses in the United States.¹ Currently, 14 to 23 million Americans, of which 75% are women, suffer from

autoimmune and inflammatory diseases (Figure 2).^{2,3} Current trends indicate there are approximately one million new diagnoses each year.⁴ Table 1 shows a list of the most common autoimmune diseases.

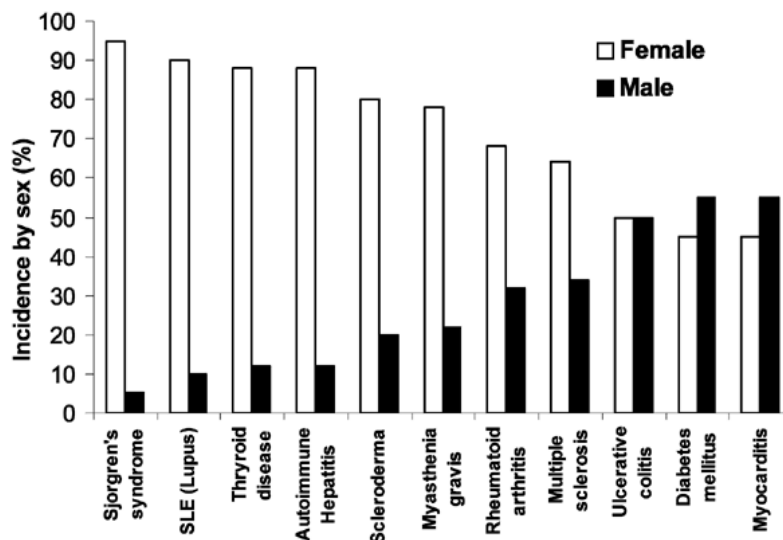


Figure 2. Incidence of common autoimmune diseases by sex¹⁴

Name of Autoimmune Disease	Annual Incidence*	Prevalence*	Pathophysiology
Crohn's Disease	6 to 7.1 in 100,000	1 in 544	autoimmune response targeted at the GI tract
Graves' Disease	1 in 2,000	1 in 89	antibodies produced against the receptor for thyroid-stimulating hormone
Hashimoto's Thyroiditis	0.8 to 1.3 in 1,000	1 in 182	T cells attack thyroid
Lupus (SLE)	1.8 to 7.6 in 100,000	1 in 200	many clinical manifestations. caused by antibodies to cell nucleus
Multiple Sclerosis	1 in 700	1 in 1,000	autoimmunity against the central nervous system
Psoriasis	6.5 in 100,000	1 in 50	autoimmune disease that affects skin and joints
Rheumatoid Arthritis	3 in 10,000	1 in 100	chronic, systemic inflammation disorder affecting mainly the joints. maybe caused by abnormal B cell/T cell interaction
Sjogren's Syndrome	1 in 200	1 in 90	immune cells attack exocrine glands that produce tears and saliva
Type I Diabetes	40 in 10,000	1 in 800	autoimmune response against insulin-producing beta cells of pancreas
* Estimates			

Table 1. List of common autoimmune diseases in the United States¹⁵⁻²³

2.2.2 Overview of the Immune System

Edward Jenner is credited as having founded the relatively new science of immunology with his 1796 discovery that cowpox provided humans with protection

against smallpox.²⁴ Following this triumph was the work of Robert Koch. In the late 19th century, Koch proved that microorganisms were responsible for infectious diseases.²⁴ Today, four categories of disease-causing microorganisms are recognized: viruses, bacteria, pathogenic fungi, and complex eukaryotic organisms collectively termed parasites. Another notable triumph occurred in the 1880s when Louis Pasteur developed a vaccine against cholera in chickens as well as a vaccine for rabies.²⁴ These breakthroughs intensified the search for the mechanism of protection and led to the development of immunology.

Other notable figures that contributed early in the development of immunology were Emil von Behring and Shibasaburo Kitasato. In the 1890s they discovered that serum from animals immune to diphtheria or tetanus contained a specific “antitoxic activity” that were later called antibodies.²⁴ This specific immune response that utilizes antibodies against a particular pathogen is known as an adaptive immune response. At the time von Behring and Kitasato were developing serum therapy, the Russian immunologist Elie Metchnikoff was gathering data showing many microorganisms could be engulfed by phagocytic cells, which he called macrophages.²⁴ These cells are a key component of the innate immune response and are non-specific.

The following sections will provide a foundation for understanding the mechanisms that allow the immune system to function. Both the innate and adaptive immune responses will be covered focusing on the cells and components that are vital for each to function properly. Finally, the mechanisms that result in autoimmunity and chronic inflammation will be discussed.

2.2.2.1 Innate immunity

The frontline defense humans have against infection are the epithelial surfaces that line our bodies.¹³ Pathogens may bind and cross internal mucosal surfaces such as the airway, gastrointestinal tract, or reproductive tract (Figure 3). Pathogens may also pass through external epithelial surfaces through wounds, abrasions, or insect bites. The epithelial surfaces contain mechanical barriers such as tight junctions between epithelial cells as well as mucus movement by cilia, chemical barriers such as antibacterial peptides and lysozymes, and microbiological barriers such as normal flora to help prevent infection.¹³ If a microorganism does manage to cross the epithelial barrier and begins to replicate, it is immediately recognized, ingested, and killed by phagocytes.

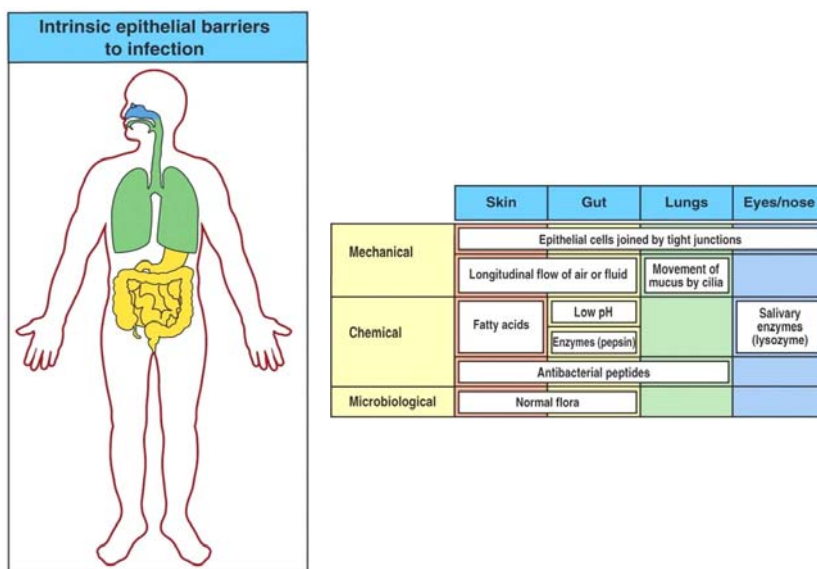


Figure 3. Epithelial barriers to infection¹³

Innate immunity is a non-specific immune response that does not result in long term immunity towards a pathogen.¹³ An innate immune response occurs within a few minutes or hours after infection. During the innate immune response, a microorganism that crosses the epithelial barrier and begins to replicate in the tissues of the host is most

often recognized by macrophages that reside in these tissues. Neutrophils are phagocytic cells that are short-lived and abundant in blood. During an encounter with a microorganism, macrophages are able to recruit neutrophils in large number to sites of infection. Both cell types use many receptors to recognize common features of microorganisms. Some of the common receptors used are the macrophage mannose receptor, scavenger receptors that bind many negatively charged ligands, and CD14 which binds lipopolysaccharide (LPS).¹³ Ligation of a pathogen to cell-surface receptors results in phagocytosis of the pathogen. The pathogen is internalized in a vesicle known as a phagosome and is destroyed as the phagosome becomes acidified.¹³ In addition, lysosomes are vesicles contained within macrophages and neutrophils that contain antimicrobial enzymes. Lysosomes fuse with the phagosome intracellularly thus destroying the pathogen.¹³ Other toxic products produced by macrophages and neutrophils used in the destruction of pathogens include nitric oxide, superoxide anion, and hydrogen peroxide.¹³

Pattern recognition is vital for cells of the innate immune system to identify pathogens.¹³ Receptors on macrophages and neutrophils identify features common to many pathogens resulting in many important functions. Phagocytic receptors ingest pathogens they recognize. Some receptors are chemotactic and bind various biomolecules produced by pathogens such as bacterial *N*-formylated peptides. By recognizing biomolecules produced by pathogens, chemotactic receptors are able to guide macrophages and neutrophils to sites of infection (Figure 4). A third function performed by some phagocytic receptors as well as specialized signaling receptors is to induce downstream effector molecules that are capable of inducing responses of the innate

immune system as well as influencing any subsequent adaptive immune response.¹³

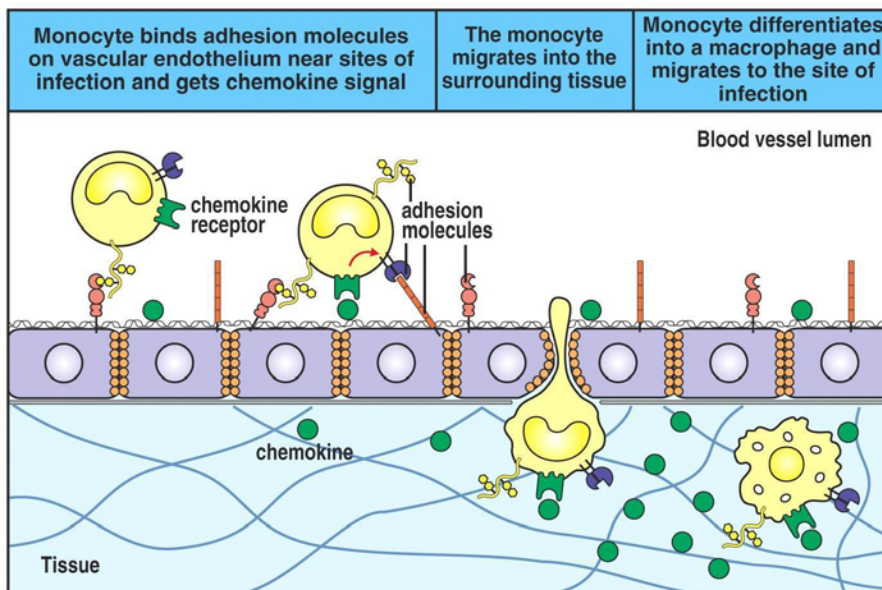


Figure 4. Migration of monocytes to sites of infection by chemokine receptors¹³

Microorganisms possess surfaces that typically contain repeating structural motifs that can be recognized by the innate immune system through pattern-recognition receptors. The mannose-binding lectin (MBL) is a receptor that is free in blood plasma that is able to recognize the spacing and orientation of certain sugar residues present on the surface of pathogens.¹³ The receptor-pathogen complex is recognized by phagocytes leading to phagocytosis and killing of the pathogen. The macrophage mannose receptor and scavenger receptors are cell-surface receptors that are able to function directly as phagocytic receptors.¹³ The macrophage mannose receptor is a calcium-dependent lectin that is able to bind certain sugars found on the surface of bacteria and some viruses (Figure 5).¹³ The structurally heterogeneous scavenger receptors identify various anionic polymers and acetylated low-density lipoproteins.¹³ Toll-like receptors (TLRs), of which there are ten, are signaling receptors present on the surface of macrophages and are able to induce the responses associated with innate immunity.¹³ Each receptor is a

transmembrane receptor able to recognize a particular structural motif present on pathogens. Activation of TLRs trigger the innate immune system resulting in the production of pro-inflammatory cytokines and chemokines as well as co-stimulatory molecules that are essential for the induction of adaptive immune responses.

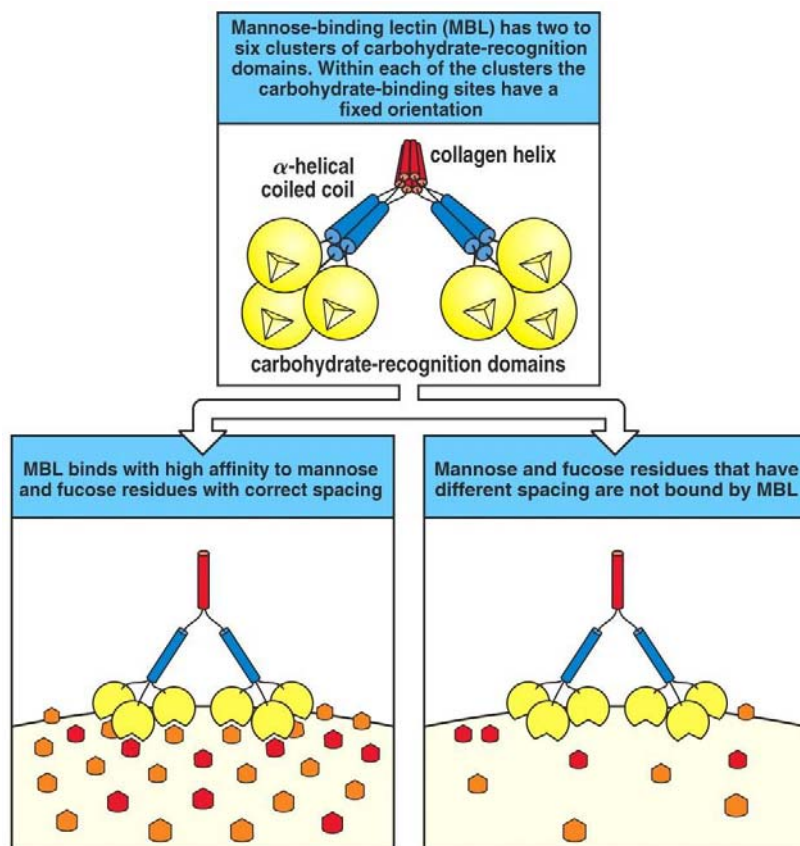


Figure 5. Mannose-binding lectin¹³

The complement system is an additional mechanism used by the innate immune system to identify and destroy pathogens.¹³ The complement system consists of many plasma proteins, many of which are proteases, that once activated undergo a number of cleavage steps ultimately leading to opsonization of pathogens (Figure 6).¹³ By opsonizing pathogens, the complement system is able to protect against infection by serving three important roles. First, opsonized pathogens are targets for phagocytes.¹³

Secondly, certain fragments generated from complement proteins are able to recruit and activate phagocytes at sites of infection.¹³ Finally, some complement components are able to lyse certain bacteria by forming pores in the bacterial membrane.¹³

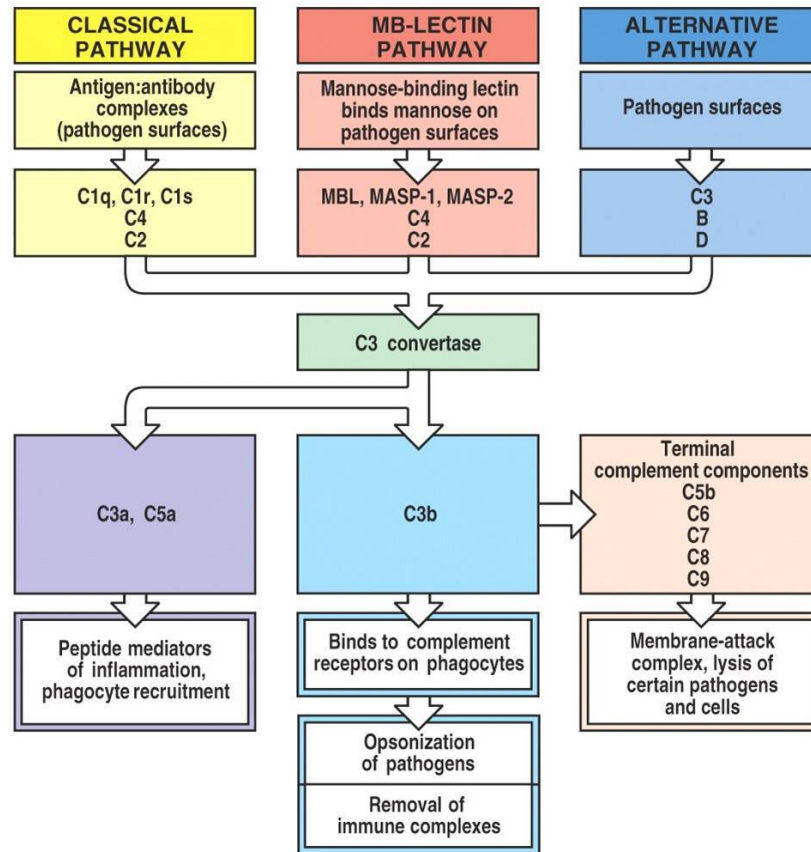


Figure 6. Activation of the complement system¹³

There are three pathways in which the complement system can be activated on the surface of pathogens. The classical pathway is activated by the binding of the complement protein C1q to the surface of pathogens.¹³ The binding of C1q can be a result of C1q binding to surface components such as cell wall proteins or polyanionic surface structures. C1q also binds to C-reactive protein which is a protein that binds to phosphocholine residues. C1q can also bind to antibody-antigen complexes of the adaptive immune system. In addition to the classical pathway of activation, the

complement cascade can be activated by the mannose-binding lectin pathway.¹³ This pathway is initiated when mannose-binding lectin binds to mannose residues found on bacteria and viruses. Finally, the alternative pathway is initiated as a result of the spontaneous activation of the complement protein C3 to the surface of pathogens.¹³ While the mechanisms of activation for the three pathways are different, they all converge to generate a critical protease, C3 convertase, on the surface of pathogens. Having the C3 convertase covalently bound to the surface of pathogens ensures that cleavage of additional complement proteins occur on the pathogen surface.

The active C3 convertase cleaves the C3 protein to generate large quantities of the C3b fragment. C3b fragments are the main effector proteins of the complement system and act as opsonins thereby targeting pathogens for destruction by phagocytes.¹³ Additionally, C3b can also bind to the C3 convertase to form yet another protease, the C5 convertase. C5b is a fragment generated by the C5 convertase and initiates the later stages of complement activation.¹³ C5b recruits and promotes the additional complement components to create a membrane-attack complex.¹³ This complex forms pores in the cell membrane of pathogens ultimately leading to their death. C3a and C5a are fragments produced along with C3b and C5b that mediate inflammation.¹³

The complement system, along with the other pattern recognition elements of the innate immune system, provides an effective yet limited and non-specific defense against pathogens. The mechanisms that govern innate immunity recognize specific components found on most pathogens but not on host cell surfaces. The recognition of these patterns leads to the destruction of the pathogen through phagocytosis by macrophages and neutrophils. The activation of phagocytes through cell surface receptors such as the

TLRs or activation of the complement system leads to the production of pro-inflammatory cytokines and chemokines as well as co-stimulatory molecules which help govern the adaptive immune response.

2.2.2.2 Adaptive immunity

The innate immune system is able to effectively defend the body from a number of pathogens; however, the defenses provided by the innate immune system are constrained in the number of pathogens that can be recognized and the lack of developing immunological memory.²⁴ An additional obstacle for innate immunity is that bacteria and viruses have developed ways to hide their components that are recognized by the innate immune system. However, these bacteria and viruses can still be taken up by dendritic cells through a non-receptor-dependent process known as macropinocytosis.²⁴ This process leads to the unmasking and identification of infectious materials that activate the dendritic cells. Antigens for these infectious materials are then presented to the lymphocytes of the adaptive immune system.²⁴ Unlike the phagocytes of the innate immune system, lymphocytes are able to recognize an almost infinite number of antigens each specific for a different pathogen.²⁴ Ultimately, activation of the adaptive immune system leads to immunological memory that provides protection from future infections with the same pathogen.

Immature dendritic cells are long-lived cells that survey tissue for pathogens, and their activation induces an adaptive immune response. Like macrophages and neutrophils, immature dendritic cells have cell surface receptors that can recognize common features associated with pathogens. Binding to a pathogen stimulates phagocytosis and destruction of the pathogen. In addition immature dendritic cells also

take up extracellular material that may contain viruses and bacteria through a process known as macropinocytosis.²⁴ Even though dendritic cells can engulf and destroy pathogens, their primary function is to carry pathogen antigens to the lymphatic system and present them to T lymphocytes. Once a pathogen is engulfed, the immature dendritic cell becomes activated and matures into an antigen-presenting cell which is then able to travel to a lymph node to activate pathogen-specific lymphocytes (Figure 7).²⁴

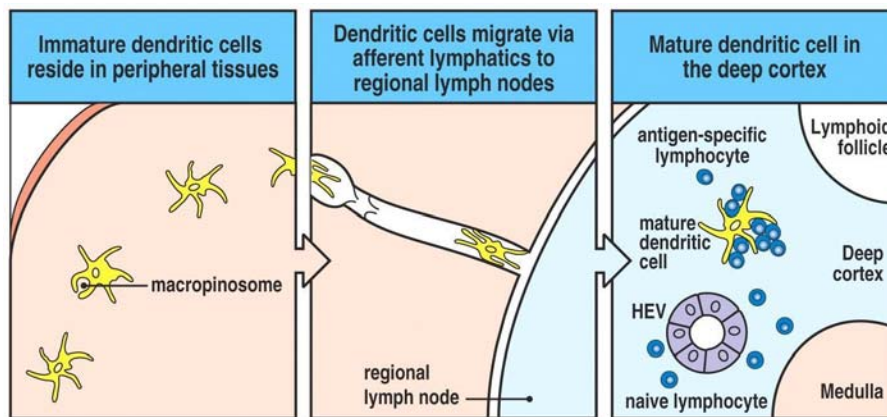


Figure 7. Lymphocyte activation by mature dendritic cells²⁴

Naive lymphocytes develop in bone marrow and the thymus where they undergo a genetic process that creates vast variants of genes encoding receptor molecules. Thus, lymphocytes collectively carry receptors for an almost infinite number of antigens, but each lymphocyte carries receptors for only one antigen (Figure 8).²⁴

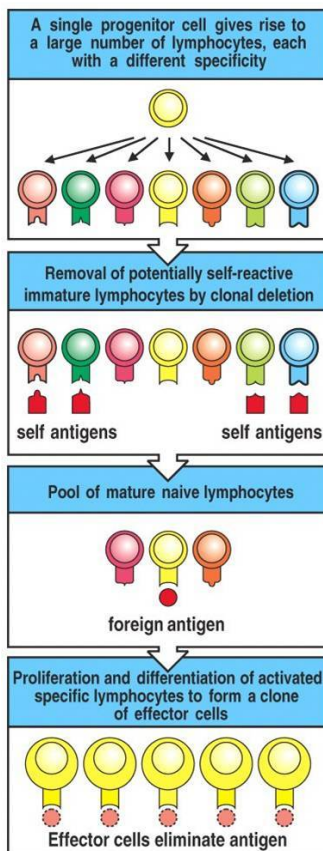


Figure 8. Generation of lymphocytes each bearing a distinct antigen receptor²⁴

In order to fight an infection efficiently, clonal expansion of an activated lymphocyte must occur in order to produce sufficient antigen-specific effector lymphocytes. Activation and proliferation of lymphocytes takes in place in lymphoid tissue where naive lymphocytes and activated antigen-presenting cells can interact. Once a lymphocyte recognizes its specific antigen, cell migration stops and cell enlargement takes place. The cell increases in volume and new proteins are synthesized resulting in a lymphoblast within a few hours. A lymphoblast then divides for three to five days producing approximately 1000 identical daughter cells that then differentiate into effector T and B cells.²⁴ Differentiated B cells are plasma cells that produce antibodies and recognize antigens outside of cells.²⁴ Differentiated T cells on the other hand become

either cells that destroy infected cells or act as helper cells to activate additional cells.²⁴ Effector cells that persist after an antigen as been removed forms the basis of immunological memory to ensure a more rapid response during future encounters with the antigen.²⁴ In order to become fully activated T and B cells must receive a second signal through a co-stimulatory molecule from another cell (Figure 9). Naive T cells can be stimulated by dendritic cells as well as B cells and macrophages presenting foreign antigens and producing co-stimulatory molecules.²⁴ Naive B cells can receive their second signal from activated effector T cells.²⁴

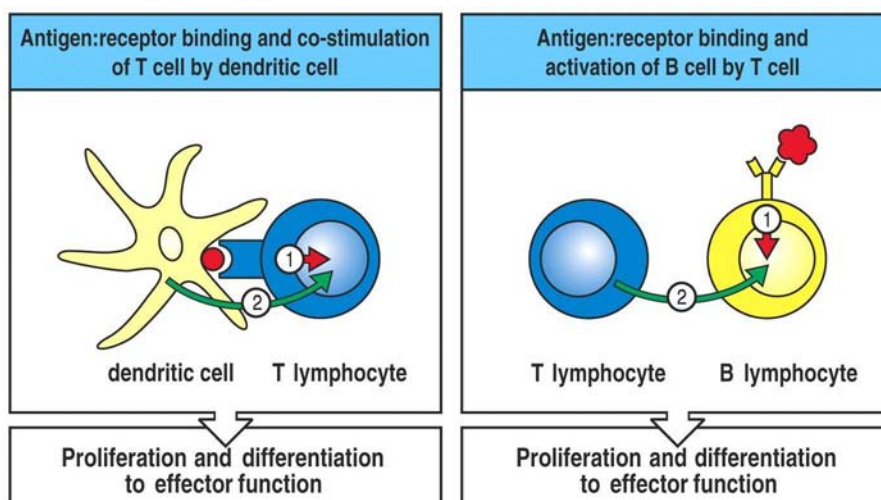


Figure 9. Co-stimulation of T and B cells²⁴

T cells are responsible for the cell-mediated immune response of adaptive immunity and therefore function to detect and destroy cells that have been infected with certain bacterial pathogens, parasites, or viruses. Cytotoxic T cells that express CD8 on their cell surfaces destroy cells that are infected.²⁴ The infected cells present antigens on their cell surface that are derived from replicating viruses. Cytotoxic T cells that recognize the presented antigens destroy the cell before viral replication is complete. Additionally, T cells may express the CD4 molecule which allows them to activate cells

they recognize.²⁴ CD4 bearing T cells are divided into T_h1 and T_h2 cells which carry out different functions in defending the body from infection.²⁴ Some bacteria are able to survive in the intracellular vesicles of macrophages because these vesicles do not fuse with lysosomes. T_h1 cells are important for controlling intracellular bacterial infections by activating macrophages and inducing their lysosomes to fuse with vesicles containing bacteria.²⁴ T_h2 bearing T cells are specialized for activating B cells which leads to the production of antibodies and the destruction of extracellular pathogens.²⁴ CD8 and T_h1 cells recognize antigens produced by pathogens that have infected or become ingested by target cells while T_h2 cells recognize and interact with B cells that have bound to and internalized foreign antigens.²⁴ These recognition events occur when T cells detect foreign peptide fragments presented to them on the cell surface by major histocompatibility complex (MHC).²⁴ The MHC traps peptide fragments as it is being synthesized in the cell and is then transported to the cell surface where it is able to present the fragments to T cells. There are two classes of MHC molecules that differ in the source of the peptide they trap. MHC class I molecules are able to trap viral peptides that form in the cytosol.²⁴ The MHC class I molecule bearing viral peptides is recognized by T cells expressing the CD8 cell surface receptors which then destroy the infected cell. MHC class II molecule traps peptides from intracellular vesicles and presents them to CD4-bearing T_h1 and T_h2 cells.²⁴ Activation of T cells by antigens is supported by co-receptors that can recognize and distinguish between the two classes of MHC molecules. Activation of T cells leads to the release of effector molecules that either have a direct effect on their target cells or are able to recruit additional effector cells.

The sole effector function of B cells is to secrete antigen receptors in the form of

antibodies (Figure 10).²⁴ Y-shaped antibodies contain both a constant and variable region that target pathogens outside of cells and in extracellular fluids. The constant region can be one of five different biochemical forms and determines how the pathogen will be destroyed. The variable region can be composed of an infinite number of sequences which gives the adaptive immune system the ability to recognize an equally vast number of antigens. The variable region therefore determines the antigen-binding specificity of an antibody. There are three main functions of antibodies that provide protection from pathogens and their toxic products. The first and simplest way antibodies provide protection is through neutralization. Neutralization of a pathogen or its toxic products is achieved when antibodies bind to them blocking them from entering into cells.²⁴ Opsonization is a second way in which antibodies provide protection. Antibody binding to pathogens such as bacteria is not sufficient to arrest cell replication. Antibodies however do enable phagocytic cells to recognize, ingest, and destroy the pathogen.²⁴ The third function of antibodies is to initiate the complement system which contributes to both innate and adaptive immunity.²⁴

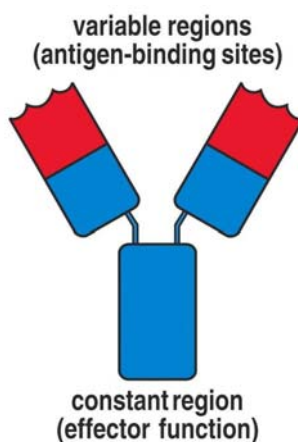


Figure 10. Antibody structure²⁴

Understanding defects in the immune system is important in the control of many diseases. One of the most severe defects of the immune system results in immunodeficiency diseases.²⁴ With no adaptive immune system present, death occurs in infancy as overwhelming infections occur. One infectious agent, HIV, can lead to AIDS and death as infectious pathogens the body normally controls cause numerous infections. In addition errant immune responses against non-infectious agents can lead to various diseases.²⁴ An allergy is an immune response against a noninfectious foreign antigen. Graft rejections occur when there is an immune response against transplanted foreign cells. Finally, autoimmune diseases occur when the immune response is against a self-antigen.

2.2.3 Autoimmunity

Immunological tolerance to self antigens prevents an immune response against self components. However, whenever immunological tolerance fails and an immune response to self antigens occur, autoimmunity can develop leading to autoimmune diseases characterized by tissue damage.¹² An autoimmune response is identical to an immune response against a pathogen except that it is activated by and targets self antigens. There are multiple mechanisms used by the immune system in order to maintain immunological tolerance. Inevitably self-reactive lymphocytes will develop in the central lymphoid organs as the genes for cell surface receptors are combined randomly. As cells are developed in the central lymphoid organs they are presented with self antigens, and cells exhibiting self-reactivity are eliminated.¹² Similarly, lymphocytes showing weak self-reactivity are rendered unresponsive through a process known as anergy.²⁵ Normally, cells that have low affinity for self antigens ignore them and remain

ignorant to these self antigens.¹² Additionally, autoimmune responses can be controlled by regulatory T cells, such as CD4 CD25 T cells, that exert their effects on activated T and B cells directly by controlling proliferation.¹² Immune responses are naturally limited in duration as a result of activation-induced cell death. Even if there is a continuous signal from antigen, many of the responding cells that are activated eventually die. Finally, a network of antibodies that are able to neutralize self-reactive antibodies exists in the human body as another mechanism to help prevent autoimmunity.¹²

As several mechanisms exist to prevent autoimmunity, there are also several genetic and environmental factors that can overcome these preventive measures and induce various autoimmune diseases. An individual may be genetically predisposed to developing certain autoimmune diseases.¹² Genes associated with immunoglobulins, T-cell receptors, and the major histocompatibility complex (MHC) have the most impact on a person's susceptibility to developing autoimmune diseases.¹² MHC class II allotypes are more strongly correlated with specific autoimmune diseases than those for MHC class I. A person's gender also plays a vital role in determining a person's susceptibility to developing autoimmune diseases as nearly 75% of those suffering with autoimmune diseases in the United States are women.³ In addition to genetic factors, many environmental factors such as drugs, toxins, and infections can increase a person's chances of developing autoimmune diseases.¹² Drugs such as procainamide can induce lupus-like autoantibodies. Toxins such as gold and mercury as well as chemicals from smoking can lead to autoimmune diseases. The mechanisms by which these substances cause autoimmunity are not well understood, but it is thought that they modify self proteins.¹² This leads to an immune response as the immune system identifies the

modified self proteins as foreign. Ultimately, the immune response is able to respond against the original unmodified self proteins. Additionally, self-reactive lymphocytes may become activated during an infection as the number of co-stimulatory molecules increase.¹² Finally, many pathogens may also prevent the apoptosis of lymphocytes and may secrete their own cytokines altering the normal balance of the immune system.¹²

There are several mechanisms that, along with genetic and environmental factors, lead to either systemic or localized autoimmune diseases. In a normal immune response, the B cell and T cell communication is very important. However, during some infections B cells can be activated without the aid of T cells by super antigens produced by the pathogen.²⁶ In addition, B cells may be activated by T cells in which the two cell types recognize different antigens.¹² Both of these mechanisms lead to erroneous immune responses. Molecular mimicry in which an exogenous antigen may possess similar structural features to host cell antigens can lead to antibodies that recognize both the exogenous and self antigens.¹² During the course of a severe immune response, many co-stimulatory receptors are produced and as a result a change from targeting the primary to structurally different epitopes may occur.^{12,27} Changes in the balance of cytokines released during an immune response that control the nature and duration of the response may lead to an exaggerated immune response.¹² Finally, self-tolerance may be compromised if dendritic cells are unable to undergo apoptosis normally leading to erroneous activation of lymphocytes.¹² While many mechanisms are present to ensure the integrity of self-tolerance, they can be overcome leading to tissue damage resulting from pro-inflammatory mediators produced during an autoimmune response.

2.2.4 Inflammation

Acute inflammation is the initial process of the immune system responding to harmful stimuli such as a pathogen, damaged cells, or irritants.²⁸ The inflammatory response is a signal to remove the harmful stimuli as well as to initiate the healing process of the damaged tissue. Macrophages, dendritic cells, histiocytes, Kupffer cells, and mastocytes are the main cells present in tissue that are responsible for initiating the acute inflammatory process.²⁴ One of the main signals in which an inflammatory response is initiated by the innate immune system during an infection is through TLRs on macrophages.²⁴ Activation of macrophages stimulates transcription of chemokines and pro-inflammatory cytokines through the NF- κ B signaling pathway (Figure 11).²⁴

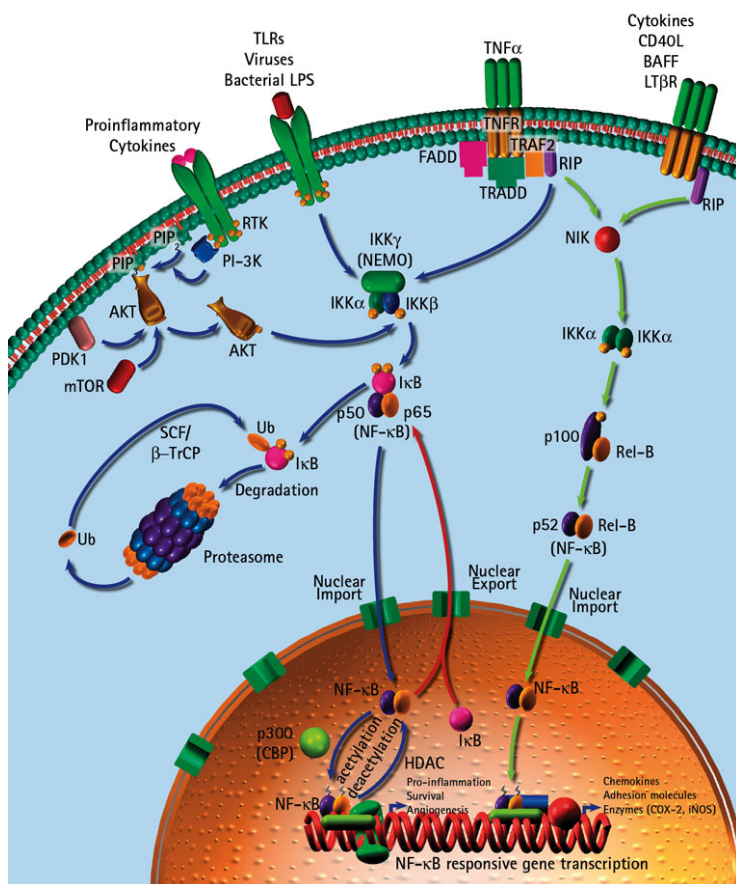


Figure 11. NF- κ B signaling pathway⁹⁹

In addition to cell-derived signals, the complement fragments C3a and C5a also can initiate a local inflammatory response.²⁴ Chemokines released during an early acute inflammatory response recruit neutrophils from the blood stream to sites of infection or damage. The onset of inflammation is associated with redness, heat, swelling, pain, and possible loss of function in the inflamed tissue. The inflammatory response ceases once the harmful stimulus has been completely removed. However, if the harmful stimulus cannot be removed rapidly, then the inflammatory response will continue and become chronic. During chronic inflammation monocytes, macrophages, lymphocytes, and mononuclear leukocytes are involved in eliminating the harmful stimulus. Inflammation due to autoimmune diseases is chronic and leads to tissue damage as a result of the high concentration of immune cells and cytokines present in the inflamed tissue.

In autoimmunity the autoantigen cannot be easily removed as it is a component of the body and exists in vast quantities.¹² Thus autoimmune diseases evolve into a chronic state leading to chronic inflammation. This situation also creates a positive feedback loop in which damaged tissue releases more autoantigens that stimulate the autoimmune response.¹² In addition, as the autoimmune response progresses, a number of nonspecific effector cells such as macrophages are attracted to the site of inflammation by released cytokines and chemokines. Furthermore, the number of B cells and dendritic cells at the site of inflammation also increases. These cells are able to take up additional antigens produced by the damaged tissue and can present these antigens to autoreactive T cells and B cells.¹² This process further exacerbates the autoimmune response and chronic inflammation as new autoantigens are created and targeted by the autoimmune response.

Many of the cytokines and chemokines involved in the immune and inflammatory

responses are controlled by the NF- κ B signaling pathway. NF- κ B is a complex that acts as a transcription factor and is activated by many stimuli such as stress, cytokines, free radicals, ultraviolet irradiation, and bacterial as well as viral components through many different cell-surface receptors.²⁹ Errant regulation of NF- κ B has been linked to many diseases such as cancer, inflammatory and autoimmune diseases, septic shock, and viral infection. NF- κ B family members can be divided into two classes. The class I members, NF- κ B1 and NF- κ B2, are produced as p105 and p100 precursor proteins, respectively.³⁰ Degradation of p105 and p100 by the ubiquitin/proteasome pathway generates the mature NF- κ B subunits p50 and p52, respectively.^{29,30} Class II members consists of RelA also known as p65, RelB, and c-Rel. These subunits contain a transactivation domain in their C-termini which is vital for activation of transcription.³⁰

In unstimulated cells, NF- κ B heterodimers reside in the cytoplasm and are bound to inhibitors of κ B (I κ Bs).^{29,30} I κ Bs contain ankyrin repeats that mask nuclear localization signals keeping NF- κ B dimers in an inactive state.²⁹ Activation of the NF- κ B pathway results in the degradation of I κ B by the I κ B kinase (IKK). IKK consists of two catalytic subunits, IKK- α and IKK- β , as well as a regulatory protein IKK- γ .^{29,30} The catalytic subunits of IKK phosphorylate I κ B at two serine residues.³⁰ This phosphorylation event leads to the modification of I κ B through ubiquitination which subsequently leads to the degradation of I κ B by proteasomes.^{29,30} The newly freed NF- κ B heterodimers are now able to translocate into the nucleus to begin transcription.

Once inside the nucleus, NF- κ B can initiate gene transcription by binding to NF- κ B sites in the promoter regions of its target genes. Before NF- κ B can begin

transcription however, its transactivation domains must first be phosphorylated.²⁹ After transactivation, NF- κ B has a much higher affinity for its target DNA sequence as well as for coactivators such as p300 and CBP.²⁹ The activated NF- κ B complex forms on DNA and recruits RNA polymerase II to begin transcription of target genes that code for cytokines and chemokines, immunoreceptors, cell adhesion molecules, acute phase proteins, cell-surface receptors, and regulators of apoptosis.

Currently, there are several hundred known and predicted NF- κ B target genes that code for many different classes of proteins.³⁰ NF- κ B target genes code for many different classes of proteins involved in stimulating and recruiting other cells to sites of infection as well as regulating the growth and apoptosis of neighboring cells. Important cytokines and chemokines that are released by macrophages and dendritic cells during an immune response are IL-1, IL-6, CXCL8 (IL-8), IL-12, and TNF- α (Figure 12).¹³

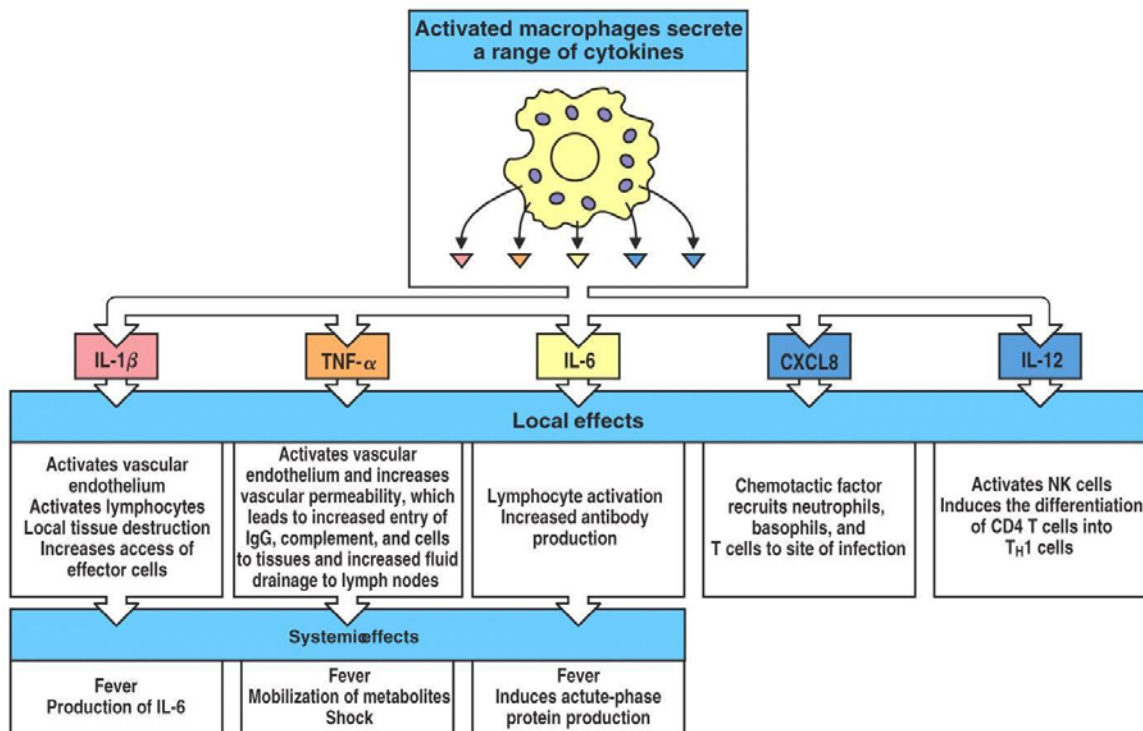


Figure 12. Important cytokines secreted by macrophages¹³

Autoimmune and overactive immune responses to harmless antigens lead to chronic inflammation and tissue damage. The typical treatment for these responses is to suppress the immune system with immunosuppressive drugs.²⁴ Current drugs target and inhibit the pathways and proteins that are involved in propagating the immune response. These drugs, however, are not selective for the cells responsible for the unwanted response. Therefore, both desirable and undesirable immune responses are suppressed.

2.2.5 Drugs Used to Treat Autoimmune/Inflammatory Diseases

Currently, a cure for autoimmune and inflammatory diseases does not exist but there are many drugs available for treatment. Since the NF- κ B signaling pathway plays a central role in regulating many cytokines and chemokines, it is being explored as a potential drug target. There are thousands of compounds known to suppress the NF- κ B pathway such as anti-oxidants and proteasome inhibitors, but a specific NF- κ B inhibitor has not yet been approved by the FDA.³⁰

Treatments and therapies currently cost over an estimated \$18 billion worldwide, and this figure is expected to reach \$50 billion by 2015.^{6,7} Americans spend an estimated \$87 billion annually for total costs associated with autoimmune and inflammatory diseases.^{4,6} While some diseases have specific treatments such as radioiodine and the anti-thyroid drugs carbimazole, methimazole, and propylthiouracil in the case of Graves' disease, many diseases can be treated with drugs coming from one of five well established drug classes. Autoimmune and inflammatory diseases are usually treated with a combination of non-steroidal anti-inflammatory drugs (NSAIDs), analgesics, steroids, disease-modifying drugs, and biologics.

Analgesics are used in patients suffering from autoimmune and inflammatory

diseases to control pain. Analgesics are not immunosuppressive and do not reduce inflammation.³¹ Acetaminophen is a common over-the-counter analgesic used to relieve pain and reduce fevers.³² There is still some debate over acetaminophen's mechanism of action. It does not appear to inhibit cyclooxygenase-1 (COX-1) or cyclooxygenase-2 (COX-2), enzymes responsible for the synthesis of prostaglandins, but rather cyclooxygenase-3 (COX-3) found at high levels in the brain and spinal cord.^{32,33} In addition to acetaminophen, opiates such as morphine, codeine, oxycodone, and hydrocodone may be used to treat pain (Figure 13). Opiates exert their analgesic effects by targeting the G-protein coupled opioid receptors of the central nervous system.³⁴ Opioids cause a decrease in pain perception as well as an increase in pain tolerance. Side effects associated with opiates include nausea, vomiting, pruritus (itching), and constipation. Furthermore, there is a risk of developing an addiction to opioids.

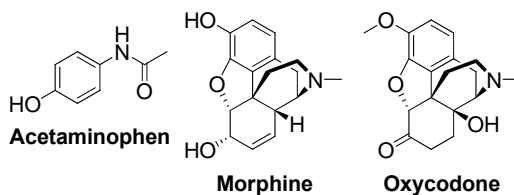


Figure 13. Commonly used analgesics

NSAIDs are able to reduce joint swelling, stiffness, and pain as well as reduce inflammation which is in contrast to analgesics. Even though NSAIDs can reduce inflammation, they are unable to stop the autoimmune disease from getting worse.^{10,35} Over-the-counter NSAIDs such as aspirin, ibuprofen, and naproxen inhibit cyclooxygenase-1 (COX-1) and cyclooxygenase-2 (COX-2) (Figure 14).³⁵ Cyclooxygenases are enzymes involved in the conversion of arachidonic acid to prostaglandins, which are messenger molecules in the inflammation process.¹⁰ Adverse

drug reactions associated with these non-selective COX inhibitors involve gastrointestinal (GI) and renal toxicities. Celebrex is an additional NSAID that is currently the only COX-2 selective inhibitor on the market (Figure 14).³⁵ It was hoped that COX-2 selective inhibitors would retain anti-inflammatory properties while avoiding GI toxicities related to COX-1 inhibition. Additionally, there is an increased risk for cardiovascular side effects such as stroke and heart attack with NSAIDs except for low-dose aspirin.

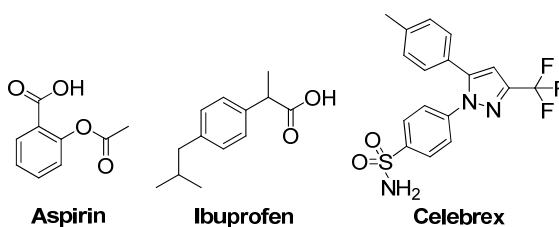


Figure 14. Structures of commonly used NSAIDS

Corticosteroids are potent anti-inflammatory agents that suppress the activation of the immune system and can prevent damage by reducing inflammation.³⁶ Examples of steroids commonly used in autoimmune and inflammatory diseases are prednisone, cortisone, and dexamethasone (Figure 15). Steroids are useful for treating acute inflammation as well as in the early stages of more severe inflammation while waiting for disease modifying drugs to exert their anti-inflammatory effects.¹⁰ Glucocorticoids, a class of corticosteroids, bind to cell surface glucocorticoid receptors forming an activated complex that is able to translocate into the cell nucleus and regulate gene transcription. The genes controlled by glucocorticoids suppress the immune system by inhibiting the genes that code for IL-1, IL-2, IL-3, IL-4, IL-5, IL-6, IL-8, and IFN- γ leading to reduced T cell proliferation.^{36,37} In addition, glucocorticoids induce apoptosis in immature T cells located in the thymus and cause B cells to express smaller amounts of IL-2 and IL-2

receptors.³⁷ The anti-inflammatory properties associated with glucocorticoids is a result of their inhibition of transcription by pro-inflammatory transcription factors by controlling genes that lead to acetylation of histones.³⁶ Long term side effects associated with corticosteroids are an increased risk of cataracts, increased blood pressure, increased blood sugar, weight gain, and connective tissue weakness.

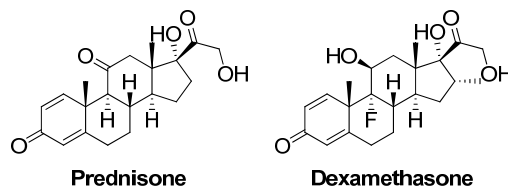


Figure 15. Structure of prednisone and dexamethasone

Disease modifying drugs, or disease modifying anti-rheumatic drugs (DMARDs) as they are sometimes referred to, interfere with the immune system processes that lead to damaging inflammation.¹⁰ Many of these drugs were approved to treat other diseases such as cancer, malaria, and skin infections but all show the ability to treat autoimmune and inflammatory diseases. Azathioprine is an immunosuppressant that inhibits purine synthesis which results in inhibiting cell proliferation, especially in leukocytes (Figure 16).³⁸ Short-term side effects are reported to be uncommon; however, there is an increased risk of developing certain types of cancer with long term use. In addition, azathioprine suppresses the bone marrow leading to an increased risk of infection. Leflunomide is a drug that inhibits pyrimidine synthesis and is used mainly to treat rheumatoid and psoriatic arthritis.³⁹ Leflunomide possesses anti-proliferation properties as a result of inhibiting the enzyme dihydroorotate dehydrogenase and has also demonstrated anti-inflammatory properties (Figure 16).³⁹ Infections, liver damage, and heart problems are some of the side effects associated with leflunomide treatment.

Cyclosporin A is an immunosuppressant drug produced by the fungus *Beauveria nivea* as a cyclic 11 amino acid peptide containing a single D-alanine amino acid.⁴⁰ Cyclosporin A is used mostly in post-allogeneic organ transplants, but it has also been used in many autoimmune and inflammatory diseases and has also been studied as a neuroprotective agent in traumatic brain injury.^{41,42} Cyclosporin A is thought to bind to the cytosolic protein cyclophilin, and this complex inhibits calcineurin.⁴³ By inhibiting calcineurin, which normally activates the transcription of IL-2, a reduced function of effector T cells is observed.⁴³ There are many adverse drug reactions associated with cyclosporin A such as convulsions, fever, vomiting, diarrhea, kidney and liver toxicity, high blood pressure, and an increased risk of infection. Cyclophosphamide is typically used to treat various types of cancer but its use is becoming more common for autoimmune and inflammatory diseases (Figure 16). Cyclophosphamide is a nitrogen mustard alkylating agent that is converted into its active form in the liver.⁴⁴ The main metabolite is 4-hydroxycyclophosphamide, which exists in equilibrium with its tautomer, aldophosphamide.⁴⁴ Aldophosphamide can be converted into its active and toxic products phosphoramidate mustard and acrolein, or it can be oxidized by aldehyde dehydrogenase (ALDH) into the nontoxic carboxyphosphamide.⁴⁴ Cells that have low levels of ALDH are therefore susceptible to cyclophosphamide treatment. Phosphoramidate is believed to form DNA cross-links between and within DNA strands leading to cell death. People taking cyclophosphamide generally do not experience side effects, but those that do experience nausea and vomiting, stomach aches, diarrhea, hair loss, lethargy, and bone marrow suppression. There is also an increased risk of cancer with cyclophosphamide.⁴⁴ Hydroxychloroquine is an anti-malarial drug that has been

shown to be effective at treating autoimmune and inflammatory diseases.⁴⁵ Hydroxychloroquine blocks the activation of toll-like receptors on dendritic cells.⁴⁵ This action inhibits dendritic cells from maturing and presenting antigen to T cells, thus avoiding the inflammatory response. The most common side effects associated with hydroxychloroquine are mild nausea, stomach aches, and diarrhea. Methotrexate inhibits the metabolism of folic acid by competitively and reversibly inhibiting dihydrofolate reductase (Figure 16).⁴⁶ Methotrexate effectively inhibits the de novo synthesis of thymidine as well as purine base synthesis.⁴⁶ Typical side effects associated with methotrexate treatment are anemia, neutropenia, nausea and vomiting, increased risk of bruising, dermatitis, diarrhea, and hepatitis. Additionally, methotrexate is a teratogenic drug and must not be taken by women that are pregnant or trying to become pregnant.

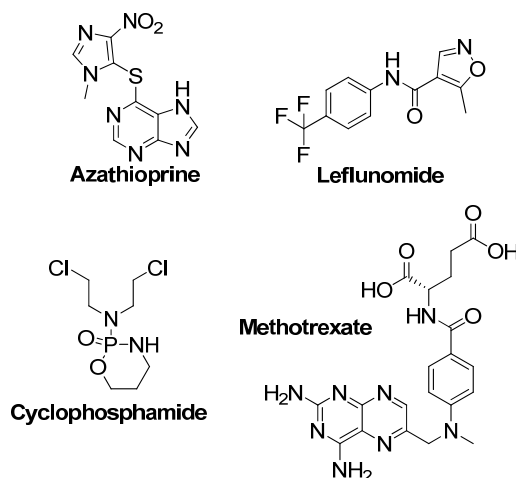


Figure 16. Structures of DMARDs

Autoimmune and inflammatory diseases are treated aggressively with biologic response modifiers or biologics, a new class of drugs.¹⁰ In addition to being good frontline treatments, biologics are also a great alternative for people that do not respond well to DMARDs or for people in which DMARDs stop working. Biologics are usually

prescribed in combination with NSAIDs and DMARDs to achieve maximum efficacy. Biologics such as enbrel, humira, kineret, orenicia, remicade, and rituxan are proteins that target the molecules that play critical roles in activating the immune system and inflammation. Enbrel is a circulating TNF- α receptor fusion protein, and humira and remicade are monoclonal antibodies that target TNF- α .⁴⁷ All three drugs help clear TNF- α from circulation, thus blocking TNF- α from binding to its receptor on cells and preventing inflammation. Kineret is an IL-1 receptor antagonist that blocks IL-1 from binding to the cell surface IL-1 receptor, thus preventing downstream inflammatory and immunological responses.⁴⁸ Orenicia is an immunoglobulin fused to the extracellular domain of CTLA-4 that is able to inhibit the co-stimulation of T cells.⁴⁹ Orenicia is typically used when TNF- α blocking biologics fail. Rituxan is a chimeric monoclonal antibody against CD20, a protein found on the surface of B cells.⁵⁰ The exact mechanism of action of rituxan is unknown, but it does increase MHC class II proteins as well as adhesion molecules, elicits shedding of CD23, downregulates the B cell receptor, and induces apoptosis in CD20 cells all of which eliminate B cells from the body.⁵⁰

While biologics have helped many people with autoimmune and inflammatory diseases, they do possess many drawbacks. Biologics must be injected and cost patients between \$10,000 and \$25,000 or more a year.⁵¹ Many health insurance plans do not cover the use of biologics, and even if they do, patients must typically fail two or even three alternative therapies before the insurance company will approve coverage.¹⁰ Even though the cost for some biologics is on the decline, their very nature and the methods used to produce them ensure they will continue to cost more than most small molecule drugs.⁵² Since biologics disrupt immune system function infections and flare-ups of

diseases in remission are common.⁹ Furthermore, biologics can stay in circulation for weeks complicating treatment due to possible adverse side effects. Lastly, biologics do not work for everyone and can even stop working for some individuals increasing the need for alternative treatments.⁹

2.3 Background

2.3.1 Triptolide as a Potent Immunosuppressant

Triptolide is a highly toxic diterpenoid triepoxide isolated from *Tripterygium wilfordii*, sometimes called thunder god vine, a vine in southern China (Figure 17).⁵³ The vine has been used in traditional Chinese medicine for centuries as a treatment for fever, chills, edema, and carbuncle and has been recently investigated for treating various forms of cancer, inflammatory disorders, and as a male oral contraceptive. Triptolide as well as other related compounds were isolated from *T. wilfordii* in the early 1970s by Kupchan.⁵³ It was discovered that triptolide possessed potent anti-cancer and anti-inflammatory properties which stimulated years of research focused on the total synthesis of triptolide. It was not until the early 1990s that work began to understand triptolide's mechanism of action. Since the early 1990s there has been an explosion of biological and synthetic interest in triptolide.

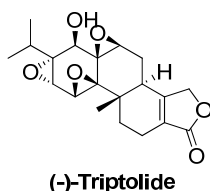


Figure 17. Structure of (-)-triptolide

2.3.2 Inhibition of the NF- κ B Signaling Pathway by Triptolide

Triptolide modulates numerous genes in many cell types, but the mechanism by which triptolide is able to modulate these genes has remained elusive. Current research indicates that triptolide might be a transcription inhibitor, although not a universal transcription inhibitor. Triptolide has been shown to suppress NF- κ B, AP-1, and HSF-1 transcription as well as have an effect on p53 transcription.⁵⁴ Furthermore, it appears

triptolide is able to suppress transcription through inhibiting transactivation of transcription factors.^{54,55}

Qiu and co-workers investigated the mechanism by which triptolide inhibits NF- κ B transcription by using phorbol-12-myristate-13-acetate (PMA) and an antibody to CD3 as well as PMA and ionomycin to stimulate Jurkat T cells.⁵⁵ Human peripheral blood lymphocytes (PBL) were stimulated with either PMA (P) and the antibody to CD3 (Figure 18 lane 4) or PMA and ionomycin (I) (Figure 18 lane 14) to give rise to a large increase in secreted IL-2 levels. These cells were treated with increasing concentrations of triptolide (PG490) (Figure 18 lanes 5-8 and lanes 15-17) or cyclosporin A (CsA) (Figure 18 lanes 9-11 and 18) resulting in a decrease in the quantity of secreted IL-2 (Figure 18). Triptolide at 200 ng/ml and 1000 ng/ml showed complete inhibition of IL-2 secretion while cyclosporin A was only able to reduce IL-2 levels indicating that triptolide and cyclosporin A possibly work by different mechanisms.⁵⁵ In addition, mRNA levels indicated that triptolide potently inhibits IL-2 and I κ B- α mRNA and upregulates NF90 mRNA. This is in contrast to cyclosporin A which showed limited inhibition of I κ B- α and NF90 mRNA indicating that triptolide and cyclosporin A work through different mechanisms.

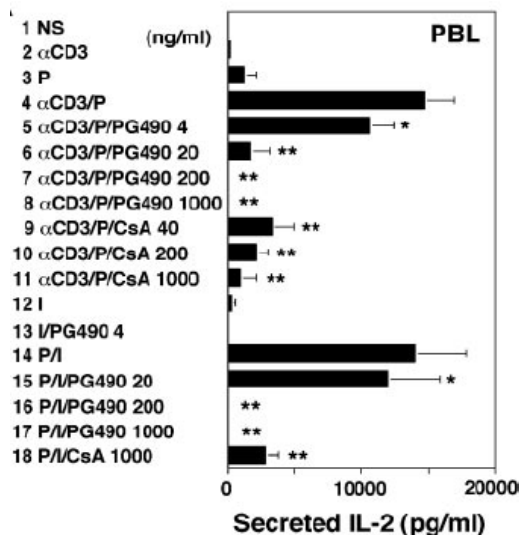


Figure 18. Inhibition of secreted IL-2 from Jurkat T cells

To further explore the differences between triptolide and cyclosporin A, Qiu and co-workers evaluated the two compounds in stimulated Jurkat cells expressing an IL-2 luciferase reporter gene (Figure 19). Cyclosporin A treated cells stimulated with PMA and ionomycin (Figure 19 left panel) showed a decrease in IL-2 luciferase reporter gene activity with increasing concentration.⁵⁵ Triptolide treated cells on the other hand showed a slight increase in reporter activity before inhibition occurred (Figure 19 left panel).⁵⁵ Furthermore, cells stimulated with PMA and antibody to CD28, conditions resistant to cyclosporin A, showed inhibition with triptolide (Figure 19 right panel).⁵⁵

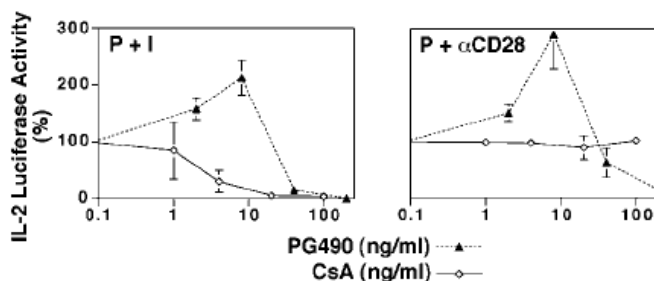


Figure 19. Inhibition of IL-2 Luciferase Activity by Triptolide and Cyclosporin A

Further experiments revealed that triptolide inhibits NF- κ B transcription activation and not DNA binding (Figure 20).⁵⁵ In both PMA stimulated (Figure 20 bottom panel) and PMA and ionomycin stimulated (not shown) Jurkat T cells, triptolide inhibited luciferase activity at 200 ng/mL and 1000 ng/mL.⁵⁵ Electrophoretic mobility shift assays (EMSA) at all concentrations of triptolide tested indicated nuclear NF- κ B DNA binding activity (Figure 20 lanes 2-5). Even though triptolide inhibited luciferase activity at the two highest concentrations tested, the NF- κ B DNA complex remained intact (Figure 20 lanes 4 and 5).⁵⁵ This indicated that triptolide does not inhibit NF- κ B binding to DNA but instead a step after DNA binding.

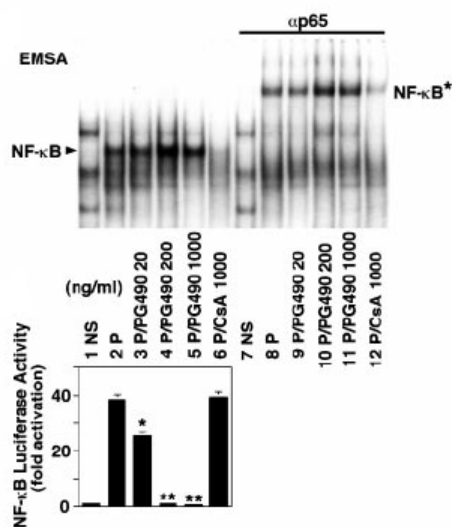


Figure 20. Triptolide inhibits NF- κ B at a step after DNA binding

Finally, triptolide's affect on NF- κ B transactivation was investigated (Figure 21). NF- κ B contains two transactivation domains, TA1 and TA2, at its C-terminal end that get phosphorylated.⁵⁵ Chimeric transcription factors were created by fusing the yeast GAL4 DNA binding domain with either TA1 or TA1 + TA2. Jurkat T cells were transfected with a GAL4 response element-luciferase reporter construct along with an expression

construct for either GAL4 DNA binding domain alone (GAL4DB), GAL4DB + TA1, or GAL4DB + TA1 + TA2. Cells expressing the GAL4DB + TA1 construct showed an increase in luciferase activity upon PMA stimulation (Figure 21 top panel lane 2).⁵⁵ This increase in luciferase activity was inhibited by increasing concentrations of triptolide but not cyclosporin A (Figure 21 top panel lanes 3-6).⁵⁵ An identical result was observed for cells expressing the GAL4DB + TA1 + TA2 construct (Figure 21 bottom panel).⁵⁵ This work indicates triptolide inhibits NF- κ B transcription at a step after NF- κ B binding DNA which is most likely inhibition of NF- κ B transactivation.

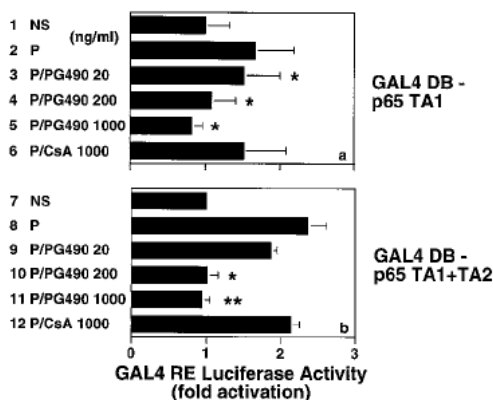


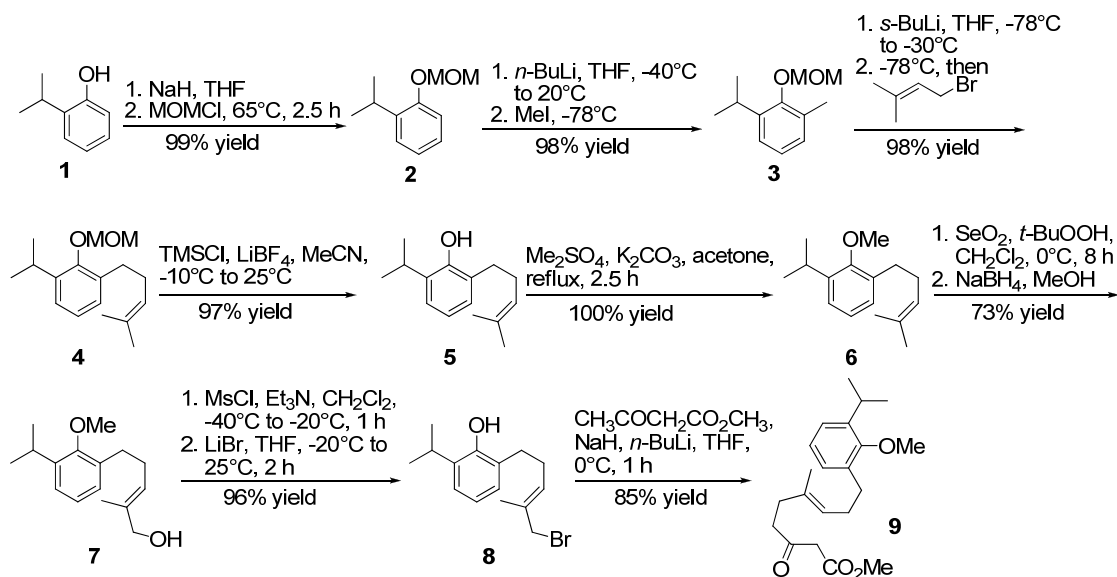
Figure 21. Triptolide's affect on NF- κ B transactivation

2.3.3 Synthesis of Triptolide

The synthesis of triptolide as well as triptolide analogues have been reported by many groups. The syntheses differ by the methods employed to construct the ring system of triptolide. Once the ring system has been established many groups utilize an oxidative dearomatization reaction in order to buildup the triepoxide motif of triptolide. The work by Yang and co-workers will be used to illustrate an efficient method for the enantioselective total synthesis of triptolide.⁵⁶

Yang and co-workers developed a lanthanide triflate-catalyzed asymmetric radical

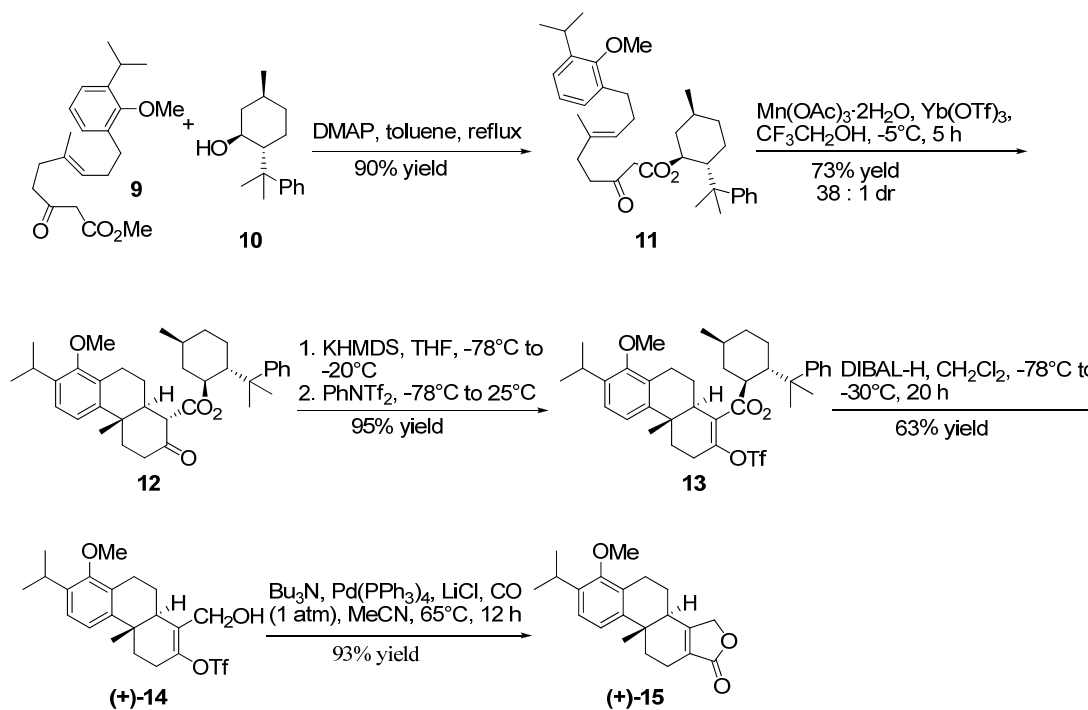
cyclization method in order to construct the ring system of triptolide.⁵⁶ The cyclization precursor was constructed starting from the commercially available 2-isopropyl phenol **1** (Scheme 1). Protection of **1** as a methoxy methyl (MOM) ether allowed for ortho-directed lithiation upon treatment with *n*-butyllithium. Addition of iodomethane provided compound **3** which was further extended by treatment with *s*-butyllithium followed by quenching with 3,3-dimethylallyl bromide. It was determined that switching from a MOM protecting group to a methyl group vastly improved the yield of the selenium oxidation to form compound **7**.⁵⁶ The resulting allylic alcohol was converted to the bromide which was then treated with the dianion generated from methyl acetoacetate to furnish the cyclization precursor **9**.



Scheme 1. Synthesis of the cyclization precursor

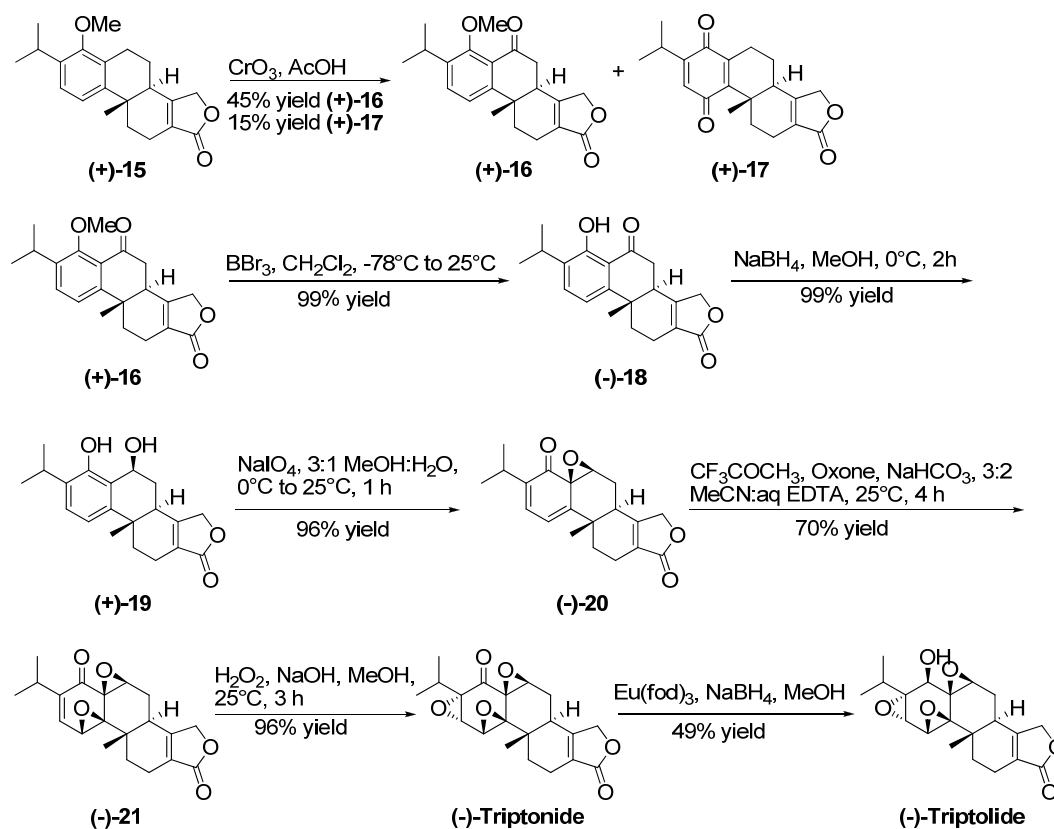
Ester exchange was carried out with (+)-8-phenylmenthol **10** prior to radical cyclization to form compound **11** (Scheme 2).⁵⁶ Treatment of **11** with manganese (III) acetate and ytterbium (III) triflate promoted the radical cyclization to give compound **12** in 73% yield with a 38:1 dr. Compound **12** was then converted into the vinyl triflate

followed by reduction with DIBAL-H to provide allylic alcohol (+)-**14**. The remaining ring of the triptolide scaffold was constructed by subjecting (+)-**14** to palladium catalyzed carbonylation conditions to afford (+)-**15**.



Scheme 2. Generation of triptolide ring system

Oxidation of (+)-**15** with chromium (VI) oxide provided the desired product (+)-**16** in modest yield along with (+)-triptoquinonide (+)-**17** (Scheme 3).⁵⁶ Deprotection of the phenol and reduction of the ketone provided the oxidative dearomatization precursor (+)-**19**. Oxidative dearomatization was induced by the addition of sodium periodate to provide the monoepoxide dienone product (-)-**20**. This compound was further oxidized with an in situ generated mixed dioxirane followed by treatment with basic hydrogen peroxide to afford (-)-triptonide.⁵⁶ (-)-Triptolide was then obtained after sodium borohydride reduction of (-)-triptonide.



Scheme 3. Completion of triptolide synthesis

2.3.4 Design and Synthesis of Monocyclic Truncated Triptolide Analogs

Triptolide possesses very potent anti-inflammatory properties; however, it suffers from high cytotoxicity.^{66,67} Developing triptolide analogs that retain immunosuppressive

properties devoid of cytotoxicity would be attractive for the treatment of chronic inflammatory diseases. We believe the cytotoxic properties of triptolide are associated with triptolide's potential of undergoing covalent modifications. Triptolide possesses a highly oxygenated triepoxide system that could function as an anchor to proteins. Once anchored to a protein, a covalent modification to the bound protein could take place through triptolide's butenolide group in a Michael addition-like process leading to an irreversible interaction. Thus, the goal of this project was to synthesize truncated triptolide analogs possessing only the triepoxide moiety (Figure 22) and assess their anti-inflammatory activity as well as their cytotoxicity. Methods for accessing the triepoxide moiety are described in the following sections.

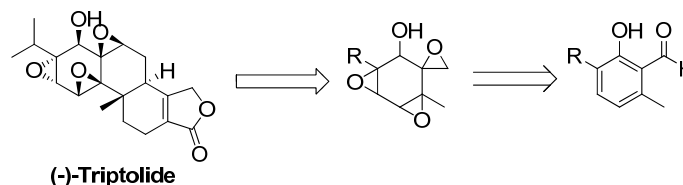


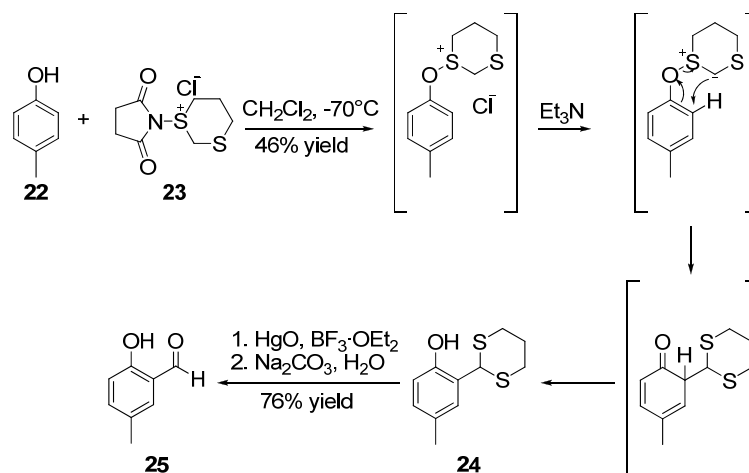
Figure 22. Truncated triptolide analogs

2.3.5 Methods for *o*-Formylation of Phenols

Many methods for the formylation of phenols have been developed such as the Duff reaction and the Vilsmeier-Haack reaction. Selective *o*-formylation of phenols relies on the phenol hydroxyl group to help direct the formylation to the ortho position. Some interesting and common methods for the *o*-formylation of phenols will be shown in this section.

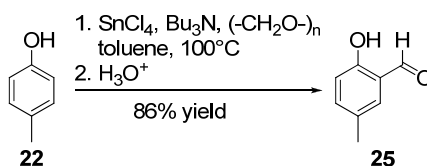
One interesting method utilized salt **23** formed from the reaction between *N*-chlorosuccinimide and dithiane to produce ortho derivatives such as **24** (Scheme 4).⁵⁷ In the presence of the salt, the phenol is believed to form an oxosulfonium species that when

treated with base forms an ylide. The ylide rearranges spontaneously to form a dienone which then tautomerizes to the *o*-substituted phenol. The desired *o*-formylated phenol is obtained in modest yield after hydrolysis of the resulting thioacetal.



Scheme 4. *o*-Formylation of *p*-cresol **22** using **23**

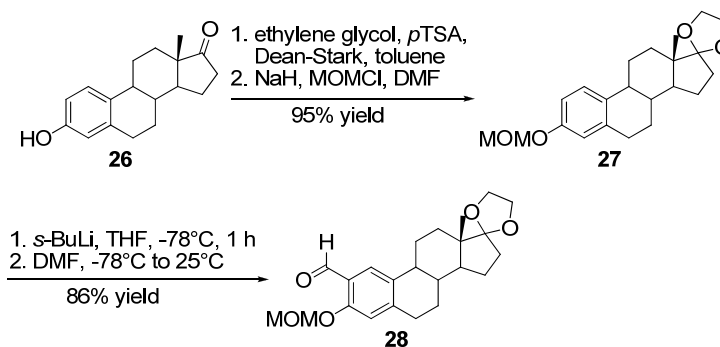
A similar strategy that is commonly used utilizes paraformaldehyde in the presence of a Lewis-acid such magnesium chloride, ferrous chloride, aluminum chloride, or stannic chloride (Scheme 5).^{58,59} The phenol and Lewis-acid form a phenoxide complex in which the metal atom is able to coordinate as well as orient formaldehyde for nucleophilic attack by the phenol. Intramolecular rearrangement through a dienone intermediate provides the saligenol derivative. Finally, a second equivalent of formaldehyde is needed for a redox reaction to provide the desired salicylaldehyde product.



Scheme 5. Lewis acid promoted *o*-formylation of *p*-cresol **22**

Ortho-directing derivatives of phenols such as a MOM ether can be used to access

o-substituted products. When treated with *sec*-butyllithium and a reagent containing a formyl group such as dimethylformamide (DMF), the *o*-formylated product can be obtained (Scheme 6).⁶⁰

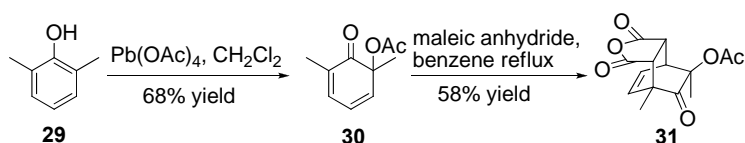


Scheme 6. Utilization of a MOM group for the *o*-formylation of a phenol

2.3.6 Methods for Oxidative Dearomatization

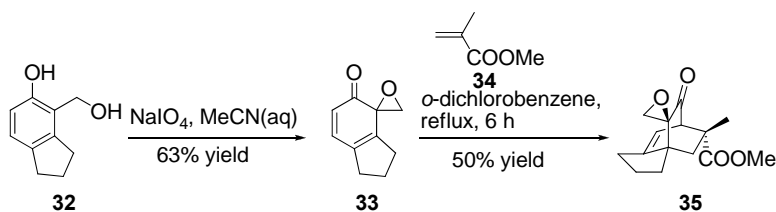
Oxidation of phenols using a variety of reagents can be used to access synthetically useful dienones and is known as the Wessely oxidation or oxidative dearomatization. During the transformation an intramolecular or intermolecular nucleophile is added to the phenol undergoing oxidation. Dienones obtained through this process are usually subjected to further modifications most commonly involving a Diels-Alder reaction or further oxidation.

Auksi and co-workers investigated 6-acetoxy-2,6-dimethyl-2,4-cyclohexadione **30** in a number of Diels-Alder reactions with maleic anhydride as well as with α,β -unsaturated carboxylic acids (Scheme 7).⁶¹ 6-Acetoxy-2,6-dimethyl-2,4-cyclohexadione **30** was obtained by treating 2,6-dimethylphenol **29** in dichloromethane with lead tetraacetate for one hour. Compound **30** was then reacted with maleic anhydride in refluxing benzene to produce compound **31**.



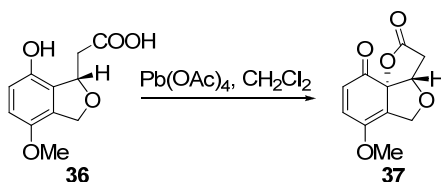
Scheme 7. Synthesis of 6-acetoxy-2,6-dimethyl-2,4-cyclohexadione

Oxidation of salicylic alcohols with either lead tetraacetate or sodium periodate leads to the formation of spiroepoxy cyclohexadiones as products. Singh and co-workers oxidized a salicylic alcohol derivative **32** in the presence of sodium periodate and then subjected the product to a Diels-Alder reaction with **34** (Scheme 8).⁶²



Scheme 8. Oxidation of a salicylic alcohol with sodium periodate

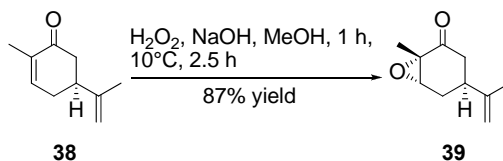
In a similar fashion, tethered carboxylic acids can give rise to lactones upon treatment of phenols with an oxidant. Cox and co-workers synthesized the tricyclic core of lactonamycin through oxidative dearomatization with lead tetraacetate (Scheme 9).⁶³



Scheme 9. Lactone formation via Wessely oxidation

2.3.7 Epoxidation of Electron Deficient Olefins

Conjugated ketones can be oxidized to give epoxy ketones by a variety of reagents. The most common conditions for the oxidization of α,β -unsaturated ketones involves alkaline hydrogen peroxide (Scheme 10); however, other reagents such as sodium borate and tetrahexylammonium hydrogen sulfate, potassium fluoride/aluminum oxide and *t*-butyl hydrogen peroxide, and 1,8-diazabicyclo[5.4.0]undec-7-ene (DBU) with *t*-butyl hydrogen peroxide can also be used. In addition, diethylzinc can be treated with oxygen in the presence of a chiral amino-alcohol to give epoxy ketones with high enantioselectivity. Peroxyacids typically do not result in epoxy ketone products.



Scheme 10. Oxidation of an enone with alkaline hydrogen peroxide⁹⁵

Asymmetric versions exist for most of the commonly used methods for epoxidation of α,β -unsaturated ketones. These methods utilize either a chiral epoxidation agent such as Shi's catalyst or a chiral ligand-metal peroxide system. Hinch and co-

workers developed a catalytic asymmetric epoxidation system in which the epoxidizing complex is generated from *t*-butyl hydrogen peroxide and diethyl tartrate in the presence of a magnesium base (Figure 23).⁶⁵ This system gives rise to reactions that proceed in 90% to 99% conversion and result in products ranging in 71% to 96% ee.

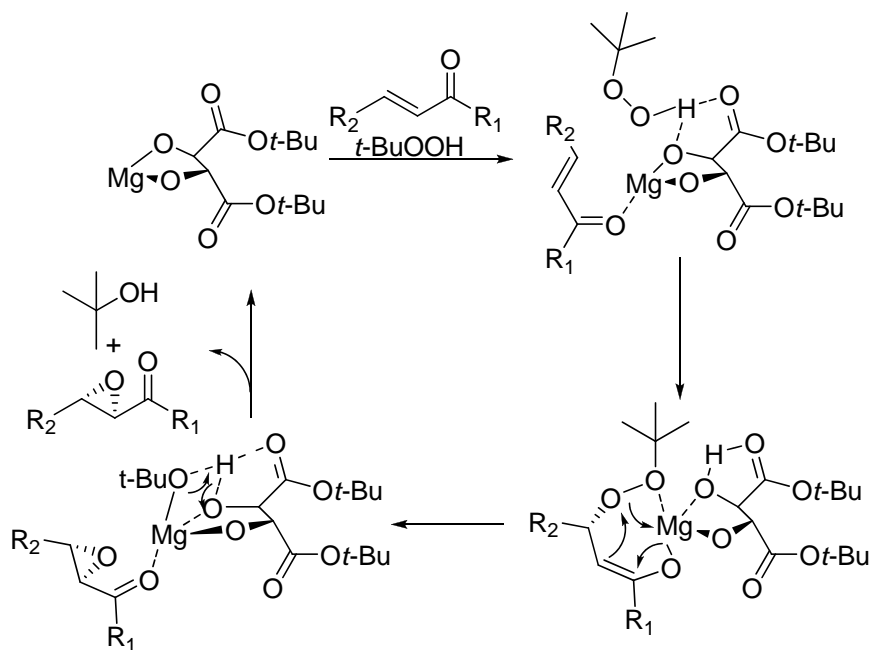


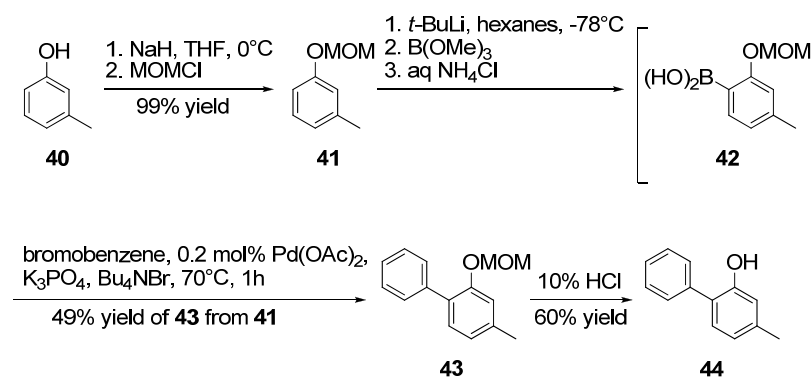
Figure 23. Proposed mechanism for the asymmetric epoxidation of enones utilizing the alkyl-tartrate magnesium system

2.4 Results and Discussion

2.4.1 Synthesis of 2,5-substituted phenols

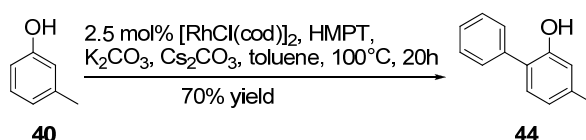
2.4.1.1 Synthesis of 5-methyl-2-phenylphenol (**44**)

Salicylic alcohols derived from phenols were used to access the triepoxide system of the truncated triptolide analogs. Phenols that were not commercially available were synthesized. 5-Methyl-2-phenylphenol **44** was successfully synthesized using three methods. Initially **44** was synthesized using a Suzuki cross-coupling approach utilizing the boronic acid **42** obtained from *m*-cresol **40** (Scheme 11).⁶⁸ Commercially available *m*-cresol was protected as its methoxy methyl (MOM) ether **41**. The MOM protecting group functioned as an ortho-directing group for the Snieckus directed *ortho* metalation of **41**. The lithiate of **41** was quenched with trimethyl borate and was then hydrolyzed to afford the boronic acid **42**. The crude boronic acid **42** was used immediately in a Suzuki cross-coupling reaction with bromobenzene to afford the MOM protected 5-methyl-2-phenylphenol **43**.^{69,70} The desired compound **44** was obtained in 29% overall yield after treating **43** with 10% hydrochloric acid solution.



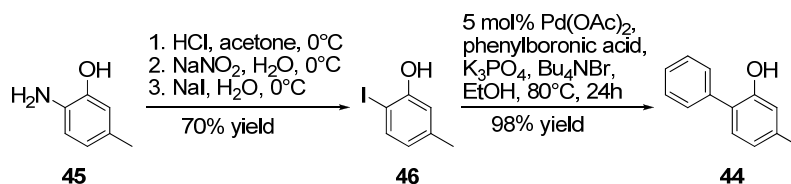
Scheme 11. Synthesis of 5-methyl-2-phenylphenol **44** utilizing the Suzuki cross-coupling reaction

Though compound **44** was successfully synthesized using the Suzuki cross-coupling method, the synthetic route that was used contained multiple steps and suffered from a low overall yield. The overall yield suffered from the inefficient *o*-lithiation of compound **41** as well as in the deprotection of **43** to obtain the desired compound **44**. A more efficient and higher yielding route to compound **44** was desired. Oi et al. synthesized compound **44** in 65% yield in a one-pot reaction utilizing a rhodium catalyst and hexamethylphosphorous triamide (HMPT).⁷¹ Utilizing the optimized conditions of Oi et al. afforded compound **44** in 70% yield (Scheme 12).



Scheme 12. One-pot synthesis of compound **44** using a rhodium (I) catalyst

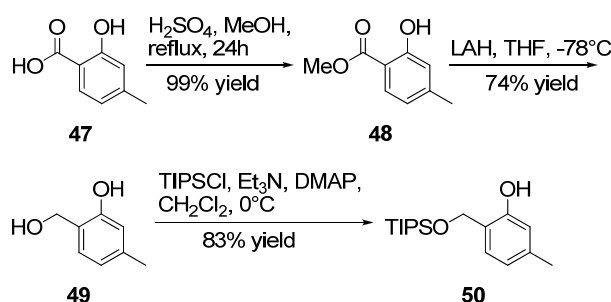
The method of Oi et al. provided **44** in one step and good yield; however, the soaring price and lack of availability of the rhodium catalyst hindered the application of this method for further use. Finally, an efficient and high yielding method for the synthesis of **44** was developed again employing a Suzuki cross-coupling reaction (Scheme 13). The commercially available 2-amino-5-methylphenol **45** was converted into the 2-iodo-5-methyl phenol **46** under Sandmeyer conditions in 75% yield.⁷² Compound **46** was then converted into compound **44** in 95% yield using palladium cross-coupling conditions.⁷³



Scheme 13. Synthesis of **44** from 2-amino-5-methylphenol **45**

2.4.1.2 Synthesis of 5-methyl-2-((triisopropylsilyloxy)methyl)phenol (**50**)

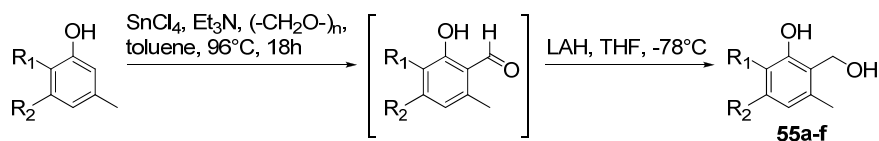
Compound **50** was generated to access triepoxide analogs possessing a hydroxyl group that could be further modified (Scheme 14). 4-Methylsalicylic acid **47** was converted to the commercially available methyl ester **48** upon treatment with sulfuric acid in methanol. ⁷⁴ The methyl ester was then reduced with lithium aluminum hydride (LAH) to the primary alcohol **49**. The primary alcohol was then treated with triisopropylsilyl chloride to obtain the desired compound **50**.



Scheme 14. Synthesis of compound **50**

2.4.2 Synthesis of salicylic alcohols

Commercial and synthetic phenols were *o*-formylated then reduced with LAH to afford salicylic alcohols (Scheme 15).⁶⁴ The desired phenols were treated with tin (IV) chloride in the presence of two equivalents of paraformaldehyde in order to obtain the *o*-formyl products. One equivalent of paraformaldehyde resulted in a mixture of starting phenol, the desired product, and the formylated phenol. Two equivalents of paraformaldehyde were used to drive the reaction to completion. The second equivalent of paraformaldehyde oxidized the salicylic alcohol-tin complex to the formylated product through an Oppenauer-type oxidation. The crude formylated products were then reduced with LAH to afford the corresponding salicylic alcohols in moderate overall yields (Table 2).



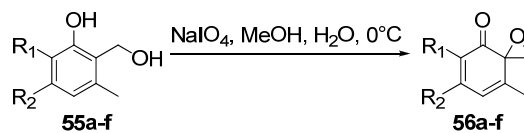
Scheme 15. Synthesis of salicylic alcohols

Phenol	R ₁	R ₂	Salicyclic Alcohol	% yield
51	Me	H	55a	68
52	Me	Me	55b	73
53	<i>i</i> -Pr	H	55c	79
54	<i>t</i> -Bu	H	55d	83
44	Ph	H	55e	55
50	TIPSOCH ₂ -	H	55f	65

Table 2. Results for the conversion of phenols into salicylic alcohols

2.4.3 Oxidative dearomatization of salicylic alcohols

The salicylic alcohols were then oxidized to obtain oxaspirocyclohexadienones which were used to access the truncated triepoxide triptolide analogs. Salicylic alcohols **55a-f** were treated with sodium periodate in methanol and water to obtain the racemic oxaspirocyclohexadienones **56a-f** (Scheme 16) as oily, yellow solids in moderate yield (Table 3).⁶⁴



Scheme 16. Sodium periodate oxidation of salicylic alcohols **55a-f**

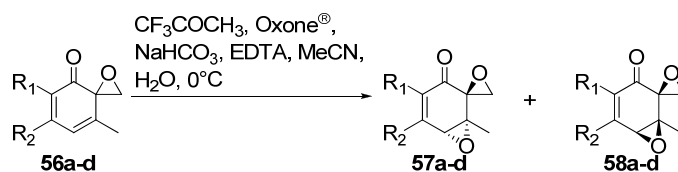
55	R ₁	R ₂	56, % Yield
a	Me	H	65
b	Me	Me	70
c	<i>i</i> -Pr	H	78
d	<i>t</i> -Bu	H	83
e	Ph	H	57
f	TIPSOCH ₂ -	H	74

Table 3. Results for the sodium periodate oxidation of salicylic alcohols **55a-f**

2.4.4 Synthesis of diepoxide analogs

2.4.4.1 Diepoxide formation

The monoepoxide dienones **56a-d** were further oxidized to their corresponding diepoxide enones with a dioxirane generated in situ from OXONE[®] and 1,1,1-trifluoroacetone (Scheme 17).⁶⁴ The reaction conditions produced both the *trans*-diepoxides **57a-d** and the *cis*-diepoxides **58a-d** for each substrate in good overall yield (Table 4). In all cases the *trans*- and *cis*- diepoxides were separated from one another using flash chromatography and were each further purified by recrystallization.



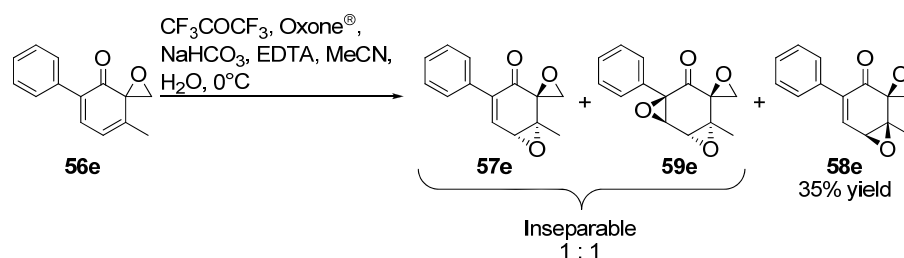
Scheme 17. Synthesis of *trans*- and *cis*- diepoxides

56	R ₁	R ₂	Overall % Yield	57 : 58
a	Me	H	65	1 : 2
b	Me	Me	72	1 : 1.8
c	<i>i</i> -Pr	H	74	1 : 2.1
d	<i>t</i> -Bu	H	85	1 : 2.2

Table 4. Results for the synthesis of diepoxides

2.4.4.2 Epoxidation of 56e

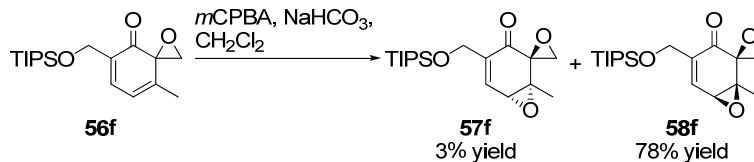
The phenyl substituted dienone **56e** was subjected to the same epoxidation conditions as described in the previous section (Scheme 18).⁶⁴ The *cis*-diepoxide **58e** was isolated in moderate yield; however, the *trans*-diepoxide **57e** was isolated along with its triepoxide **59e** in a 1:1 ratio. Attempts to separate the *trans*-diepoxide from its triepoxide were conducted but failed.



Scheme 18. Oxidation of dienone **56e**

2.4.4.3 Epoxidation of **56f**

The monoepoxide **56f** was converted into its corresponding diepoxides upon treatment with *m*CPBA in dichloromethane (Scheme 19).⁷⁵ While the *cis*-diepoxide was isolated in good yield, only a trace quantity of the *trans*-diepoxide was isolated.

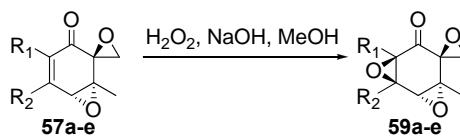


Scheme 19. Treatment of monoepoxide **56f** with *m*CPBA

2.4.5 Triepoxide formation

2.4.5.1 Epoxidation of *trans*-diepoxides

All *trans*-diepoxides were treated with basic hydrogen peroxide in methanol (Scheme 20) to afford a single triepoxide product (Table 5).⁶⁴



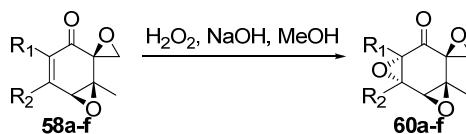
Scheme 20. Epoxidation of *trans*-diepoxides

57	R ₁	R ₂	59 % Yield
a	Me	H	78
b	Me	Me	81
c	<i>i</i> -Pr	H	89
d	<i>t</i> -Bu	H	92
e	Ph	H	76
f	TIPSOCH ₂ -	H	77

Table 5. Results for the epoxidation of **57a-e**

2.4.5.2 Epoxidation of *cis*-diepoxides

The *cis*-diepoxides **58a-f** were also treated with basic hydrogen peroxide in methanol (Scheme 21) affording a single triepoxide product (Table 6).⁶⁴



Scheme 21. Epoxidation of *cis*-diepoxides

58	R ₁	R ₂	60, % Yield
a	Me	H	82
b	Me	Me	80
c	<i>i</i> -Pr	H	88
d	<i>t</i> -Bu	H	93
e	Ph	H	79
f	TIPSOCH ₂ -	H	67

Table 6. Results for the epoxidation of *cis*-diepoxides **58a-f**

X-ray crystallography was used to confirm the relative stereochemistry of compounds **60a** and **60b** (Figure 24).⁶⁴ The structure received for compound **60a** was in agreement with the structure published by Yang and co-workers. Since both compounds **60a** and **60b** shared the same relative stereochemistry, it was assumed the other triepoxides in this series also possessed this stereochemistry. Since the epoxidation of the α,β position is anti to the γ,δ position, compounds **60a** and **60b** came from compounds **58a** and **58b** respectfully.

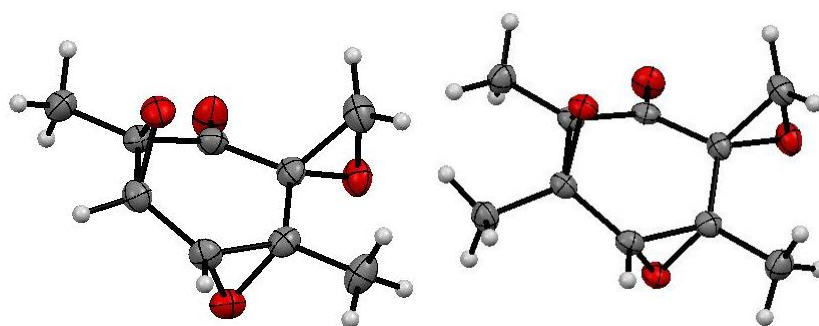
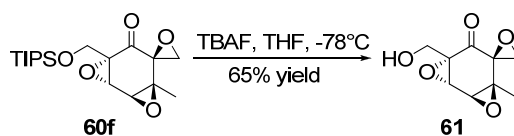


Figure 24. X-ray structures of compounds **60a** and **60b**

2.4.6 Deprotection of the triisopropylsilyl protected analogs

Compound **58f** as well as **60f** were treated with tetrabutylammonium fluoride (TBAF) in THF to unmask the primary alcohol in each compound.⁷⁶ The product for the deprotection of **58f** rapidly decomposed yielding no isolated product. In contrast, the desired product resulting from the deprotection of **60f** was isolated in moderate yield (Scheme 22).



Scheme 22. Deprotection of compound **60f**

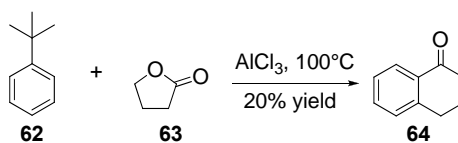
2.4.7 Design and synthesis of bicyclic truncated triptolide analogs

Synthesizing analogs that focused on the highly oxygenated region of triptolide

eliminated a large portion of the triptolide molecule potentially altering recognition elements that allow triptolide to bind to its target. In order to recover the lost recognition elements analogs more closely resembling triptolide were synthesized.

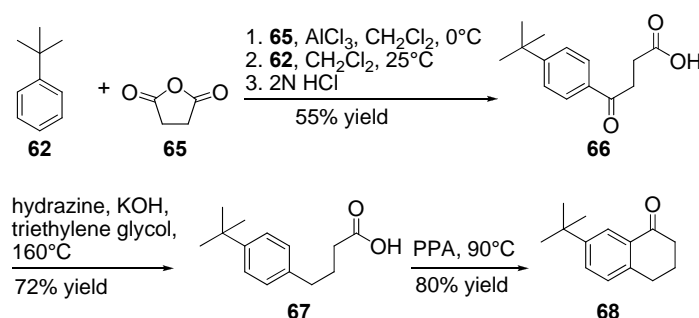
2.4.7.1 Synthesis of 7-*tert*-butyl-8-hydroxytetralol 70

Pal et al. converted toluene into 7-methyl-tetralone under Friedel-Crafts conditions.⁷⁷ Initially these conditions were used for the conversion of *tert*-butylbenzene **62** into 7-*tert*-butyl-tetralone **68**. However, under the conditions of Pal et al. elimination of the *tert*-butyl group occurred resulting in the isolation of the known and commercially available α -tetralone **64** in 20% yield (Scheme 23).



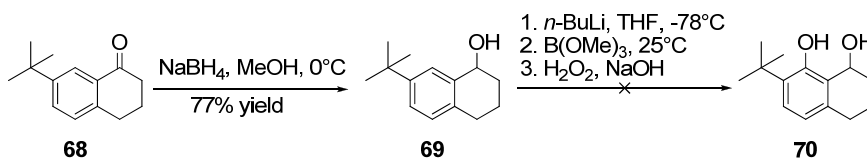
Scheme 23. Attempted synthesis of 7-*tert*-butyl-tetralone **68**

Since the one-step method failed to produce the desired tetralone, a more traditional multi-step route was investigated (Scheme 24). Reducing the number of equivalents of aluminum chloride used as well as allowing the reaction to proceed at ambient temperature afforded the desired condensation product **66**.⁷⁸ Compound **66** was then subjected to Wolff-Kishner conditions to afford 4-(4-*tert*-butylphenyl)butanoic acid **67**.⁷⁹ The desired 7-*tert*-butyl-tetralone **68** was formed after dehydration and ring-closing of **67** promoted by polyphosphoric acid (PPA) at elevated temperature.⁸⁰



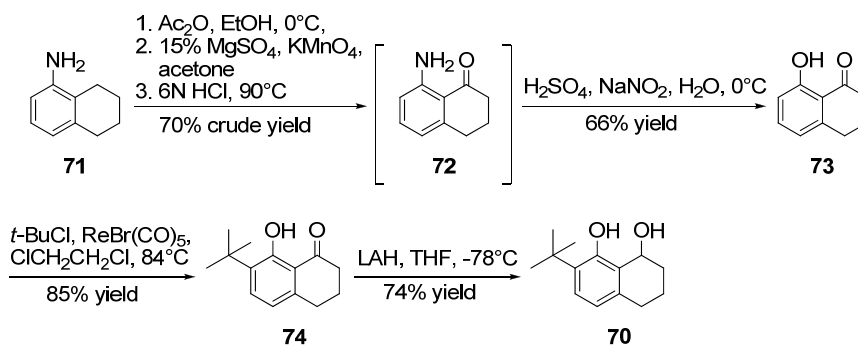
Scheme 24. Synthesis of 7-*tert*-butyl-tetralone **68**

The next step was to reduce the ketone of **68** and then introduce a hydroxyl group to form the desired 7-*tert*-butyl-8-hydroxytetralol **70**. The reduction of **68** with sodium borohydride (NaBH_4) proceeded in excellent yield (Scheme 25).⁶⁴ The resulting alcohol was treated with multiple equivalents of *n*-butyllithium in order to form the dianion. The goal was to quench the dianion with trimethylborate followed by treatment with basic hydrogen peroxide to form 7-*tert*-butyl-8-hydroxytetralol **70**. However, all attempts to install the hydroxyl group failed resulting in the isolation of only starting material.



Scheme 25. Attempted synthesis of 7-*tert*-butyl-8-hydroxytetralol **70**

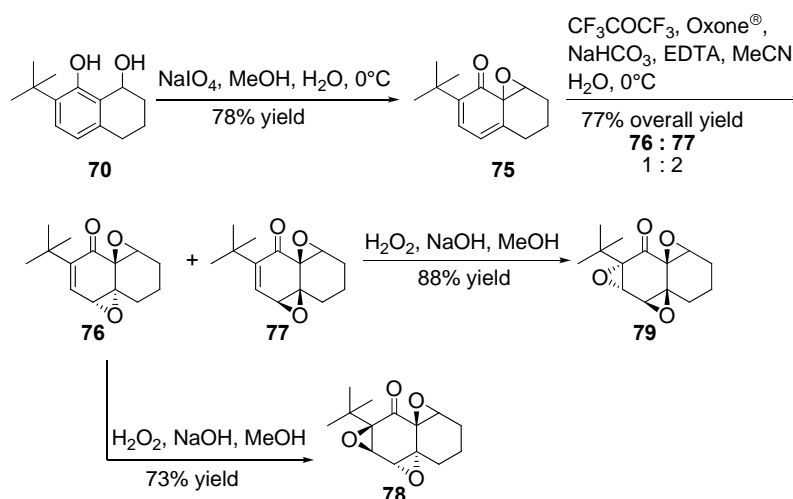
Finally, 7-*tert*-butyl-8-hydroxytetralol **70** was successfully synthesized starting from the commercially available 5,6,7,8-tetrahydro-1-naphthylamine **71** (Scheme 26). Using the one-pot regioselective oxidation method of Nguyen and co-workers, compound **71** was converted into the known 8-aminotetralone **72** in moderate yield.⁸¹ Compound **72** was then subjected to Sandmeyer conditions and converted into 8-hydroxytetralone **73**.⁸² The *tert*-butyl group was installed by using a rhenium catalyzed Friedel-Crafts reaction to produce compound **74**.⁸³ Finally, compound **74** was reduced with LiAlH₄ to afford the desired 7-*tert*-butyl-8-hydroxytetralol **70**.



Scheme 26. Synthesis of 7-*tert*-butyl-8-hydroxytetralol **70**

2.4.7.2 Synthesis of bicyclic diepoxides and triepoxides

Compound **70** was subjected directly to the oxidative dearomatization conditions previously described in order to form the dienone **75** (Scheme 27).⁶⁴ The dienone was then further oxidized using the in situ generated dioxirane described previously yielding two diastereoisomers.⁶⁴ The two diastereoisomers were separated by flash chromatography and then were converted to their corresponding triepoxides upon treatment with basic hydrogen peroxide.⁶⁴



Scheme 27. Synthesis of bicyclic diepoxides and triepoxides

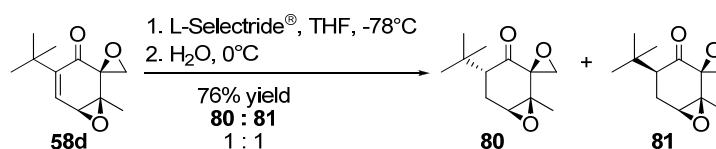
2.4.8 Minimization of reactive functional groups

Even though the main goal was to synthesize analogs of the highly oxygenated region of triptolide, the presence of reactive functional groups such as epoxides and enones were a concern. These reactive functional groups can undergo covalent modifications themselves presenting a liability for the treatment of chronic inflammatory disorders. Therefore, the synthesis of a series of analogs focused on minimizing the presence of reactive functional groups was undertaken. The aim was to generate truncated triptolide analogs that retained activity with minimal reactive functional groups

present.

2.4.8.1 Reduction of the carbon-carbon double bond in **58d**

One way in which the enone was eliminated in compound **58d** was by reducing the carbon-carbon double bond. This transformation was carried out by treating **58d** with L-Selectride[®] in THF affording two diastereoisomers (Scheme 28).⁸⁴



Scheme 28. Treatment of **58d** with L-Selectride[®]

The relative stereochemistry for compounds **80** and **81** was established using X-ray crystallography (Figure 25).

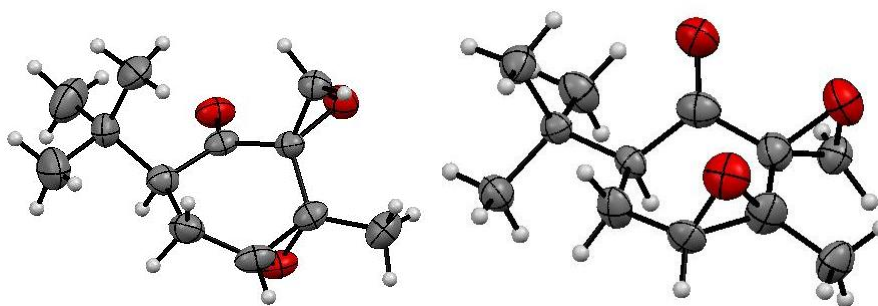
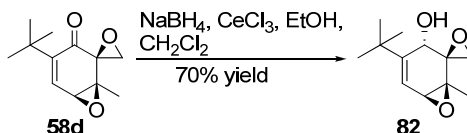


Figure 25. X-ray structures of compounds **80** and **81**

2.4.8.2 Carbonyl reduction

Additionally, the enone in **58d** was removed by reduction of the carbonyl group, thus disrupting the conjugated enone system. Compound **58d** was treated with cerium trichloride and NaBH₄ in dichloromethane and ethanol to afford a single diastereoisomer in good yield (Scheme 29).⁸⁵



Scheme 29. Reduction of the carbonyl in **58d**

X-ray crystallography was used to establish the relative stereochemistry of compound **82** (Figure 26).

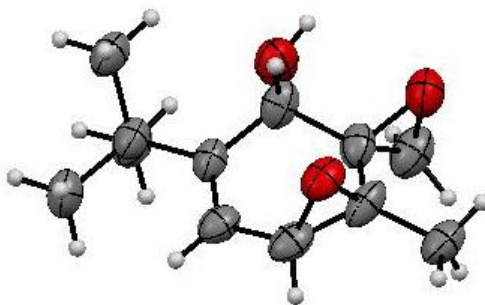
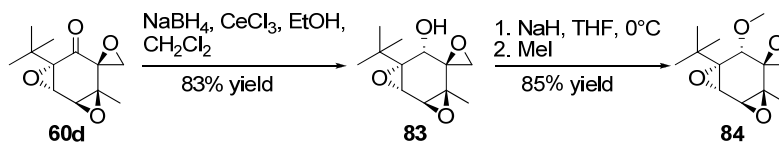


Figure 26. Relative stereochemistry of compound **82**

In a similar fashion the carbonyl of **60d** was reduced to give a single product **83** (Scheme 30).⁸⁵ Compound **83** was then converted to the methyl ether **84**.⁸⁶ All attempts to invert the stereochemistry of compound **83** failed.



Scheme 30. Reduction of **60d**

X-ray Crystallography was used to determine the relative stereochemistry of compound **83** (Figure 27).

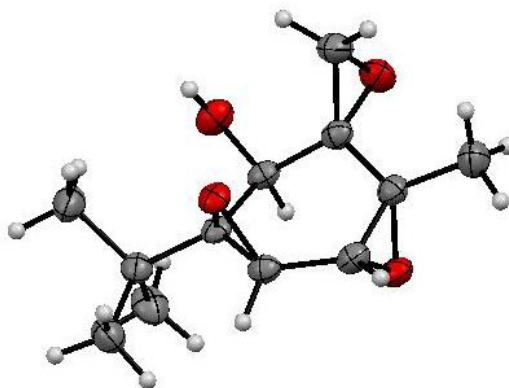
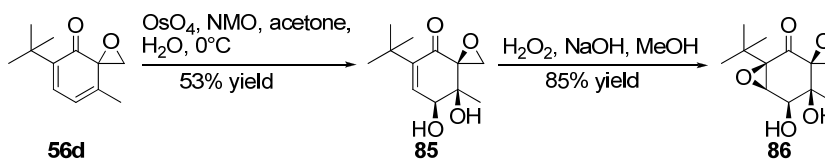


Figure 27. X-ray structure of compound **83**

2.4.8.3 Substitution of epoxides with diols

In continuing our efforts to minimize reactive functional groups, it was determined that a diol would be a suitable substitute for an epoxide. Therefore, each epoxide was systematically replaced with a diol in order to determine the contribution each epoxide had on activity. First, dienone **56d** was treated with a catalytic amount of osmium tetroxide in the presence of 4-methylmorpholine *N*-oxide (NMO) to afford the diol **85** in moderate yield (Scheme 31).⁸⁷ Compound **85** was then further oxidized to the triepoxide **86** upon treatment with basic hydrogen peroxide.⁶⁴



Scheme 31. Synthesis of diol **85**

The X-ray structures for compounds **85** and **86** were solved and showed the relative stereochemistry in each compound (Figure 28).

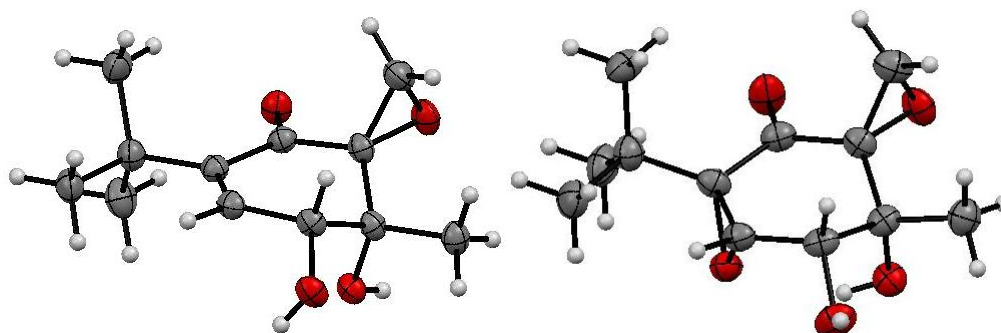
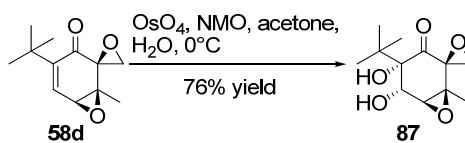


Figure 28. X-ray structures of compounds **85** and **86**

In addition, **58d** was converted to the diol **87** using the same oxidation conditions used in the synthesis of **85**. Thus, **59d** was treated with osmium tetroxide and NMO to afford a single product in good yield (Scheme 32).⁸⁷



Scheme 32. Synthesis of diol **87**

The relative stereochemistry of compound **87** was established through X-ray crystallography (Figure 29).

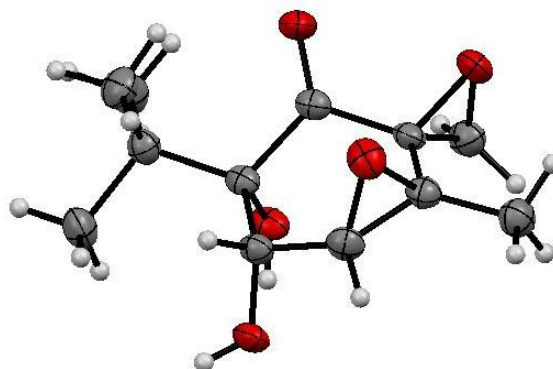
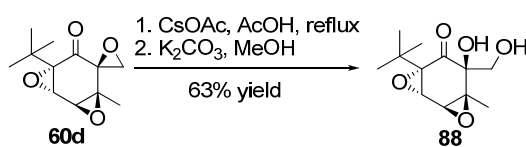


Figure 29. X-ray structure of compound **87**

Since the spiro epoxide is formed during the sodium periodate promoted oxidative dearomatization reaction giving access to the di- and tri- epoxide analogs, conditions to selectively open the spiro epoxide to form the diol were investigated. Compound **60d** was treated with cesium acetate in refluxing acetic acid to open the epoxide. Next the acetic acid was removed under reduced pressure. The resulting residue was treated with potassium carbonate in methanol providing the diol **88** (Scheme 33).⁸⁸



Scheme 33. Synthesis of diol **88**

X-ray crystallography was used to confirm the structure and establish the relative stereochemistry of compound **88** (Figure 30).

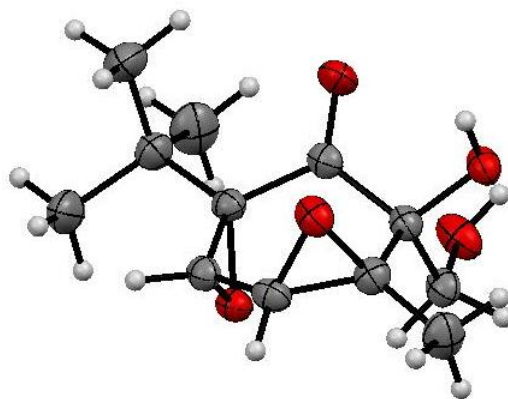
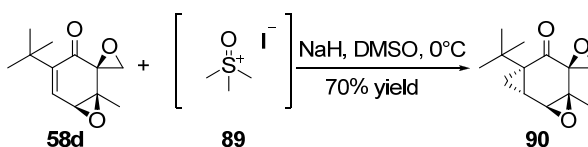


Figure 30. X-ray structure of compound **88**

2.4.8.4 Cyclopropanation of **58d**

A cyclopropanation reaction was conducted on **58d** in addition to the dihydroxylation and reduction reactions. The cyclopropyl group was thought to occupy the same space as the epoxide without participating in any possible covalent modifications. Thus, a Corey-Chaykovsky cyclopropanation reaction was carried out on **58d** using dimethylsulfoxonium methylide generated in situ from trimethylsulfoxonium iodide **89** and sodium hydride (Scheme 34).^{89,90}



Scheme 34. Corey-Chaykovsky cyclopropanation of **58d**

The relative stereochemistry of compound **90** was established using X-ray crystallography (Figure 31).

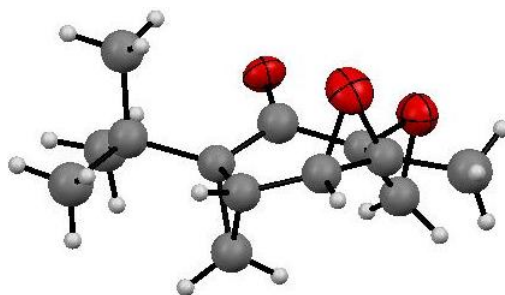
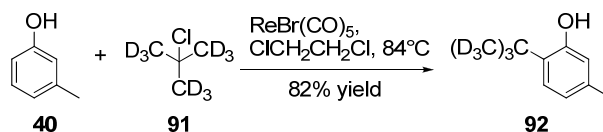


Figure 31. X-ray structure of compound **90**

2.4.9 Synthesis of deuterated analogs for use as biological standards

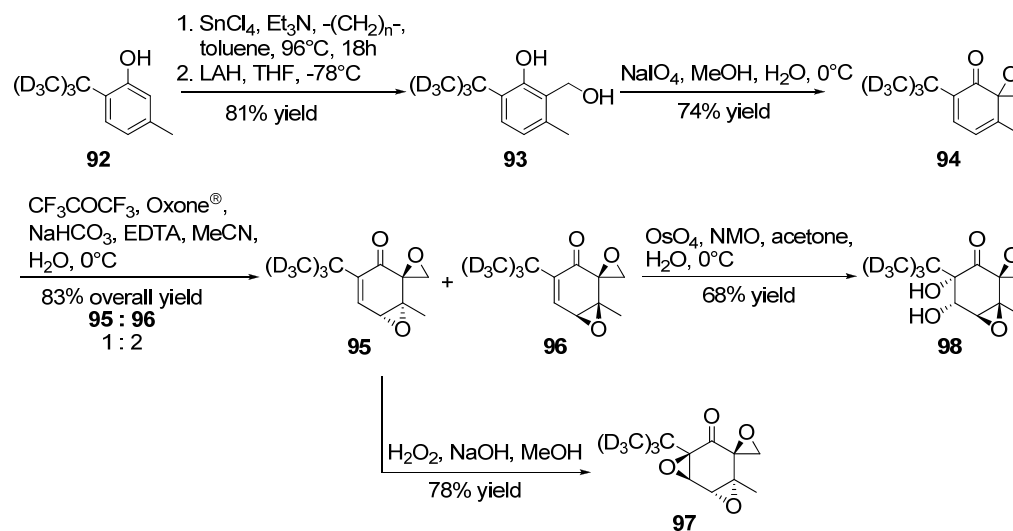
Compounds **58d**, **59d**, and **87** were administered orally to mice in a pharmacokinetic study to determine plasma half-life, distribution, and rate of clearance. In order to quantitate the levels of each compound in plasma deuterated analogs of each compound were synthesized for use as internal standards for mass spectrometry. A deuterated *tert*-butyl group was introduced into *m*-cresol **40** affording **92**. Thus, *m*-cresol **40** was treated with 2-chloro-2-methylpropane- d_9 **91** in the presence of a rhenium catalyst to afford **92** in good yield (Scheme 35).⁸³



Scheme 35. Synthesis of deuterated 2-*tert*-butyl-5-methylphenol

Compound **92** was then subjected to the same reactions as described before to obtain the desired deuterated products (Scheme 36). Compound **92** was converted into the salicylic alcohol **93** as described previously followed by oxidation with sodium periodate to obtain the dienone **94**.⁶⁴ After treating **94** with OXONE[®] and 1,1,1-

trifluoroacetone, the two diepoxides, **95** and **96**, were obtained.⁶⁴ Compound **95** was then treated with basic hydrogen peroxide to afford **97** in good overall yield.⁶⁴ A portion of **96** was treated with osmium tetroxide in the presence of NMO in order to obtain **98**.⁸⁷



Scheme 36. Synthesis of deuterated analogs

2.4.10 Biological evaluation of truncated triptolide analogs

The goals of the in vitro assays were to show that the triptolide analogs are less toxic than triptolide, more water soluble than triptolide, and retain anti-inflammatory properties. A XTT cell proliferation and viability assay was used to determine the cytotoxicity of all test articles. The triptolide analogs were screened for their ability to reduce inflammation in two animal models as well as reduce pro-inflammatory cytokine levels in various cellular assays. Finally, nephelometry was used to determine water solubility.

2.4.10.1 XTT cell proliferation and viability assay

The XTT cell proliferation and viability assay was used to determine if the truncated triptolide analogs were cytotoxic. The colorimetric assay is based on the cleavage of the yellow XTT tetrazolium salt into an orange formazan dye by mitochondrial dehydrogenase (Figure 32). Thus, conversion only occurs in viable cells and is dependent on the number of viable cells.

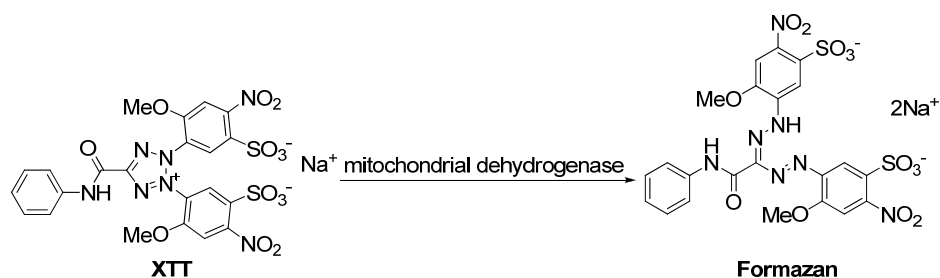


Figure 32. Conversion of XTT into formazan dye

The XTT assay was used to evaluate the effects triptolide, triptonide, the synthetic NF- κ B inhibitor QNZ, and a selection of truncated triptolide analogs had on cell proliferation (Figure 33).⁹⁸

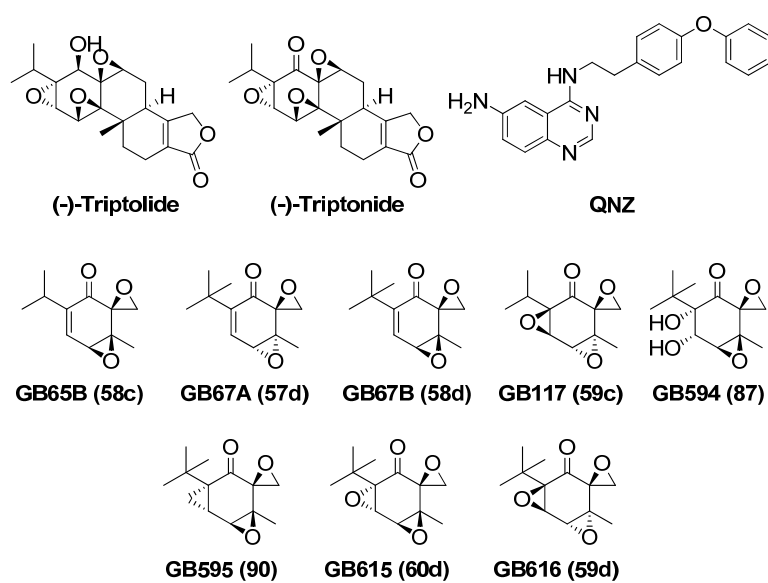


Figure 33. Compounds screened in XTT assay

Initially, the compounds were screened for cytotoxicity in peripheral blood mononuclear cells (PBMCs) stimulated with and without lipopolysaccharide (LPS) (Appendix A). Both (-)-triptolide and (-)-triptonide at 100 nM and 1000 nM impaired cell proliferation (Figure 34). QNZ and the truncated triptolide analogs that were screened did not impair PBMC proliferation at any of the concentrations tested.

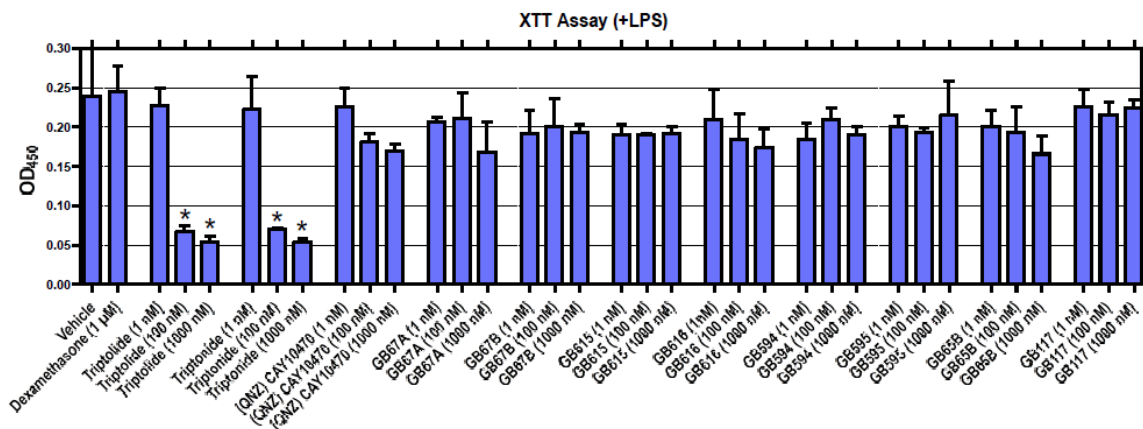


Figure 34. LPS stimulated PBMC proliferation results

In addition, triptolide, QNZ, **GB67B**, and **GB594** were also screened for their effects on cell proliferation in Jurkat cells stimulated with and without phorbol 12-myristate 13-acetate (PMA) and phytohemagglutinin (PHA) (Appendix B). Inhibition of cell proliferation was only observed with triptolide at 50 nM (Figure 35).

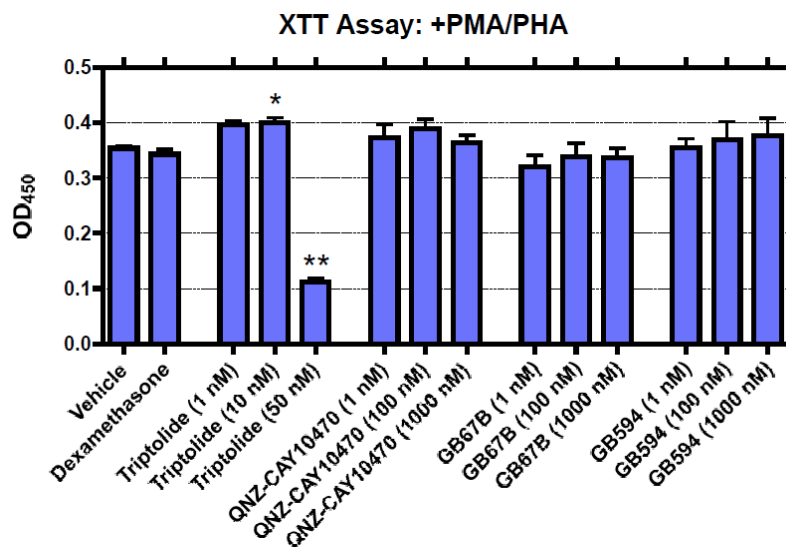


Figure 35. Cell proliferation assay in Jurkat cells with PMA and PHA

Mouse splenocytes were incubated with triptolide, QNZ, **GB67B**, and **GB594** in a XTT assay (Appendix C). Surprisingly, triptolide did not appear to be cytotoxic at any of the concentrations tested (Figure 36). In contrast to the previous XTT assays performed on these compounds, triptolide, **GB67B**, and **GB594** enhanced cell proliferation at some of the concentrations tested.

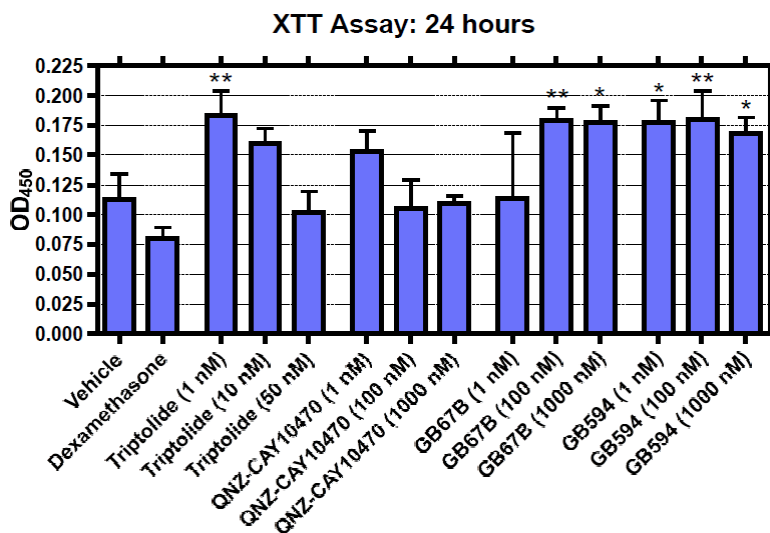


Figure 36. Mouse splenocyte XTT assay results

2.4.10.2 Carrageenan edema mouse model

The triptolide analogs (Figure 37) were screened in a carrageenan edema mouse model (Experimental).

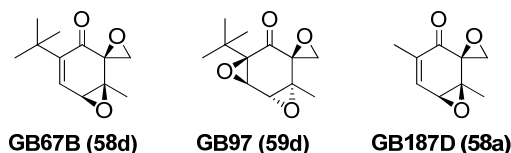


Figure 37. Analogs screened in carrageenan edema model

Acute inflammation was induced in mice by injecting λ -carrageenan into the right hind paw of the mice. The left hind paw was injected with saline as a control. Triptolide

analogs, suspended in 9:1 45% β -cyclodextrin/DMSO, were administered i.p. at 30 mg/kg daily for 3 days. Two hours after the final injection of test articles, the final paw measurements were taken. The volume of the control paws were subtracted from the paws injected with λ -carrageenan to obtain the edema volume. The results, shown in Table 7 and Figure 38, indicate **GB67B** significantly reduced the edema with a change of paw volume = 0.48 were as the change in paw volume for the control was = 0.86.

		Control		97B		67B		187D	
		R	L	R	L	R	L	R	L
M1		2	1.1	1.8	1.1	1.8	1.2	1.6	1.2
M2		2	1.2	2	1.1	1.5	1.1	1.9	1.2
M3		2	1.3	1.8	1.2	1.5	1.2	2.4	1.1
M4		2.4	1.4	1.9	1.2	2	1.2	1.9	1.3
M5		2.1	1.2	1.9	1.1	1.5	1.2	1.8	1.2
Average		2.1	1.24	1.88	1.14	1.66	1.18	1.92	1.2
Δ Paw		0.86		0.74		0.48		0.72	

Table 7. Results of the carrageenan paw edema model

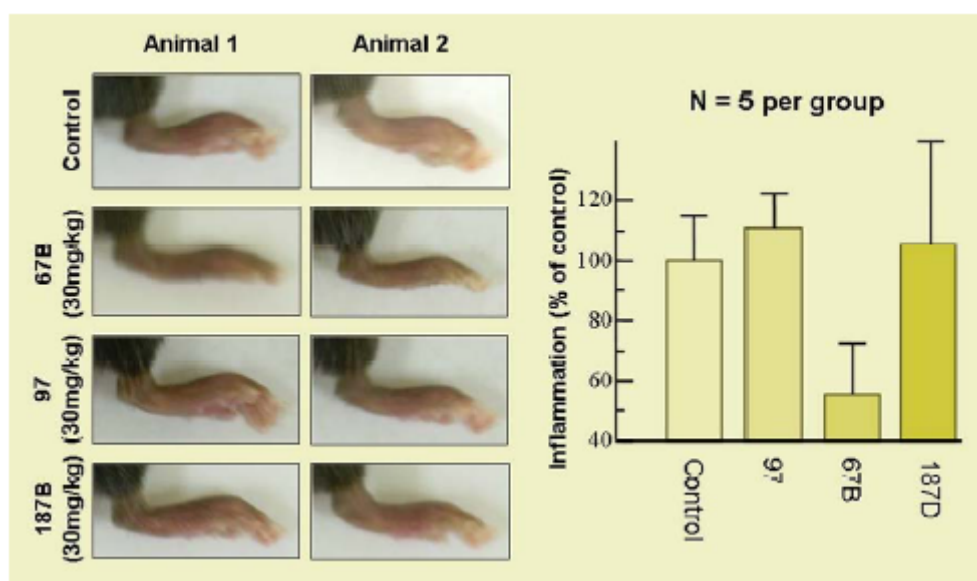


Figure 38. Pictures of paw edema

In addition to the observed changes in paw volume, RNA levels for pro-inflammatory cytokines were measured. RNA was isolated from livers of mice challenged with carrageenan, and the levels were measured in a RNase protection assay.

The introduction of carrageenan greatly increased the levels of TNF- α , IL-1 α , and IL-1 β RNA levels (Figure 39). The three triptolide analogs were able to reduce the cytokine upregulation induced by carrageenan; however, **GB67B** was the only analog to significantly reduce paw inflammation. Interestingly, **GB67B** greatly reduced TNF- α RNA levels (Figure 39).

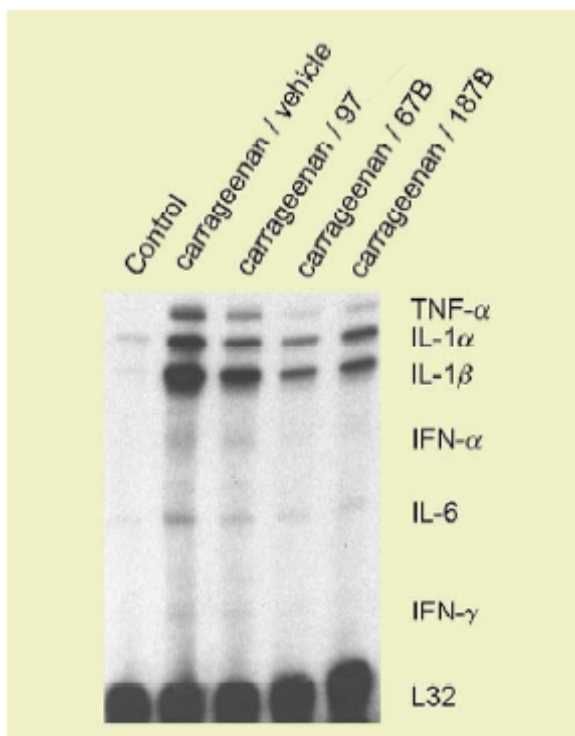


Figure 39. RNA levels of pro-inflammatory cytokines from livers of mice challenged with carrageenan

2.4.10.3 Adjuvant induced arthritis in rats

Two animal models, an adjuvant induced arthritis model and a carrageenan edema model, were used to determine if the truncated analogs retained anti-inflammatory properties. Compound **GB67B** (Figure 40) was chosen for evaluation in an adjuvant induced arthritis model in rats (Appendix D). Arthritis in Lewis rats was induced following exposure to inactivated *Mycobacterium tuberculosis*. Two groups of rats were

administered **GB67B** orally. One group received **GB67B** at a dose of 10 mg/kg once daily, and the other group received **GB67B** at 30mg/kg once daily. The groups receiving **GB67B** were compared to rats receiving a 1 mg/kg intraperitoneal injection of dexamethasone once daily. Administration of **GB67B** and dexamethasone continued for 28 days.

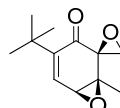


Figure 40. Structure of **GB67B (58d)**

During the course of the study, the body weights of the animals were monitored (Figure 41). Animals in the vehicle treated group gained 15% of body weight during the course of the study. The groups receiving **GB67B** gained 21% of body weight during the 28 day study. However, rats receiving dexamethasone only gained 2% of body weight which is a typical result.

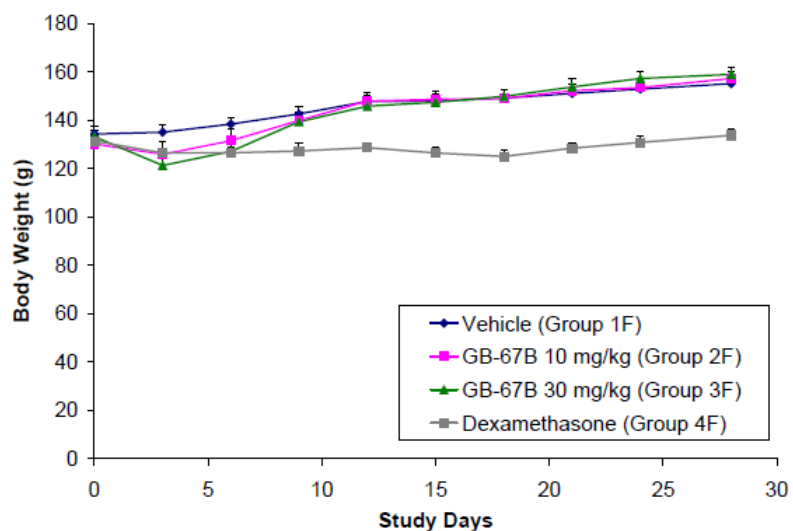


Figure 41. Body weights of animals during study

In addition, the paw volumes of the animals were monitored during the 28 day

study (Figure 42). Dexamethasone completely prevented an increase in paw volume during the course of the study. The highest dose of **GB67B** was able to reduce paw volume by 50%.

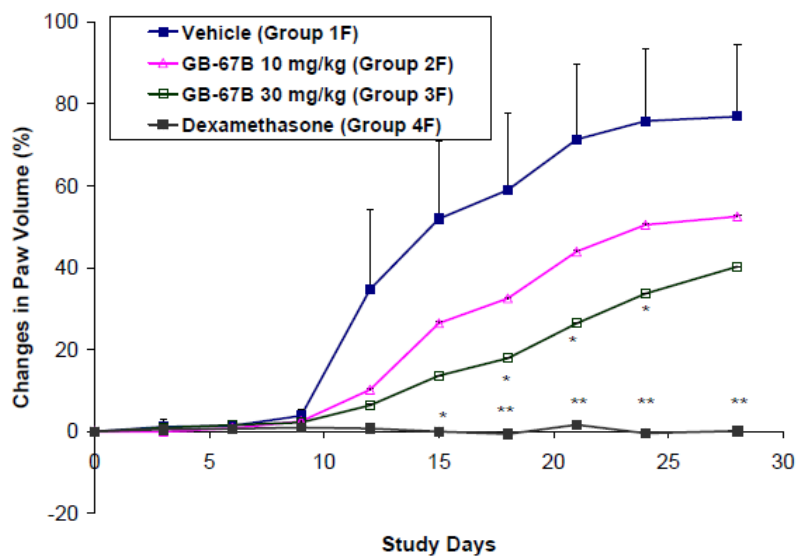


Figure 42. Changes in paw volume

The ability for **GB67B** and dexamethasone to reduce signs of arthritogenic responses in peripheral joints were scored throughout the 28 day study (Figure 43). Dexamethasone completely prevented the development of disease. Compound **GB67B** at the highest dose tested was slightly active in reducing signs of the disease.

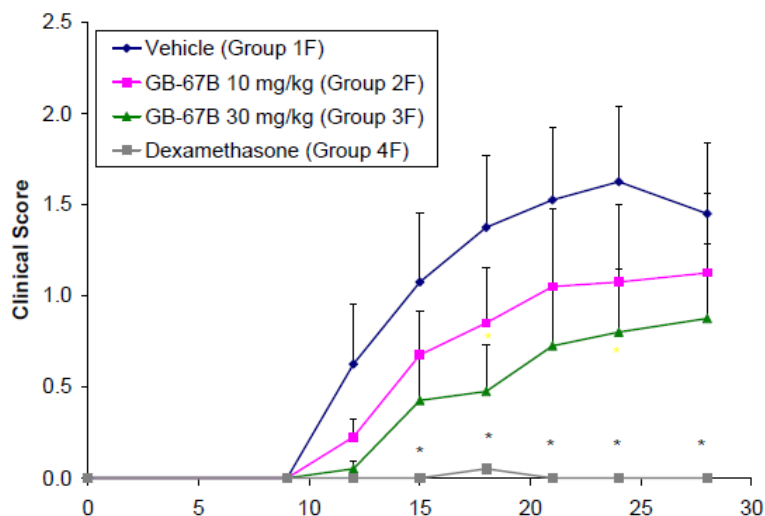


Figure 43. Arthritis score for **GB67B** and dexamethasone

2.4.10.4 Inhibition of NF- κ B activation

Triptolide is known to inhibit the transactivation of NF- κ B resulting in decreased gene transcription. In order to determine if the truncated triptolide analogs possessed the ability to inhibit NF- κ B activation, **GB67B** and **GB594** were compared to triptolide and QNZ in a NF- κ B luciferase reporter gene assay (Figure 44) (Appendix B).

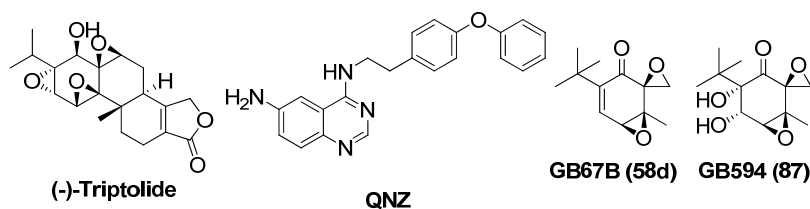


Figure 44. Compounds screened in NF- κ B activation assay

In this assay Jurkat cells were transfected with a plasmid containing a luciferase gene controlled by a promoter region containing five NF- κ B binding sites. The cells were stimulated with PMA/PHA and were allowed to grow for 6, 12, 24, and 36 hours. Cellular stimulation with PMA/PHA led to NF- κ B activation and luciferase gene transcription. In this assay luciferase activity was measured with relative light units (RLUs). Surprisingly, triptolide had little effect on NF- κ B activation except for at the highest concentration tested which is mostly likely due to cytotoxicity. This is in contrast to earlier reports but maybe due to differences in stimulating conditions. QNZ inhibited luciferase production in a dose dependent manner at six hours which is consistent with earlier reports (Figure 45).⁹⁸ However, **GB67B** and **GB594** failed to inhibit luciferase production at any of the time points tested. In light of the results from the adjuvant arthritis model and carrageenan paw edema model, these results suggest that the triptolide analogs have a different mechanism of action than triptolide.

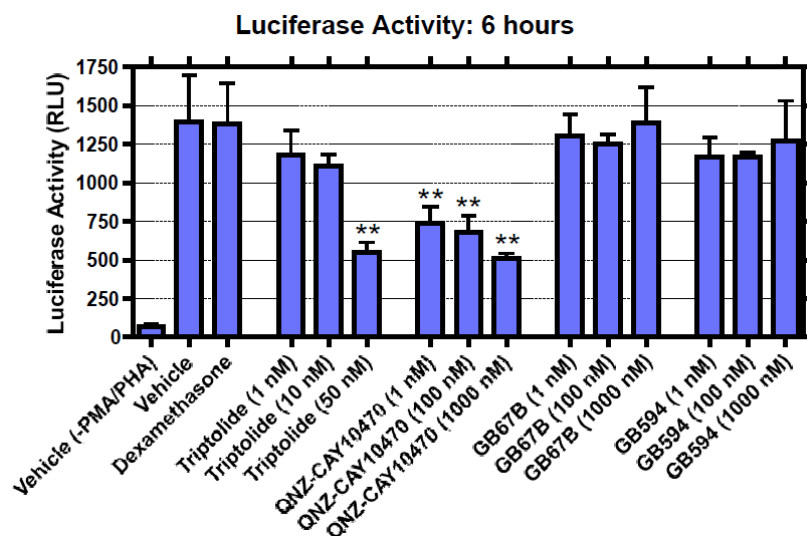


Figure 45. NF- κ B luciferase reporter gene assay six hour results

2.4.10.5 Cytokine release assays

In order to gain better insight into the cytokine modulating abilities of the triptolide analogs, a number of cytokine release assays were performed.

PBMCs stimulated with LPS were incubated with the compounds shown in figure 46 and pro-inflammatory cytokine levels were measured (Appendix A).

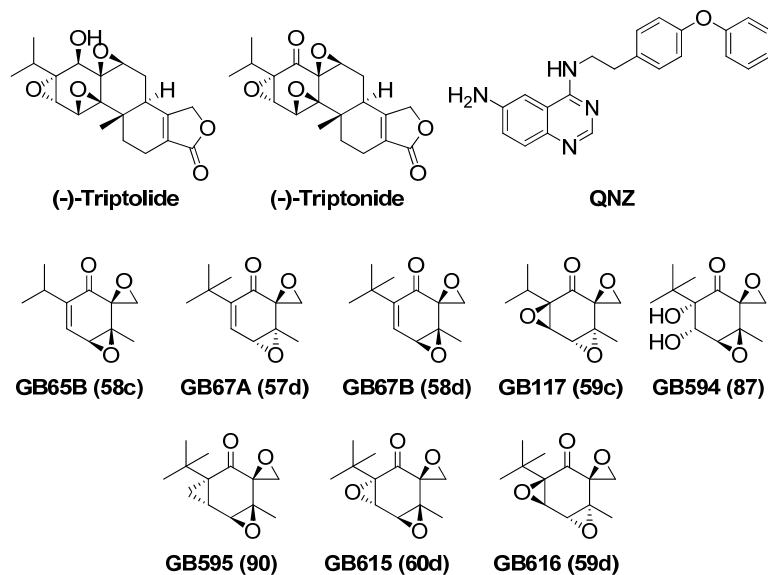


Figure 46. Compounds screened in cytokine release assays

The levels of the pro-inflammatory cytokines IL-1, IL-6, IL-8, and IL-12 were evaluated after 24 hours (Figure 47). Triptolide and triptonide at 100 nM and 1000 nM significantly decreased IL-1, IL-6, IL-8, and IL-12 levels; however, this was probably due to cytotoxicity at these concentrations. Triptolide and triptonide at 1 nM did significantly reduce IL-8 levels as a result of inhibiting the inflammatory response. The triptolide analogs **GB65B**, **GB67A**, and **GB67B** at 1000 nM showed weak inhibition of IL-1 levels. None of the analogs seemed to reduce IL-6, IL-8, or IL-12 levels at any of the concentrations tested (Appendix A).

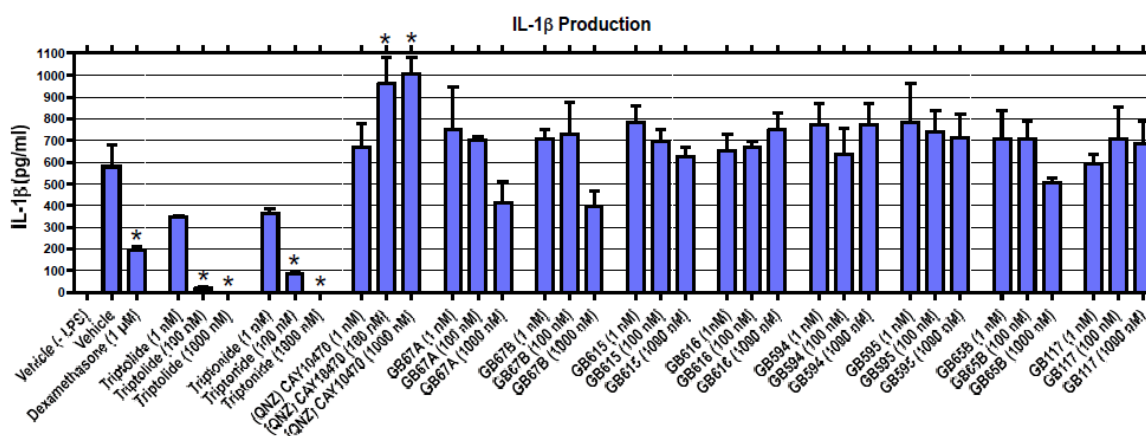


Figure 47. IL-1 cytokine levels from LPS stimulated PBMCs

In a separate experiment, PBMCs were stimulated with either the CD3 antibody or the CD3 and the CD28 antibodies (Appendix E). The cells were incubated with the compounds from figure 47 for 48 hours and assayed for IL-2 (Figure 48 and Figure 49) and TNF- α (Figure 50 and Figure 51). Triptolide and triptonide at 10 nM and 50 nM reduced IL-2 and TNF- α levels under all stimulation conditions; however, the reduction of IL-2 and TNF- α by triptolide and triptonide at 50 nM was probably due to cytotoxicity. The triptolide analogs gave higher IL-2 levels than the vehicle controls when the PBMCs were stimulated with both the CD3 and CD28 antibodies. Under no

conditions did the triptolide analogs inhibit IL-2 or TNF- α levels.

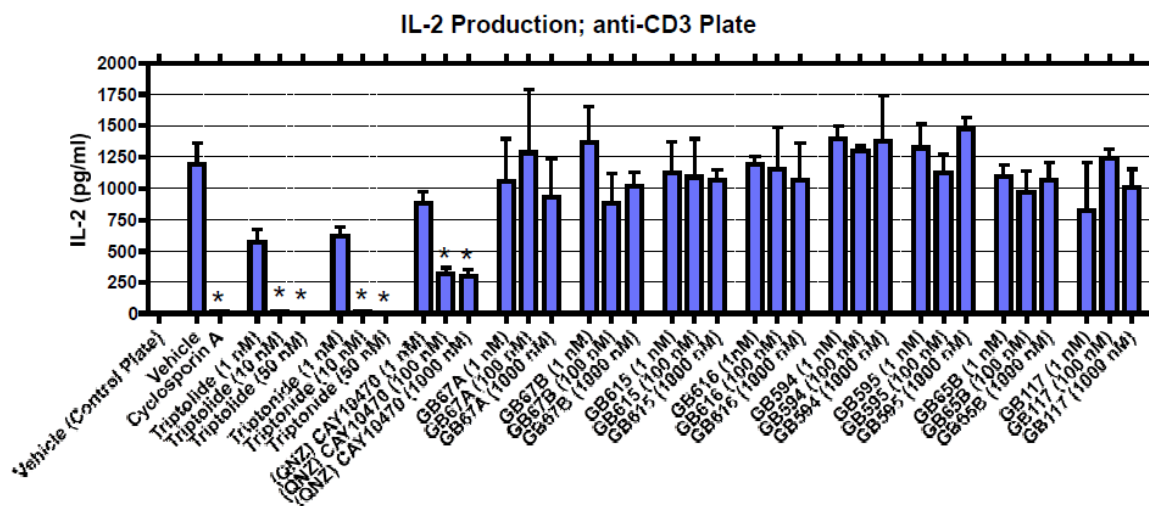


Figure 48. Inhibition of IL-2 from PBMCs stimulated with anti-CD3

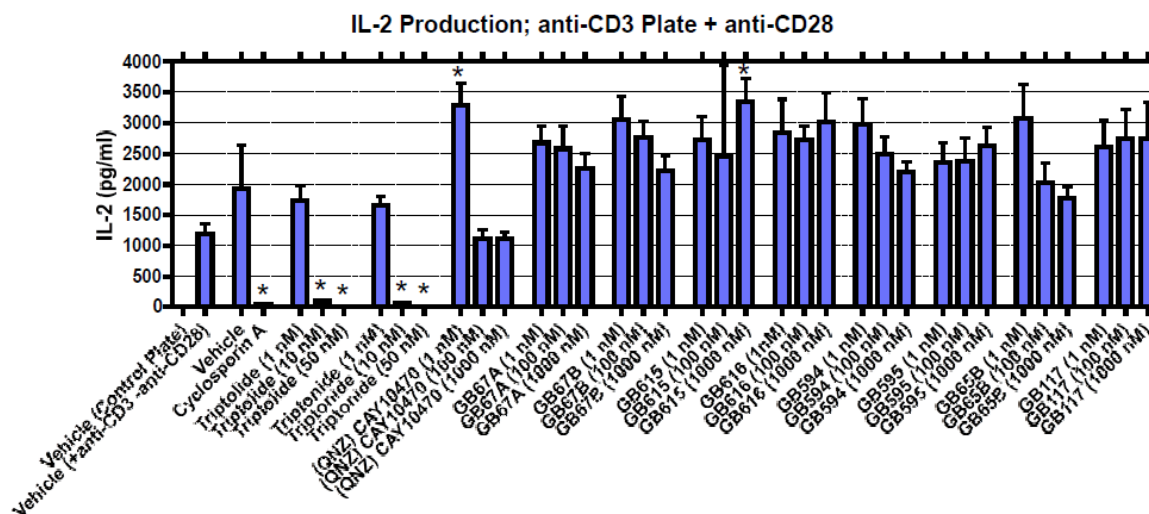


Figure 49. Inhibition of IL-2 from PBMCs stimulated with anti-CD3 and anti-CD28

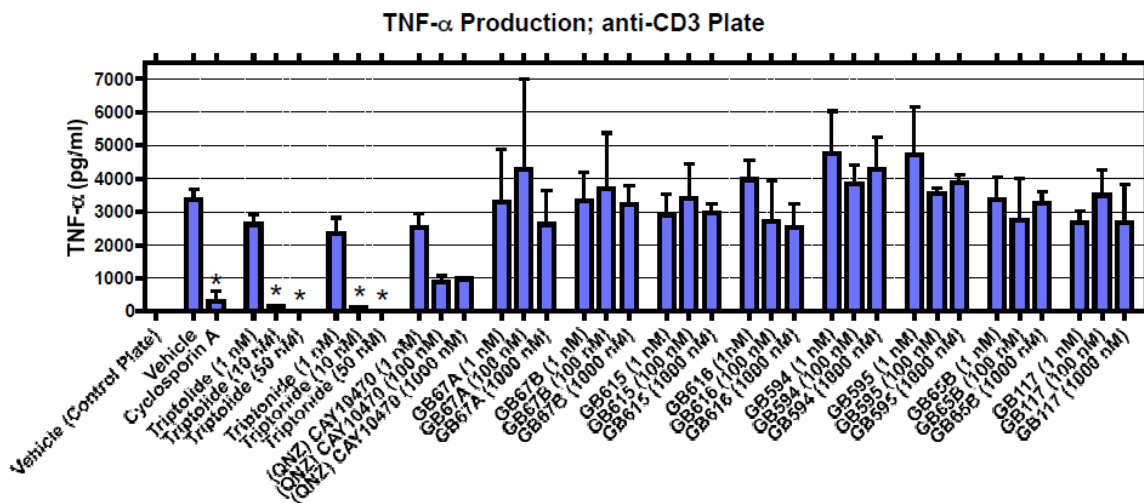


Figure 50. Inhibition of TNF- α from PBMCs stimulated with anti-CD3

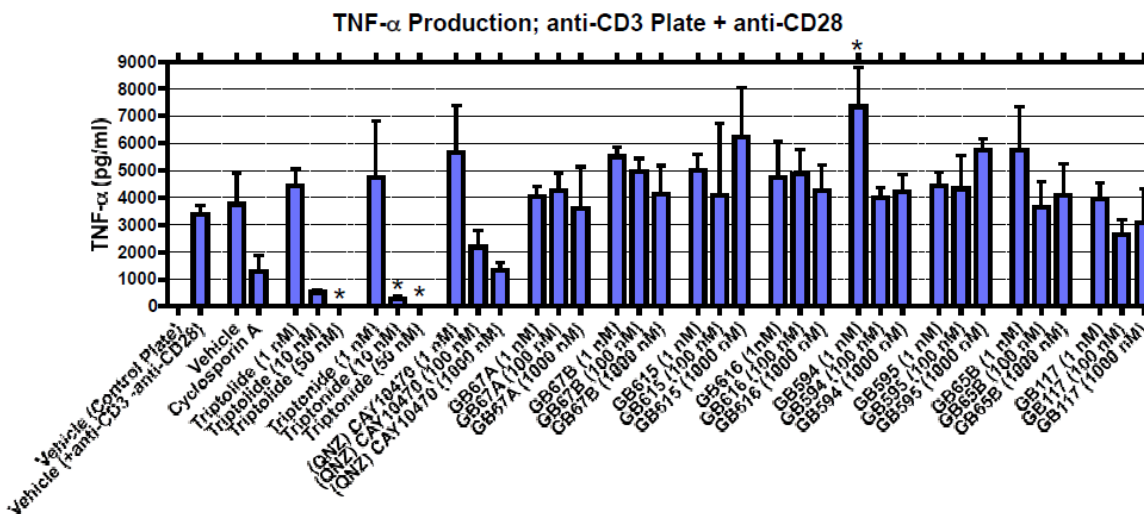


Figure 51. Inhibition of TNF- α from PBMCs stimulated with anti-CD3 and anti-CD28

Triptolide, QNZ, **GB67B**, and **GB594**, shown in figure 52, were evaluated in mouse splenocytes stimulated with LPS at different time points for their ability to reduce TNF- α levels (Appendix C).

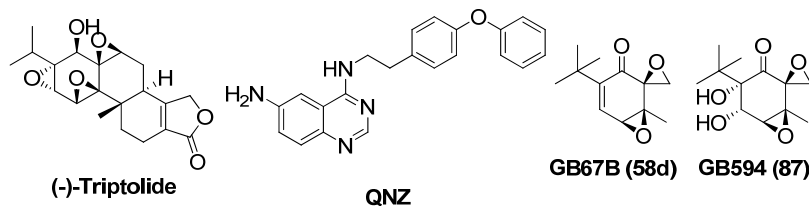


Figure 52. Compounds screened for inhibition of TNF- α

All test articles significantly reduced TNF- α levels at all concentrations tested at the 12 hour time point (Figure 53). Triptolide, QNZ, and **GB67B** reduced TNF- α in a dose dependent manner. These results help support the findings obtained from the carrageenan edma model.

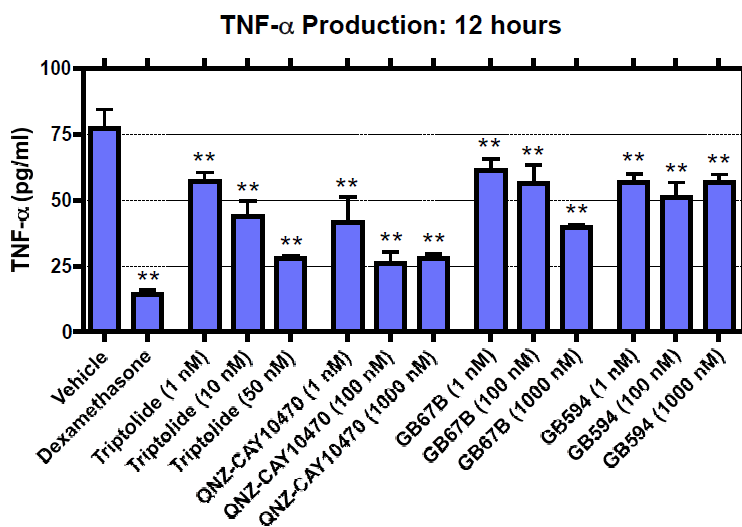


Figure 53. Inhibition of TNF- α levels from LPS stimulated mouse splenocytes

A second set of experiments evaluated TNF- α production from Jurkat cells stimulated with PMA and ionomycin (I) (Experimental). The truncated triptolide analogs (Figure 54) were tested at 1 nM, 100 nM, and 1000 nM. After six hours of incubation the cell supernatants were assayed for TNF- α using ELISA.

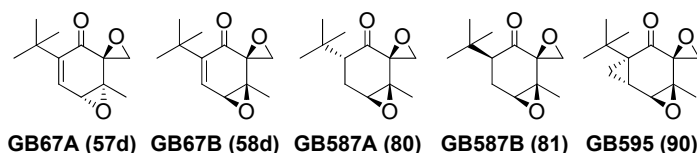


Figure 54. Truncated triptolide analogs evaluated in TNF- α release assay for which the results are shown in figure 55

As in the TNF- α release assay in mouse splenocytes, **GB67B** also showed a weak inhibition of TNF- α production from Jurkat cells (Figure 55).

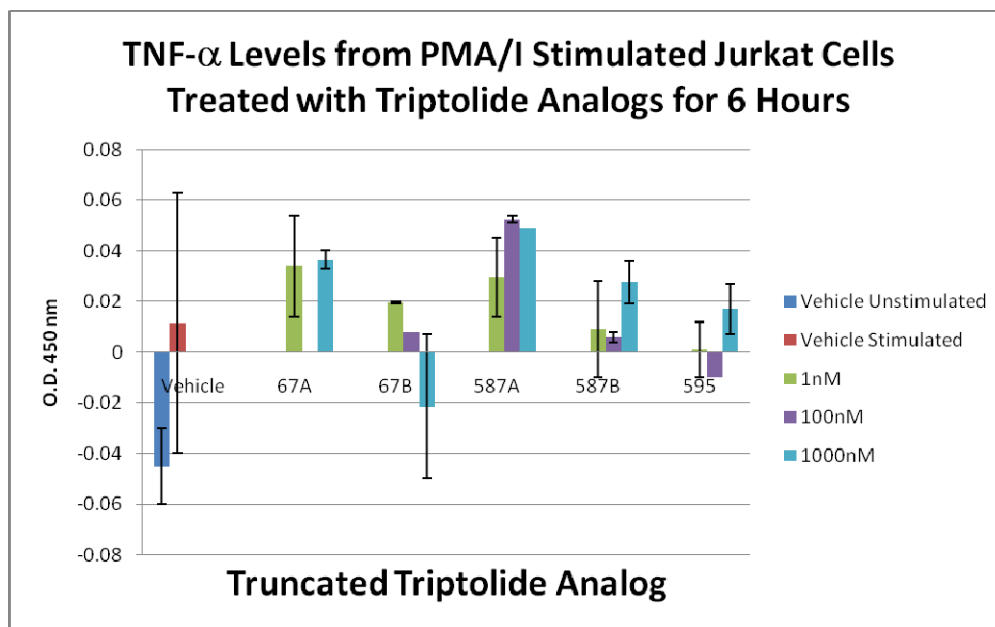


Figure 55. TNF- α levels from PMA/I stimulated Jurkat cells treated with truncated triptolide analogs

Additional triptolide analogs (Figure 56) were screened in the TNF- α release assay. Compounds **GB615** and **GB768A** also showed inhibition of TNF- α levels in a dose dependent manner (Figure 57).

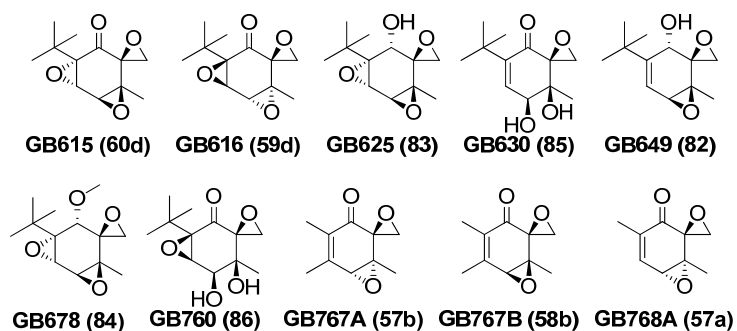


Figure 56. Truncated analogs screened in TNF- α release assay

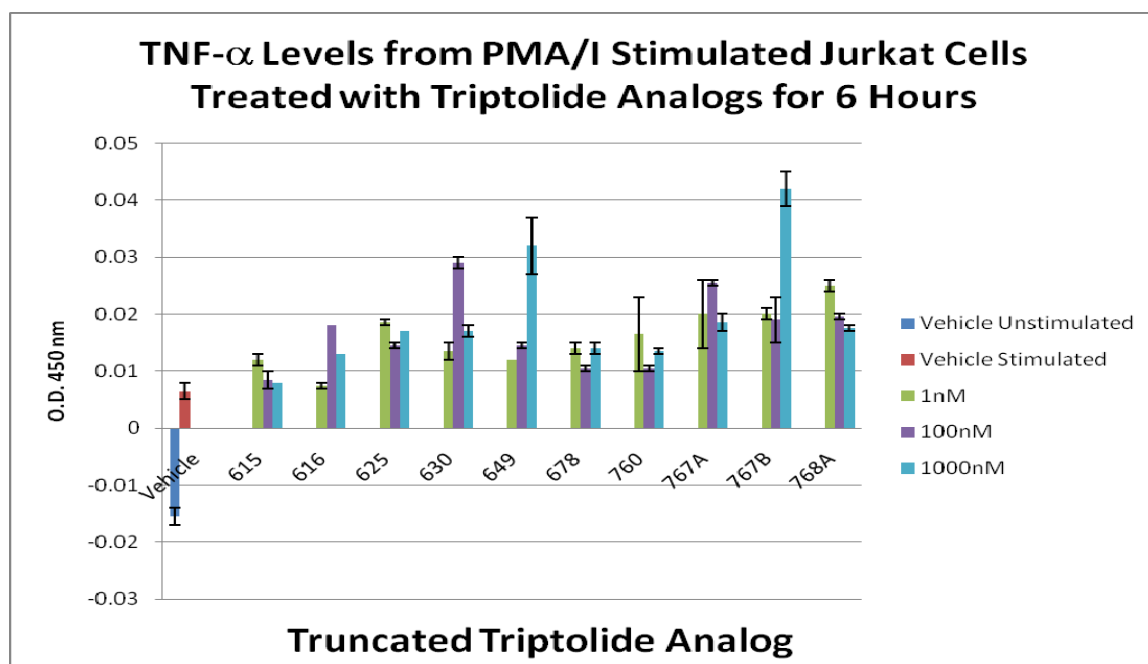


Figure 57. Affect of truncated triptolide analogs on TNF- α levels from PMA/I stimulated Jurkat cells

Compounds **GB769B** and **GB782** (Figure 58) also showed inhibition of TNF- α levels from PMA/I stimulated Jurkat cells in a dose dependent manner (Figure 59).

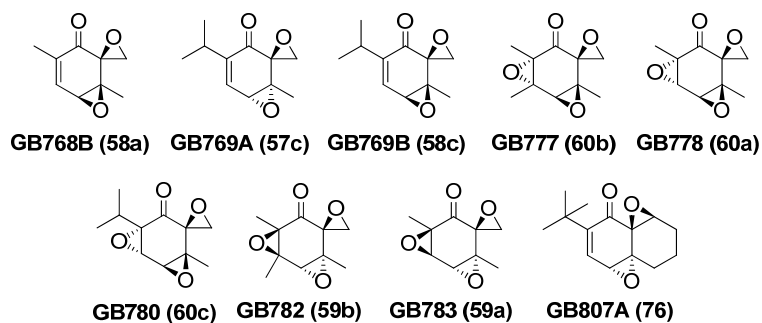


Figure 58. Additional truncated triptolide analogs screened in TNF- α release assay

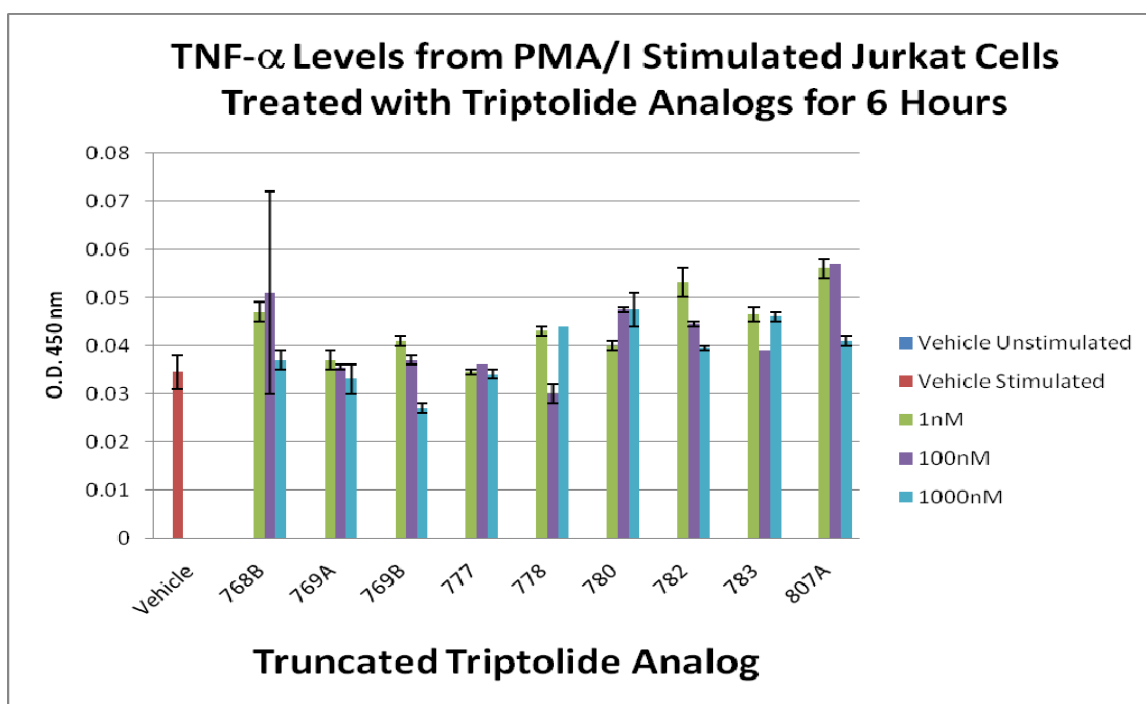


Figure 59. Results for TNF- α production from PMA/I stimulated Jurkat cells incubated with truncated triptolide analogs

Finally, compounds **GB810**, **GB816B**, and **GB828** (Figure 60) inhibited TNF- α from PMA/I stimulated Jurkat cells in a dose dependent manner (Figure 61). However, the overall TNF- α levels for these compounds were slightly higher than the control.

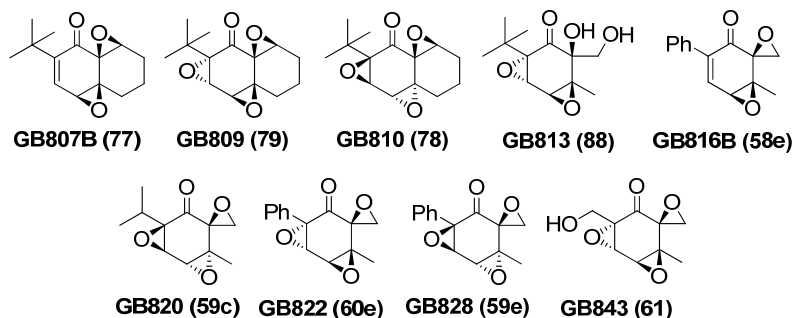


Figure 60. Final selection of triptolide analogs tested in TNF- α release assay

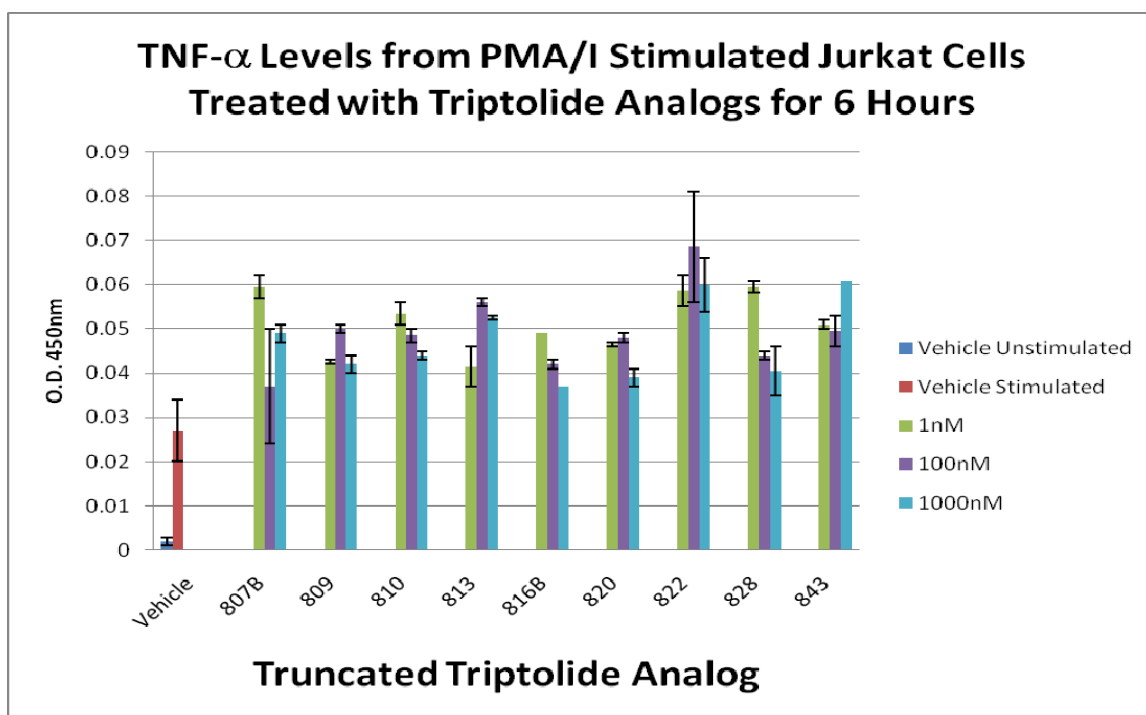


Figure 61. Results for TNF- α production from PMA/I stimulated Jurkat cells incubated with truncated triptolide analogs

2.4.10.6 AMES II and GreenScreen mutagenicity and genotoxicity assays

Two compounds, **GB67B** and **GB594** (Figure 62), were evaluated in the AMES II mutagenicity assay (Appendix F) as well as the GreenScreen genotoxicity assay (Appendix G). The AMES II assay detects base pair substitutions in TA98 and TAMix *Salmonella typhi* strains. The test articles were evaluated at six doses in the presence and absence of S9 metabolic activators. Neither analog displayed a significant increase in positive wells (Tables 8-11). Therefore, both compounds were determined to be non-mutagenic.

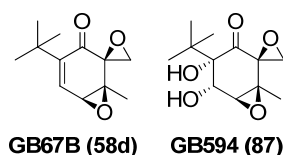


Figure 62. Compounds screened in AMES II and GreenScreen Assays

TA98 Dose (µg/mL)	Without S9 Activation			With S9 Activation		
	Mean Number of Positive Wells	Standard Deviation	Fold Induction as Compared to Negative Control	Mean Number of Positive Wells	Standard Deviation	Fold Induction as Compared to Negative Control
Negative Control (DMSO)	1.0*	0.6	NA	1.7	1.2	NA
0.975	0.0	0.0	0.0	3.7	2.9	2.2
3.9	0.3	0.6	0.3	2.3	0.6	1.4
15.6	1.7	2.1	1.7	4.7	2.5	2.8
62.5	0.7	0.6	0.7	1.7	1.5	1.0
250	0.3	0.6	0.3	1.7	0.6	1.0
1000	0.0	0.0	0.0	0.0	0.0	0.0
Positive Control	48.0	0.0	48.0	48.0	0.0	28.8

* = Because the mean revertant value was less than 1.0, 1.0 was substituted for the actual control mean value for purposes of calculations.

Table 8. AMES II results for **GB67B** in TA98 strain

TAMix Dose (µg/mL)	Without S9 Activation			With S9 Activation		
	Mean Number of Positive Wells	Standard Deviation	Fold Induction as Compared to Negative Control	Mean Number of Positive Wells	Standard Deviation	Fold Induction as Compared to Negative Control
Negative Control (DMSO)	1.7	2.1	NA	1.0	1.0	NA
0.975	0.0	0.0	0.0	1.7	1.5	1.7
3.9	1.0	1.0	0.6	1.0	1.0	1.0
15.6	3.3	2.9	2.0	1.7	0.6	1.7
62.5	1.7	1.5	1.0	0.0	0.0	0.0
250	2.0	1.0	1.2	1.0	0.0	1.0
1000	0.0	0.0	0.0	0.3	0.6	0.3
Positive Control	30.7	1.2	18.4	44.0	1.7	44.0

* = Because the mean revertant value was less than 1.0, 1.0 was substituted for the actual control mean value for purposes of calculations.

Table 9. AMES II results for **GB67B** in TAMix strain

TA98 Dose (µg/mL)	Without S9 Activation			With S9 Activation		
	Mean Number of Positive Wells	Standard Deviation	Fold Induction as Compared to Negative Control	Mean Number of Positive Wells	Standard Deviation	Fold Induction as Compared to Negative Control
Negative Control (DMSO)	1.0	0.0	NA	1.0*	0.6	NA
0.975	2.0	2.0	2.0	0.3	0.6	0.3
3.9	1.3	2.3	1.3	2.3	1.5	2.3
15.6	0.7	1.2	0.7	0.0	0.0	0.0
62.5	2.0	1.7	2.0	1.7	0.6	1.7
250	1.7	2.1	1.7	2.0	2.0	2.0
1000	1.7	0.6	1.7	1.3	1.2	1.3
Positive Control	38.0	8.7	38.0	48.0	0.0	48.0

* = Because the mean revertant value was less than 1.0, 1.0 was substituted for the actual control mean value for purposes of calculations.

Table 10. AMES II results for **GB594** in TA98 strain

TAMix Dose ($\mu\text{g/mL}$)	Without S9 Activation			With S9 Activation		
	Mean Number of Positive Wells	Standard Deviation	Fold Induction as Compared to Negative Control	Mean Number of Positive Wells	Standard Deviation	Fold Induction as Compared to Negative Control
Negative Control (DMSO)	1.0*	0.0	NA	2.0	1.0	NA
0.975	0.7	0.6	0.7	1.7	1.2	0.8
3.9	0.3	0.6	0.3	1.3	1.2	0.7
15.6	0.3	0.6	0.3	1.7	0.6	0.8
62.5	0.7	0.6	0.7	0.7	0.6	0.3
250	0.0	0.0	0.0	0.3	0.6	0.2
1000	0.3	0.6	0.3	1.0	1.0	0.5
Positive Control	48.0	0.0	48.0	40.7	3.5	20.3

* = Because the mean revertant value was less than 1.0, 1.0 was substituted for the actual control mean value for purposes of calculations.

Table 11. AMES II results for **GB594** in TAMix strain

Additionally, both **GB67B** and **GB594** were evaluated in a GreenScreen assay. The GreenScreen assay is a green fluorescent protein (GFP) reporter assay that shows transcription of the human growth arrest and DNA damage (GADD45a) gene. The GADD45a gene is involved in DNA damage and repair, apoptosis, and cell cycle control. Compound **GB67B** was found not to be genotoxic at any of the concentrations tested (Table 12).

BioReliance Test Code	AC13JU
Sponsor Test Article ID	GB67B
Maximum test article solubility in Dimethyl Sulfoxide (DMSO)	100 mg/mL
Maximum test article solubility in Sterile Water with 2% DMSO	0.50 mg/mL
Highest concentration of test article tested on microplate	250 µg/mL
Test article concentrations tested on microplate	250, 125, 62.5, 31.25, 15.63, 7.81, 3.91, 1.95, and 0.98 µg/mL
Concentrations of positive control (Methyl Methanesulfonate) tested on microplate	50 and 10 µg/mL
Genotoxicity Results	Not Genotoxic
Lowest Effective Concentration (LEC) to give positive result	Not Applicable
Cytotoxicity Results	Cytotoxic
Lowest Effective Concentration (LEC) to give positive result	125 µg/mL

Table 12. GreenScreen results for **GB67B**

Compound **GB594** was initially found to be genotoxic at 7.81 mg/mL. However, these initial findings were not observed in an additional experiment. Compound **GB594**

was determined not to be genotoxic (Table 13).

BioReliance Test Code	AC13JV
Sponsor Test Article ID	GB594
Maximum test article solubility in Dimethyl Sulfoxide (DMSO)	100 mg/mL
Maximum test article solubility in Sterile Water with 2% DMSO	2.0 mg/mL (B1), 0.08 mg/mL (B2)
Highest concentration of test article tested on microplate	1000 µg/mL (B1), 40 µg/mL (B2)
Test article concentrations tested on microplate	1000, 500, 250, 125, 62.5, 31.25, 15.63, 7.81, and 3.91 µg/mL (B1) 40, 20, 10, 5.0, 2.5, 1.25, 0.63, 0.31, and 0.16 µg/mL (B2)
Concentrations of positive control (Methyl Methanesulfonate) tested on microplate	50 and 10 µg/mL
Genotoxicity Results (Experiment B2)	Not Genotoxic
Lowest Effective Concentration (LEC) to give positive result	Not Applicable
Cytotoxicity Results (Experiment B2)	Not Cytotoxic
Lowest Effective Concentration (LEC) to give positive result	Not Applicable

Table 13. GreenScreen results for **GB594**

2.4.10.7 Toxicogenomic analysis

A gene expression experiment was performed to predict possible toxicities associated with the truncated triptonide analogs (Appendix H). Male Sprague-Dawley rat primary hepatocytes were treated with triptonide and **GB67B** (Figure 63) at a single dose that killed 20% of the cells (TC₂₀) for 16 and 24 hours. The TC₂₀ for triptonide was found to be 100 µM, and the TC₂₀ for **GB67B** was found to be 32.5 µM. After the

indicated times, RNA was extracted and used to determine changes in gene expression.

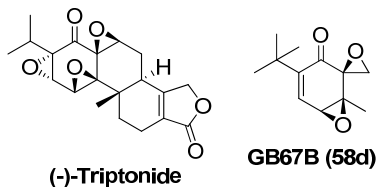


Figure 63. Structures of triptonide and **GB67B**

Even though the rat hepatocytes were treated with equitoxic doses of triptonide and **GB67B**, triptonide perturbed a far greater number of genes (16 hours = 42%, 24 hours = 47%) than **GB67B** (16 hours = 8%, 24 hours = 4%) (Figure 64).

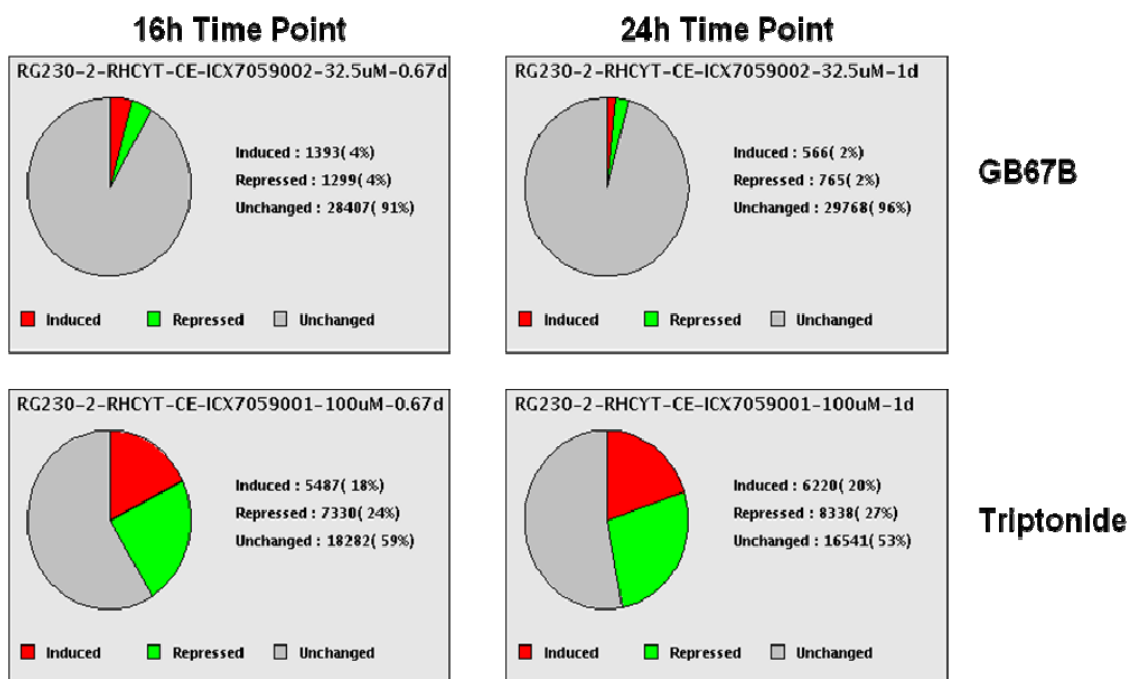


Figure 64. Number of genes perturbed by triptonide and **GB67B** at 16 and 24 hours

Based on the gene expression profile obtained from rat hepatocytes treated with triptonide, moderate liver toxicity is expected. Triptonide induced genes involved in mitochondrial oxidative phosphorylation, oxidative stress response mediated by Nrf2, acute phase response, and ubiquitin-proteasome and protein degradation pathways. In

addition, triptonide repressed gene expression for TGF- β signaling, Bcr-Abl signaling, and MAP kinase signaling pathways. **GB67B** is expected to be less toxic than triptonide. **GB67B** induced gene expression associated with oxidative stress response mediated by Nrf2 and xenobiotic metabolism pathways. **GB67B** repressed gene expression for complement activation, P450 family, and integrin signaling pathways.

2.4.10.8 Pharmacokinetic study results

Mouse plasma from a pharmacokinetic (PK) study performed on three truncated triptonide analogs was analyzed in a bioanalytical study (Appendix I). The truncated analogs **GB67B**, **GB97**, and **GB594** were administered to mice in a single intraperitoneal injection of 30 mg/kg (Figure 65). Samples were analyzed using mass spectrometry and quantitated using the appropriate deuterated compound **96**, **97**, or **98** as an internal standard.

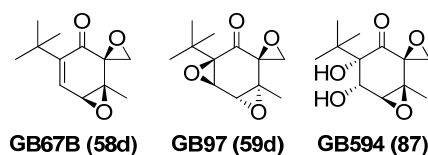


Figure 65. Compounds evaluated in the pharmacokinetic study

Compound **GB67B** was not detected in mouse plasma at any of the time points evaluated (Figure 66).

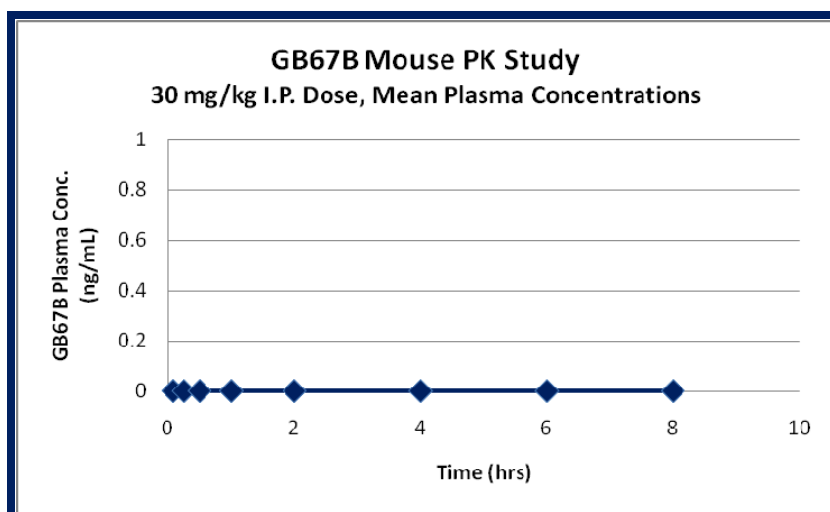


Figure 66. GB67B mouse plasma concentration

Compound **GB97** was detected at the early time points but rapidly disappeared (Figure 67). The maximum concentration (C_{max}) reached by **GB97** in mouse plasma was determined to be 1600 ng/ml with a mean terminal plasma half-life of 0.153 hours. In addition administration of **GB97** to mice results in very high clearance of 61000 ml/min/kg as well as a high volume of distribution determined to be 13000 ml/kg.

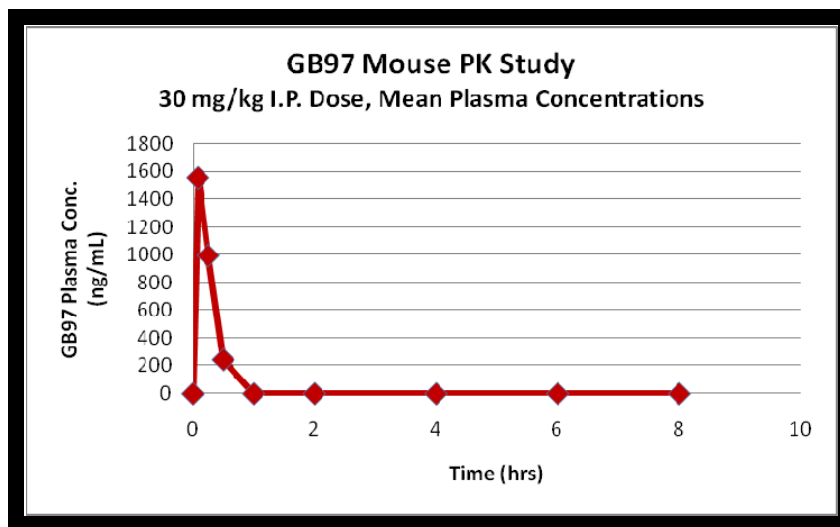


Figure 67. GB97 mouse plasma concentration

Compound **GB594** was also detected but rapidly disappeared (Figure 68). The C_{max} for **GB594** in mouse plasma was determined to be 1800 ng/ml with a mean terminal plasma half-life of 0.168 hours. Administration of **GB594** resulted in a very high clearance of 400000 ml/min/kg and a high volume of distribution of 9700 ml/kg.

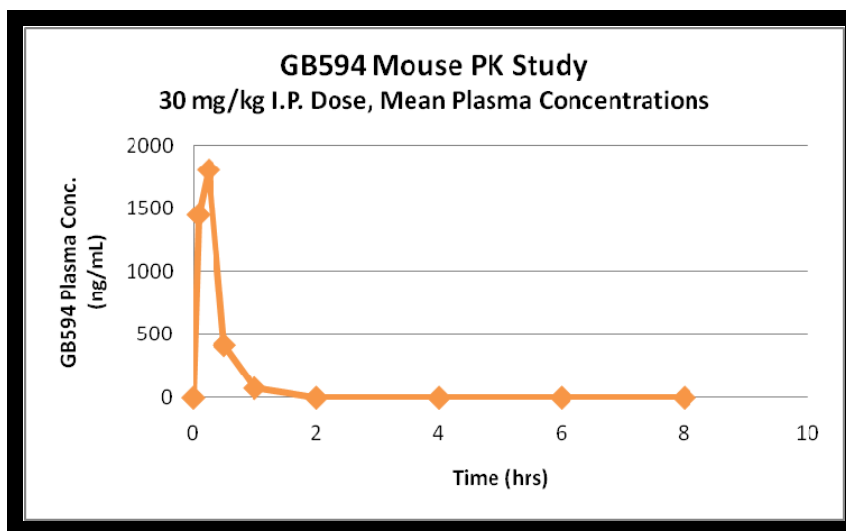


Figure 68. **GB594** mouse plasma concentration

2.4.10.9 Toxicity study results

Severe toxicity has hindered the use of triptolide as a therapeutic agent in humans as seen in one clinical trial.⁹⁶ The LD_{50} of triptolide in mice for an intraperitoneal injection has been determined to be 1.93 mg/kg.⁹⁶ For oral administration of triptolide in rats, the LD_{50} has been determined to be 1.0 mg/kg.⁹⁷ In order to determine if the truncated triptolide analogs had an improved toxicity profile compared to triptolide, **GB67B** was chosen for a five day toxicity study in rats (Appendix J). Initially, Sprague-Dawley rats were to receive an intraperitoneal injection of various concentrations of **GB67B** once a day for five days (Table 14). However, the injections were stopped after the first day due to excessive animal deaths in the two groups receiving the highest doses of **GB67B**. By the second day all three males and two females in Group 6 were found

dead. In addition, all the males and one female in Group 5 were found dead. The two other females in Group 5 were sacrificed due to severe morbidity. Additionally, by the second day, two males and one female in Group 4 were found dead. All surviving animals were followed until Day 6 of the study and appeared normal. Even though the injections were terminated after the first injection, it appears rats are able to tolerate higher doses of **GB67B** compared to triptolide.

Group	Dose Level (mg/kg)	Concentration (mg/ml)	Dose Volume (ml/kg)	Number of Animals	
				Male	Female
1. Vehicle	0	0	10	3	3
2. Low dose	100	10	10	3	3
3. Low-mid dose	200	20	10	3	3
4. Mid dose	500	50	10	3	3
5. Mid-high dose	1000	100	10	3	3
6. High dose	2000	200	10	3	3

Table 14. Toxicology groups

2.4.10.10 Toxicity and toxicokinetic study results

A seven day toxicity and toxicokinetic study was performed on **GB67B** in Sprague-Dawley rats (Appendix K). Rats in both the toxicology and toxicokinetic groups were dosed with 30, 90, and 180 mg/kg of **GB67B** once daily via oral gavage for seven consecutive days (Table 15).

Toxicology Groups

Group	Daily Dose Level (mg/kg/day)	Concentration (mg/ml)	Dose Volume* (ml/kg)	Number of Animals**	
				Male	Female
1. Control (Vehicle)	0	0	5	2	2
2. Low-Dose	30	6	5	2	2
3. Mid-Dose	90	18	5	2	2
4. High-Dose	180	36	5	2	2

Toxicokinetic Groups

Group	Daily Dose Level (mg/kg/day)	Concentration (mg/ml)	Dose Volume* (ml/kg)	Number of Animals**	
				Male	Female
5. Low dose	30	6	5	4	4
6. Mid dose	90	18	5	4	4
7. High Dose	180	36	5	4	4

Table 15. Toxicology and toxicokinetic groups

All animals survived until their scheduled sacrifice on Day 8. However, there were clinical signs of intolerance to **GB67B** in the group receiving 180 mg/kg of **GB67B**. One animal in the high dose group exhibited soft feces as well as a ruffled fur coat. The animals in the high dose group also had reduced body weights, reduced body weight gains, and consumed less food when compared to animals in the control group. Male animals in the high dose group also had reduced spleen weights. Rats receiving 180 mg/kg of **GB67B** showed increased levels of white blood cells, platelets, absolute

neutrophils, and absolute monocytes when compared to control rats. Erythrocyte morphology was unaffected by the test article.

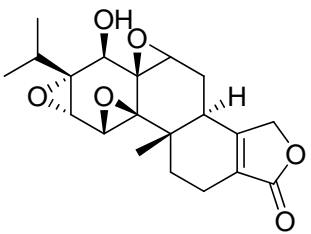
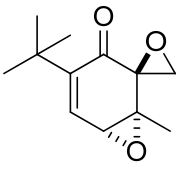
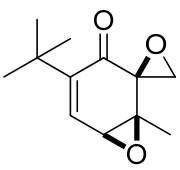
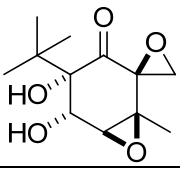
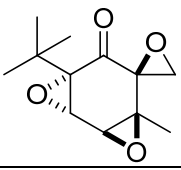
The spleen is an organ found in almost all vertebrate animals. The spleen contains a reserve of red blood cells as well as a large reserve of monocytes. White pulp, contained within the spleen, is rich in B-lymphocytes and T-lymphocytes and is thus a major site for the production of antibodies. The red pulp of the spleen contains a large reserve of monocytes that are able to move to sites of infection and differentiate into dendritic cells or macrophages. **GB67B** does not appear to be Cytotoxic to any of the cell lines investigated including mouse splenocytes (Figure 36). It appears then that **GB67B** is working through an unknown pathway causing the spleen to release its reserve of blood and monocytes. This would explain the decrease in spleen weight as well as the increase in white blood cells, platelets, neutrophils, and monocytes observed in rats receiving 180 mg/kg of **GB67B**.

Blood collected from the animals in the toxicokinetic groups was analyzed for **GB67B**. However, **GB67B** was not detected in any of the blood samples. This is consistent with the mouse PK data that was obtained on **GB67B**.

2.4.10.11 Aqueous solubility of truncated triptolide analogs

Triptolide is a largely hydrophobic compound that is water insoluble making its application as an orally administered drug difficult. However, by truncating triptolide and focusing on analogs of the highly oxygenated triepoxide region, the water solubility was expected to increase. The aqueous solubility of a selection of triptolide analogs was determined by laser nephelometry (Appendix J). In general the water solubility of the triptolide analogs was greater than triptolide itself (Table 16). Triptolide was found to

have an aqueous solubility of 142 $\mu\text{g/mL}$. All the triptolide analogs screened except for **GB807B** were found to be soluble. **GB67A** and **GB594** were found to have aqueous solubilities above 300 $\mu\text{g/mL}$ which was the limit of detection for the assay. **GB807B** was found to have a partial aqueous solubility of 83 $\mu\text{g/mL}$.

Compound	Structure	MW (g/mol)	Solubility by Nephelometer	
			$\mu\text{g/mL}$	μM
Triptolide Lot N ^o : NA		360.40	>100	>275
GB67A Lot N ^o : NA		208.25	>100	>480
GB67B Lot N ^o : NA		208.25	>100	>480
GB594 Lot N ^o : NA		242.27	>100	>400
GB615 Lot N ^o : NA		224.25	>100	>440

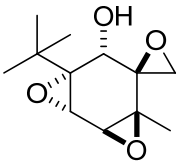
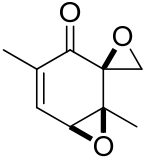
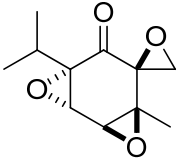
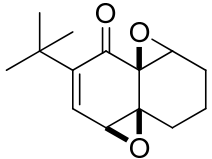
GB625 Lot N ^o : NA		226.27	>100	>440
GB768B Lot N ^o : NA		166.17	>100	>600
GB780 Lot N ^o : NA		210.23	>100	>475
GB807B Lot N ^o : NA		234.29	83	354

Table 16. Aqueous solubility of triptolide and triptolide analogs

2.5 Conclusion

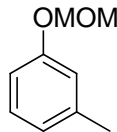
A series of di- and tri- epoxide truncated triptolide analogs were successfully synthesized from phenols. In addition a series of analogs attempting to reduce the number of reactive functional groups, such as epoxides and enones, were synthesized. The analogs were noticeably less toxic than triptolide in *in vitro* experiments. Triptolide showed cytotoxicity at 100 nM and 1000 nM in PBMCs as well as at 50 nM in Jurkat cells. None of the triptolide analogs tested showed cytotoxicity in PMBCs or Jurkat cells up to 1000 nM. In addition, **GB67B** and **GB594** did not show cytotoxicity in mouse splenocytes up to 1000 nM. In order to determine if the analogs retained anti-inflammatory properties, **GB67B**, **GB97**, and **GB187D** were screened in a carrageenan edema model in mice. They were found to reduce pro-inflammatory cytokines induced by carrageenan. **GB67B** was found to greatly reduce TNF- α levels and was the only analog that reduced paw inflammation. To further study this compound, **GB67B** at 10 mg/kg and 30 mg/kg was given orally to rats once daily for 28 consecutive days in an adjuvant arthritis model. **GB67B** was found to give a dose-dependent reduction of paw volume and arthritic score. Cell based assays were used to further probe the anti-inflammatory properties of **GB67B**. Unlike triptolide, **GB67B** did not inhibit NF- κ B activation as seen in a luciferase reporter gene assay. However, **GB67B** was found to inhibit TNF- α levels from LPS stimulated mouse splenocytes in a dose-dependent manner supporting results obtained from the carrageenan edema model. Triptolide is known to be lethal to mice and rats at a single dose at 1 mg/kg. In order to observe toxicity of the truncated analogs, **GB67B** was dosed at 30, 90, and 180 mg/kg in rats for 7 days. While no animals died during the study there were signs of clinical intolerance for **GB67B** in the 180 mg/kg

group. Blood extracted from the rats showed increased levels of white blood cells, platelets, neutrophils, and monocytes. In addition, rats receiving 180 mg/kg of **GB67B** had reduced spleen weights. Finally, the aqueous solubility of a selection of compounds was determined using laser nephelometry. Out of the compounds screened, **GB807B** was shown to be partially soluble. All other analogs as well as triptolide were shown to be soluble. Triptolide was found to have an aqueous solubility of 142 $\mu\text{g/mL}$, and the analogs **GB67A** and **GB594** had aqueous solubilities $>300 \mu\text{g/mL}$, which was the maximum limit for the method used to measure solubility.

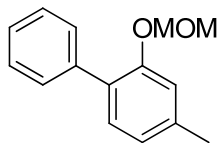
2.6 Experimental

General Notes

Unless otherwise noted, all reagents were obtained from commercial suppliers and used without further purification. All solvents used were anhydrous or kept dry over activated 4Å molecular sieves. Specific reactions were performed in oven-dried glassware under an atmosphere of argon gas. Reaction progress was monitored through thin layer chromatography (TLC) on pre-coated aluminum plates purchased from EM Sciences. Organic extracts were dried over commercially available anhydrous magnesium sulfate, and the solvents were removed at 42°C with a Büchi rotary evaporator. Brine refers to saturated aqueous sodium chloride solution. Flash chromatography was carried out with silica gel 60 (230-400 mesh) from either Sorbent Technologies or Silicycle. ¹H NMR and ¹³C NMR spectra were recorded on a Mercury 300 or Varian 400 spectrometer (300 or 400 MHz for ¹H and 100 MHz for ¹³C). Unless otherwise stated, all NMR spectra were recorded in deuterated chloroform (CDCl₃) or dimethylsulfoxide (DMSO-d₆) with the residual solvent peak serving as the internal standards (CDCl₃: ¹H δ 7.27 and ¹³C δ 77.23, DMSO-d₆: ¹H δ 2.500). Chemical shifts (δ) are reported in parts per million, and the coupling constants (J) are reported in Hertz. Mass spectra were obtained on either a VG 70-S Nier Johnson or JEOL Mass Spectrometer. Infrared spectra were recorded on a Thermo Nicolet Avatar 370 FT-IR spectrometer as neat films. Elemental analyses were performed by Atlantic Microlab (Norcross, GA).

1-(Methoxymethoxy)-3-methylbenzene (41)

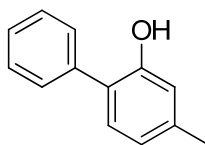
To a dry round bottomed flask under argon containing dry THF (500 mL) was added 60% NaH dispersion in mineral oil (8.88 g, 222 mmol). Next the reaction flask was cooled to 0°C followed by the dropwise addition of *m*-cresol **40** (20.0 g, 185 mmol) in 100 mL of dry THF. The reaction mixture was allowed to stir for 1 hour at 0°C after addition of *m*-cresol was complete. Next, chloromethyl methyl ether (16.9 mL, 222 mmol) was added dropwise over a period of 30 minutes while maintaining the reaction temperature at 0°C. After addition of the chloromethyl methyl ether was complete, the reaction was allowed to warm to room temperature and stir for 12 hours. Water was added to the reaction and the contents of the flask were then transferred to a separatory funnel. The organic layer was separated and then washed with brine. The organic layer was dried over anhydrous MgSO₄, filtered, and concentrated to give an oil. The oil was purified on silica eluting with 15:1 hexanes/ethyl acetate providing 27.9 g of product as a colorless oil in 99% yield. (Rf: 0.65; 8:1 hexanes/ethyl acetate). ¹H NMR (CDCl₃, 300 MHz): δ: 2.35 (s, 3H), 3.50 (s, 3H), 5.18 (s, 2H), 6.83-6.87 (m, 3H), 7.19 (t, 1H, J = 7.8 Hz). ¹³C NMR (CDCl₃, 100 MHz): δ: 21.5, 55.9, 94.4, 113.3, 117.0, 122.8, 129.3, 139.6, 157.4. HRMS (APCI): expected for C₁₂H₁₂O₂ (M)⁺ 152.08318. Found 152.08300. IR (neat): ν_{max} 3040, 2921, 1152, 1078, 1013, 984 cm⁻¹. Elemental Analysis for C₁₂H₁₂O₂: Found: C, 71.04; H, 7.92. Calculated: C, 71.03; H, 7.95.

2-(Methoxymethoxy)-4-methylbiphenyl (43)

To a dry round bottomed flask at -78°C under argon containing dry THF (500 ml) and compound **41** (10.0 g, 66 mmol) was added a 1.7 M solution of *tert*-butyllithium in pentane (46 mL, 79 mmol). The reaction mixture was allowed to stir at -78°C for 5 hours after addition was complete. To the resulting solution at -78°C was added $\text{B}(\text{OMe})_3$ (74 mL, 660 mmol). The reaction mixture was allowed to warm to room temperature and continue stirring for 24 hours. The reaction mixture was then cooled to 0°C followed by the addition of 3 M HCl (260 mL). After addition of acid the reaction mixture was allowed to stir for a further 5 hours before being transferred to a separatory funnel. The reaction mixture was diluted with water and the product was extracted with diethyl ether. The combined organic layers were washed with brine, dried over MgSO_4 , and concentrated to give the crude boronic acid which was used without further purification. A round bottomed flask containing water (40 mL) was degassed by bubbling argon through the water for 30 minutes. Next the crude boronic acid (6.4 g, 33 mmol), bromobenzene (3.8 mL, 36 mmol), $\text{Pd}(\text{OAc})_2$ (14.8 mg, 0.066 mmol), K_2CO_3 (11.5 g, 83 mmol), and Bu_4NBr (10.6 g, 33 mmol) were all added to the degassed water. The mixture was stirred vigorously and heated to 70°C with continued degassing. The reaction mixture was then cooled to room temperature, diluted with water, and the product was extracted with ethyl acetate. The organic layer was washed with brine, dried over MgSO_4 , filtered, and concentrated. The resulting residue was purified on silica eluting with 15:1 hexanes/ethyl acetate to give 7.4 g of the desired product **43** in 49%

yield as a colorless oil. (Rf: 0.55; 8:1 hexanes/ethyl acetate). ^1H NMR (CDCl_3 , 300 MHz): δ : 2.40 (s, 3H), 3.41 (s, 3H), 5.12 (s, 2H), 6.93 (d, 1H, $J = 7.8$ Hz), 7.05 (s, 1H), 7.24 (d, 1H, $J = 8.1$), 7.33 (d, 1H, $J = 6.9$ Hz), 7.41 (t, 2H, $J = 7.2$ Hz), 7.52 (d, 2H, $J = 7.5$ Hz). ^{13}C NMR (CDCl_3 , 100 MHz): δ : 21.6, 56.2, 95.1, 116.5, 123.2, 126.9, 128.1, 129.1, 129.7, 130.9, 138.8, 138.9, 154.2. HRMS (APCI): expected for $\text{C}_{15}\text{H}_{16}\text{O}_2$ (M^+) 228.11448. Found 228.11462. IR (neat): ν_{max} 3023, 2949, 1152, 1078, 1004 cm^{-1} . Elemental Analysis for $\text{C}_{15}\text{H}_{16}\text{O}_2$: Found: C, 78.99; H, 7.08. Calculated: C, 78.91; H, 7.07.

4-Methylbiphenyl-2-ol (44)

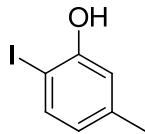


Method A: Compound **43** (5.0 g, 22 mmol) was placed in a round bottomed flask and dissolved in THF (200 mL) and 10% aqueous HCl (100 mL). The reaction was then heated to 50°C and stirred for 3 hours. The reaction was allowed to cool to room temperature and was then transferred to a separatory funnel. Water was added and the product was extracted with ethyl acetate. The organic layer was washed with brine, dried over MgSO_4 , filtered, and concentrated. The resulting residue was purified on silica eluting with 12:1 hexanes/ethyl acetate to give 2.4 g of the desired product **44** in 60% yield.

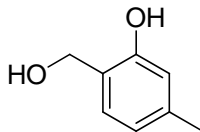
Method B: To a dry round bottomed flask under argon was added K_2CO_3 (11.1 g, 80.0 mmol), Cs_2CO_3 (26.1 g, 80.0 mmol), and chloro(1,5-cyclooctadiene)rhodium (I) dimer (0.50 g, 1.0 mmol). Next was added *m*-cresol (4.2 mL, 40.0 mmol), HMPT (1.5 mL, 8.0

mmol), and bromobenzene (10.1 mL, 96.0 mmol). The reaction mixture was stirred rapidly and heated at reflux for 20 hours. The reaction mixture was then cooled and diluted with water (100 mL). Concentrated HCl was added until the pH was acidic. Additional portion of water (100 mL) was added along with diethyl ether (100 mL). The organic layer was separated and washed with brine, dried over MgSO₄, filtered, and concentrated. The residue was purified on silica eluting with 12:1 hexanes/ethyl acetate to give the desired product in 70% yield.

Method C: To a dry round bottomed flask under argon was added compound **46** (10.0 g, 42.7 mmol) along with ethanol (170 mL) and TBAB (0.69 g, 2.1 mmol). Next was added K₃PO₄ (18.1 g, 85.5 mmol) and phenylboronic acid (6.8 g, 55.5 mmol) followed by Pd(OAc)₂ (0.48 g, 2.1 mmol). The reaction mixture was stirred at 80°C until compound **46** was completely consumed (monitored by TLC). The reaction mixture was allowed to cool to room temperature and was then transferred to a separatory funnel. The reaction mixture was diluted with water and the product was extracted with ethyl acetate. The organic layer was washed with water and brine. The organic layer was dried over MgSO₄, filtered, and concentrated. The resulting residue was purified on silica eluting with 12:1 hexanes/ethyl acetate to give 7.7 g of the desired product in 98% yield as a colorless oil. (Rf: 0.30; 8:1 hexanes/ethyl acetate). ¹H NMR (CDCl₃, 300 MHz): δ: 2.37 (s, 3H), 5.15 (s, 1H), 6.82-6.84 (m, 2H), 7.15 (d, 1H, J = 8.2 Hz), 7.37-7.42 (m, 1H), 7.45-7.52 (m, 4H). ¹³C NMR (CDCl₃, 100 MHz): δ: 21.4, 116.6, 121.9, 125.5, 127.8, 129.3, 129.4, 130.2, 137.4, 139.5, 152.3. HRMS (APCI): expected for C₁₃H₁₃O (M+H)⁺ 185.09609. Found 185.09636. IR (neat): ν_{max} 3525, 3329, 3027, 2917, 1491, 1409, 1294, 1074, 759, 698 cm⁻¹.

2-Iodo-5-methylphenol (46)

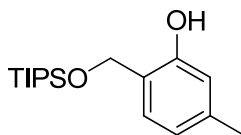
To a 250 mL round bottomed flask containing 2-amino-5-methylphenol **45** (10.0 g, 81 mmol) was added 140 mL of acetone. The reaction flask was cooled to -10°C using a dry ice-acetone bath. Next, 17 mL of concentrated HCl was added slowly to the reaction flask followed by the dropwise addition of NaNO_2 (5.6 g, 81 mmol) dissolved in 15 mL of water. Once addition of the NaNO_2 was complete the reaction mixture was allowed to stir for 1 hours at -10°C followed by the addition of NaI (24.0 g, 162 mmol) dissolved in 27 mL of water. The reaction was allowed to stir at -10°C for 4 hours and was then transferred into a separatory funnel. The product was extracted with ethyl acetate and was then washed with water, NaHSO_3 (6 g in 100 mL of water), and brine. The organic layer was dried with anhydrous MgSO_4 , filtered, and concentrated. The resulting dark residue was purified on silica eluting with 12:1 hexanes/ethyl acetate to give 13.3 g (70% yield) of product as an orange oil. (Rf: 0.29; 8:1 hexanes/ethyl acetate). ^1H NMR (CDCl_3 , 300 MHz): δ : 2.30 (s, 3H), 5.18 (s, 1H), 6.52 (d, 1H, $J = 8.1$ Hz), 6.84 (s, 1H), 7.51 (d, 1H, $J = 8.1$ Hz). ^{13}C NMR (CDCl_3 , 100 MHz): δ : 21.2, 81.7, 116.0, 123.7, 138.0, 140.7, 154.6. HRMS (APCI): expected for $\text{C}_7\text{H}_7\text{OI}$ (M^+) 233.95362. Found 233.95396. IR (neat): ν_{max} 3473, 3031, 2917, 1479, 1291, 1197, 1152, 792 cm^{-1} . Elemental Analysis for $\text{C}_7\text{H}_7\text{OI}$: Found: C, 35.79; H, 3.02. Calculated: C, 35.90; H, 3.02.

2-(Hydroxymethyl)-5-methylphenol (49)

To a round bottomed flask was added 4-methylsalicylic acid (50.0 g, 329 mmol) which was then dissolved in methanol (500 mL). As the solution was stirring concentrated sulfuric acid (30 mL) was added very slowly. Once addition of the sulfuric acid was complete the reaction was heated to reflux and allowed to stir for 12 hours. After cooling to room temperature the reaction mixture was transferred to a separatory funnel and diluted with water (300 mL). The product was extracted with diethyl ether. The combined organic layers were washed with saturated aqueous NaHCO_3 , brine, dried over MgSO_4 , filtered, and concentrated to give the intermediate methyl ester. To a dry round bottomed flask under argon was added the methyl ester (34.4 g, 207 mmol) and dry THF (750 mL). The reaction was cooled to 0°C followed by addition of LiAlH_4 (10.2 g, 269 mmol) in small portions. The reaction was allowed to stir at room temperature for 1 hour before being quenched with saturated aqueous NH_4Cl . The product was extracted with ethyl acetate. The combined organic layers were washed with brine, dried over MgSO_4 , filtered, and concentrated. The resulting residue was purified on silica eluting with 4:1 hexanes/ethyl acetate to afford 21.1 g of the desired product in 74% yield as a white solid. (Rf: 0.14; 3:1 hexanes/ethyl acetate). mp: $104\text{--}106^\circ\text{C}$. ^1H NMR (CDCl_3 , 300 MHz): δ : 2.04 (t, 1H, $J = 5.4$ Hz), 2.31 (s, 3H), 4.85 (d, 2H, $J = 5.7$ Hz), 6.68 (d, 1H, $J = 7.8$ Hz), 6.74 (s, 1H), 6.93 (d, 1H, $J = 7.8$ Hz), 7.12 (s, 1H). ^{13}C NMR (CDCl_3 , 100 MHz): δ : 21.4, 64.6, 117.3, 121.0, 121.9, 127.9, 140.0, 156.1. HRMS (APCI): expected for $\text{C}_8\text{H}_9\text{O}$ ($\text{M}+\text{H}-\text{H}_2\text{O}$) $^+$ 121.06479. Found 121.06496. IR (neat): ν_{max} 3440, 3162,

3031, 2921, 1434, 1413, 1286, 993, 817 cm^{-1} . Elemental Analysis for $\text{C}_8\text{H}_{10}\text{O}_2$: Found: C, 69.52; H, 7.20. Calculated: C, 69.55; H, 7.29.

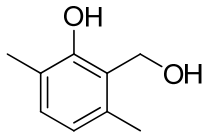
5-Methyl-2-((triisopropylsilyloxy)methyl)phenol (50)



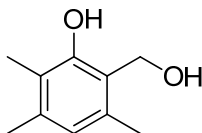
To a dry round bottomed flask under argon was added compound **49** (12.5 g, 90.5 mmol) and dry CH_2Cl_2 (500 mL). Next was added DMAP (1.11 g, 9.05 mmol) and triethylamine (15.1 mL, 109 mmol). Finally TIPSCl (20.9 g, 109 mmol) was added to the stirred solution. The reaction was allowed to stir for 20 hours before being quenched with ethanol. The reaction mixture was transferred to a separatory funnel and washed with water and brine. The organic layer was dried over MgSO_4 , filtered, and concentrated. The resulting residue was purified on silica eluting with 20:1 hexanes/ethyl acetate to give 24.4 g of the desired product in 83% yield as a colorless oil. (Rf: 0.70; 8:1 hexanes/ethyl acetate). ^1H NMR (CDCl_3 , 300 MHz): δ : 1.09 (d, 18H, $J = 6.3$ Hz), 1.14-1.24 (m, 3H, $J = 6.0$ Hz), 2.30 (s, 3H), 4.96 (s, 2H), 6.63 (d, 1H, $J = 6.6$ Hz), 6.71 (s, 1H), 6.82 (d, 1H, $J = 7.8$ Hz), 8.18 (s, 1H). ^{13}C NMR (CDCl_3 , 100 MHz): δ : 11.8, 18.0, 21.3, 66.3, 117.4, 120.4, 121.4, 126.6, 139.1, 156.7. HRMS (APCI): expected for $\text{C}_{17}\text{H}_{29}\text{OSi}$ ($\text{M}+\text{H}-\text{H}_2\text{O}$) $^+$ 277.19822. Found 277.19875. IR (neat): ν_{max} 3375, 2946, 2860, 1462, 1042, 882, 682 cm^{-1} . Elemental Analysis for $\text{C}_{17}\text{H}_{30}\text{O}_2\text{Si}$: Found: C, 69.10; H, 10.27. Calculated: C, 69.33; H, 10.27.

General procedure for the synthesis of salicylic alcohols:

The appropriate phenol (1 eq) was added to a dry 3-necked round bottomed flask equipped with a reflux condenser under argon followed by the addition of dry toluene (0.5 mL/mmol of phenol). Next was added dry triethylamine (0.4 eq) followed by the dropwise addition of a 1.0 M solution of SnCl₄ in CH₂Cl₂ (0.1 eq). After stirring for 30 minutes paraformaldehyde (2 eq) was added in one portion to the reaction flask. The reaction was then heated to 95°C and allowed to stir for 12 hours. The reaction was then allowed to cool to room temperature and transferred to a separatory funnel. Water (10 mL) and diethyl ether (30 mL) were added to the funnel, and the product was extracted with gentle swirling. The organic layer was dried with anhydrous MgSO₄, filtered, and concentrated to give the desired salicylic aldehyde as an orange oil. The crude aldehyde was then transferred to a new dry round bottomed flask under argon followed by the addition of THF (5 mL/mmol). The flask was cooled to -78°C using a dry ice-acetone bath. Next powdered LAH (1.1 eq) was added in small portions over a period of 30 minutes. Once the addition of LAH was complete, the reaction mixture was allowed to stir at -78°C for one hour. The reaction was warmed to 0°C and was quenched by the addition of saturated aqueous NH₄Cl followed by the addition of water (20 mL). Next, the pH of the reaction mixture was adjusted to pH 2 through the dropwise addition of concentrated HCl resulting in the formation of two layers. The reaction mixture was transferred to a separatory funnel, and the aqueous layer was removed. The organic layer was washed with brine, dried with anhydrous MgSO₄, filtered, and concentrated. The residue was purified on silica eluting with 8:1 hexanes/ethyl acetate to give the desired salicylic alcohol.

2-(Hydroxymethyl)-3,6-dimethylphenol (55a)

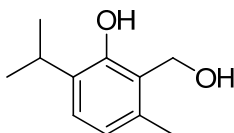
Following the general procedure for the formation of salicylic alcohols, 2,5-dimethylphenol (20.0 g, 164 mmol) resulted in the formation of 16.9 g of **55a** in 68% overall yield as a white solid. (Rf: 0.40; 3:1 hexanes/ethyl acetate). mp: 53-56 °C. ¹H NMR (CDCl₃, 300 MHz): δ: 2.11 (t, 1H, J = 5.4 Hz), 2.23 (s, 3H), 2.25 (s, 3H), 4.96 (d, 2H, J = 5.4 Hz), 6.63 (d, 1H, J = 7.2 Hz), 6.97 (d, 1H, J = 7.8 Hz), 7.73 (s, 1H). ¹³C NMR (CDCl₃, 100 MHz): δ: 15.7, 19.2, 61.0, 121.7, 122.2, 123.2, 130.1, 133.4, 154.7. HRMS (APCI): expected for C₉H₁₁O (M+H-H₂O)⁺ 135.08044. Found 135.08064. IR (neat): ν_{max} 3309, 3023, 3031, 2921, 1467, 1426, 1266, 1221, 984, 805 cm⁻¹. Elemental Analysis for C₉H₁₂O₂: Found: C, 71.01; H, 7.96. Calculated: C, 71.03; H, 7.95.

2-(Hydroxymethyl)-3,5,6-trimethylphenol (55b)

Following the general procedure for the formation of salicylic alcohols, 2,3,5-trimethylphenol (20.0 g, 147 mmol) resulted in the formation of 17.8 g of **55b** in 73% overall yield as a white solid. (Rf: 0.65; 3:1 hexanes/ethyl acetate). mp: 95-96 °C. ¹H NMR (CDCl₃, 300 MHz): δ: 1.99 (t, 1H, J = 5.4 Hz), 2.15 (s, 3H), 2.22 (s, 3H), 2.23 (s, 3H), 4.93 (d, 2H, J = 5.4 Hz), 6.55 (s, 1H), 7.70 (s, 1H). ¹³C NMR (CDCl₃, 100 MHz): δ: 11.4, 19.0, 20.0, 61.0, 119.9, 121.7, 123.5, 132.3, 137.5, 154.6. HRMS (APCI): expected for C₁₀H₁₃O (M+H-H₂O)⁺ 149.09609. Found 149.09635. IR (neat): ν_{max} 3460,

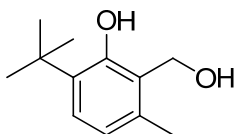
3330, 3023, 2917, 1307, 1221, 1095, 1041, 1021 cm^{-1} . Elemental Analysis for $\text{C}_{10}\text{H}_{14}\text{O}_2$: Found: C, 72.26; H, 8.63. Calculated: C, 72.26; H, 8.49.

2-(Hydroxymethyl)-6-isopropyl-3-methylphenol (55c)



Following the general procedure for the formation of salicylic alcohols, thymol (18.0 g, 122 mmol) resulted in the formation of 18.7 g of **55c** in 79% overall yield as a white solid. (Rf: 0.49; 3:1 hexanes/ethyl acetate). mp: 46-48 $^{\circ}\text{C}$. ^1H NMR (CDCl_3 , 300 MHz): δ : 1.24 (d, 6H, $J = 6.9$ Hz), 2.09 (t, 1H, $J = 6.0$ Hz), 2.25 (s, 3H), 3.31 (m, 1H, $J = 6.9$ Hz), 4.97 (d, 2H, $J = 5.4$ Hz), 6.70 (d, 1H, $J = 7.8$ Hz), 7.06 (d, 1H, $J = 8.1$ Hz), 7.87 (s, 1H). ^{13}C NMR (CDCl_3 , 100 MHz): δ : 19.3, 22.9, 26.6, 61.3, 122.0, 122.3, 125.7, 133.1, 133.9, 154.1. HRMS (APCI): expected for $\text{C}_{11}\text{H}_{15}\text{O}$ ($\text{M}+\text{H}-\text{H}_2\text{O}$) $^+$ 163.11174. Found 163.11203. IR (neat): ν_{max} 3322, 3040, 2958, 1450, 1422, 1262, 1209, 993, 805 cm^{-1} . Elemental Analysis for $\text{C}_{11}\text{H}_{16}\text{O}_2$: Found: C, 73.62; H, 8.92. Calculated: C, 73.30; H, 8.95.

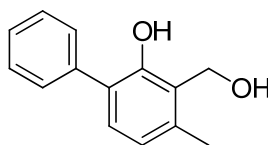
6-tert-Butyl-2-(hydroxymethyl)-3-methylphenol (55d)



Following the general procedure for the formation of salicylic alcohols, 2-tert-butyl-5-methylphenol (20.0 g, 122 mmol) resulted in the formation of 19.7 g of **55d** in 83% overall yield as a white solid. (Rf: 0.33; 8:1 hexanes/ethyl acetate). mp: 50-52 $^{\circ}\text{C}$. ^1H

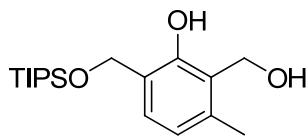
NMR (CDCl₃, 300 MHz): δ : 1.42 (s, 9H), 2.02 (t, 1H, $J = 5.7$ Hz), 2.26 (s, 3H), 4.97 (d, 2H, $J = 5.4$ Hz), 6.65 (d, 1H, $J = 8.1$ Hz), 7.13 (d, 1H, $J = 7.8$ Hz), 8.07 (s, 1H). ¹³C NMR (CDCl₃, 100 MHz): δ : 19.3, 29.8, 34.7, 61.3, 121.6, 123.1, 126.5, 133.5, 135.4, 156.2. HRMS (APCI): expected for C₁₂H₁₇O (M+H-H₂O)⁺ 177.12739. Found 177.12772. IR (neat): ν_{\max} 3334, 3093, 3007, 2962, 2946, 1405, 1221, 1185, 1005, 817 cm⁻¹. Elemental Analysis for C₁₂H₁₈O₂: Found: C, 74.35; H, 9.34. Calculated: C, 74.19; H, 9.34.

3-(Hydroxymethyl)-4-methylbiphenyl-2-ol (**55e**)



Following the general procedure for the formation of salicylic alcohols, 4-methylbiphenyl-2-ol **44** (5.1 g, 28 mmol) resulted in the formation of 3.3 g of **55e** in 55% overall yield as a pale yellow oil. (Rf: 0.11; 8:1 hexanes/ethyl acetate). ¹H NMR (CDCl₃, 300 MHz): δ : 2.38 (s, 3H), 4.94 (s, 2H), 6.82 (d, 1H, $J = 7.8$ Hz), 6.90 (s, 1H), 7.14 (d, 1H, $J = 7.5$ Hz), 7.35-7.40 (m, 1H), 7.44-7.53 (m, 4H). ¹³C NMR (CDCl₃, 100 MHz): δ : 19.3, 59.7, 122.4, 123.8, 127.0, 127.4, 128.8, 129.4, 129.6, 136.3, 137.8, 152.6. HRMS (APCI): expected for C₁₄H₁₄O₂ (M)⁺ 214.09883. Found 214.09913. IR (neat): ν_{\max} 3530, 3305, 3052, 3032, 2966, 2917, 1462, 1413, 1270, 1225, 988, 768, 698 cm⁻¹. Elemental Analysis for C₁₄H₁₄O₂: Found: C, 78.66; H, 6.56. Calculated: C, 78.47; H, 6.59.

2-(Hydroxymethyl)-3-methyl-6-((triisopropylsilyloxy)methyl)phenol (55f)



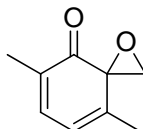
Following the general procedure for the formation of salicylic alcohols, 5-methyl-2-((triisopropylsilyloxy)methyl)phenol **50** (23.0 g, 78 mmol) resulted in the formation of 16.4 g of **55f** in 65% overall yield as a white solid. During the workup the pH was adjusted to 7.0 instead of 2.0. (Rf: 0.16; 8:1 hexanes/ethyl acetate). mp: 59-61 °C. ¹H NMR (CDCl₃, 300 MHz): δ: 1.10 (d, 18H, J = 6.3 Hz), 1.15-1.26 (m, 3H, J = 6.0 Hz), 2.36 (s, 3H), 2.47 (t, 1H, J = 6.6 Hz), 4.80 (d, 2H, J = 6.3 Hz), 4.96 (s, 2H), 6.67 (d, 1H, J = 7.5 Hz), 6.81 (d, 1H, J = 8.1 Hz), 8.66 (s, 1H). ¹³C NMR (CDCl₃, 100 MHz): δ: 11.9, 18.0, 19.3, 58.3, 65.9, 121.6, 122.3, 125.9, 126.0, 136.8, 155.5. HRMS (APCI): expected for C₁₈H₃₃O₃Si (M+H)⁺ 325.21935. Found 325.21944. IR (neat): ν_{max} 3314, 2942, 2864, 1462, 1070, 1037, 1013, 988, 878, 800, 682 cm⁻¹. Elemental Analysis for C₁₈H₃₂O₃Si: Found: C, 66.90; H, 9.95. Calculated: C, 66.62; H, 9.94.

General procedure for the synthesis of the monoepoxides:

To a round bottomed flask containing the appropriate salicylic alcohol (1 eq) was added methanol (5 mL/mmol of salicylic alcohol) and water (1.5 mL/mmol of salicylic alcohol). The flask was cooled to 0°C in a ice water bath. Sodium periodate (1.1 eq) was added to the flask in portions over 30 minutes. As the reaction proceeded a precipitate formed and the reaction mixture turned yellow. Once the reaction was complete the reaction mixture was vacuum filtered to remove the precipitate, and the filter was washed with CH₂Cl₂. The filtrate containing the product was transferred to a separatory funnel and was washed

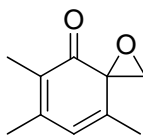
with water and brine. The organic layer was dried with MgSO₄, filtered, and concentrated. The resulting residue was purified on silica eluting with 12:1 hexanes/ethyl acetate.

5,8-Dimethyl-1-oxaspiro[2.5]octa-5,7-dien-4-one (56a)



Following the general procedure for the formation of monoepoxides, compound **55a** (9.1 g, 60 mmol) resulted in the formation of 5.9 g of **56a** in 65% yield as a yellow solid. (Rf: 0.23; 8:1 hexanes/ethyl acetate). mp: 26-27 °C. ¹H NMR (CDCl₃, 300 MHz): δ: 1.81 (s, 3H), 1.91 (s, 3H), 3.16 (d, 1H, J = 8.7 Hz), 3.23 (d, 1H, J = 8.4 Hz), 6.24 (d, 1H, J = 5.4 Hz), 6.93 (d, 1H, J = 6.3 Hz). ¹³C NMR (CDCl₃, 100 MHz): δ: 15.3, 16.3, 58.8, 58.9, 124.0, 131.9, 139.1, 144.9, 196.5. HRMS (APCI): expected for C₉H₁₁O₂ (M+H)⁺ 151.07536. Found 151.07536. IR (neat): ν_{max} 2983, 2917, 1663, 1642 cm⁻¹. Elemental Analysis for C₉H₁₀O₂: Found: C, 71.61; H, 6.63. Calculated: C, 71.98; H, 6.71.

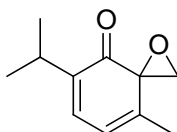
5,6,8-Trimethyl-1-oxaspiro[2.5]octa-5,7-dien-4-one (56b)



Following the general procedure for the formation of monoepoxides, compound **55b** (3.0 g, 18 mmol) resulted in the formation of 2.1 g of **56b** in 70% yield as an orange solid. (Rf: 0.16; 8:1 hexanes/ethyl acetate). mp: 82-84 °C. ¹H NMR (CDCl₃, 300 MHz): δ: 1.80 (s, 3H), 1.89 (s, 3H), 2.09 (s, 3H), 3.15 (d, 1H, J = 8.4 Hz), 3.20 (d, 1H, J = 8.4 Hz),

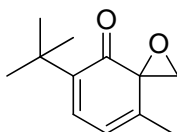
6.20 (s, 1H). ^{13}C NMR (CDCl_3 , 100 MHz): δ : 10.8, 16.0, 20.9, 57.7, 58.2, 128.0, 129.3, 142.7, 149.0, 194.9. HRMS (APCI): expected for $\text{C}_{10}\text{H}_{13}\text{O}_2$ ($\text{M}+\text{H}$) $^+$ 165.09101. Found 165.09080. IR (neat): ν_{max} 3019, 2974, 2917, 2852, 1642 cm^{-1} . Elemental Analysis for $\text{C}_{10}\text{H}_{12}\text{O}_2$: Found: C, 73.01; H, 7.37. Calculated: C, 73.15; H, 7.37.

5-Isopropyl-8-methyl-1-oxaspiro[2.5]octa-5,7-dien-4-one (56c)



Following the general procedure for the formation of monoepoxides, compound **55c** (12.0 g, 66.6 mmol) resulted in the formation of 9.3 g of **56c** in 78% yield as a yellow solid. (Rf: 0.31; 8:1 hexanes/ethyl acetate). mp: 32-34 °C. ^1H NMR (CDCl_3 , 300 MHz): δ : 1.08 (d, 3H, J = 6.9 Hz), 1.08 (d, 3H, J = 6.9 Hz), 1.81 (d, 3H, J = 1.5 Hz), 2.93 (m, 1H, J = 6.9 Hz), 3.15 (d, 1H, J = 8.4 Hz), 3.22 (d, 1H, J = 8.1 Hz), 6.30 (m, 1H, J = 6.3 Hz, 1.5 Hz), 6.88 (d, 1H, J = 6.3 Hz). ^{13}C NMR (CDCl_3 , 100 MHz): δ : 16.3, 21.7, 22.0, 26.3, 58.8, 59.2, 124.1, 135.8, 141.8, 144.5, 195.5. HRMS (APCI): expected for $\text{C}_{11}\text{H}_{15}\text{O}_2$ ($\text{M}+\text{H}$) $^+$ 179.10666. Found 179.10634. IR (neat): ν_{max} 2958, 2868, 1671, 1642 cm^{-1} . Elemental Analysis for $\text{C}_{11}\text{H}_{14}\text{O}_2$: Found: C, 74.23; H, 7.92. Calculated: C, 74.13; H, 7.92.

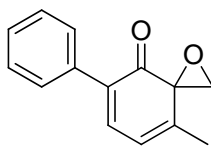
5-tert-Butyl-8-methyl-1-oxaspiro[2.5]octa-5,7-dien-4-one (56d)



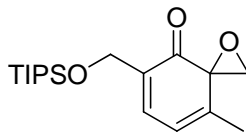
Following the general procedure for the formation of monoepoxides, compound **55d**

(25.0 g, 129 mmol) resulted in the formation of 20.6 g of **56d** in 83% yield of an orange oil. (Rf: 0.35; 8:1 hexanes/ethyl acetate). ^1H NMR (CDCl_3 , 300 MHz): δ : 1.22 (s, 9H), 1.80 (d, 3H, $J = 1.5$ Hz), 3.10 (d, 1H, $J = 8.1$ Hz), 3.16 (d, 1H, $J = 8.1$ Hz), 6.27 (dq, 1H, $J = 6.9$ Hz, 1.5 Hz), 6.94 (d, 1H, $J = 6.9$ Hz). ^{13}C NMR (CDCl_3 , 100 MHz): δ : 16.0, 29.0, 34.1, 58.2, 59.7, 123.8, 136.3, 142.8, 145.0, 194.9. HRMS (APCI): expected for $\text{C}_{12}\text{H}_{17}\text{O}_2$ ($\text{M}+\text{H}$) $^+$ 193.12231. Found 193.12204. IR (neat): ν_{max} 2954, 2917, 2868, 1667, 1638 cm^{-1} . Elemental Analysis for $\text{C}_{12}\text{H}_{16}\text{O}_2$: Found: C, 74.71; H, 8.37. Calculated: C, 74.97; H, 8.39.

8-Methyl-5-phenyl-1-oxaspiro[2.5]octa-5,7-dien-4-one (**56e**)



Following the general procedure for the formation of monoepoxides, compound **55e** (4.1 g, 19 mmol) resulted in the formation of 2.3 g of **56e** in 57% yield as an orange solid. (Rf: 0.09; 8:1 hexanes/ethyl acetate). mp: 84-86 °C. ^1H NMR (CDCl_3 , 300 MHz): δ : 1.90 (d, 3H, $J = 1.5$ Hz), 3.23 (d, 1H, $J = 8.1$ Hz), 3.30 (d, 1H, $J = 8.1$ Hz), 6.46 (m, 1H, $J = 6.3$ Hz, 1.5 Hz), 7.25 (d, 1H, $J = 6.3$ Hz), 7.33-7.41 (m, 3H), 7.46-7.49 (m, 2H). ^{13}C NMR (CDCl_3 , 100 MHz): δ : 16.6, 59.5, 59.9, 124.4, 128.4, 128.6, 129.4, 134.7, 135.1, 140.1, 147.3, 194.3. HRMS (APCI): expected for $\text{C}_{14}\text{H}_{13}\text{O}_2$ ($\text{M}+\text{H}$) $^+$ 213.09101. Found 213.09133. IR (neat): ν_{max} 3056, 3040, 2978, 1671, 1634 cm^{-1} . Elemental Analysis for $\text{C}_{14}\text{H}_{12}\text{O}_2$: Found: C, 78.97; H, 5.72. Calculated: C, 79.21; H, 5.70.

8-Methyl-5-((triisopropylsilyloxy)methyl)-1-oxaspiro[2.5]octa-5,7-dien-4-one (56f)

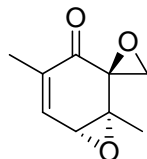
Following the general procedure for the formation of monoepoxides, compound **55f** (7.3 g, 22 mmol) resulted in the formation of 5.3 g of **56f** in 74% yield as an orange solid. (Rf: 0.68; 8:1 hexanes/ethyl acetate). mp: 55-57 °C. ¹H NMR (CDCl₃, 300 MHz): δ: 1.08 (d, 18H, J = 6.0 Hz), 1.12-1.15 (m, 3H, J = 5.4 Hz), 1.84 (s, 3H), 3.17 (d, 1H, J = 8.1 Hz), 3.25 (d, 1H, J = 8.4 Hz), 4.54 (d, 2H, J = 7.2 Hz), 6.40 (d, 1H, J = 6.0 Hz), 7.27 (d, 1H, J = 6.0 Hz). ¹³C NMR (CDCl₃, 100 MHz): δ: 12.1, 16.3, 18.1, 58.8, 58.9, 59.6, 124.2, 134.9, 136.9, 145.2, 195.2. HRMS (APCI): expected for C₁₈H₃₁O₃Si (M+H)⁺ 323.20370. Found 323.20421. IR (neat): ν_{max} 2938, 2856, 1667, 1642, 1123, 1095, 882 cm⁻¹. Elemental Analysis for C₁₈H₃₀O₃Si: Found: C, 67.22; H, 9.40. Calculated: C, 67.04; H, 9.38.

General procedure for the synthesis of the diepoxides:

To a round bottomed flask containing the appropriate monoepoxide (1mmol) was added acetonitrile (7.5 ml/mmol of monoepoxide) and a 0.4 mM aqueous solution of EDTA (5 mL/mmol of monoepoxide). The reaction flask was cooled to 0°C followed by the addition of NaHCO₃ (7.75 eq) and 1,1,1-trifluoroacetone (0.5 mL/mmol of monoepoxide). Next Oxone[®] (5 eq) was added to the reaction in portions over the period of one hour. When the reaction was complete the contents of the flask were transferred into a separatory funnel and diluted with water. The product was extracted with CH₂Cl₂. The organic layers were pooled and washed with water and then brine. The organic layer

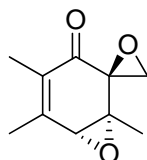
was dried with MgSO_4 , filtered, and concentrated. The residue was purified on silica eluting with 12:1 hexanes/ethyl acetate to afford the desired products. Each of the diepoxides were recrystallized from hexanes and ethyl acetate.

(±)-1,4-Dimethyl-7-oxaspiro[bicyclo[4.1.0]hept[4]ene-2,2'-oxiran]-3-one (57a)



Following the general procedure for the synthesis of diepoxides, compound **56a** (6.2 g, 41 mmol) was converted into 1.5 g of compound **57a** in a 22% yield as a white solid. (Rf: 0.17; 8:1 hexanes/ethyl acetate). mp: 62-64 °C. ^1H NMR (CDCl_3 , 300 MHz): δ : 1.34 (s, 3H), 1.87 (d, 3H, $J = 1.5$ Hz), 3.14 (d, 1H, $J = 6.3$ Hz), 3.42 (d, 1H, $J = 3.9$ Hz), 3.44 (d, 1H, $J = 6.6$ Hz), 7.04 (dd, 1H, $J = 3.9$ Hz, 1.5 Hz). ^{13}C NMR (CDCl_3 , 100 MHz): δ : 16.1, 16.4, 50.3, 54.3, 55.2, 61.8, 140.0, 140.1, 191.8. HRMS (APCI): expected for $\text{C}_9\text{H}_{11}\text{O}_3$ ($\text{M}+\text{H}$) $^+$ 167.07027. Found 167.07031. IR (neat): ν_{max} 2987, 2929, 1683 cm^{-1} . Elemental Analysis for $\text{C}_9\text{H}_{10}\text{O}_3$: Found: C, 64.88; H, 6.10. Calculated: C, 65.05; H, 6.07.

(±)-1,4,5-Trimethyl-7-oxaspiro[bicyclo[4.1.0]hept[4]ene-2,2'-oxiran]-3-one (57b)

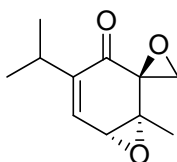


Following the general procedure for the synthesis of diepoxides, compound **56b** (2.8 g, 17 mmol) was converted into 0.79 g of compound **57b** in a 26% yield as a white solid.

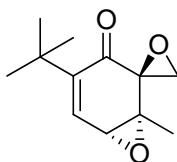
(Rf: 0.14; 8:1 hexanes/ethyl acetate). mp: 44-46 °C. ^1H NMR (CDCl_3 , 400 MHz): δ : 1.33 (s, 3H), 1.83 (s, 3H), 2.21 (s, 3H), 3.11 (d, 1H, $J = 6.8$ Hz), 3.35 (s, 1H), 3.41 (d, 1H, $J = 6.8$ Hz). ^{13}C NMR (CDCl_3 , 100 MHz): δ : 12.0, 16.1, 50.3, 54.7, 59.8, 61.0, 134.7, 150.1, 190.9. HRMS (APCI): expected for $\text{C}_{10}\text{H}_{13}\text{O}_3$ ($\text{M}+\text{H}$) $^+$ 181.08592. Found 181.08600. IR (neat): ν_{max} 2983, 2933, 1732, 1377, 1250, 1042 cm^{-1} . Elemental Analysis for $\text{C}_{10}\text{H}_{12}\text{O}_3$: Found: C, 66.40; H, 6.76. Calculated: C, 66.65; H, 6.71.

(±)-4-Isopropyl-1-methyl-7-oxaspiro[bicyclo[4.1.0]hept[4]ene-2,2'-oxiran]-3-one

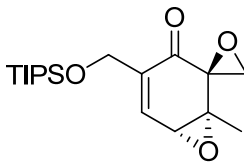
(57c)



Following the general procedure for the synthesis of diepoxides, compound **56c** (9.7 g, 54 mmol) was converted into 2.5 g of compound **57c** in a 24% yield as a pale yellow oil. (Rf: 0.26; 8:1 hexanes/ethyl acetate). ^1H NMR (CDCl_3 , 400 MHz): δ : 1.05 (t, 6H, $J = 6.4$ Hz), 1.34 (s, 3H), 2.88 (m, 1H, $J = 6.8$ Hz), 3.13 (d, 1H, $J = 6.4$ Hz), 3.44 (d, 1H, $J = 6.0$ Hz), 3.47 (d, 1H, $J = 4.4$ Hz), 6.96 (d, 1H, $J = 4.8$). ^{13}C NMR (CDCl_3 , 100 MHz): δ : 15.8, 21.4, 27.1, 49.9, 54.1, 55.4, 61.1, 137.0, 149.2, 190.8. HRMS (APCI): expected for $\text{C}_{11}\text{H}_{15}\text{O}_3$ ($\text{M}+\text{H}$) $^+$ 195.10157. Found 195.10158. IR (neat): ν_{max} 2966, 2929, 2880, 1671, 890 cm^{-1} . Elemental Analysis for $\text{C}_{11}\text{H}_{14}\text{O}_3$: Found: C, 67.87; H, 7.24. Calculated: C, 68.02; H, 7.26.

(±)-4-tert-Butyl-1-methyl-7-oxaspiro[bicyclo[4.1.0]hept[4]ene-2,2'-oxiran]-3-one**(57d)**

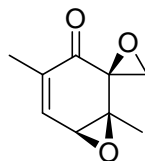
Following the general procedure for the synthesis of diepoxides, compound **56d** (7.7 g, 40 mmol) was converted into 2.2 g of compound **57d** in a 27% yield a white solid. (Rf: 0.31; 8:1 hexanes/ethyl acetate). mp: 61-63 °C. ¹H NMR (CDCl₃, 300 MHz): δ: 1.17 (s, 9H), 1.32 (s, 3H), 3.08 (d, 1H, J = 6.0 Hz), 3.45 (d, 1H, J = 5.7 Hz), 3.46 (d, 1H, J = 4.5 Hz), 7.01 (d, 1H, J = 4.8 Hz). ¹³C NMR (CDCl₃, 100 MHz): δ: 15.8, 29.0, 35.3, 49.3, 54.5, 56.7, 60.8, 137.6, 150.9, 190.7. HRMS (APCI): expected for C₁₂H₁₇O₃ (M+H)⁺ 209.11722. Found 209.11703. IR (neat): ν_{max} 2999, 2958, 2917, 2868, 1679, 882 cm⁻¹. Elemental Analysis for C₁₂H₁₆O₃: Found: C, 69.29; H, 7.76. Calculated: C, 69.21; H, 7.74.

(±)-1-Methyl-4-((triisopropylsilyloxy)methyl)-7-oxaspiro[bicyclo[4.1.0]hept[4]ene-2,2'-oxiran]-3-one (57f)

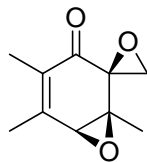
To a dry round bottomed flask containing compound **56f** (10 g, 31 mmol, 1.0 eq) was added dry CH₂Cl₂ (225 mL) and Na₂CO₃ (4.9 g, 47 mmol, 1.5 eq). The reaction was cooled to 0°C followed by the added of 70% mCPBA (9.1 g, 37 mmol, 1.2 eq). Once complete the reaction mixture was transferred into a separatory funnel and the organic

layer was washed with water and brine. The organic layer was dried over MgSO_4 , filtered, and concentrated. The resulting solid was purified on silica eluting with 8:1 hexanes/ethyl acetate to afford a trace amount of compound **57f** as a pale yellow residue. (Rf: 0.39; 8:1 hexanes/ethyl acetate). ^1H NMR (CDCl_3 , 400 MHz): δ : 1.07 (d, 18H, J = 6.4 Hz), 1.11-1.14 (m, 3H, J = 6.0 Hz), 1.35 (s, 3H), 3.14 (d, 1H, J = 6.4 Hz), 3.41 (d, 1H, J = 6.0 Hz), 3.55 (d, 1H, J = 4.4 Hz), 4.45 (dd, 1H, J = 8.4 Hz, 2.4 Hz), 7.37 (m, 1H, J = 2.4 Hz). ^{13}C NMR (CDCl_3 , 100 MHz): δ : 12.1, 16.2, 18.2, 50.3, 54.3, 55.4, 60.2, 61.8, 138.5, 142.6, 191.0. HRMS (APCI): expected for $\text{C}_{18}\text{H}_{31}\text{O}_4\text{Si}$ ($\text{M}+\text{H}$) $^+$ 339.19861. Found 339.19870. IR (neat): ν_{max} 2942, 2868, 1687, 1123 cm^{-1} . Elemental Analysis for $\text{C}_{18}\text{H}_{30}\text{O}_4\text{Si}$: Found: C, 63.47; H, 8.69. Calculated: C, 63.87; H, 8.93.

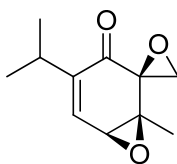
(±)-1,4-Dimethyl-7-oxaspiro[bicyclo[4.1.0]hept[4]ene-2,2'-oxiran]-3-one (58a)



In the formation of diepoxides, 3.0 g of compound **58a** was produced in 43% yield as a white solid along with compound **57a**. (Rf: 0.11; 3:1 hexanes/ethyl acetate). mp: 72-73 °C. ^1H NMR (CDCl_3 , 300 MHz): δ : 1.36 (s, 3H), 1.87 (d, 3H, J = 1.5 Hz), 2.97 (d, 1H, J = 6.3 Hz), 3.01 (d, 1H, J = 6.0 Hz), 3.47 (d, 1H, J = 4.5 Hz), 7.02 (m, 1H, J = 4.2 Hz, 1.5 Hz). ^{13}C NMR (CDCl_3 , 100 MHz): δ : 15.7, 16.0, 53.0, 54.0, 58.2, 58.9, 139.8, 140.3, 191.9. HRMS (APCI): expected for $\text{C}_9\text{H}_{11}\text{O}_3$ ($\text{M}+\text{H}$) $^+$ 167.07027. Found 167.07030. IR (neat): ν_{max} 2987, 2929, 1683, 903 cm^{-1} . Elemental Analysis for $\text{C}_9\text{H}_{10}\text{O}_3$: Found: C, 65.13; H, 6.01. Calculated: C, 65.05; H, 6.07.

(±)-1,4,5-Trimethyl-7-oxaspiro[bicyclo[4.1.0]hept[4]ene-2,2'-oxiran]-3-one (58b)

In the formation of diepoxides, 1.4 g of compound **58a** was produced in 51% yield as a white solid along with compound **57a**. (Rf: 0.04; 8:1 hexanes/ethyl acetate). mp: 130-132 °C. ¹H NMR (CDCl₃, 300 MHz): δ: 1.36 (s, 3H), 1.83 (d, 3H, J = 1.2 Hz), 2.22 (d, 3H, J = 1.2 Hz), 2.94 (d, 1H, J = 6.3 Hz), 2.98 (d, 1H, J = 6.6 Hz), 3.40 (s, 1H). ¹³C NMR (CDCl₃, 100 MHz): δ: 12.2, 15.7, 20.7, 52.8, 57.7, 58.6, 60.0, 134.5, 149.9, 190.9. HRMS (APCI): expected for C₁₀H₁₃O₃ (M+H)⁺ 181.08592. Found 181.08596. IR (neat): ν_{max} 2987, 2909, 1679, 923 cm⁻¹. Elemental Analysis for C₁₀H₁₂O₃: Found: C, 66.48; H, 6.77. Calculated: C, 66.65; H, 6.71.

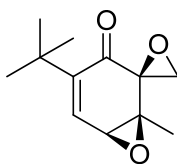
(±)-4-Isopropyl-1-methyl-7-oxaspiro[bicyclo[4.1.0]hept[4]ene-2,2'-oxiran]-3-one (58c)**(58c)**

In the formation of diepoxides, 5.3 g of compound **58c** was produced in 48% yield as a white solid along with compound **57c**. (Rf: 0.05; 8:1 hexanes/ethyl acetate). mp: 75-76 °C. ¹H NMR (CDCl₃, 300 MHz): δ: 1.00 (d, 3H, J = 7.2 Hz), 1.10 (d, 3H, J = 6.6 Hz), 1.36 (s, 3H), 2.86 (m, 1H, J = 6.6 Hz), 2.91 (d, 1H, J = 6.0 Hz), 2.98 (d, 1H, J = 6.3 Hz), 3.53 (d, 1H, J = 4.8 Hz), 6.92 (d, 1H, J = 4.2 Hz). ¹³C NMR (CDCl₃, 100 MHz): δ: 15.6, 21.5, 21.6, 27.4, 52.6, 54.5, 57.9, 59.6, 136.5, 150.2, 191.3. HRMS (APCI): expected for

$C_{11}H_{15}O_3$ (M+H)⁺ 195.10157. Found 195.10157. IR (neat): ν_{\max} 3032, 2962, 2938, 2868, 1687, 902 cm^{-1} . Elemental Analysis for $C_{11}H_{14}O_3$: Found: C, 68.05; H, 7.32. Calculated: C, 68.02; H, 7.26.

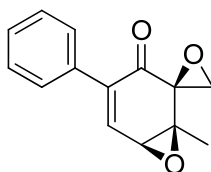
(±)-4-*tert*-Butyl-1-methyl-7-oxaspiro[bicyclo[4.1.0]hept[4]ene-2,2'-oxiran]-3-one

(58d)



In the formation of diepoxides, 4.9 g of compound **58d** was produced in 53% yield as a white solid along with compound **57d**. (Rf: 0.07; 8:1 hexanes/ethyl acetate). mp: 74-78 °C. ¹H NMR (CDCl₃, 300 MHz): δ : 1.16 (s, 9H), 1.33 (s, 3H), 2.81 (d, 1H, J = 6.0 Hz), 2.91 (d, 1H, J = 5.7 Hz), 3.52 (d, 1H, J = 4.8 Hz), 6.94 (d, 1H, J = 4.8 Hz). ¹³C NMR (CDCl₃, 100 MHz): δ : 15.1, 29.0, 35.2, 51.7, 54.6, 57.5, 60.8, 136.7, 151.8, 191.2. HRMS (ESI): expected for $C_{12}H_{17}O_3$ (M+H)⁺ 209.11722. Found 209.11720. IR (neat): ν_{\max} 2995, 2954, 2913, 2864, 1687 cm^{-1} . Elemental Analysis for $C_{12}H_{16}O_3$: Found: C, 69.10; H, 7.71. Calculated: C, 69.21; H, 7.74.

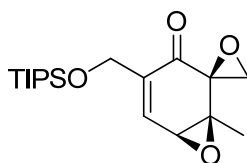
(±)-1-Methyl-4-phenyl-7-oxaspiro[bicyclo[4.1.0]hept[4]ene-2,2'-oxiran]-3-one (58e)



Following the general procedure for the synthesis of diepoxides, compound **56e** (2.0 g, 9.4 mmol) was converted into 0.75 g of compound **58e** in a 35% yield as a white solid.

(Rf: 0.20; 3:1 hexanes/ethyl acetate). mp: 123-125 °C. ^1H NMR (CDCl_3 , 300 MHz): δ : 1.43 (s, 3H), 3.02 (d, 1H, $J = 6.0$ Hz), 3.07 (d, 1H, $J = 6.3$ Hz), 3.68 (d, 1H, $J = 4.2$ Hz), 7.29 (d, 1H, $J = 4.2$ Hz), 7.32-7.39 (m, 5H). ^{13}C NMR (CDCl_3 , 100 MHz): δ : 15.3, 52.6, 54.5, 58.4, 60.1, 128.3, 128.5, 128.9, 134.1, 141.0, 142.8, 190.6. HRMS (APCI): expected for $\text{C}_{14}\text{H}_{13}\text{O}_3$ ($\text{M}+\text{H}$) $^+$ 229.08592. Found 229.08596. IR (neat): ν_{max} 3056, 3031, 2987, 2938, 1699 cm^{-1} . Elemental Analysis for $\text{C}_{14}\text{H}_{12}\text{O}_3$: Found: C, 73.38; H, 5.29. Calculated: C, 73.67; H, 5.30.

(±)-1-Methyl-4-((triisopropylsilyloxy)methyl)-7-oxaspiro[bicyclo[4.1.0]hept[4]ene-2,2'-oxiran]-3-one (58f)



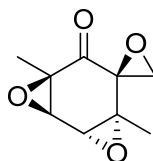
In the formation of diepoxides, 8.2 g of compound **58f** was isolated in 78% yield as a white solid along with compound **57f**. (Rf: 0.10; 8:1 hexanes/ethyl acetate). mp: 104-106 °C. ^1H NMR (CDCl_3 , 300 MHz): δ : 1.07 (d, 18H, $J = 6.0$ Hz), 1.06-1.16 (m, 3H, $J = 6.05.7$ Hz), 1.38 (s, 3H), 2.96 (d, 1H, $J = 6.3$ Hz), 3.02 (d, 1H, $J = 6.0$ Hz), 3.60 (d, 1H, $J = 3.9$ Hz), 4.34 (dd, 1H, $J = 16.8$ Hz, 2.1 Hz), 4.55 (dd, 1H, $J = 16.8$ Hz, 2.1 Hz), 7.33 (m, 1H, $J = 3.9$ Hz, 2.4 Hz). ^{13}C NMR (CDCl_3 , 100 MHz): δ : 12.0, 15.8, 18.2, 53.0, 54.4, 58.2, 59.0, 60.2, 138.5, 143.1, 191.0. HRMS (APCI): expected for $\text{C}_{18}\text{H}_{31}\text{O}_4\text{Si}$ ($\text{M}+\text{H}$) $^+$ 339.19861. Found 339.19877. IR (neat): ν_{max} 2946, 2872, 1679, 1123 cm^{-1} . Elemental Analysis for $\text{C}_{18}\text{H}_{30}\text{O}_4\text{Si}$: Found: C, 63.81; H, 8.82. Calculated: C, 63.87; H, 8.93.

General procedure for the synthesis of the triepoxides:

To a round bottomed flask containing the appropriate diepoxide (1 eq) was added methanol (10 mL/mmol of diepoxide). Next 1M NaOH (0.47 mL/mmol of diepoxide) was added followed immediately by 30% H₂O₂ (1.5 eq). The reaction was allowed to stir for one hour and was then transferred to a separatory funnel and diluted with water. The product was extracted with ethyl acetate (3 x 30 mL). The organic layer was dried with MgSO₄, filtered, and concentrated. The resulting residue was purified on silica eluting with 8:1 hexanes/ethyl acetate to afford the desired product. Each of the triepoxides were recrystallized from hexanes and ethyl acetate.

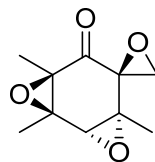
(±)-4',7'-Dimethyl-3',8'-dioxaspiro[oxirane-2,5'-tricyclo[5.1.0.0^{2,4}]octan]-6'-one

(59a)



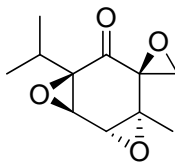
Following the general procedure for the formation of triepoxides, compound **57a** (6.2 g, 41 mmol) resulted in the formation of 5.3 g of **59a** in 78% yield as a white solid. (Rf: 0.11; 8:1 hexanes/ethyl acetate). mp: 44-45 °C. ¹H NMR (CDCl₃, 300 MHz): δ: 1.26 (s, 3H), 1.47 (s, 3H), 3.02 (d, 1H, J = 5.4 Hz), 3.43 (d, 1H, J = 5.1 Hz), 3.64 (d, 1H, J = 2.4 Hz), 3.84 (d, 1H, J = 2.1 Hz). ¹³C NMR (CDCl₃, 100 MHz): δ: 15.3, 15.5, 47.2, 55.9, 58.7, 58.8, 60.7, 62.6, 198.4. HRMS (APCI): expected for C₉H₁₁O₄ (M+H)⁺ 183.06519. Found 183.06523. IR (neat): ν_{max} 3003, 2942, 1724 cm⁻¹. Elemental Analysis for C₉H₁₀O₄: Found: C, 59.60; H, 5.52. Calculated: C, 59.34; H, 5.53.

(±)-1',4',7'-Trimethyl-3',8'-dioxaspiro[oxirane-2,5'-tricyclo[5.1.0.0^{2,4}]octan]-6'-one (59b)



Following the general procedure for the formation of triepoxides, compound **57b** (0.23 g, 1.27 mmol) resulted in the formation of 0.21 g of **59a** in 81% yield as a white solid. (Rf: 0.18; 8:1 hexanes/ethyl acetate). mp: 107-109 °C. ¹H NMR (CDCl₃, 400 MHz): δ: 1.24 (s, 3H), 1.46 (s, 3H), 1.71 (s, 3H), 3.01 (d, 1H, J = 5.6 Hz), 3.39 (d, 1H, J = 5.2 Hz), 3.46 (s, 1H). ¹³C NMR (CDCl₃, 100 MHz): δ: 11.8, 15.5, 18.1, 47.2, 55.9, 58.4, 63.9, 64.8, 67.2, 199.0. HRMS (APCI): expected for C₁₀H₁₃O₄ (M+H)⁺ 197.08084. Found 197.08092. IR (neat): ν_{max} 2991, 2966, 2933, 1728 cm⁻¹. Elemental Analysis for C₁₀H₁₂O₄: Found: C, 61.20; H, 6.16. Calculated: C, 61.22; H, 6.16.

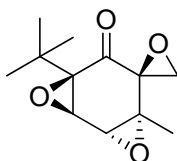
(±)-7'-Isopropyl-4'-methyl-3',8'-dioxaspiro[oxirane-2,5'-tricyclo[5.1.0.0^{2,4}]octan]-6'-one (59c)



Following the general procedure for the formation of triepoxides, compound **57c** (1.5 g, 7.7 mmol) resulted in the formation of 1.4 g of **59c** in 89% yield as a white solid. (Rf: 0.20; 8:1 hexanes/ethyl acetate). mp: 52 °C. ¹H NMR (CDCl₃, 300 MHz): δ: 0.89 (d, 3H, J = 6.9 Hz), 0.97 (d, 3H, J = 6.9 Hz), 1.23 (s, 3H), 2.41 (m, 1H, J = 6.6 Hz), 3.00 (d,

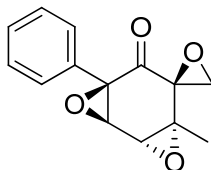
1H, J = 5.1 Hz), 3.40 (d, 1H, J = 5.4 Hz), 3.63 (d, 1H, J = 2.4 Hz), 3.83 (d, 1H, J = 2.7 Hz). ¹³C NMR (CDCl₃, 100 MHz): δ: 15.5, 16.3, 18.2, 26.0, 47.4, 56.5, 58.4, 68.6, 59.2, 66.1, 198.0. HRMS (APCI): expected for C₁₁H₁₅O₄ (M+H)⁺ 211.09649. Found 211.09650. IR (neat): ν_{max} 2966, 2938, 2868, 1728 cm⁻¹. Elemental Analysis for C₁₁H₁₄O₄: Found: C, 62.86; H, 6.76. Calculated: C, 62.85; H, 6.71.

(±)-7'-(*tert*-Butyl)-4'-methyl-3',8'-dioxaspiro[oxirane-2,5'-tricyclo[5.1.0.0^{2,4}]octan]-6'-one (59d)



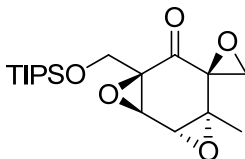
Following the general procedure for the formation of triepoxides, compound **57d** (0.50 g, 2.4 mmol) resulted in the formation of 0.50 g of **59d** in 92% yield as a white solid. (Rf: 0.17; 8:1 hexanes/ethyl acetate). mp: 88-89 °C. ¹H NMR (CDCl₃, 300 MHz): δ: 1.05 (s, 9H), 1.24 (s, 3H), 2.96 (d, 1H, J = 5.1 Hz), 3.33 (d, 1H, J = 5.1 Hz), 3.60 (d, 1H, J = 2.7 Hz), 3.93 (d, 1H, J = 2.7 Hz). ¹³C NMR (CDCl₃, 100 MHz): δ: 15.5, 25.8, 32.4, 47.3, 58.0, 58.4, 58.6, 59.3, 67.6, 197.3. HRMS (APCI): expected for C₁₂H₁₇O₄ (M+H)⁺ 225.11214. Found 225.11172. IR (neat): ν_{max} 2987, 2962, 2929, 2876, 1720 cm⁻¹. Elemental Analysis for C₁₂H₁₆O₄: Found: C, 64.56; H, 7.16. Calculated: C, 64.27; H, 7.19.

(±)-4'-Methyl-7'-phenyl-3',8'-dioxaspiro[oxirane-2,5'-tricyclo[5.1.0.0^{2,4}]octan]-6'-one (59e)



Following the general procedure for the formation of triepoxides, compound **57e** (1.1 g, 4.8 mmol) resulted in the formation of 0.89 g of **59e** in 76% yield as a white solid. (Rf: 0.13; 8:1 hexanes/ethyl acetate). mp: 100-103 °C. ¹H NMR (CDCl₃, 300 MHz): δ: 1.33 (s, 3H), 3.08 (d, 1H, J = 5.4 Hz), 3.46 (d, 1H, J = 5.1 Hz), 3.74 (d, 1H, J = 2.4 Hz), 3.95 (d, 1H, J = 2.4 Hz), 7.35-7.38 (m, 5H). ¹³C NMR (CDCl₃, 100 MHz): δ: 15.8, 47.7, 56.5, 58.5, 58.9, 63.9, 64.2, 127.6, 128.4, 129.2, 131.8, 196.7. HRMS (APCI): expected for C₁₄H₁₃O₄ (M+H)⁺ 245.08084. Found 245.08094. IR (neat): ν_{max} 3060, 3036, 3011, 2933, 1720 cm⁻¹. Elemental Analysis for C₁₄H₁₂O₄: Found: C, 68.94; H, 4.98. Calculated: C, 68.85; H, 4.95.

(±)-4'-Methyl-7'-(((triisopropylsilyl)oxy)methyl)-3',8'-dioxaspiro[oxirane-2,5'-tricyclo[5.1.0.0^{2,4}]octan]-6'-one (59f)

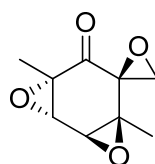


Following the general procedure for the formation of triepoxides, compound **57f** (0.050 g, 0.15 mmol) resulted in the formation of 0.040 g of **59f** in 77% yield as a residue. (Rf: 0.42; 8:1 hexanes/ethyl acetate). ¹H NMR (CDCl₃, 300 MHz): δ: 1.05 (d, 18H, J = 4.2 Hz), 1.07 (m, 3H), 1.26 (s, 3H), 3.02 (d, 1H, J = 5.7 Hz), 3.41 (d, 1H, J = 5.7 Hz), 3.68

(d, 1H, J = 2.7 Hz), 4.02 (d, 1H, J = 12.3 Hz), 4.21 (d, 1H, J = 2.4 Hz), 4.27 (d, 1H, J = 2.4 Hz) 12.3. ^{13}C NMR (CDCl_3 , 100 MHz): δ : 12.0, 15.6, 18.0, 47.3, 56.1, 57.6, 58.3, 58.5, 58.8, 62.6, 198.5. HRMS (APCI): expected for $\text{C}_{18}\text{H}_{31}\text{O}_5\text{Si}$ ($\text{M}+\text{H}$) $^+$ 355.19353. Found 355.19311. IR (neat): ν_{max} 2942, 2864, 1724, 1127 cm^{-1} . Elemental Analysis for $\text{C}_{18}\text{H}_{30}\text{O}_5\text{Si}$: Found: C, 60.94; H, 8.49. Calculated: C, 60.98; H, 8.53.

(±)-4',7'-Dimethyl-3',8'-dioxaspiro[oxirane-2,5'-tricyclo[5.1.0.0^{2,4}]octan]-6'-one

(60a)



Following the general procedure for the formation of triepoxides, compound **58a** (0.67 g, 4.0 mmol) resulted in the formation of 0.60 g of **60a** in 82% yield as a white solid. (Rf: 0.20; 3:1 hexanes/ethyl acetate). mp: 128-129 °C. ^1H NMR (CDCl_3 , 300 MHz): δ : 1.26 (s, 3H), 1.48 (s, 3H), 2.79 (d, 1H, J = 5.4 Hz), 2.98 (d, 1H, J = 5.4 Hz), 3.70 (d, 1H, J = 2.4 Hz), 3.87 (d, 1H, J = 2.4 Hz). ^{13}C NMR (CDCl_3 , 100 MHz): δ : 14.8, 14.9, 50.9, 58.5, 59.7, 59.9, 61.7, 63.5, 198.2. HRMS (APCI): expected for $\text{C}_9\text{H}_{11}\text{O}_4$ ($\text{M}+\text{H}$) $^+$ 183.06519. Found 183.06523. IR (neat): ν_{max} 2999, 2946, 1724 cm^{-1} . Elemental Analysis for $\text{C}_9\text{H}_{10}\text{O}_4$: Found: C, 59.53; H, 5.58. Calculated: C, 59.34; H, 5.53. The relative stereochemistry was established by X-ray crystallographic analysis.

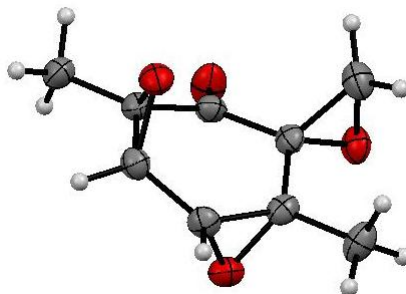


Table 17. Crystal data and structure refinement for GB2s.

Identification code	gb2s	
Empirical formula	C ₉ H ₁₀ O ₄	
Formula weight	182.17	
Temperature	173(2) K	
Wavelength	1.54178 Å	
Crystal system	Orthorhombic	
Space group	Fdd2	
Unit cell dimensions	a = 26.5082(16) Å	α = 90°.
	b = 27.8923(14) Å	β = 90°.
	c = 4.5594(3) Å	γ = 90°.
Volume	3371.1(3) Å ³	
Z	16	
Density (calculated)	1.436 Mg/m ³	
Absorption coefficient	0.964 mm ⁻¹	
F(000)	1536	
Crystal size	0.51 x 0.10 x 0.09 mm ³	
Theta range for data collection	4.60 to 63.84°.	
Index ranges	-28 ≤ h ≤ 30, -32 ≤ k ≤ 22, -5 ≤ l ≤ 4	
Reflections collected	4138	
Independent reflections	1110 [R(int) = 0.0230]	
Completeness to theta = 63.84°	95.5 %	
Absorption correction	Semi-empirical from equivalents	
Max. and min. transmission	0.9182 and 0.6391	
Refinement method	Full-matrix least-squares on F ²	
Data / restraints / parameters	1110 / 1 / 160	
Goodness-of-fit on F ²	1.041	
Final R indices [I > 2σ(I)]	R1 = 0.0244, wR2 = 0.0640	

R indices (all data)	R1 = 0.0261, wR2 = 0.0654
Absolute structure parameter	0(6)
Extinction coefficient	0.00016(5)
Largest diff. peak and hole	0.149 and -0.122 e.Å ⁻³

Table 18. Atomic coordinates ($\times 10^4$) and equivalent isotropic displacement parameters ($\text{\AA}^2 \times 10^3$) for GB2s. $U(\text{eq})$ is defined as one third of the trace of the orthogonalized U_{ij} tensor.

	x	y	z	U(eq)
O(1)	1307(1)	992(1)	4899(4)	41(1)
O(2)	355(1)	1179(1)	-222(3)	32(1)
O(3)	452(1)	2083(1)	5192(3)	31(1)
O(4)	1637(1)	1889(1)	3465(3)	32(1)
C(1)	1009(1)	1235(1)	3540(5)	26(1)
C(2)	494(1)	1053(1)	2760(5)	25(1)
C(3)	104(1)	1416(1)	2169(5)	28(1)
C(4)	224(1)	1936(1)	2450(5)	28(1)
C(5)	745(1)	2103(1)	2483(5)	27(1)
C(6)	1151(1)	1729(1)	2426(5)	25(1)
C(7)	358(1)	555(1)	3738(6)	33(1)
C(8)	874(1)	2599(1)	1441(6)	37(1)
C(9)	1585(1)	1756(1)	424(6)	36(1)

Table 19. Bond lengths [Å] and angles [°] for GB2s.

O(1)-C(1)	1.210(2)
O(2)-C(3)	1.439(2)
O(2)-C(2)	1.451(3)
O(3)-C(4)	1.448(3)
O(3)-C(5)	1.461(3)
O(4)-C(9)	1.442(3)
O(4)-C(6)	1.444(2)
C(1)-C(2)	1.501(3)
C(1)-C(6)	1.517(3)
C(2)-C(3)	1.472(2)
C(2)-C(7)	1.504(3)
C(3)-C(4)	1.489(2)
C(3)-H(3)	1.02(2)
C(4)-C(5)	1.459(3)
C(4)-H(4)	0.989(19)
C(5)-C(6)	1.499(2)
C(5)-C(8)	1.500(3)
C(6)-C(9)	1.470(3)
C(7)-H(7A)	0.99(3)
C(7)-H(7B)	0.99(3)
C(7)-H(7C)	0.96(3)
C(8)-H(8A)	0.94(3)
C(8)-H(8B)	1.02(3)
C(8)-H(8C)	0.94(2)
C(9)-H(9A)	1.03(2)
C(9)-H(9B)	0.95(3)
C(3)-O(2)-C(2)	61.24(12)
C(4)-O(3)-C(5)	60.22(12)
C(9)-O(4)-C(6)	61.24(13)
O(1)-C(1)-C(2)	121.71(17)
O(1)-C(1)-C(6)	121.28(17)
C(2)-C(1)-C(6)	116.95(16)
O(2)-C(2)-C(3)	59.00(12)
O(2)-C(2)-C(1)	111.77(16)

C(3)-C(2)-C(1)	116.76(14)
O(2)-C(2)-C(7)	116.13(18)
C(3)-C(2)-C(7)	121.51(17)
C(1)-C(2)-C(7)	117.40(17)
O(2)-C(3)-C(2)	59.77(12)
O(2)-C(3)-C(4)	114.51(16)
C(2)-C(3)-C(4)	120.29(16)
O(2)-C(3)-H(3)	116.3(13)
C(2)-C(3)-H(3)	117.0(11)
C(4)-C(3)-H(3)	116.5(11)
O(3)-C(4)-C(5)	60.31(13)
O(3)-C(4)-C(3)	116.03(18)
C(5)-C(4)-C(3)	120.95(15)
O(3)-C(4)-H(4)	114.2(11)
C(5)-C(4)-H(4)	118.1(10)
C(3)-C(4)-H(4)	115.3(10)
C(4)-C(5)-O(3)	59.47(13)
C(4)-C(5)-C(6)	117.22(14)
O(3)-C(5)-C(6)	111.70(16)
C(4)-C(5)-C(8)	120.44(17)
O(3)-C(5)-C(8)	115.12(16)
C(6)-C(5)-C(8)	118.18(18)
O(4)-C(6)-C(9)	59.30(13)
O(4)-C(6)-C(5)	114.93(14)
C(9)-C(6)-C(5)	122.50(17)
O(4)-C(6)-C(1)	112.99(15)
C(9)-C(6)-C(1)	116.58(16)
C(5)-C(6)-C(1)	116.70(16)
C(2)-C(7)-H(7A)	109.1(13)
C(2)-C(7)-H(7B)	108.8(15)
H(7A)-C(7)-H(7B)	116(2)
C(2)-C(7)-H(7C)	109.8(15)
H(7A)-C(7)-H(7C)	101.9(19)
H(7B)-C(7)-H(7C)	111(2)
C(5)-C(8)-H(8A)	111.0(14)
C(5)-C(8)-H(8B)	112.4(15)

H(8A)-C(8)-H(8B)	109(2)
C(5)-C(8)-H(8C)	111.3(14)
H(8A)-C(8)-H(8C)	103(2)
H(8B)-C(8)-H(8C)	110.4(19)
O(4)-C(9)-C(6)	59.45(13)
O(4)-C(9)-H(9A)	113.5(16)
C(6)-C(9)-H(9A)	120.2(13)
O(4)-C(9)-H(9B)	111.9(14)
C(6)-C(9)-H(9B)	119.2(13)
H(9A)-C(9)-H(9B)	117(2)

Symmetry transformations used to generate equivalent atoms:

Table 20. Anisotropic displacement parameters ($\text{\AA}^2 \times 10^3$) for GB2s. The anisotropic displacement factor exponent takes the form: $-2\pi^2 [h^2 a^{*2} U^{11} + \dots + 2 h k a^* b^* U^{12}]$

	U11	U22	U33	U23	U13	U12
O(1)	29(1)	32(1)	62(1)	12(1)	-8(1)	4(1)
O(2)	35(1)	35(1)	25(1)	-5(1)	-2(1)	-3(1)
O(3)	37(1)	28(1)	27(1)	-2(1)	0(1)	5(1)
O(4)	25(1)	38(1)	34(1)	0(1)	-5(1)	-8(1)
C(1)	25(1)	25(1)	30(1)	-3(1)	1(1)	4(1)
C(2)	26(1)	24(1)	26(1)	-4(1)	2(1)	-1(1)
C(3)	23(1)	30(1)	29(1)	1(1)	-1(1)	0(1)
C(4)	26(1)	28(1)	31(1)	3(1)	-2(1)	5(1)
C(5)	32(1)	25(1)	23(1)	0(1)	-4(1)	-1(1)
C(6)	24(1)	28(1)	23(1)	-3(1)	-3(1)	-4(1)
C(7)	34(1)	24(1)	41(1)	-3(1)	2(1)	-2(1)
C(8)	40(1)	26(1)	44(2)	5(1)	-10(1)	-4(1)
C(9)	32(1)	43(1)	32(1)	3(1)	2(1)	-6(1)

Table 21. Hydrogen coordinates ($\times 10^4$) and isotropic displacement parameters ($\text{\AA}^2 \times 10^3$) for GB2s.

	x	y	z	U(eq)
H(3)	-260(8)	1320(7)	2540(60)	35(5)
H(4)	-39(7)	2157(6)	1710(50)	23(5)
H(7A)	22(10)	470(7)	2940(60)	45(6)
H(7B)	391(9)	536(9)	5900(70)	44(7)
H(7C)	572(9)	326(9)	2780(70)	52(7)
H(8A)	933(9)	2602(8)	-590(60)	39(7)
H(8B)	1182(9)	2735(8)	2480(80)	56(7)
H(8C)	598(9)	2807(8)	1640(50)	38(6)
H(9A)	1779(8)	1451(8)	-130(60)	37(6)
H(9B)	1617(8)	2024(8)	-840(60)	39(7)

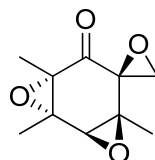
Table 22. Torsion angles [$^\circ$] for GB2s.

C(3)-O(2)-C(2)-C(1)	-109.00(16)
C(3)-O(2)-C(2)-C(7)	112.60(19)
O(1)-C(1)-C(2)-O(2)	-137.7(2)
C(6)-C(1)-C(2)-O(2)	39.5(2)
O(1)-C(1)-C(2)-C(3)	157.1(2)
C(6)-C(1)-C(2)-C(3)	-25.7(3)
O(1)-C(1)-C(2)-C(7)	0.1(3)
C(6)-C(1)-C(2)-C(7)	177.35(19)
C(2)-O(2)-C(3)-C(4)	112.08(19)
C(1)-C(2)-C(3)-O(2)	100.5(2)
C(7)-C(2)-C(3)-O(2)	-103.5(2)
O(2)-C(2)-C(3)-C(4)	-102.5(2)
C(1)-C(2)-C(3)-C(4)	-2.0(3)
C(7)-C(2)-C(3)-C(4)	154.0(2)
C(5)-O(3)-C(4)-C(3)	112.36(17)
O(2)-C(3)-C(4)-O(3)	-119.99(19)

C(2)-C(3)-C(4)-O(3)	-52.0(3)
O(2)-C(3)-C(4)-C(5)	-50.5(3)
C(2)-C(3)-C(4)-C(5)	17.5(3)
C(3)-C(4)-C(5)-O(3)	-104.3(2)
O(3)-C(4)-C(5)-C(6)	100.3(2)
C(3)-C(4)-C(5)-C(6)	-4.0(3)
O(3)-C(4)-C(5)-C(8)	-103.0(2)
C(3)-C(4)-C(5)-C(8)	152.7(2)
C(4)-O(3)-C(5)-C(6)	-109.68(16)
C(4)-O(3)-C(5)-C(8)	111.91(19)
C(9)-O(4)-C(6)-C(5)	-114.4(2)
C(9)-O(4)-C(6)-C(1)	108.3(2)
C(4)-C(5)-C(6)-O(4)	-159.5(2)
O(3)-C(5)-C(6)-O(4)	-93.68(19)
C(8)-C(5)-C(6)-O(4)	43.3(3)
C(4)-C(5)-C(6)-C(9)	132.3(2)
O(3)-C(5)-C(6)-C(9)	-161.88(17)
C(8)-C(5)-C(6)-C(9)	-24.9(3)
C(4)-C(5)-C(6)-C(1)	-23.7(3)
O(3)-C(5)-C(6)-C(1)	42.0(2)
C(8)-C(5)-C(6)-C(1)	179.1(2)
O(1)-C(1)-C(6)-O(4)	-7.1(3)
C(2)-C(1)-C(6)-O(4)	175.61(17)
O(1)-C(1)-C(6)-C(9)	58.8(3)
C(2)-C(1)-C(6)-C(9)	-118.5(2)
O(1)-C(1)-C(6)-C(5)	-143.7(2)
C(2)-C(1)-C(6)-C(5)	39.1(3)
C(5)-C(6)-C(9)-O(4)	101.72(19)
C(1)-C(6)-C(9)-O(4)	-102.18(19)

Symmetry transformations used to generate equivalent atoms:

**(±)-1',4',7'-Trimethyl-3',8'-dioxaspiro[oxirane-2,5'-tricyclo[5.1.0.0^{2,4}]octan]-6'-one
(60b)**



Following the general procedure for the formation of triepoxides, compound **58b** (0.10 g, 0.55 mmol) resulted in the formation of 0.086 g of **60b** in 80% yield as a white solid. (Rf: 0.26; 3:1 hexanes/ethyl acetate). mp: 175-177 °C. ¹H NMR (CDCl₃, 300 MHz): δ: 1.25 (s, 3H), 1.46 (s, 3H), 1.72 (s, 3H), 2.79 (d, 1H, J = 5.4 Hz), 2.97 (d, 1H, J = 5.1 Hz), 3.52 (s, 1H). ¹³C NMR (CDCl₃, 100 MHz): 11.9, 14.7, 18.0, 50.7, 59.3, 60.0, 63.7, 65.5, 68.2, 198.7. HRMS (APCI): expected for C₁₀H₁₃O₄ (M+H)⁺ 197.08084. Found 197.08089. IR (neat): ν_{max} 3019, 2987, 2942, 1728 cm⁻¹. Elemental Analysis for C₁₀H₁₂O₄: Found: C, 61.46; H, 6.20. Calculated: C, 61.22; H, 6.16. The relative stereochemistry was established by X-ray crystallographic analysis.

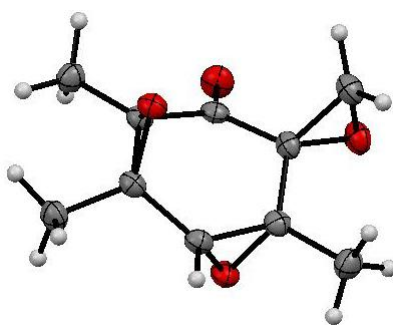


Table 23. Crystal data and structure refinement for GB1.

Identification code	GB1
Empirical formula	C ₁₀ H ₁₂ O ₄
Formula weight	196.20
Temperature	173(2) K
Wavelength	1.54178 Å
Crystal system	Monoclinic

Space group	P2(1)/n	
Unit cell dimensions	a = 7.0181(8) Å	$\alpha = 90^\circ$.
	b = 11.0756(12) Å	$\beta = 102.745(6)^\circ$.
	c = 11.8936(14) Å	$\gamma = 90^\circ$.
Volume	901.71(18) Å ³	
Z	4	
Density (calculated)	1.445 Mg/m ³	
Absorption coefficient	0.942 mm ⁻¹	
F(000)	416	
Crystal size	0.44 x 0.41 x 0.31 mm ³	
Theta range for data collection	5.52 to 65.96°.	
Index ranges	-6 ≤ h ≤ 8, -12 ≤ k ≤ 12, -13 ≤ l ≤ 13	
Reflections collected	4284	
Independent reflections	1394 [R(int) = 0.0196]	
Completeness to theta = 65.96°	88.5 %	
Absorption correction	Semi-empirical from equivalents	
Max. and min. transmission	0.7589 and 0.6821	
Refinement method	Full-matrix least-squares on F ²	
Data / restraints / parameters	1394 / 0 / 131	
Goodness-of-fit on F ²	1.014	
Final R indices [I > 2σ(I)]	R1 = 0.0297, wR2 = 0.0781	
R indices (all data)	R1 = 0.0307, wR2 = 0.0789	
Extinction coefficient	0.0183(12)	
Largest diff. peak and hole	0.196 and -0.157 e.Å ⁻³	

Table 24. Atomic coordinates ($\times 10^4$) and equivalent isotropic displacement parameters ($\text{Å}^2 \times 10^3$) for GB1. $U(\text{eq})$ is defined as one third of the trace of the orthogonalized U_{ij} tensor.

	x	y	z	$U(\text{eq})$
C(1)	10318(2)	3649(1)	1676(1)	20(1)
C(2)	8945(2)	3412(1)	538(1)	20(1)
C(3)	6829(2)	3589(1)	486(1)	20(1)
C(4)	6223(2)	3943(1)	1568(1)	21(1)
C(5)	7593(2)	4458(1)	2556(1)	21(1)

C(6)	9691(2)	4554(1)	2470(1)	20(1)
C(7)	9721(2)	2588(1)	-254(1)	26(1)
C(8)	5280(2)	2964(1)	-394(1)	28(1)
C(9)	6887(2)	5257(1)	3398(1)	30(1)
C(10)	10811(2)	5683(1)	2687(1)	27(1)
O(1)	11876(1)	3138(1)	1945(1)	29(1)
O(2)	7941(1)	4509(1)	43(1)	22(1)
O(3)	6989(1)	3198(1)	2567(1)	24(1)
O(4)	11076(1)	4736(1)	3535(1)	28(1)

Table 25. Bond lengths [\AA] and angles [$^\circ$] for GB1.

C(1)-O(1)	1.2098(16)
C(1)-C(2)	1.5016(19)
C(1)-C(6)	1.5072(18)
C(2)-O(2)	1.4616(15)
C(2)-C(3)	1.4860(18)
C(2)-C(7)	1.4977(18)
C(3)-O(2)	1.4515(15)
C(3)-C(4)	1.4939(19)
C(3)-C(8)	1.5013(19)
C(4)-O(3)	1.4496(16)
C(4)-C(5)	1.4604(19)
C(4)-H(4)	1.0000
C(5)-O(3)	1.4597(15)
C(5)-C(9)	1.5002(19)
C(5)-C(6)	1.5026(19)
C(6)-O(4)	1.4310(17)
C(6)-C(10)	1.4681(18)
C(7)-H(7A)	0.9800
C(7)-H(7B)	0.9800
C(7)-H(7C)	0.9800
C(8)-H(8A)	0.9800
C(8)-H(8B)	0.9800
C(8)-H(8C)	0.9800

C(9)-H(9A)	0.9800
C(9)-H(9B)	0.9800
C(9)-H(9C)	0.9800
C(10)-O(4)	1.4382(17)
C(10)-H(10A)	0.9900
C(10)-H(10B)	0.9900
O(1)-C(1)-C(2)	121.23(12)
O(1)-C(1)-C(6)	121.18(13)
C(2)-C(1)-C(6)	117.59(11)
O(2)-C(2)-C(3)	58.99(8)
O(2)-C(2)-C(7)	117.63(11)
C(3)-C(2)-C(7)	123.56(12)
O(2)-C(2)-C(1)	111.96(10)
C(3)-C(2)-C(1)	116.80(12)
C(7)-C(2)-C(1)	115.08(11)
O(2)-C(3)-C(2)	59.66(8)
O(2)-C(3)-C(4)	113.97(10)
C(2)-C(3)-C(4)	118.10(12)
O(2)-C(3)-C(8)	115.80(11)
C(2)-C(3)-C(8)	122.09(12)
C(4)-C(3)-C(8)	114.94(11)
O(3)-C(4)-C(5)	60.21(8)
O(3)-C(4)-C(3)	115.58(10)
C(5)-C(4)-C(3)	122.24(11)
O(3)-C(4)-H(4)	115.7
C(5)-C(4)-H(4)	115.7
C(3)-C(4)-H(4)	115.7
O(3)-C(5)-C(4)	59.53(8)
O(3)-C(5)-C(9)	114.75(11)
C(4)-C(5)-C(9)	120.79(12)
O(3)-C(5)-C(6)	111.08(10)
C(4)-C(5)-C(6)	117.01(12)
C(9)-C(5)-C(6)	118.47(12)
O(4)-C(6)-C(10)	59.47(9)
O(4)-C(6)-C(5)	115.70(11)
C(10)-C(6)-C(5)	122.89(11)

O(4)-C(6)-C(1)	114.41(11)
C(10)-C(6)-C(1)	117.22(11)
C(5)-C(6)-C(1)	114.91(11)
C(2)-C(7)-H(7A)	109.5
C(2)-C(7)-H(7B)	109.5
H(7A)-C(7)-H(7B)	109.5
C(2)-C(7)-H(7C)	109.5
H(7A)-C(7)-H(7C)	109.5
H(7B)-C(7)-H(7C)	109.5
C(3)-C(8)-H(8A)	109.5
C(3)-C(8)-H(8B)	109.5
H(8A)-C(8)-H(8B)	109.5
C(3)-C(8)-H(8C)	109.5
H(8A)-C(8)-H(8C)	109.5
H(8B)-C(8)-H(8C)	109.5
C(5)-C(9)-H(9A)	109.5
C(5)-C(9)-H(9B)	109.5
H(9A)-C(9)-H(9B)	109.5
C(5)-C(9)-H(9C)	109.5
H(9A)-C(9)-H(9C)	109.5
H(9B)-C(9)-H(9C)	109.5
O(4)-C(10)-C(6)	58.98(8)
O(4)-C(10)-H(10A)	117.9
C(6)-C(10)-H(10A)	117.9
O(4)-C(10)-H(10B)	117.9
C(6)-C(10)-H(10B)	117.9
H(10A)-C(10)-H(10B)	115.0
C(3)-O(2)-C(2)	61.34(8)
C(4)-O(3)-C(5)	60.26(8)
C(6)-O(4)-C(10)	61.55(8)

Symmetry transformations used to generate equivalent atoms:

Table 26. Anisotropic displacement parameters ($\text{\AA}^2 \times 10^3$) for GB1. The anisotropic displacement factor exponent takes the form: $-2\pi^2 [h^2 a^{*2} U_{11} + \dots + 2 h k a^* b^* U_{12}]$

	U11	U22	U33	U23	U13	U12
C(1)	19(1)	18(1)	24(1)	5(1)	6(1)	-2(1)
C(2)	20(1)	17(1)	22(1)	2(1)	5(1)	0(1)
C(3)	19(1)	18(1)	23(1)	2(1)	3(1)	0(1)
C(4)	19(1)	20(1)	26(1)	2(1)	5(1)	1(1)
C(5)	24(1)	17(1)	24(1)	2(1)	6(1)	0(1)
C(6)	21(1)	19(1)	18(1)	2(1)	0(1)	0(1)
C(7)	27(1)	27(1)	27(1)	-3(1)	8(1)	2(1)
C(8)	23(1)	30(1)	29(1)	-5(1)	2(1)	-3(1)
C(9)	34(1)	29(1)	28(1)	-4(1)	10(1)	1(1)
C(10)	28(1)	22(1)	29(1)	0(1)	2(1)	-4(1)
O(1)	21(1)	33(1)	31(1)	1(1)	2(1)	8(1)
O(2)	21(1)	20(1)	24(1)	5(1)	4(1)	1(1)
O(3)	27(1)	19(1)	26(1)	3(1)	7(1)	-3(1)
O(4)	29(1)	29(1)	22(1)	0(1)	-3(1)	-3(1)

Table 27. Hydrogen coordinates ($\times 10^4$) and isotropic displacement parameters ($\text{\AA}^2 \times 10^3$) for GB1.

	x	y	z	U(eq)
H(4)	4831	4202	1471	26
H(7A)	8674	2392	-922	40
H(7B)	10204	1843	157	40
H(7C)	10791	2988	-515	40
H(8A)	4110	3472	-579	42
H(8B)	4955	2190	-84	42
H(8C)	5765	2822	-1095	42
H(9A)	6907	6100	3152	44
H(9B)	7743	5162	4164	44

H(9C)	5550	5029	3429	44
H(10A)	11863	5815	2266	32
H(10B)	10112	6421	2837	32

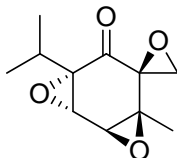
Table 28. Torsion angles [°] for GB1.

O(1)-C(1)-C(2)-O(2)	-142.46(12)
C(6)-C(1)-C(2)-O(2)	37.11(15)
O(1)-C(1)-C(2)-C(3)	152.29(12)
C(6)-C(1)-C(2)-C(3)	-28.14(16)
O(1)-C(1)-C(2)-C(7)	-4.66(18)
C(6)-C(1)-C(2)-C(7)	174.91(11)
C(7)-C(2)-C(3)-O(2)	-104.52(14)
C(1)-C(2)-C(3)-O(2)	100.67(12)
O(2)-C(2)-C(3)-C(4)	-102.78(12)
C(7)-C(2)-C(3)-C(4)	152.70(12)
C(1)-C(2)-C(3)-C(4)	-2.11(16)
O(2)-C(2)-C(3)-C(8)	103.19(13)
C(7)-C(2)-C(3)-C(8)	-1.33(19)
C(1)-C(2)-C(3)-C(8)	-156.14(12)
O(2)-C(3)-C(4)-O(3)	-118.25(11)
C(2)-C(3)-C(4)-O(3)	-51.15(15)
C(8)-C(3)-C(4)-O(3)	104.70(13)
O(2)-C(3)-C(4)-C(5)	-48.69(16)
C(2)-C(3)-C(4)-C(5)	18.41(18)
C(8)-C(3)-C(4)-C(5)	174.26(12)
C(3)-C(4)-C(5)-O(3)	-103.13(13)
O(3)-C(4)-C(5)-C(9)	-102.40(13)
C(3)-C(4)-C(5)-C(9)	154.47(12)
O(3)-C(4)-C(5)-C(6)	99.70(12)
C(3)-C(4)-C(5)-C(6)	-3.43(18)
O(3)-C(5)-C(6)-O(4)	-97.70(13)
C(4)-C(5)-C(6)-O(4)	-163.27(11)
C(9)-C(5)-C(6)-O(4)	38.30(16)
O(3)-C(5)-C(6)-C(10)	-166.59(12)

C(4)-C(5)-C(6)-C(10)	127.84(14)
C(9)-C(5)-C(6)-C(10)	-30.59(19)
O(3)-C(5)-C(6)-C(1)	39.12(15)
C(4)-C(5)-C(6)-C(1)	-26.45(16)
C(9)-C(5)-C(6)-C(1)	175.12(11)
O(1)-C(1)-C(6)-O(4)	-0.20(17)
C(2)-C(1)-C(6)-O(4)	-179.77(10)
O(1)-C(1)-C(6)-C(10)	66.60(17)
C(2)-C(1)-C(6)-C(10)	-112.97(14)
O(1)-C(1)-C(6)-C(5)	-137.58(13)
C(2)-C(1)-C(6)-C(5)	42.85(15)
C(5)-C(6)-C(10)-O(4)	102.60(14)
C(1)-C(6)-C(10)-O(4)	-103.66(13)
C(4)-C(3)-O(2)-C(2)	109.69(13)
C(8)-C(3)-O(2)-C(2)	-113.63(13)
C(7)-C(2)-O(2)-C(3)	114.41(13)
C(1)-C(2)-O(2)-C(3)	-108.96(12)
C(3)-C(4)-O(3)-C(5)	114.05(13)
C(9)-C(5)-O(3)-C(4)	112.50(13)
C(6)-C(5)-O(3)-C(4)	-109.75(13)
C(5)-C(6)-O(4)-C(10)	-114.57(13)
C(1)-C(6)-O(4)-C(10)	108.39(12)

Symmetry transformations used to generate equivalent atoms:

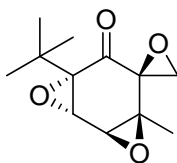
(±)-7'-Isopropyl-4'-methyl-3',8'-dioxaspiro[oxirane-2,5'-tricyclo[5.1.0.0^{2,4}]octan]-6'-one (**60c**)



Following the general procedure for the formation of triepoxides, compound **58c** (0.26 g, 1.3 mmol) resulted in the formation of 0.24 g of **60c** in 88% yield as a white solid. (Rf:

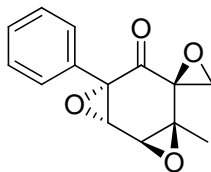
0.21; 3:1 hexanes/ethyl acetate). mp: 86-87 °C. ^1H NMR (CDCl_3 , 300 MHz): δ : 0.89 (d, 3H, $J = 6.9$ Hz), 0.98 (d, 3H, $J = 6.9$ Hz), 1.26 (s, 3H), 2.43 (m, 1H, $J = 6.9$ Hz), 2.76 (d, 1H, $J = 5.1$ Hz), 2.96 (d, 1H, $J = 5.1$ Hz), 3.69 (d, 1H, $J = 2.7$ Hz), 3.87 (d, 1H, $J = 2.7$ Hz). ^{13}C NMR (CDCl_3 , 100 MHz): δ : 14.4, 16.3, 17.8, 25.5, 50.4, 58.1, 59.2, 60.1, 66.9, 197.7. HRMS (APCI): expected for $\text{C}_{11}\text{H}_{15}\text{O}_4$ ($\text{M}+\text{H}$) $^+$ 211.09649. Found 211.09671. IR (neat): ν_{max} 2970, 2933, 2876, 1732 cm^{-1} . Elemental Analysis for $\text{C}_{11}\text{H}_{14}\text{O}_4$: Found: C, 62.78; H, 6.69. Calculated: C, 62.85; H, 6.71.

(\pm)-7'-(*tert*-Butyl)-4'-methyl-3',8'-dioxaspiro[oxirane-2,5'-tricyclo[5.1.0.0 2,4]octan]-6'-one (60d)



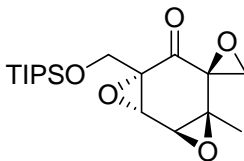
Following the general procedure for the formation of triepoxides, compound **58d** (1.5 g, 7.2 mmol) resulted in the formation of 1.5 g of **60d** in 93% yield as a white solid. (Rf: 0.31; 3:1 hexanes/ethyl acetate). mp: 105-107 °C. ^1H NMR (CDCl_3 , 300 MHz): δ : 1.05 (s, 9H), 1.24 (s, 3H), 2.71 (d, 1H, $J = 5.4$ Hz), 2.92 (d, 1H, $J = 5.1$ Hz), 3.66 (d, 1H, $J = 3.0$ Hz), 3.97 (d, 1H, $J = 3.0$ Hz). ^{13}C NMR (CDCl_3 , 100 MHz): δ : 14.5, 25.7, 32.3, 50.2, 58.1, 59.5, 60.2, 61.1, 68.5, 196.9. HRMS (APCI): expected for $\text{C}_{12}\text{H}_{17}\text{O}_4$ ($\text{M}+\text{H}$) $^+$ 225.11214. Found 225.11192. IR (neat): ν_{max} 2991, 2962, 2913, 2868, 1736, 739 cm^{-1} . Elemental Analysis for $\text{C}_{12}\text{H}_{16}\text{O}_4$: Found: C, 64.11; H, 7.19. Calculated: C, 64.27; H, 7.19.

(±)-4'-Methyl-7'-phenyl-3',8'-dioxaspiro[oxirane-2,5'-tricyclo[5.1.0.0^{2,4}]octan]-6'-one (60e)



Following the general procedure for the formation of triepoxides, compound **58e** (0.15 g, 0.66 mmol) resulted in the formation of 0.13 g of **60e** in 79% yield as a white solid. (Rf: 0.23; 3:1 hexanes/ethyl acetate). mp: 140-142 °C. ¹H NMR (CDCl₃, 300 MHz): δ: 1.33 (s, 3H), 2.85 (d, 1H, J = 5.4 Hz), 3.05 (d, 1H, J = 5.1 Hz), 3.78 (d, 1H, J = 2.4 Hz), 3.97 (d, 1H, J = 2.4 Hz), 7.38 (s, 5H). ¹³C NMR (CDCl₃, 100 MHz): δ: 14.7, 50.9, 58.0, 59.7, 60.1, 64.5, 65.1, 127.4, 128.2, 129.0, 131.2, 196.2. HRMS (APCI): expected for C₁₄H₁₃O₄ (M+H)⁺ 245.08084. Found 245.08105. IR (neat): ν_{max} 3068, 2995, 1736 cm⁻¹. Elemental Analysis for C₁₄H₁₂O₄: Found: C, 68.61; H, 4.92. Calculated: C, 68.85; H, 4.95.

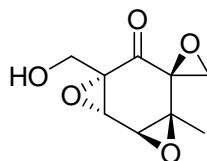
(±)-4'-Methyl-7'-(((triisopropylsilyl)oxy)methyl)-3',8'-dioxaspiro[oxirane-2,5'-tricyclo[5.1.0.0^{2,4}]octan]-6'-one (60f)



Following the general procedure for the formation of triepoxides, compound **58f** (0.25 g, 0.74 mmol) resulted in the formation of 0.18 g of **60f** in 67% yield as a white solid. (Rf: 0.18; 8:1 hexanes/ethyl acetate). mp: 45-47 °C. ¹H NMR (CDCl₃, 300 MHz): δ: 1.02-1.09 (m, 21H), 1.27 (s, 3H), 2.80 (d, 1H, J = 5.1 Hz), 2.99 (d, 1H, J = 5.4 Hz), 3.73 (d,

1H, J = 2.4 Hz), 4.05 (d, 1H, J = 12.9 Hz), 4.25 (d, 1H, J = 2.4 Hz), 4.32 (d, 1H, J = 12.9 Hz). ¹³C NMR (CDCl₃, 100 MHz): δ: 11.9, 14.7, 17.9, 50.9, 57.2, 58.4, 59.2, 59.4, 60.0, 63.8, 198.0. HRMS (APCI): expected for C₁₈H₃₁O₅Si (M+H)⁺ 355.19353. Found 355.19375. IR (neat): ν_{max} 2942, 2864, 1728 cm⁻¹. Elemental Analysis for C₁₈H₃₀O₅Si: Found: C, 61.27; H, 8.55. Calculated: C, 60.98; H, 8.53.

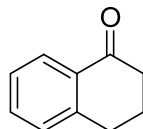
(±)-7'-(Hydroxymethyl)-4'-methyl-3',8'-dioxaspiro[oxirane-2,5'-tricyclo[5.1.0.0^{2,4}]octan]-6'-one (61)



Compound **60f** (0.10 g, 0.28 mmol, 1.0 eq) was added to a dry flask under argon and was dissolved in dry THF (10 mL). The solution was cooled to -78°C followed by the dropwise addition of 1.0 M TBAF in THF (0.34 mL, 0.34 mmol, 1.2 eq). The reaction was allowed to warm to room temperature as it stirred for 4 hours. The reaction solution was then transferred to a separatory funnel and was diluted with water (50 mL). The aqueous phase was extracted with ethyl acetate (3 x 30 mL). The organic layers were pooled, dried with MgSO₄, filtered, and concentrated. The product was purified on silica eluting with 2:1 hexanes/ethyl acetate. Compound **61** (0.036 g) was isolated in 65% yield as a white solid. (R_f: 0.03; 3:1 hexanes/ethyl acetate). mp: 128-133 °C (decomposition). ¹H NMR (CDCl₃, 300 MHz): δ: 1.28 (s, 3H), 1.80 (dd, 1H, J = 8.4 Hz, 5.4 Hz), 2.82 (d, 1H, J = 5.4 Hz), 3.02 (d, 1H, J = 5.4 Hz), 3.74 (d, 1H, J = 2.4 Hz), 3.94 (dd, 1H, J = 13.5 Hz, 8.1 Hz), 4.06 (dd, 1H, J = 13.2 Hz, 5.4 Hz), 4.13 (d, 1H, J = 2.1 Hz). ¹³C NMR (CDCl₃, 100 MHz): δ: 14.8, 51.1, 58.2, 58.9, 59.6, 60.0, 60.6, 63.1, 198.6. HRMS

(APCI): expected for $C_9H_{11}O_5$ (M+H)⁺ 199.06010. Found 199.06012. IR (neat): ν_{max} 3314, 2999, 2938, 2880, 1732 cm^{-1} . Elemental Analysis for $C_9H_{10}O_5$: Found: C, 54.67; H, 5.09. Calculated: C, 54.55; H, 5.09.

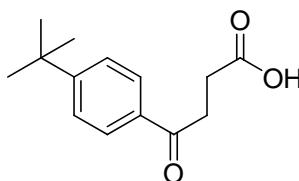
3,4-Dihydronaphthalen-1(2H)-one (64)



To a dry flask under argon was added *tert*-butylbenzene (57.7 mL, 373 mmol, 1.0 eq) followed by γ -butyrolactone (48.1 g, 559 mmol, 1.5 eq). This mixture was stirred vigorously as $AlCl_3$ (124 g, 931 mmol, 2.5 eq) was added. This mixture was heated to 100°C and allowed to stir for 10 hours. The reaction mixture was allowed to cool to room temperature and was then quenched slowly with water. The reaction was transferred to a separatory funnel and was extracted with diethyl ether (3 x 150 mL). The organic layers were pooled, washed with water, washed with brine, dried with $MgSO_4$, filtered, and concentrated. The resulting sludge was passed through silica eluting with 15:1 hexanes/ethyl acetate. The fractions containing product were pooled and concentrated. The product was further purified by distillation. The 15.0 g of product was isolated at 68°C under reduced pressure (1.5 mmHg) in 20% yield as a colorless oil. (Rf: 0.38; 8:1 hexanes/ethyl acetate). 1H NMR ($CDCl_3$, 300 MHz): δ : 2.15 (pent, 2H, J = 6.3 Hz), 2.67 (t, 2H, J = 6.0 Hz), 2.98 (t, 2H, J = 6.0 Hz), 7.26 (d, 1H, J = 7.8 Hz), 7.31 (t, 1H, J = 7.5 Hz), 7.48 (dt, 1H, J = 7.2 Hz, 1.5 Hz), 8.04 (dd, 1H, J = 7.5 Hz, 1.2 Hz). ^{13}C NMR ($CDCl_3$, 100 MHz): δ : 22.9, 29.2, 38.7, 126.1, 126.5, 128.4, 132.1, 132.9, 144.1, 197.6. HRMS (APCI): expected for $C_{10}H_{11}O$ (M+H)⁺ 147.08044. Found 147.08025. IR

(neat): ν_{\max} 3064, 3019, 2942, 2868, 2827, 1679 cm^{-1} . Elemental Analysis for $\text{C}_{10}\text{H}_{10}\text{O}$: Found: C, 81.75; H, 6.98. Calculated: C, 82.16; H, 6.89.

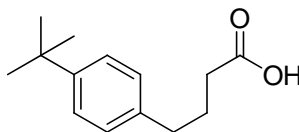
4-(4-*tert*-Butylphenyl)-4-oxobutanoic acid (66)



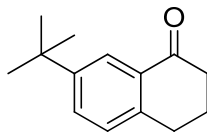
To a dry round bottomed flask under argon was added AlCl_3 (103 g, 770 mmol, 1.1 eq) and CH_2Cl_2 (500 mL). The reaction was cooled to 0°C and then succinic anhydride (70.1 g, 700 mmol, 1.0 eq) was added. The reaction was allowed to warm to ambient temperature followed by the dropwise addition of *tert*-butylbenzene (66.3 g, 700 mmol, 1.0 eq) in CH_2Cl_2 (500 mL). The reaction was allowed to stir at ambient temperature for 20 hours and was then poured into a separatory funnel containing 2N HCl (500 mL). The product was extracted with CH_2Cl_2 (2 x 400 mL). The organic layers were pooled and then washed with brine, dried over MgSO_4 , filtered, and concentrated. The product was purified on silica eluting with 2:1 hexanes/ethyl acetate. The product was further purified through recrystallization from hexanes/ethyl acetate. 90.2 g of the desired product was isolated in 55% yield as a white solid. (Rf: 0.68; ethyl acetate). mp: $112\text{--}113^\circ\text{C}$ ^1H NMR (CDCl_3 , 300 MHz): δ : 1.35 (s, 9H), 2.82 (t, 2H, $J = 6.3$ Hz), 3.32 (t, 2H, $J = 6.3$ Hz), 7.50 (d, 2H, $J = 8.1$ Hz), 7.94 (t, 2H, $J = 8.7$ Hz). ^{13}C NMR (CDCl_3 , 100 MHz): δ : 28.3, 31.3, 33.2, 35.3, 125.8, 128.2, 134.0, 157.3, 179.3, 197.7. HRMS (APCI): expected for $\text{C}_{14}\text{H}_{19}\text{O}_3$ ($\text{M}+\text{H}$) $^+$ 235.13287. Found 235.13299. IR (neat): ν_{\max} 3048, 2962, 2913, 2872, 1704, 1679, 1250 cm^{-1} . Elemental Analysis for $\text{C}_{14}\text{H}_{18}\text{O}_3$: Found: C, 71.69; H,

7.74. Calculated: C, 71.77; H, 7.74.

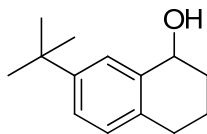
4-(4-*tert*-Butylphenyl)butanoic acid (67)



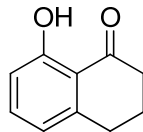
To a dry 1 L round bottomed flask under argon with compound **66** (90.0 g, 384 mmol, 1.0 eq) was added triethylene glycol (345 mL). Next sodium hydroxide (57.6 g, 1441 mmol, 3.75 eq) was added followed by the dropwise addition of anhydrous hydrazine (42.2 mL, 1344 mmol, 3.5 eq). The flask was heated to 165°C for 12 hours. The reaction was then cooled to ambient temperature and acidified with concentrated HCl. The contents of the reaction flask were transferred into a separatory funnel, diluted with water, and the product was extracted with ethyl acetate. The organic layer was washed with water and brine, dried over MgSO₄, filtered, and concentrated. The resulting residue was purified on silica eluting with 8:1 hexanes/ethyl acetate. The product was further purified by recrystallization from hexanes/ethyl acetate. 60.9 g of the desired product was isolated in 72% yield as a white solid. (Rf: 0.12; 8:1 hexanes/ethyl acetate). mp: 54-55 °C ¹H NMR (CDCl₃, 300 MHz): δ: 1.32 (s, 9H), 1.97 (pent, 2H, J = 7.8 Hz), 2.39 (t, 2H, J = 7.8 Hz), 2.66 (t, 2H, J = 7.2 Hz), 7.13 (d, 2H, J = 8.1 Hz), 7.32 (t, 2H, J = 8.4 Hz). ¹³C NMR (CDCl₃, 100 MHz): δ: 26.3, 31.6, 33.6, 34.6, 34.6, 125.5, 128.3, 138.3, 149.0, 180.4. HRMS (APCI): expected for C₁₄H₁₉O₂ (M-H)⁻ 219.13905. Found 219.13911. IR (neat): ν_{max} 3019, 2954, 2905, 2864, 1712 cm⁻¹. Elemental Analysis for C₁₄H₂₀O₂: Found: C, 76.26; H, 9.19. Calculated: C, 76.33; H, 9.15.

7-tert-Butyl-3,4-dihydronaphthalen-1(2H)-one (68)

To a dry round bottomed flask under argon containing 200 mL of polyphosphoric acid was added compound **67** (75.0 g, 340 mmol). Next an additional portion of polyphosphoric acid (175 mL) was added. The reaction was heated to 90°C and allowed to stir for one hour. Once the reaction cooled to room temperature the contents of the reaction flask were poured into ice water (1 L) and then extracted with CH₂Cl₂. The combined organic layers were washed with brine, dried with MgSO₄, filtered, and concentrated. The resulting residue was purified on silica eluting with 15:1 hexanes/ethyl acetate providing 55.0 g of the desired product in 80% yield as a white solid. (Rf: 0.51; 8:1 hexanes/ethyl acetate). mp: 96-98 °C ¹H NMR (CDCl₃, 300 MHz): δ: 1.34 (s, 9H), 2.14 (pent, 2H, J = 6.3 Hz), 2.66 (t, 2H, J = 6.3 Hz), 2.95 (t, 2H, J = 6.3 Hz), 7.21 (d, 1H, J = 7.8 Hz), 7.54 (dd, 1H, J = 7.8 Hz, 2.1 Hz), 8.08 (d, 1H, J = 1.8 Hz). ¹³C NMR (CDCl₃, 100 MHz): δ: 23.5, 29.4, 31.4, 34.8, 39.4, 123.8, 128.8, 131.0, 132.3, 141.9, 149.9, 199.0. HRMS (APCI): expected for C₁₄H₁₉O (M+H)⁺ 203.14304. Found 203.14307. IR (neat): ν_{max} 2958, 2942, 2868, 1683 cm⁻¹. Elemental Analysis for C₁₄H₁₈O: Found: C, 83.23; H, 8.95. Calculated: C, 83.12; H, 8.97.

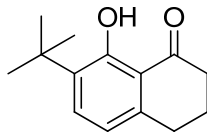
(±)-7-tert-Butyl-1,2,3,4-tetrahydronaphthalen-1-ol (69)

To a round bottomed flask containing compound **68** (26.1 g, 129 mmol, 1.0 eq) was added methanol (375 mL). The flask was then cooled to 0°C followed by the addition of NaBH₄ (13.7 g, 361 mmol, 2.8 eq) in small portions over a period of 30 minutes. Once complete the reaction was quenched with saturated aqueous NH₄Cl. The reaction mixture was transferred to a separatory funnel and diluted with water (250 mL). The product was extracted with ethyl acetate. The organic extracts were combined, washed with brine, dried over MgSO₄, filtered, and concentrated. The product was purified on silica eluting with 8:1 hexanes/ethyl acetate. The product (20.3 g) was isolated in 77% yield as a white solid. (Rf: 0.19; 8:1 hexanes/ethyl acetate). mp: 122-123 °C ¹H NMR (CDCl₃, 300 MHz): δ: 1.33 (s, 9H), 1.65 (d, 1H, J = 6.9 Hz), 1.78-1.81 (m, 1H), 1.92-2.01 (m, 3H), 2.67-2.86 (m, 2H), 4.77-4.80 (m, 1H), 7.07 (d, 1H, J = 8.1 Hz), 7.27 (dd, 1H, J = 8.1 Hz, 1.8 Hz), 7.47 (d, 1H, J = 1.8 Hz). ¹³C NMR (CDCl₃, 100 MHz): δ: 19.0, 29.0, 31.6, 32.6, 34.6, 68.6, 125.1, 125.5, 129.0, 134.4, 138.4, 149.3. HRMS (APCI): expected for C₁₄H₁₉ (M+H-H₂O)⁺ 187.14813. Found 187.14820. IR (neat): ν_{max} 3256, 2958, 2925, 2897, 2872 cm⁻¹. Elemental Analysis for C₁₄H₂₀O: Found: C, 82.12; H, 10.04. Calculated: C, 82.30; H, 9.87.

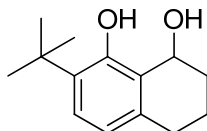
8-Hydroxy-3,4-dihydronaphthalen-1(2H)-one (73)

Compound **73** was prepared following the procedure of Nguyen and co-workers. 5,6,7,8-Tetrahydro-1-naphthylamine (26.0 g, 179 mmol, 1.0 eq) in dry ethanol (100 mL) was added dropwise to a dry round bottomed flask under argon containing acetic anhydride (34 mL, 359 mmol, 2.0 eq) in ethanol (400 mL) at 0°C. The mixture was allowed to stir for 20 hours at room temperature. The solvents were then removed under room temperature and the crude product was used without further purification. The crude product (32.6 g, 172 mmol) was transferred to a new round bottomed flask and dissolved with acetone (1 L) and 15% aqueous MgSO₄ (160 mL). Next KMnO₄ (65.2 g, 413 mmol, 2.4 eq) was added at room temperature. The reaction mixture was allowed to stir for 3 hours and was then filtered through celite. The solids were washed with CH₂Cl₂ and water. The filtrate was transferred into a separatory funnel and the organic layer was separated. The aqueous layer was extracted several times with CH₂Cl₂. The organic layers were combined, washed with brine, and dried over MgSO₄. The dried organic layer was then filtered and concentrated to provide crude *N*-(8-oxo-5,6,7,8-tetrahydro-naphthyl)-acetamide. Next the crude *N*-(8-oxo-5,6,7,8-tetrahydro-naphthyl)-acetamide (35.8 g, 176 mmol) was added to a round bottomed flask containing 6N HCl (475 mL). The reaction mixture was then heated to 90°C for 3 hours. Once cooled ice was added to the reaction flask followed by 2M NaOH until the mixture was at pH 8.0. The reaction mixture was transferred to a separatory funnel and the product was extracted with ethyl acetate. The organic layers were combined and washed with brine, dried with MgSO₄,

filtered, and concentrated to give crude 8-amino-1-tetralone **72**. Finally compound **72** (4.50 g, 27.9 mmol) in a round bottomed flask was dissolved in water (18 mL) and concentrated sulfuric acid (13.5 mL). The reaction was cooled to 0°C followed by the addition of NaNO₂ (2.12 g, 30.7 mmol, 1.1 eq) in water (45 mL). After an hour of stirring at 0°C the reaction was heated to 120°C. Stirring continued at the elevated temperature for 1 hour before being cooled back to room temperature. The dark brown reaction mixture was transferred to a separatory funnel and extracted with ethyl acetate. The combined organic layers were washed with water and brine. The organic layer was dried over MgSO₄, filtered, and concentrated. The resulting residue was applied to silica and eluted with 12:1 hexanes/ethyl acetate to provide 19.2 g of 8-Hydroxy-3,4-dihydronaphthalen-1(2H)-one **73** in 66% yield as a tan oil. (Rf: 0.36; 8:1 hexanes/ethyl acetate). ¹H NMR (CDCl₃, 300 MHz): δ: 2.12 (pent, 2H, J = 6.6 Hz), 2.70 (t, 2H, J = 6.0 Hz), 2.94 (t, 2H, J = 6.3 Hz), 6.72 (dd, 1H, J = 7.2 Hz, 0.9 Hz), 6.80 (d, 1H, J = 8.4 Hz), 7.37 (t, 1H, J = 8.1 Hz), 12.44 (s, 1H). ¹³C NMR (CDCl₃, 100 MHz): δ: 22.8, 29.6, 38.8, 115.3, 116.9, 118.8, 136.2, 145.5, 162.8, 205.1. HRMS (APCI): expected for C₁₀H₁₁O₂ (M+H)⁺ 163.07536. Found 163.07564. IR (neat): ν_{max} 3040, 2942, 2864, 2835, 1630, 1450, 1234, 1217 cm⁻¹. Elemental Analysis for C₁₀H₁₀O₂: Found: C, 74.20; H, 6.22. Calculated: C, 74.06; H, 6.21.

7-tert-Butyl-8-hydroxy-3,4-dihydronaphthalen-1(2H)-one (74)

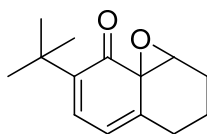
To a dry round bottomed flask under argon was added compound **73** (3.5 g, 22 mmol, 1.0 eq) and anhydrous 1,2-dichloroethane (38.5 mL). Next was added 2-chloro-2-methylpropane (7.0 mL, 65 mmol, 3.0 eq) followed by bromopentacarbonylrhenium (I) (0.088 g, 0.22 mmol, 0.01 eq). The reaction mixture was heated to 84°C and stirring was allowed to continue for 3 hours. The reaction mixture was concentrated and then purified on silica eluting with 15:1 hexanes/ethyl acetate. The desired compound (4.1 g) was isolated in 85% yield as a white solid. (Rf: 0.51; 8:1 hexanes/ethyl acetate). mp: 58-60 °C. ¹H NMR (CDCl₃, 300 MHz): δ: 1.41 (s, 9H), 2.09 (pent, 2H, J = 6.6 Hz), 2.69 (t, 2H, J = 6.3 Hz), 2.90 (t, 2H, J = 6.3 Hz), 6.64 (d, 1H, J = 8.1 Hz), 7.38 (d, 1H, J = 7.8 Hz), 13.32 (s, 1H). ¹³C NMR (CDCl₃, 100 MHz): δ: 23.1, 29.4, 29.7, 34.7, 39.3, 116.9, 117.9, 133.4, 135.7, 143.0, 162.7, 205.8. HRMS (APCI): expected for C₁₄H₁₉O₂ (M+H)⁺ 219.13796. Found 219.13771. IR (neat): ν_{max} 3032, 2999, 2954, 2868, 1634, 1417, 1225, 809 cm⁻¹. Elemental Analysis for C₁₄H₁₈O₂: Found: C, 77.11; H, 8.34. Calculated: C, 77.02; H, 8.32.

(±)-7-tert-Butyl-1,2,3,4-tetrahydronaphthalene-1,8-diol (70)

Compound **74** (3.5 g, 16 mmol, 1.0 eq) was added to a dry round bottomed flask under argon followed by the addition of THF (75 mL). The reaction was cooled to -78°C and

powdered LAH (0.61 g, 16 mmol, 1.0 eq) was added. The reaction was allowed to stir for 1 hour at -78°C before being allowed to warm to 0°C . The reaction was quenched with saturated aqueous NH_4Cl . The pH was adjusted to 2.0 using concentrated HCl. The reaction mixture was then transferred to a separatory funnel. The product was extracted with diethyl ether. The organic layers were combined, dried over MgSO_4 , filtered, and concentrated. The resulting residue was purified on silica eluting with 12:1 hexanes/ethyl acetate to afford 2.6 g of the desired product in 74% yield as a white solid. (Rf: 0.32; 8:1 hexanes/ethyl acetate). mp: $111\text{-}113^{\circ}\text{C}$. ^1H NMR (CDCl_3 , 300 MHz): δ : 1.42 (s, 9H), 1.73-1.92 (m, 3H), 1.93 (d, 1H, $J = 9.3$ Hz), 2.19-2.27 (m, 1H), 2.62-2.84 (m, 2H), 5.02-5.10 (m, 1H), 6.62 (d, 1H, $J = 8.1$ Hz), 7.15 (d, 1H, $J = 7.8$ Hz), 8.12 (s, 1H). ^{13}C NMR (CDCl_3 , 100 MHz): δ : 20.4, 29.7, 29.9, 34.0, 34.7, 68.6, 120.0, 123.8, 126.5, 134.7, 136.5, 156.0. HRMS (APCI): expected for $\text{C}_{14}\text{H}_{21}\text{O}_2$ ($\text{M}+\text{H}$) $^+$ 221.15361. Found 221.15420. IR (neat): ν_{max} 3334, 2954, 2872, 1417 cm^{-1} . Elemental Analysis for $\text{C}_{14}\text{H}_{20}\text{O}_2$: Found: C, 76.61; H, 9.16. Calculated: C, 76.31; H, 9.16.

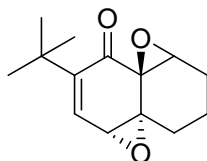
(\pm)-3-*tert*-Butyl-6,7,8,8a-tetrahydro-2H-naphtho[1-b]oxiren-2-one (75)



Following the general procedure for the formation of monoepoxides, compound **70** (3.2 g, 15 mmol) resulted in the formation of 2.6 g of **75** in 78 % yield as a yellow solid. (Rf: 0.32; 8:1 hexanes/ethyl acetate). mp: $68\text{-}71^{\circ}\text{C}$. ^1H NMR (CDCl_3 , 400 MHz): δ : 1.22 (s, 9H), 1.51-1.62 (m, 1H), 1.81-1.90 (m, 1H), 2.00-2.14 (m, 2H), 2.23 (dt, 1H, $J = 14.4$ Hz, 4.4 Hz), 2.51 (m, 1H, $J = 10.0$ Hz, 4.4 Hz, 2.0 Hz), 3.79 (d, 1H, $J = 3.2$ Hz), 6.26 (dd,

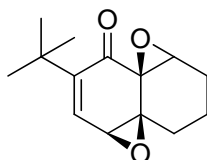
1H, J = 6.8 Hz, 2.0 Hz), 6.97 (d, 1H, J = 6.4 Hz). ¹³C NMR (CDCl₃, 100 MHz): δ: 24.2, 25.0, 29.0, 29.2, 34.4, 59.5, 70.6, 121.2, 136.7, 143.0, 149.0, 194.8. HRMS (APCI): expected for C₁₄H₁₉O₂ (M+H)⁺ 219.13796. Found 219.13778. IR (neat): ν_{max} 3048, 2995, 2946, 2913, 2868, 1663, 1634 cm⁻¹. Elemental Analysis for C₁₄H₁₈O₂: Found: C, 76.69; H, 8.37. Calculated: C, 77.03; H, 8.31.

(±)-3-(*tert*-Butyl)-6,7,8,8a-tetrahydronaphtho[1,8a-b:4a,5b']bis(oxirene)-2(4a*H*)-one
(76)



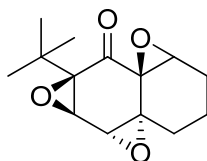
Following the general procedure for the synthesis of diepoxides, compound **75** (2.4 g, 11 mmol) was converted into 0.66 g of compound **76** in a 26% yield as a white solid. (Rf: 0.30; 8:1 hexanes/ethyl acetate). mp: 96 °C. ¹H NMR (CDCl₃, 300 MHz): δ: 1.18 (s, 9H), 1.31 (dt, 1H, J = 13.5 Hz, 3.9 Hz), 1.66-1.77 (m, 2H), 1.97-2.08 (m, 1H), 2.17-2.27 (m, 2H), 3.59 (d, 1H, J = 4.5 Hz), 4.09 (d, 1H, J = 4.2 Hz), 7.00 (d, 1H, J = 4.5 Hz). ¹³C NMR (CDCl₃, 100 MHz): δ: 18.5, 23.1, 26.6, 29.0, 35.2, 54.2, 57.0, 57.3, 60.9, 137.3, 151.4, 191.4. HRMS (APCI): expected for C₁₄H₁₉O₃ (M+H)⁺ 235.13287. Found 235.13292. IR (neat): ν_{max} 2995, 2962, 2868, 1683, 911 cm⁻¹. Elemental Analysis for C₁₄H₁₈O₃: Found: C, 71.48; H, 7.77. Calculated: C, 71.77; H, 7.74.

(±)-3-(*tert*-Butyl)-6,7,8,8a-tetrahydronaphtho[1,8a-b:4a,5b']bis(oxirene)-2(4a*H*)-one
(77)



In the formation of diepoxides, 1.3 g of compound **77** was produced in 51% yield as a white solid along with compound **76**. (Rf: 0.30; 3:1 hexanes/ethyl acetate). mp: 124-125 °C. ¹H NMR (CDCl₃, 300 MHz): δ: 1.19 (s, 9H), 1.41-1.59 (m, 2H), 1.81 (m, 1H), 1.94-2.02 (m, 3H), 3.47 (m, 1H), 3.48 (d, 1H, J = 5.1 Hz), 7.00 (d, 1H, J = 4.5 Hz). ¹³C NMR (CDCl₃, 100 MHz): δ: 20.2, 23.7, 27.4, 29.0, 35.2, 54.2, 59.5, 59.9, 62.3, 137.5, 151.3, 190.9. HRMS (APCI): expected for C₁₄H₁₉O₃ (M+H)⁺ 235.13287. Found 235.13290. IR (neat): ν_{max} 2995, 2962, 2937, 2904, 2868, 1683 cm⁻¹. Elemental Analysis for C₁₄H₁₈O₃: Found: C, 71.96; H, 7.73. Calculated: C, 71.77; H, 7.74.

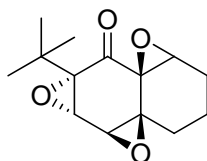
(±)-6a-(*tert*-Butyl)hexahydronaphtho[1,8a-b:2,3-b':4a,5-b']tris(oxirene)-7(5a*H*)-one
(78)



Following the general procedure for the formation of triepoxides, compound **76** (0.10 g, 0.43 mmol) resulted in the formation of 0.079 g of **78** in 73 % yield as a white solid. (Rf: 0.20; 8:1 hexanes/ethyl acetate). mp: 116-119 °C. ¹H NMR (CDCl₃, 300 MHz): δ: 0.99-1.26 (m, 1H), 1.06 (s, 9H), 1.50-1.63 (m, 2H), 1.88-1.99 (m, 1H), 2.10-2.23 (m, 2H), 3.65 (d, 1H, J = 3.0 Hz), 3.81 (d, 1H, J = 4.5 Hz), 3.95 (d, 1H, J = 2.7 Hz). ¹³C NMR (CDCl₃,

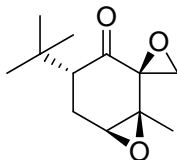
100 MHz): δ : 18.2, 23.1, 25.7, 26.7, 32.4, 55.8, 57.9, 58.1, 58.1, 60.2, 68.4, 197.9. HRMS (APCI): expected for $C_{14}H_{19}O_4$ ($M+H$)⁺ 251.12779. Found 251.12783. IR (neat): ν_{\max} 2962, 2917, 2880, 1720 cm^{-1} . Elemental Analysis for $C_{14}H_{18}O_4$: Found: C, 66.97; H, 7.25. Calculated: C, 67.18; H, 7.25.

(±)-6a-(*tert*-Butyl)hexahydronaphtho[1,8a-b:2,3-b':4a,5-b']tris(oxirene)-7(5a*H*)-one (79)



Following the general procedure for the formation of triepoxides, compound **77** (0.20 g, 0.85 mmol) resulted in the formation of 0.19 g of **79** in 88 % yield as a white solid. (Rf: 0.08; 8:1 hexanes/ethyl acetate). mp: 107-108 °C. ¹H NMR (CDCl₃, 300 MHz): δ : 1.07 (s, 9H), 1.16 (dt, 1H, J = 13.8 Hz), 1.68 (m, 1H), 1.78 (m, 1H), 1.88-1.96 (m, 1H), 2.05 (dt, 2H, J = 13.2 Hz, 3.3 Hz), 3.29 (d, 1H, J = 3.9 Hz), 3.66 (d, 1H, J = 3.0 Hz), 3.97 (d, 1H, J = 2.4 Hz). ¹³C NMR (CDCl₃, 100 MHz): δ : 21.4, 22.9, 25.8, 26.9, 32.4, 58.4, 59.9, 61.2, 61.7, 61.9, 68.1, 197.2. HRMS (APCI): expected for $C_{14}H_{19}O_4$ ($M+H$)⁺ 251.12779. Found 251.12791. IR (neat): ν_{\max} 2958, 2913, 2868, 1723 cm^{-1} . Elemental Analysis for $C_{14}H_{18}O_4$: Found: C, 67.14; H, 7.26. Calculated: C, 67.18; H, 7.25.

(±)-4-*tert*-Butyl-1-methyl-7-oxaspiro[bicyclo[4.1.0]heptane-2,2'-oxiran]-3-one (**80**)



Compound **58d** (0.50 g, 2.4 mmol, 1.0 eq) was added to a dry round bottomed flask under argon followed by the addition of dry THF (5 mL). The flask was cooled to -78°C and then a 1.0 M L-Selectride[®] solution in THF (2.4 mL, 2.4 mmol, 1.0 eq) was added dropwise. The reaction was allowed to stir at -78°C for 3 hours and then was allowed to warm to 0°C . The reaction was then quenched with saturated aqueous NH_4Cl (10 mL). The reaction was allowed to warm to room temperature. The reaction mixture was transferred to a separatory funnel and diluted with diethyl ether. The organic layer was separated, dried over MgSO_4 , filtered, and concentrated. The resulting residue was purified on silica eluting with 5:1 hexanes/ethyl acetate to give 0.19 g of compound **80** in 38% yield as a white solid. A portion of compound **80** was recrystallized from hexanes and ethyl acetate for x-ray crystallography. (Rf: 0.26; 3:1 hexanes/ethyl acetate). mp: $81\text{--}82^{\circ}\text{C}$. ^1H NMR (CDCl_3 , 400 MHz): δ : 0.99 (s, 9H), 1.24 (s, 3H), 2.19 (ddd, 1H, $J = 14.8$ Hz, 10.0 Hz, 1.2 Hz), 2.39–2.44 (m, 1H), 2.47–2.54 (m, 1H), 2.83 (d, 1H, $J = 6.0$ Hz), 2.90 (d, 1H, $J = 5.6$ Hz), 3.45 (dd, 1H, $J = 4.0$ Hz, 1.2 Hz). ^{13}C NMR (CDCl_3 , 100 MHz): δ : 15.2, 23.7, 28.3, 33.7, 50.6, 53.7, 58.3, 59.3, 61.2, 204.5. HRMS (ESI): expected for $\text{C}_{12}\text{H}_{19}\text{O}_3$ ($\text{M}+\text{H}$)⁺ 211.13287. Found 211.13264. IR (neat): ν_{max} 2999, 2954, 2876, 1712 cm^{-1} . Elemental Analysis for $\text{C}_{12}\text{H}_{18}\text{O}_3$: Found: C, 68.49; H, 8.60. Calculated: C, 68.55; H, 8.63. The relative stereochemistry was established by X-ray crystallographic analysis.

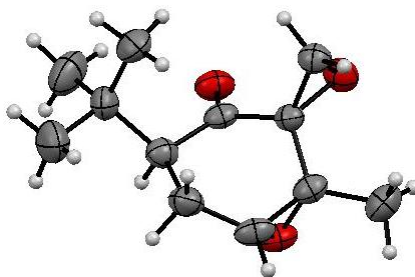


Table 29. Crystal data and structure refinement for gb587_1_0m.

Identification code	gb587_1_0m	
Empirical formula	C ₁₂ H ₁₈ O ₃	
Formula weight	210.26	
Temperature	173(2) K	
Wavelength	1.54178 Å	
Crystal system	Monoclinic	
Space group	P2(1)/c	
Unit cell dimensions	a = 9.058(3) Å	α = 90°.
	b = 9.967(3) Å	β = 95.873(11)°.
	c = 12.799(4) Å	γ = 90°.
Volume	1149.5(6) Å ³	
Z	4	
Density (calculated)	1.215 Mg/m ³	
Absorption coefficient	0.697 mm ⁻¹	
F(000)	456	
Crystal size	0.45 x 0.11 x 0.06 mm ³	
Theta range for data collection	8.26 to 58.59°.	
Index ranges	-9 ≤ h ≤ 9, -9 ≤ k ≤ 9, -11 ≤ l ≤ 12	
Reflections collected	3395	
Independent reflections	1304 [R(int) = 0.0318]	
Completeness to theta = 58.59°	80.7 %	
Absorption correction	None	
Max. and min. transmission	0.9594 and 0.7445	
Refinement method	Full-matrix least-squares on F ²	
Data / restraints / parameters	1304 / 0 / 140	
Goodness-of-fit on F ²	1.004	
Final R indices [I > 2σ(I)]	R1 = 0.0461, wR2 = 0.1115	

R indices (all data)

R1 = 0.0750, wR2 = 0.1240

Largest diff. peak and hole

0.159 and -0.180 e.Å⁻³**Table 30.** Atomic coordinates ($\times 10^4$) and equivalent isotropic displacement parameters ($\text{\AA}^2 \times 10^3$) for gb587_1_0m. U(eq) is defined as one third of the trace of the orthogonalized U^{ij} tensor.

	x	y	z	U(eq)
C(1)	9075(3)	2257(3)	7135(2)	37(1)
C(2)	10567(3)	2866(3)	7493(2)	34(1)
C(3)	10787(3)	3033(3)	8659(2)	42(1)
C(4)	9466(3)	3471(3)	9127(2)	46(1)
C(5)	8105(3)	3851(3)	8433(2)	48(1)
C(6)	7708(3)	2885(3)	7519(2)	41(1)
C(7)	6657(3)	3520(3)	6602(2)	46(1)
C(8)	7518(3)	4443(3)	5942(2)	55(1)
C(9)	5923(3)	2410(4)	5904(3)	77(1)
C(10)	5442(3)	4333(4)	7053(3)	77(1)
C(11)	11335(3)	3699(3)	6777(2)	40(1)
C(12)	12325(3)	3269(3)	9186(2)	54(1)
O(1)	9002(2)	1275(2)	6564(2)	49(1)
O(2)	11798(2)	2342(2)	7005(2)	48(1)
O(3)	9877(2)	2057(2)	9170(2)	49(1)

Table 31. Bond lengths [\AA] and angles [$^\circ$] for gb587_1_0m.

C(1)-O(1)	1.219(3)
C(1)-C(2)	1.509(4)
C(1)-C(6)	1.514(4)
C(2)-O(2)	1.431(3)
C(2)-C(11)	1.465(4)
C(2)-C(3)	1.494(4)

C(3)-C(4)	1.459(4)
C(3)-O(3)	1.470(3)
C(3)-C(12)	1.503(4)
C(4)-O(3)	1.457(3)
C(4)-C(5)	1.492(4)
C(4)-H(4)	1.0000
C(5)-C(6)	1.530(4)
C(5)-H(5A)	0.9900
C(5)-H(5B)	0.9900
C(6)-C(7)	1.567(4)
C(6)-H(6)	1.0000
C(7)-C(8)	1.518(4)
C(7)-C(10)	1.527(4)
C(7)-C(9)	1.531(4)
C(8)-H(8A)	0.9800
C(8)-H(8B)	0.9800
C(8)-H(8C)	0.9800
C(9)-H(9A)	0.9800
C(9)-H(9B)	0.9800
C(9)-H(9C)	0.9800
C(10)-H(10A)	0.9800
C(10)-H(10B)	0.9800
C(10)-H(10C)	0.9800
C(11)-O(2)	1.437(3)
C(11)-H(11A)	0.9900
C(11)-H(11B)	0.9900
C(12)-H(12A)	0.9800
C(12)-H(12B)	0.9800
C(12)-H(12C)	0.9800
O(1)-C(1)-C(2)	119.8(2)
O(1)-C(1)-C(6)	122.0(3)
C(2)-C(1)-C(6)	118.2(3)
O(2)-C(2)-C(11)	59.48(15)
O(2)-C(2)-C(3)	116.5(2)
C(11)-C(2)-C(3)	122.6(2)
O(2)-C(2)-C(1)	115.7(2)

C(11)-C(2)-C(1)	120.4(2)
C(3)-C(2)-C(1)	111.8(2)
C(4)-C(3)-O(3)	59.67(17)
C(4)-C(3)-C(2)	114.4(2)
O(3)-C(3)-C(2)	110.3(2)
C(4)-C(3)-C(12)	122.0(3)
O(3)-C(3)-C(12)	116.1(2)
C(2)-C(3)-C(12)	119.2(2)
O(3)-C(4)-C(3)	60.55(18)
O(3)-C(4)-C(5)	117.4(2)
C(3)-C(4)-C(5)	119.6(3)
O(3)-C(4)-H(4)	116.0
C(3)-C(4)-H(4)	116.0
C(5)-C(4)-H(4)	116.0
C(4)-C(5)-C(6)	114.3(2)
C(4)-C(5)-H(5A)	108.7
C(6)-C(5)-H(5A)	108.7
C(4)-C(5)-H(5B)	108.7
C(6)-C(5)-H(5B)	108.7
H(5A)-C(5)-H(5B)	107.6
C(1)-C(6)-C(5)	111.9(2)
C(1)-C(6)-C(7)	112.2(2)
C(5)-C(6)-C(7)	113.3(2)
C(1)-C(6)-H(6)	106.3
C(5)-C(6)-H(6)	106.3
C(7)-C(6)-H(6)	106.3
C(8)-C(7)-C(10)	108.7(3)
C(8)-C(7)-C(9)	109.3(3)
C(10)-C(7)-C(9)	108.5(2)
C(8)-C(7)-C(6)	110.7(2)
C(10)-C(7)-C(6)	109.8(2)
C(9)-C(7)-C(6)	109.8(2)
C(7)-C(8)-H(8A)	109.5
C(7)-C(8)-H(8B)	109.5
H(8A)-C(8)-H(8B)	109.5
C(7)-C(8)-H(8C)	109.5

H(8A)-C(8)-H(8C)	109.5
H(8B)-C(8)-H(8C)	109.5
C(7)-C(9)-H(9A)	109.5
C(7)-C(9)-H(9B)	109.5
H(9A)-C(9)-H(9B)	109.5
C(7)-C(9)-H(9C)	109.5
H(9A)-C(9)-H(9C)	109.5
H(9B)-C(9)-H(9C)	109.5
C(7)-C(10)-H(10A)	109.5
C(7)-C(10)-H(10B)	109.5
H(10A)-C(10)-H(10B)	109.5
C(7)-C(10)-H(10C)	109.5
H(10A)-C(10)-H(10C)	109.5
H(10B)-C(10)-H(10C)	109.5
O(2)-C(11)-C(2)	59.10(17)
O(2)-C(11)-H(11A)	117.9
C(2)-C(11)-H(11A)	117.9
O(2)-C(11)-H(11B)	117.9
C(2)-C(11)-H(11B)	117.9
H(11A)-C(11)-H(11B)	115.0
C(3)-C(12)-H(12A)	109.5
C(3)-C(12)-H(12B)	109.5
H(12A)-C(12)-H(12B)	109.5
C(3)-C(12)-H(12C)	109.5
H(12A)-C(12)-H(12C)	109.5
H(12B)-C(12)-H(12C)	109.5
C(2)-O(2)-C(11)	61.42(17)
C(4)-O(3)-C(3)	59.78(17)

Symmetry transformations used to generate equivalent atoms:

Table 32. Anisotropic displacement parameters ($\text{\AA}^2 \times 10^3$) for gb587_1_0m. The anisotropic displacement factor exponent takes the form: $-2\pi^2 [h^2 a^{*2} U^{11} + \dots + 2 h k a^* b^* U^{12}]$

	U11	U22	U33	U23	U13	U12
C(1)	50(2)	33(2)	29(2)	7(2)	2(1)	-1(2)
C(2)	38(2)	34(2)	29(2)	1(1)	5(1)	4(1)
C(3)	52(2)	37(2)	35(2)	4(2)	-1(2)	1(2)
C(4)	69(2)	37(2)	31(2)	-4(2)	5(2)	-4(2)
C(5)	52(2)	53(2)	40(2)	1(2)	12(2)	4(2)
C(6)	44(2)	41(2)	38(2)	0(2)	5(1)	-6(1)
C(7)	33(2)	57(2)	47(2)	3(2)	1(1)	-3(2)
C(8)	55(2)	63(2)	46(2)	12(2)	-2(2)	8(2)
C(9)	68(2)	84(3)	73(3)	7(2)	-22(2)	-18(2)
C(10)	48(2)	105(3)	79(3)	13(2)	9(2)	18(2)
C(11)	45(2)	37(2)	40(2)	2(2)	6(1)	0(2)
C(12)	57(2)	52(2)	48(2)	1(2)	-11(2)	1(2)
O(1)	65(1)	46(2)	38(2)	-4(1)	6(1)	-6(1)
O(2)	50(1)	46(2)	50(2)	-4(1)	11(1)	6(1)
O(3)	68(1)	46(2)	33(1)	6(1)	5(1)	-4(1)

Table 33. Hydrogen coordinates ($\times 10^4$) and isotropic displacement parameters ($\text{\AA}^2 \times 10^3$) for gb587_1_0m.

	x	y	z	U(eq)
H(4)	9646	3978	9802	55
H(5A)	8249	4758	8146	58
H(5B)	7258	3897	8864	58
H(6)	7138	2134	7805	49
H(8A)	6825	4926	5437	83
H(8B)	8200	3910	5562	83
H(8C)	8086	5089	6400	83

H(9A)	5311	2813	5310	116
H(9B)	5296	1858	6314	116
H(9C)	6691	1847	5641	116
H(10A)	5886	5106	7440	116
H(10B)	4933	3767	7530	116
H(10C)	4726	4647	6479	116
H(11A)	10818	3890	6074	49
H(11B)	11977	4433	7084	49
H(12A)	12983	2547	8997	80
H(12B)	12298	3282	9950	80
H(12C)	12696	4132	8955	80

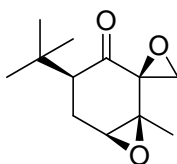
Table 34. Torsion angles [$^{\circ}$] for gb587_1_0m.

O(1)-C(1)-C(2)-O(2)	8.6(4)
C(6)-C(1)-C(2)-O(2)	-172.5(2)
O(1)-C(1)-C(2)-C(11)	76.8(4)
C(6)-C(1)-C(2)-C(11)	-104.3(3)
O(1)-C(1)-C(2)-C(3)	-128.0(3)
C(6)-C(1)-C(2)-C(3)	50.9(3)
O(2)-C(2)-C(3)-C(4)	-175.5(2)
C(11)-C(2)-C(3)-C(4)	115.2(3)
C(1)-C(2)-C(3)-C(4)	-39.3(3)
O(2)-C(2)-C(3)-O(3)	-110.6(3)
C(11)-C(2)-C(3)-O(3)	-179.8(2)
C(1)-C(2)-C(3)-O(3)	25.7(3)
O(2)-C(2)-C(3)-C(12)	27.5(4)
C(11)-C(2)-C(3)-C(12)	-41.7(4)
C(1)-C(2)-C(3)-C(12)	163.8(3)
C(2)-C(3)-C(4)-O(3)	100.2(2)
C(12)-C(3)-C(4)-O(3)	-103.6(3)
O(3)-C(3)-C(4)-C(5)	-106.7(3)
C(2)-C(3)-C(4)-C(5)	-6.5(4)
C(12)-C(3)-C(4)-C(5)	149.7(3)
O(3)-C(4)-C(5)-C(6)	-25.6(3)

C(3)-C(4)-C(5)-C(6)	44.3(4)
O(1)-C(1)-C(6)-C(5)	165.1(3)
C(2)-C(1)-C(6)-C(5)	-13.8(4)
O(1)-C(1)-C(6)-C(7)	-66.2(4)
C(2)-C(1)-C(6)-C(7)	114.9(3)
C(4)-C(5)-C(6)-C(1)	-32.0(3)
C(4)-C(5)-C(6)-C(7)	-160.1(2)
C(1)-C(6)-C(7)-C(8)	-50.7(3)
C(5)-C(6)-C(7)-C(8)	77.3(3)
C(1)-C(6)-C(7)-C(10)	-170.7(3)
C(5)-C(6)-C(7)-C(10)	-42.7(3)
C(1)-C(6)-C(7)-C(9)	70.2(3)
C(5)-C(6)-C(7)-C(9)	-161.9(2)
C(3)-C(2)-C(11)-O(2)	103.8(3)
C(1)-C(2)-C(11)-O(2)	-103.8(3)
C(3)-C(2)-O(2)-C(11)	-113.9(3)
C(1)-C(2)-O(2)-C(11)	111.5(3)
C(5)-C(4)-O(3)-C(3)	110.2(3)
C(2)-C(3)-O(3)-C(4)	-107.0(3)
C(12)-C(3)-O(3)-C(4)	113.4(3)

Symmetry transformations used to generate equivalent atoms:

(±)-4-*tert*-Butyl-1-methyl-7-oxaspiro[bicyclo[4.1.0]heptane-2,2'-oxiran]-3-one (81)



In addition to the formation of compound **80**, 0.19 g of compound **81** was isolated in 38% yield as a white solid during the reduction of compound **58d**. A portion of compound **81** was recrystallized from hexanes and ethyl acetate for x-ray crystallography. (R_f: 0.15; 3:1 hexanes/ethyl acetate). mp: 146-147 °C. ¹H NMR (CDCl₃, 300 MHz): δ: 0.98 (s, 9H), 1.25 (s, 3H), 2.18 (dd, 1H, J = 14.7 Hz, 11.1 Hz), 2.42-2.48 (m, 1H), 2.53-2.63 (m,

1H), 2.69 (d, 1H, J = 5.1 Hz), 2.96 (d, 1H, J = 5.4 Hz), 3.41 (d, 1H, J = 4.8 Hz). ¹³C NMR (CDCl₃, 100 MHz): δ: 15.5, 27.2, 32.0, 50.4, 55.4, 59.8, 59.8, 62.2, 62.9, 203.4. HRMS (ESI): expected for C₁₂H₁₉O₃ (M+H)⁺ 211.13287. Found 211.13306. IR (neat): ν_{max} 2995, 2958, 2909, 2872, 1728 cm⁻¹. Elemental Analysis for C₁₂H₁₈O₃: Found: C, 68.41; H, 8.66. Calculated: C, 68.55; H, 8.63. The relative stereochemistry was established by X-ray crystallographic analysis.

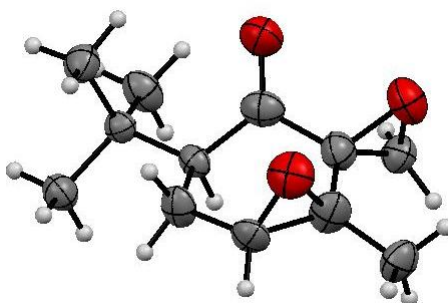


Table 35. Crystal data and structure refinement for GB587_2s.

Identification code	gb587_2s	
Empirical formula	C ₁₂ H ₁₈ O ₃	
Formula weight	210.26	
Temperature	173(2) K	
Wavelength	1.54178 Å	
Crystal system	Orthorhombic	
Space group	Pbca	
Unit cell dimensions	a = 9.601(3) Å	α = 90°.
	b = 12.659(4) Å	β = 90°.
	c = 18.736(5) Å	γ = 90°.
Volume	2277.2(11) Å ³	
Z	8	
Density (calculated)	1.227 Mg/m ³	
Absorption coefficient	0.704 mm ⁻¹	
F(000)	912	
Crystal size	0.38 x 0.09 x 0.05 mm ³	
Theta range for data collection	8.45 to 61.09°.	
Index ranges	-10 ≤ h ≤ 9, -12 ≤ k ≤ 12, -18 ≤ l ≤ 20	

Reflections collected	8115
Independent reflections	1512 [R(int) = 0.0886]
Completeness to theta = 61.09°	86.5 %
Absorption correction	Semi-empirical from equivalents
Max. and min. transmission	0.9657 and 0.7759
Refinement method	Full-matrix least-squares on F ²
Data / restraints / parameters	1512 / 0 / 141
Goodness-of-fit on F ²	1.025
Final R indices [I > 2sigma(I)]	R1 = 0.1286, wR2 = 0.2844
R indices (all data)	R1 = 0.1748, wR2 = 0.3084
Extinction coefficient	0.0022(5)
Largest diff. peak and hole	1.483 and -0.317 e.Å ⁻³

Table 36. Atomic coordinates ($\times 10^4$) and equivalent isotropic displacement parameters ($\text{\AA}^2 \times 10^3$) for GB587_2s. $U(\text{eq})$ is defined as one third of the trace of the orthogonalized U_{ij} tensor.

	x	y	z	$U(\text{eq})$
C(1)	9729(9)	6932(7)	2995(5)	47(2)
C(2)	9433(9)	6715(7)	2210(4)	45(2)
C(3)	9195(10)	5579(7)	2034(5)	51(3)
C(4)	8989(9)	4852(7)	2629(4)	42(2)
C(5)	8887(10)	5206(6)	3390(4)	43(2)
C(6)	8747(7)	6419(6)	3498(4)	31(2)
C(7)	8736(7)	6776(6)	4287(4)	31(2)
C(8)	10134(9)	6537(7)	4655(4)	46(2)
C(9)	8447(9)	7963(7)	4321(5)	49(2)
C(10)	7576(9)	6207(7)	4696(4)	43(2)
C(11)	8807(8)	7601(7)	1804(4)	44(2)
C(12)	8781(10)	5303(7)	1297(4)	50(3)
O(1)	10701(7)	7510(5)	3168(3)	59(2)
O(2)	10283(6)	7310(5)	1713(3)	58(2)
O(3)	10396(7)	4961(5)	2317(3)	60(2)

Table 37. Bond lengths [\AA] and angles [$^\circ$] for GB587_2s.

C(1)-O(1)	1.230(10)
C(1)-C(6)	1.482(11)
C(1)-C(2)	1.522(12)
C(2)-O(2)	1.450(10)
C(2)-C(11)	1.483(12)
C(2)-C(3)	1.493(13)
C(3)-C(4)	1.459(12)
C(3)-C(12)	1.479(12)
C(3)-O(3)	1.490(11)
C(4)-O(3)	1.478(10)
C(4)-C(5)	1.498(11)

C(4)-H(4)	1.0000
C(5)-C(6)	1.555(11)
C(5)-H(5A)	0.9900
C(5)-H(5B)	0.9900
C(6)-C(7)	1.547(10)
C(6)-H(6)	1.0000
C(7)-C(9)	1.530(12)
C(7)-C(10)	1.532(10)
C(7)-C(8)	1.538(11)
C(8)-H(8A)	0.9800
C(8)-H(8B)	0.9800
C(8)-H(8C)	0.9800
C(9)-H(9A)	0.9800
C(9)-H(9B)	0.9800
C(9)-H(9C)	0.9800
C(10)-H(10A)	0.9800
C(10)-H(10B)	0.9800
C(10)-H(10C)	0.9800
C(11)-O(2)	1.474(10)
C(11)-H(11A)	0.9900
C(11)-H(11B)	0.9900
C(12)-H(12A)	0.9800
C(12)-H(12B)	0.9800
C(12)-H(12C)	0.9800
O(1)-C(1)-C(6)	125.2(8)
O(1)-C(1)-C(2)	120.2(8)
C(6)-C(1)-C(2)	114.6(7)
O(2)-C(2)-C(11)	60.3(5)
O(2)-C(2)-C(3)	116.4(7)
C(11)-C(2)-C(3)	123.6(8)
O(2)-C(2)-C(1)	115.0(7)
C(11)-C(2)-C(1)	115.8(8)
C(3)-C(2)-C(1)	114.6(7)
C(4)-C(3)-C(12)	121.9(8)
C(4)-C(3)-O(3)	60.2(5)
C(12)-C(3)-O(3)	114.6(7)

C(4)-C(3)-C(2)	117.4(8)
C(12)-C(3)-C(2)	118.3(8)
O(3)-C(3)-C(2)	108.0(7)
C(3)-C(4)-O(3)	61.0(6)
C(3)-C(4)-C(5)	123.2(8)
O(3)-C(4)-C(5)	114.1(7)
C(3)-C(4)-H(4)	115.6
O(3)-C(4)-H(4)	115.6
C(5)-C(4)-H(4)	115.6
C(4)-C(5)-C(6)	115.1(7)
C(4)-C(5)-H(5A)	108.5
C(6)-C(5)-H(5A)	108.5
C(4)-C(5)-H(5B)	108.5
C(6)-C(5)-H(5B)	108.5
H(5A)-C(5)-H(5B)	107.5
C(1)-C(6)-C(7)	119.0(7)
C(1)-C(6)-C(5)	107.2(7)
C(7)-C(6)-C(5)	114.4(6)
C(1)-C(6)-H(6)	105.0
C(7)-C(6)-H(6)	105.0
C(5)-C(6)-H(6)	105.0
C(9)-C(7)-C(10)	108.0(7)
C(9)-C(7)-C(8)	109.5(7)
C(10)-C(7)-C(8)	108.6(6)
C(9)-C(7)-C(6)	109.1(6)
C(10)-C(7)-C(6)	110.2(6)
C(8)-C(7)-C(6)	111.4(6)
C(7)-C(8)-H(8A)	109.5
C(7)-C(8)-H(8B)	109.5
H(8A)-C(8)-H(8B)	109.5
C(7)-C(8)-H(8C)	109.5
H(8A)-C(8)-H(8C)	109.5
H(8B)-C(8)-H(8C)	109.5
C(7)-C(9)-H(9A)	109.5
C(7)-C(9)-H(9B)	109.5
H(9A)-C(9)-H(9B)	109.5

C(7)-C(9)-H(9C)	109.5
H(9A)-C(9)-H(9C)	109.5
H(9B)-C(9)-H(9C)	109.5
C(7)-C(10)-H(10A)	109.5
C(7)-C(10)-H(10B)	109.5
H(10A)-C(10)-H(10B)	109.5
C(7)-C(10)-H(10C)	109.5
H(10A)-C(10)-H(10C)	109.5
H(10B)-C(10)-H(10C)	109.5
O(2)-C(11)-C(2)	58.7(5)
O(2)-C(11)-H(11A)	117.9
C(2)-C(11)-H(11A)	117.9
O(2)-C(11)-H(11B)	117.9
C(2)-C(11)-H(11B)	117.9
H(11A)-C(11)-H(11B)	115.1
C(3)-C(12)-H(12A)	109.5
C(3)-C(12)-H(12B)	109.5
H(12A)-C(12)-H(12B)	109.5
C(3)-C(12)-H(12C)	109.5
H(12A)-C(12)-H(12C)	109.5
H(12B)-C(12)-H(12C)	109.5
C(2)-O(2)-C(11)	61.0(5)
C(4)-O(3)-C(3)	58.9(5)

Symmetry transformations used to generate equivalent atoms:

Table 38. Anisotropic displacement parameters ($\text{\AA}^2 \times 10^3$) for GB587_2s. The anisotropic displacement factor exponent takes the form: $-2\pi^2 [h^2 a^{*2} U^{11} + \dots + 2 h k a^* b^* U^{12}]$

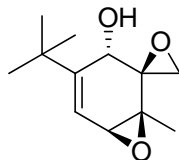
	U11	U22	U33	U23	U13	U12
C(1)	45(5)	35(6)	61(6)	-2(4)	-2(4)	-1(5)
C(2)	46(5)	49(7)	40(5)	2(4)	5(4)	-1(4)
C(3)	74(7)	28(6)	52(6)	-5(4)	-8(5)	0(5)
C(4)	51(5)	25(5)	50(5)	1(4)	-2(4)	-8(4)

C(5)	64(6)	25(6)	41(5)	2(4)	5(4)	0(4)
C(6)	30(4)	26(5)	36(4)	5(3)	2(3)	2(3)
C(7)	34(4)	26(5)	35(4)	3(3)	-2(3)	-1(3)
C(8)	47(5)	52(6)	40(5)	3(4)	-5(4)	2(4)
C(9)	57(6)	36(6)	54(6)	-1(4)	13(4)	-1(4)
C(10)	47(5)	41(6)	42(5)	3(4)	4(4)	-5(4)
C(11)	44(5)	45(6)	41(5)	4(4)	-5(4)	1(4)
C(12)	62(6)	49(6)	40(5)	-10(4)	-6(4)	2(5)
O(1)	65(4)	53(5)	59(4)	3(3)	-1(3)	-12(4)
O(2)	64(4)	55(5)	54(4)	6(3)	15(3)	1(3)
O(3)	55(4)	52(5)	71(4)	1(3)	-1(3)	15(3)

Table 39. Hydrogen coordinates ($\times 10^4$) and isotropic displacement parameters ($\text{\AA}^2 \times 10^3$) for GB587_2s.

	x	y	z	U(eq)
H(4)	8487	4182	2511	50
H(5A)	9726	4960	3648	52
H(5B)	8070	4858	3611	52
H(6)	7800	6599	3313	37
H(8A)	10875	6950	4427	69
H(8B)	10345	5782	4611	69
H(8C)	10074	6727	5161	69
H(9A)	8449	8195	4820	74
H(9B)	7535	8111	4108	74
H(9C)	9170	8344	4056	74
H(10A)	7552	6462	5190	65
H(10B)	7755	5444	4694	65
H(10C)	6679	6349	4466	65
H(11A)	8154	7427	1413	52
H(11B)	8593	8261	2066	52
H(12A)	7817	5526	1215	75
H(12B)	8856	4537	1231	75
H(12C)	9397	5663	958	75

(±)-4-*tert*-Butyl-1-methyl-7-oxaspiro[bicyclo[4.1.0]hept[4]ene-2,2'-oxiran]-3-ol (**82**)



To a round bottomed flask containing compound **58d** (1.5 g, 7.2 mmol, 1.0 eq) was added ethanol (100 mL) and CH₂Cl₂ (100 mL). Next was added CeCl₃·7H₂O (3.5 g, 9.0 mmol, 1.25 eq) and then the reaction was cooled to -25°C. Once cooled NaBH₄ (1.2 g, 32.4 mmol, 4.5 eq) was added. The reaction was allowed to stir for 1 hour and then was quenched with saturated aqueous NH₄Cl. The reaction mixture was transferred into a separatory funnel and was diluted with water (200 mL). The product was extracted with CH₂Cl₂. The organic layers were dried over MgSO₄, filtered, and concentrated. The resulting residue was purified on silica eluting with 8:1 hexanes/ethyl acetate. The concentrated product was stored at 4°C for 1 week for it to solidify. 1.1 g of the desired product **82** was isolated in 70% yield as a white solid. (R_f: 0.37; 3:1 hexanes/ethyl acetate). mp: 70-73 °C. ¹H NMR (CDCl₃, 300 MHz): δ: 1.18 (s, 9H), 1.34 (s, 3H), 1.72 (d, 1H, J = 3.3 Hz), 2.83 (d, 1H, J = 4.8 Hz), 3.08 (d, 1H, J = 4.5 Hz), 3.30 (d, 1H, J = 3.9 Hz), 4.63 (t, 1H, J = 2.7 Hz), 5.73-5.75 (m, 1H). ¹³C NMR (CDCl₃, 100 MHz): δ: 16.4, 29.4, 36.1, 47.1, 56.6, 57.3, 62.6, 67.2, 115.4, 155.5. HRMS (APCI): expected for C₁₂H₁₉O₃ (M+H)⁺ 211.13287. Found 211.13288. IR (neat): ν_{max} 3469, 3003, 2958, 2904, 2872, 1082, 878 cm⁻¹. Elemental Analysis for C₁₂H₁₈O₃: Found: C, 67.31; H, 8.63. Calculated: C, 68.55; H, 8.63. The relative stereochemistry was established by X-ray crystallographic analysis.

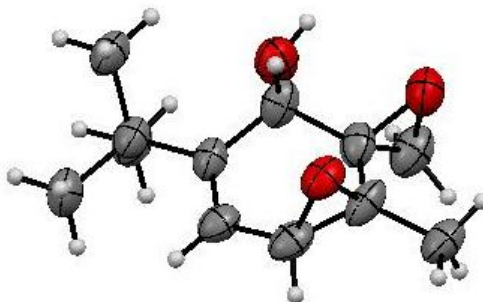


Table 40. Crystal data and structure refinement for GB649.

Identification code	GB649	
Empirical formula	C ₁₂ H ₁₈ O ₃	
Formula weight	210.26	
Temperature	173(2) K	
Wavelength	1.54178 Å	
Crystal system	Monoclinic	
Space group	P2(1)/c	
Unit cell dimensions	a = 17.893(3) Å	α = 90°.
	b = 11.719(2) Å	β = 107.279(8)°.
	c = 11.4984(16) Å	γ = 90°.
Volume	2302.4(6) Å ³	
Z	8	
Density (calculated)	1.213 Mg/m ³	
Absorption coefficient	0.696 mm ⁻¹	
F(000)	912	
Crystal size	0.53 x 0.47 x 0.42 mm ³	
Theta range for data collection	2.59 to 65.86°.	
Index ranges	-20 ≤ h ≤ 19, -13 ≤ k ≤ 10, -12 ≤ l ≤ 13	
Reflections collected	10782	
Independent reflections	3612 [R(int) = 0.0663]	
Completeness to theta = 65.86°	90.1 %	
Absorption correction	Semi-empirical from equivalents	
Max. and min. transmission	0.7587 and 0.7093	
Refinement method	Full-matrix least-squares on F ²	
Data / restraints / parameters	3612 / 0 / 272	
Goodness-of-fit on F ²	1.003	
Final R indices [I > 2σ(I)]	R1 = 0.1254, wR2 = 0.2935	

R indices (all data)	R1 = 0.1936, wR2 = 0.3503
Extinction coefficient	0.0022(5)
Largest diff. peak and hole	0.583 and -0.692 e.Å ⁻³

Table 41. Atomic coordinates ($\times 10^4$) and equivalent isotropic displacement parameters ($\text{\AA}^2 \times 10^3$) for GB649. $U(\text{eq})$ is defined as one third of the trace of the orthogonalized U_{ij} tensor.

	x	y	z	U(eq)
C(1)	2166(4)	7920(6)	4482(5)	46(2)
C(2)	1653(4)	8793(7)	4096(5)	49(2)
C(3)	817(4)	8615(7)	3470(6)	54(2)
C(4)	524(4)	7514(7)	2910(5)	54(2)
C(5)	1155(4)	6627(7)	3094(6)	53(2)
C(6)	1840(4)	6719(7)	4237(6)	53(2)
C(7)	3002(4)	8132(7)	5264(6)	49(2)
C(8)	3165(4)	7426(7)	6441(6)	59(2)
C(9)	3607(4)	7805(7)	4621(7)	60(2)
C(10)	3153(4)	9403(7)	5632(6)	58(2)
C(11)	-200(4)	7421(8)	1842(6)	60(2)
C(12)	1229(5)	5994(8)	2020(7)	69(2)
C(1B)	3304(4)	3534(7)	6201(6)	53(2)
C(2B)	3210(4)	4248(7)	7063(6)	52(2)
C(3B)	2426(4)	4534(7)	7149(6)	54(2)
C(4B)	1772(4)	3782(6)	6594(6)	48(2)
C(5B)	2006(3)	2704(6)	6056(5)	40(2)
C(6B)	2595(4)	2922(6)	5385(5)	46(2)
C(7B)	4109(4)	3320(7)	5997(6)	54(2)
C(8B)	4379(4)	2091(8)	6390(8)	72(2)
C(9B)	4735(4)	4141(9)	6715(9)	80(3)
C(10B)	4027(4)	3481(9)	4645(7)	77(3)
C(11B)	967(4)	4264(7)	6012(6)	53(2)
C(12B)	1501(4)	1690(6)	5786(6)	51(2)
O(1)	394(3)	7848(5)	4054(4)	55(1)
O(2)	851(3)	5461(5)	2841(4)	63(1)

O(3)	2447(3)	5944(5)	4192(5)	66(2)
O(1B)	2071(3)	3818(5)	7907(4)	60(1)
O(2B)	2183(3)	1728(4)	6863(4)	54(1)
O(3B)	2226(3)	3616(4)	4356(4)	54(1)

Table 42. Bond lengths [\AA] and angles [$^\circ$] for GB649.

C(1)-C(2)	1.358(10)
C(1)-C(7)	1.520(8)
C(1)-C(6)	1.517(10)
C(2)-C(3)	1.470(9)
C(2)-H(2A)	0.9500
C(3)-O(1)	1.461(8)
C(3)-C(4)	1.467(11)
C(3)-H(3A)	1.0000
C(4)-O(1)	1.455(7)
C(4)-C(5)	1.502(10)
C(4)-C(11)	1.502(8)
C(5)-O(2)	1.468(9)
C(5)-C(12)	1.480(10)
C(5)-C(6)	1.512(9)
C(6)-O(3)	1.428(8)
C(6)-H(6A)	1.0000
C(7)-C(9)	1.530(9)
C(7)-C(8)	1.539(9)
C(7)-C(10)	1.550(11)
C(8)-H(8A)	0.9800
C(8)-H(8B)	0.9800
C(8)-H(8C)	0.9800
C(9)-H(9A)	0.9800
C(9)-H(9B)	0.9800
C(9)-H(9C)	0.9800
C(10)-H(10A)	0.9800
C(10)-H(10B)	0.9800

C(10)-H(10C)	0.9800
C(11)-H(11A)	0.9800
C(11)-H(11B)	0.9800
C(11)-H(11C)	0.9800
C(12)-O(2)	1.455(9)
C(12)-H(12A)	0.9900
C(12)-H(12B)	0.9900
C(1B)-C(2B)	1.344(10)
C(1B)-C(6B)	1.516(9)
C(1B)-C(7B)	1.547(9)
C(2B)-C(3B)	1.474(10)
C(2B)-H(2BA)	0.9500
C(3B)-C(4B)	1.453(10)
C(3B)-O(1B)	1.482(8)
C(3B)-H(3BA)	1.0000
C(4B)-O(1B)	1.445(7)
C(4B)-C(11B)	1.507(9)
C(4B)-C(5B)	1.519(9)
C(5B)-O(2B)	1.447(8)
C(5B)-C(12B)	1.469(9)
C(5B)-C(6B)	1.501(9)
C(6B)-O(3B)	1.426(8)
C(6B)-H(6BA)	1.0000
C(7B)-C(9B)	1.521(10)
C(7B)-C(10B)	1.529(10)
C(7B)-C(8B)	1.544(11)
C(8B)-H(8BA)	0.9800
C(8B)-H(8BB)	0.9800
C(8B)-H(8BC)	0.9800
C(9B)-H(9BA)	0.9800
C(9B)-H(9BB)	0.9800
C(9B)-H(9BC)	0.9800
C(10B)-H(10D)	0.9800
C(10B)-H(10E)	0.9800
C(10B)-H(10F)	0.9800
C(11B)-H(11D)	0.9800

C(11B)-H(11E)	0.9800
C(11B)-H(11F)	0.9800
C(12B)-O(2B)	1.458(8)
C(12B)-H(12C)	0.9900
C(12B)-H(12D)	0.9900
O(3)-H(3B)	0.8400
O(3B)-H(3BB)	0.8400
C(2)-C(1)-C(7)	121.4(7)
C(2)-C(1)-C(6)	117.0(6)
C(7)-C(1)-C(6)	121.2(6)
C(1)-C(2)-C(3)	122.9(7)
C(1)-C(2)-H(2A)	118.6
C(3)-C(2)-H(2A)	118.6
O(1)-C(3)-C(4)	59.6(4)
O(1)-C(3)-C(2)	117.0(5)
C(4)-C(3)-C(2)	121.2(6)
O(1)-C(3)-H(3A)	115.7
C(4)-C(3)-H(3A)	115.7
C(2)-C(3)-H(3A)	115.7
O(1)-C(4)-C(3)	60.0(4)
O(1)-C(4)-C(5)	112.0(5)
C(3)-C(4)-C(5)	113.1(6)
O(1)-C(4)-C(11)	115.3(5)
C(3)-C(4)-C(11)	122.1(7)
C(5)-C(4)-C(11)	119.6(7)
O(2)-C(5)-C(12)	59.1(5)
O(2)-C(5)-C(4)	113.5(6)
C(12)-C(5)-C(4)	118.7(6)
O(2)-C(5)-C(6)	113.3(6)
C(12)-C(5)-C(6)	120.7(6)
C(4)-C(5)-C(6)	117.0(6)
O(3)-C(6)-C(5)	110.6(6)
O(3)-C(6)-C(1)	110.0(5)
C(5)-C(6)-C(1)	113.3(6)
O(3)-C(6)-H(6A)	107.6
C(5)-C(6)-H(6A)	107.6

C(1)-C(6)-H(6A)	107.6
C(1)-C(7)-C(9)	112.8(5)
C(1)-C(7)-C(8)	109.2(6)
C(9)-C(7)-C(8)	108.3(6)
C(1)-C(7)-C(10)	112.3(6)
C(9)-C(7)-C(10)	106.4(6)
C(8)-C(7)-C(10)	107.7(6)
C(7)-C(8)-H(8A)	109.5
C(7)-C(8)-H(8B)	109.5
H(8A)-C(8)-H(8B)	109.5
C(7)-C(8)-H(8C)	109.5
H(8A)-C(8)-H(8C)	109.5
H(8B)-C(8)-H(8C)	109.5
C(7)-C(9)-H(9A)	109.5
C(7)-C(9)-H(9B)	109.5
H(9A)-C(9)-H(9B)	109.5
C(7)-C(9)-H(9C)	109.5
H(9A)-C(9)-H(9C)	109.5
H(9B)-C(9)-H(9C)	109.5
C(7)-C(10)-H(10A)	109.5
C(7)-C(10)-H(10B)	109.5
H(10A)-C(10)-H(10B)	109.5
C(7)-C(10)-H(10C)	109.5
H(10A)-C(10)-H(10C)	109.5
H(10B)-C(10)-H(10C)	109.5
C(4)-C(11)-H(11A)	109.5
C(4)-C(11)-H(11B)	109.5
H(11A)-C(11)-H(11B)	109.5
C(4)-C(11)-H(11C)	109.5
H(11A)-C(11)-H(11C)	109.5
H(11B)-C(11)-H(11C)	109.5
O(2)-C(12)-C(5)	60.0(5)
O(2)-C(12)-H(12A)	117.8
C(5)-C(12)-H(12A)	117.8
O(2)-C(12)-H(12B)	117.8
C(5)-C(12)-H(12B)	117.8

H(12A)-C(12)-H(12B)	114.9
C(2B)-C(1B)-C(6B)	119.1(6)
C(2B)-C(1B)-C(7B)	122.6(6)
C(6B)-C(1B)-C(7B)	118.4(6)
C(1B)-C(2B)-C(3B)	121.4(6)
C(1B)-C(2B)-H(2BA)	119.3
C(3B)-C(2B)-H(2BA)	119.3
C(4B)-C(3B)-C(2B)	119.4(7)
C(4B)-C(3B)-O(1B)	59.0(4)
C(2B)-C(3B)-O(1B)	119.6(6)
C(4B)-C(3B)-H(3BA)	115.7
C(2B)-C(3B)-H(3BA)	115.7
O(1B)-C(3B)-H(3BA)	115.7
O(1B)-C(4B)-C(3B)	61.5(4)
O(1B)-C(4B)-C(11B)	117.4(5)
C(3B)-C(4B)-C(11B)	120.4(7)
O(1B)-C(4B)-C(5B)	112.9(6)
C(3B)-C(4B)-C(5B)	113.6(6)
C(11B)-C(4B)-C(5B)	118.3(6)
O(2B)-C(5B)-C(12B)	60.0(4)
O(2B)-C(5B)-C(6B)	114.2(5)
C(12B)-C(5B)-C(6B)	120.7(6)
O(2B)-C(5B)-C(4B)	115.5(5)
C(12B)-C(5B)-C(4B)	122.1(6)
C(6B)-C(5B)-C(4B)	112.8(5)
O(3B)-C(6B)-C(5B)	107.5(5)
O(3B)-C(6B)-C(1B)	109.8(6)
C(5B)-C(6B)-C(1B)	110.4(5)
O(3B)-C(6B)-H(6BA)	109.7
C(5B)-C(6B)-H(6BA)	109.7
C(1B)-C(6B)-H(6BA)	109.7
C(9B)-C(7B)-C(10B)	107.9(7)
C(9B)-C(7B)-C(8B)	108.3(7)
C(10B)-C(7B)-C(8B)	109.8(7)
C(9B)-C(7B)-C(1B)	112.6(6)
C(10B)-C(7B)-C(1B)	108.8(6)

C(8B)-C(7B)-C(1B)	109.4(6)
C(7B)-C(8B)-H(8BA)	109.5
C(7B)-C(8B)-H(8BB)	109.5
H(8BA)-C(8B)-H(8BB)	109.5
C(7B)-C(8B)-H(8BC)	109.5
H(8BA)-C(8B)-H(8BC)	109.5
H(8BB)-C(8B)-H(8BC)	109.5
C(7B)-C(9B)-H(9BA)	109.5
C(7B)-C(9B)-H(9BB)	109.5
H(9BA)-C(9B)-H(9BB)	109.5
C(7B)-C(9B)-H(9BC)	109.5
H(9BA)-C(9B)-H(9BC)	109.5
H(9BB)-C(9B)-H(9BC)	109.5
C(7B)-C(10B)-H(10D)	109.5
C(7B)-C(10B)-H(10E)	109.5
H(10D)-C(10B)-H(10E)	109.5
C(7B)-C(10B)-H(10F)	109.5
H(10D)-C(10B)-H(10F)	109.5
H(10E)-C(10B)-H(10F)	109.5
C(4B)-C(11B)-H(11D)	109.5
C(4B)-C(11B)-H(11E)	109.5
H(11D)-C(11B)-H(11E)	109.5
C(4B)-C(11B)-H(11F)	109.5
H(11D)-C(11B)-H(11F)	109.5
H(11E)-C(11B)-H(11F)	109.5
O(2B)-C(12B)-C(5B)	59.2(4)
O(2B)-C(12B)-H(12C)	117.9
C(5B)-C(12B)-H(12C)	117.9
O(2B)-C(12B)-H(12D)	117.9
C(5B)-C(12B)-H(12D)	117.9
H(12C)-C(12B)-H(12D)	115.0
C(4)-O(1)-C(3)	60.4(5)
C(12)-O(2)-C(5)	60.8(5)
C(6)-O(3)-H(3B)	109.5
C(4B)-O(1B)-C(3B)	59.5(4)
C(5B)-O(2B)-C(12B)	60.8(4)

C(6B)-O(3B)-H(3BB) 109.5

Table 43. Anisotropic displacement parameters ($\text{\AA}^2 \times 10^3$) for GB649. The anisotropic displacement factor exponent takes the form: $-2\pi^2 [h^2 a^{*2} U_{11} + \dots + 2 h k a^* b^* U_{12}]$

	U11	U22	U33	U23	U13	U12
C(1)	37(3)	63(5)	36(3)	-5(3)	9(3)	-6(3)
C(2)	45(4)	63(5)	40(3)	9(3)	14(3)	4(3)
C(3)	49(4)	76(6)	40(3)	10(4)	17(3)	8(4)
C(4)	33(3)	94(6)	34(3)	2(4)	7(3)	5(4)
C(5)	51(4)	67(5)	39(3)	-7(3)	13(3)	-12(3)
C(6)	34(3)	73(5)	50(4)	-9(4)	12(3)	5(3)
C(7)	41(3)	67(5)	37(3)	0(3)	8(3)	-5(3)
C(8)	45(4)	79(6)	45(4)	3(4)	3(3)	-3(4)
C(9)	45(4)	80(6)	55(4)	-3(4)	13(3)	-5(4)
C(10)	48(4)	67(5)	52(4)	-10(4)	5(3)	-8(4)
C(11)	47(4)	88(6)	41(3)	9(4)	8(3)	3(4)
C(12)	56(4)	98(7)	51(4)	-3(4)	15(3)	2(4)
C(1B)	43(4)	71(5)	45(3)	4(4)	12(3)	-1(3)
C(2B)	50(4)	69(5)	36(3)	-2(3)	10(3)	-6(3)
C(3B)	59(4)	65(5)	40(3)	-8(3)	19(3)	-9(4)
C(4B)	46(4)	65(5)	38(3)	-10(3)	20(3)	-6(3)
C(5B)	41(3)	41(4)	36(3)	2(3)	5(3)	-3(3)
C(6B)	44(4)	58(5)	35(3)	-9(3)	9(3)	1(3)
C(7B)	38(3)	71(5)	49(4)	-1(4)	8(3)	-5(3)
C(8B)	50(4)	83(6)	88(6)	15(5)	27(4)	14(4)
C(9B)	34(4)	105(8)	97(6)	-15(6)	12(4)	-8(4)
C(10B)	47(4)	129(9)	58(4)	7(5)	22(4)	-3(5)
C(11B)	46(4)	60(5)	58(4)	5(4)	22(3)	5(3)
C(12B)	41(4)	65(5)	47(3)	-6(3)	15(3)	-4(3)
O(1)	46(3)	79(4)	43(2)	6(2)	18(2)	0(2)
O(2)	56(3)	73(4)	56(3)	-9(3)	11(2)	-11(3)
O(3)	50(3)	66(4)	77(3)	-3(3)	10(3)	4(3)
O(1B)	70(3)	70(4)	41(2)	-2(2)	21(2)	-1(3)

O(2B)	55(3)	64(3)	44(2)	2(2)	15(2)	-1(2)
O(3B)	57(3)	67(3)	37(2)	5(2)	16(2)	6(2)

Table 44. Hydrogen coordinates ($\times 10^4$) and isotropic displacement parameters ($\text{\AA}^2 \times 10^3$) for GB649.

	x	y	z	U(eq)
H(2A)	1844	9553	4237	59
H(3A)	521	9303	3066	65
H(6A)	1651	6491	4939	63
H(8A)	3077	6616	6235	88
H(8B)	2813	7672	6902	88
H(8C)	3709	7540	6936	88
H(9A)	3508	8239	3862	91
H(9B)	3568	6987	4437	91
H(9C)	4134	7980	5152	91
H(10A)	3058	9873	4897	87
H(10B)	3696	9499	6137	87
H(10C)	2799	9640	6094	87
H(11A)	-550	8061	1853	90
H(11B)	-468	6701	1891	90
H(11C)	-55	7440	1085	90
H(12A)	893	6233	1207	82
H(12B)	1755	5716	2040	82
H(2BA)	3658	4575	7627	63
H(3BA)	2299	5366	7127	64
H(6BA)	2760	2182	5106	55
H(8BA)	4885	1950	6247	108
H(8BB)	3991	1549	5914	108
H(8BC)	4434	1995	7258	108
H(9BA)	4566	4928	6494	120
H(9BB)	5226	3995	6526	120
H(9BC)	4817	4028	7589	120

H(10D)	3857	4262	4401	115
H(10E)	3639	2941	4163	115
H(10F)	4534	3341	4505	115
H(11D)	888	4935	6471	80
H(11E)	572	3686	6017	80
H(11F)	916	4486	5171	80
H(12C)	977	1744	5908	61
H(12D)	1528	1198	5100	61
H(3B)	2299	5271	4253	100
H(3BB)	2304	3335	3730	80

Table 45. Torsion angles [°] for GB649.

C(7)-C(1)-C(2)-C(3)	-172.2(6)
C(6)-C(1)-C(2)-C(3)	0.2(9)
C(1)-C(2)-C(3)-O(1)	51.3(9)
C(1)-C(2)-C(3)-C(4)	-17.9(9)
C(2)-C(3)-C(4)-O(1)	105.0(6)
O(1)-C(3)-C(4)-C(5)	-103.0(6)
C(2)-C(3)-C(4)-C(5)	2.0(9)
O(1)-C(3)-C(4)-C(11)	102.7(7)
C(2)-C(3)-C(4)-C(11)	-152.3(6)
O(1)-C(4)-C(5)-O(2)	98.9(7)
C(3)-C(4)-C(5)-O(2)	164.4(5)
C(11)-C(4)-C(5)-O(2)	-40.6(8)
O(1)-C(4)-C(5)-C(12)	165.3(6)
C(3)-C(4)-C(5)-C(12)	-129.2(7)
C(11)-C(4)-C(5)-C(12)	25.8(10)
O(1)-C(4)-C(5)-C(6)	-36.0(9)
C(3)-C(4)-C(5)-C(6)	29.5(8)
C(11)-C(4)-C(5)-C(6)	-175.4(6)
O(2)-C(5)-C(6)-O(3)	54.6(8)
C(12)-C(5)-C(6)-O(3)	-12.2(10)
C(4)-C(5)-C(6)-O(3)	-170.5(6)
O(2)-C(5)-C(6)-C(1)	178.6(5)

C(12)-C(5)-C(6)-C(1)	111.8(8)
C(4)-C(5)-C(6)-C(1)	-46.4(8)
C(2)-C(1)-C(6)-O(3)	155.0(6)
C(7)-C(1)-C(6)-O(3)	-32.5(8)
C(2)-C(1)-C(6)-C(5)	30.6(8)
C(7)-C(1)-C(6)-C(5)	-156.9(6)
C(2)-C(1)-C(7)-C(9)	-115.2(7)
C(6)-C(1)-C(7)-C(9)	72.7(8)
C(2)-C(1)-C(7)-C(8)	124.3(7)
C(6)-C(1)-C(7)-C(8)	-47.8(8)
C(2)-C(1)-C(7)-C(10)	5.0(8)
C(6)-C(1)-C(7)-C(10)	-167.1(6)
C(4)-C(5)-C(12)-O(2)	-101.7(7)
C(6)-C(5)-C(12)-O(2)	100.4(7)
C(6B)-C(1B)-C(2B)-C(3B)	-6.2(11)
C(7B)-C(1B)-C(2B)-C(3B)	173.1(7)
C(1B)-C(2B)-C(3B)-C(4B)	20.5(11)
C(1B)-C(2B)-C(3B)-O(1B)	89.4(8)
C(2B)-C(3B)-C(4B)-O(1B)	108.9(7)
C(2B)-C(3B)-C(4B)-C(11B)	-144.4(6)
O(1B)-C(3B)-C(4B)-C(11B)	106.8(6)
C(2B)-C(3B)-C(4B)-C(5B)	4.6(9)
O(1B)-C(3B)-C(4B)-C(5B)	-104.2(6)
O(1B)-C(4B)-C(5B)-O(2B)	24.5(7)
C(3B)-C(4B)-C(5B)-O(2B)	92.1(7)
C(11B)-C(4B)-C(5B)-O(2B)	-118.2(6)
O(1B)-C(4B)-C(5B)-C(12B)	93.8(7)
C(3B)-C(4B)-C(5B)-C(12B)	161.4(6)
C(11B)-C(4B)-C(5B)-C(12B)	-48.9(8)
O(1B)-C(4B)-C(5B)-C(6B)	-109.5(6)
C(3B)-C(4B)-C(5B)-C(6B)	-41.9(7)
C(11B)-C(4B)-C(5B)-C(6B)	107.8(6)
O(2B)-C(5B)-C(6B)-O(3B)	160.2(5)
C(12B)-C(5B)-C(6B)-O(3B)	92.0(7)
C(4B)-C(5B)-C(6B)-O(3B)	-65.1(6)
O(2B)-C(5B)-C(6B)-C(1B)	-79.9(7)

C(12B)-C(5B)-C(6B)-C(1B)	-148.2(6)
C(4B)-C(5B)-C(6B)-C(1B)	54.7(7)
C(2B)-C(1B)-C(6B)-O(3B)	87.4(7)
C(7B)-C(1B)-C(6B)-O(3B)	-91.9(7)
C(2B)-C(1B)-C(6B)-C(5B)	-31.0(9)
C(7B)-C(1B)-C(6B)-C(5B)	149.7(6)
C(2B)-C(1B)-C(7B)-C(9B)	-9.6(11)
C(6B)-C(1B)-C(7B)-C(9B)	169.7(7)
C(2B)-C(1B)-C(7B)-C(10B)	-129.2(8)
C(6B)-C(1B)-C(7B)-C(10B)	50.1(9)
C(2B)-C(1B)-C(7B)-C(8B)	110.9(8)
C(6B)-C(1B)-C(7B)-C(8B)	-69.8(8)
C(6B)-C(5B)-C(12B)-O(2B)	102.0(6)
C(4B)-C(5B)-C(12B)-O(2B)	-103.0(6)
C(5)-C(4)-O(1)-C(3)	104.7(7)
C(11)-C(4)-O(1)-C(3)	-113.9(8)
C(2)-C(3)-O(1)-C(4)	-112.1(7)
C(4)-C(5)-O(2)-C(12)	110.5(7)
C(6)-C(5)-O(2)-C(12)	-113.0(7)
C(11B)-C(4B)-O(1B)-C(3B)	-111.5(8)
C(5B)-C(4B)-O(1B)-C(3B)	105.4(6)
C(2B)-C(3B)-O(1B)-C(4B)	-108.5(7)
C(6B)-C(5B)-O(2B)-C(12B)	-112.8(6)
C(4B)-C(5B)-O(2B)-C(12B)	113.9(6)

Symmetry transformations used to generate equivalent atoms:

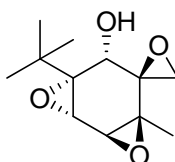
Table 46. Hydrogen bonds for GB649 [\AA and $^\circ$].

D-H...A	d(D-H)	d(H...A)	d(D...A)	$\angle(\text{DHA})$
O(3)-H(3B)...O(3B)	0.84	1.95	2.770(8)	165.1
O(3B)-H(3BB)...O(2B)#1	0.84	2.09	2.874(6)	154.1

Symmetry transformations used to generate equivalent atoms:

#1 $x, -y+1/2, z-1/2$

(±)-7'-(*tert*-Butyl)-4'-methyl-3',8'-dioxaspiro[oxirane-2,5'-tricyclo[5.1.0.0^{2,4}]octan]-6'-ol (**83**)



To a round bottomed flask containing compound **60d** (0.75 g, 3.3 mmol, 1.1 eq) was added ethanol (50 mL) and CH₂Cl₂ (50 mL). Next was added CeCl₃·7H₂O (1.6 g, 4.2 mmol, 1.25 eq) and then the reaction was cooled to -25°C. Once cooled NaBH₄ (0.57 g, 15.0 mmol, 4.5 eq) was added. The reaction was allowed to stir for 1 hour and then was quenched with saturated aqueous NH₄Cl. The reaction mixture was transferred into a separatory funnel and was diluted with water (200 mL). The product was extracted with CH₂Cl₂. The organic layers were dried over MgSO₄, filtered, and concentrated. The resulting residue was purified on silica eluting with 5:1 hexanes/ethyl acetate. The desired product (0.62 g) was isolated as a white solid in 83% yield. A portion of compound **83** was recrystallized from hexanes and ethyl acetate for x-ray crystallography. (R_f: 0.36; 3:1 hexanes/ethyl acetate). mp: 117-118 °C. ¹H NMR (CDCl₃, 300 MHz): δ: 1.04 (s, 9H), 1.26 (s, 3H), 2.03 (d, 1H, J = 3.9 Hz), 2.88 (d, 1H, J = 4.2 Hz), 3.05 (d, 1H, J = 4.2 Hz), 3.39 (d, 1H, J = 2.4 Hz), 3.60 (d, 1H, J = 2.7 Hz), 4.29 (d, 1H, J = 3.3 Hz). ¹³C NMR (CDCl₃, 100 MHz): δ: 16.8, 26.5, 33.5, 47.8, 55.7, 58.1, 58.5, 59.7, 67.4, 67.7. HRMS (APCI): expected for C₁₂H₁₉O₄ (M+H)⁺ 227.12779. Found 227.12794. IR (neat): ν_{max} 3501, 3003, 2966, 2913, 2876 cm⁻¹. Elemental Analysis for C₁₂H₁₈O₄: Found: C, 63.92; H, 8.04. Calculated: C, 63.70; H, 8.02. The relative stereochemistry was established by X-ray crystallographic analysis.

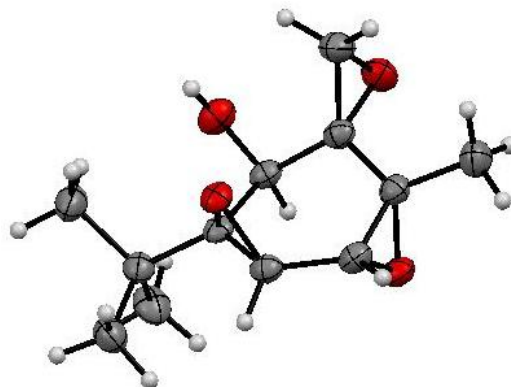


Table 47. Crystal data and structure refinement for GB625s.

Identification code	gb625s	
Empirical formula	C ₁₂ H ₁₈ O ₄	
Formula weight	226.26	
Temperature	173(2) K	
Wavelength	1.54178 Å	
Crystal system	Monoclinic	
Space group	P2(1)/c	
Unit cell dimensions	a = 9.8311(10) Å	α = 90°.
	b = 18.3625(18) Å	β = 105.612(5)°.
	c = 6.5753(6) Å	γ = 90°.
Volume	1143.20(19) Å ³	
Z	4	
Density (calculated)	1.315 Mg/m ³	
Absorption coefficient	0.807 mm ⁻¹	
F(000)	488	
Crystal size	0.35 x 0.18 x 0.03 mm ³	
Theta range for data collection	4.67 to 66.86°.	
Index ranges	-10 ≤ h ≤ 11, -21 ≤ k ≤ 18, -7 ≤ l ≤ 7	
Reflections collected	4965	
Independent reflections	1833 [R(int) = 0.0197]	
Completeness to theta = 66.86°	90.6 %	
Absorption correction	Semi-empirical from equivalents	
Max. and min. transmission	0.9762 and 0.7654	
Refinement method	Full-matrix least-squares on F ²	
Data / restraints / parameters	1833 / 0 / 150	

Goodness-of-fit on F^2	1.081
Final R indices [$I > 2\sigma(I)$]	$R1 = 0.0425$, $wR2 = 0.1127$
R indices (all data)	$R1 = 0.0483$, $wR2 = 0.1167$
Largest diff. peak and hole	0.515 and -0.306 e. \AA^{-3}

Table 48. Atomic coordinates ($\times 10^4$) and equivalent isotropic displacement parameters ($\text{\AA}^2 \times 10^3$) for GB625s. $U(\text{eq})$ is defined as one third of the trace of the orthogonalized U_{ij} tensor.

	x	y	z	$U(\text{eq})$
C(1)	1356(2)	1276(1)	3315(3)	25(1)
C(2)	295(2)	1208(1)	4629(3)	26(1)
C(3)	-1210(2)	1402(1)	3381(3)	27(1)
C(4)	-1734(2)	1039(1)	1276(3)	29(1)
C(5)	-678(2)	917(1)	101(3)	29(1)
C(6)	811(2)	1138(1)	1029(3)	27(1)
C(7)	2935(2)	1163(1)	4421(3)	29(1)
C(8)	3531(2)	1827(1)	5796(4)	40(1)
C(9)	3801(2)	1075(1)	2810(3)	38(1)
C(10)	3115(2)	473(1)	5781(4)	41(1)
C(11)	-1837(2)	2093(1)	3775(3)	36(1)
C(12)	-3274(2)	1094(1)	111(3)	39(1)
O(1)	697(2)	1584(1)	6573(2)	37(1)
O(2)	-2206(1)	1424(1)	4640(2)	38(1)
O(3)	-1143(1)	317(1)	1192(2)	32(1)
O(4)	1051(1)	1880(1)	1821(2)	27(1)

Table 49. Bond lengths [\AA] and angles [$^\circ$] for GB625s.

C(1)-O(4)	1.459(2)	C(2)-C(3)	1.529(3)
C(1)-C(6)	1.475(3)	C(2)-H(2)	1.0000
C(1)-C(2)	1.528(2)	C(3)-O(2)	1.443(2)
C(1)-C(7)	1.541(2)	C(3)-C(11)	1.464(3)
C(2)-O(1)	1.412(2)	C(3)-C(4)	1.497(3)

C(4)-O(3)	1.454(2)	O(1)-C(2)-C(3)	111.51(14)
C(4)-C(5)	1.468(3)	C(1)-C(2)-C(3)	112.75(15)
C(4)-C(12)	1.505(3)	O(1)-C(2)-H(2)	106.0
C(5)-O(3)	1.454(2)	C(1)-C(2)-H(2)	106.0
C(5)-C(6)	1.483(3)	C(3)-C(2)-H(2)	106.0
C(5)-H(5)	1.0000	O(2)-C(3)-C(11)	59.45(12)
C(6)-O(4)	1.455(2)	O(2)-C(3)-C(4)	115.13(15)
C(6)-H(6)	1.0000	C(11)-C(3)-C(4)	119.57(16)
C(7)-C(10)	1.533(3)	O(2)-C(3)-C(2)	113.98(14)
C(7)-C(9)	1.535(3)	C(11)-C(3)-C(2)	119.98(16)
C(7)-C(8)	1.538(3)	C(4)-C(3)-C(2)	115.79(15)
C(8)-H(8A)	0.9800	O(3)-C(4)-C(5)	59.66(11)
C(8)-H(8B)	0.9800	O(3)-C(4)-C(3)	113.55(15)
C(8)-H(8C)	0.9800	C(5)-C(4)-C(3)	116.00(15)
C(9)-H(9A)	0.9800	O(3)-C(4)-C(12)	113.56(15)
C(9)-H(9B)	0.9800	C(5)-C(4)-C(12)	119.95(16)
C(9)-H(9C)	0.9800	C(3)-C(4)-C(12)	119.27(16)
C(10)-H(10A)	0.9800	O(3)-C(5)-C(4)	59.68(11)
C(10)-H(10B)	0.9800	O(3)-C(5)-C(6)	114.28(15)
C(10)-H(10C)	0.9800	C(4)-C(5)-C(6)	120.05(16)
C(11)-O(2)	1.442(3)	O(3)-C(5)-H(5)	116.8
C(11)-H(11A)	0.9900	C(4)-C(5)-H(5)	116.8
C(11)-H(11B)	0.9900	C(6)-C(5)-H(5)	116.8
C(12)-H(12A)	0.9800	O(4)-C(6)-C(1)	59.71(11)
C(12)-H(12B)	0.9800	O(4)-C(6)-C(5)	116.81(14)
C(12)-H(12C)	0.9800	C(1)-C(6)-C(5)	120.93(16)
O(1)-H(1)	0.8400	O(4)-C(6)-H(6)	115.9
		C(1)-C(6)-H(6)	115.9
O(4)-C(1)-C(6)	59.47(11)	C(5)-C(6)-H(6)	115.9
O(4)-C(1)-C(2)	113.24(14)	C(10)-C(7)-C(9)	108.50(16)
C(6)-C(1)-C(2)	116.52(15)	C(10)-C(7)-C(8)	110.27(17)
O(4)-C(1)-C(7)	114.73(14)	C(9)-C(7)-C(8)	107.13(16)
C(6)-C(1)-C(7)	120.09(15)	C(10)-C(7)-C(1)	109.27(15)
C(2)-C(1)-C(7)	118.44(15)	C(9)-C(7)-C(1)	111.33(15)
O(1)-C(2)-C(1)	113.92(14)	C(8)-C(7)-C(1)	110.31(15)

C(7)-C(8)-H(8A)	109.5
C(7)-C(8)-H(8B)	109.5
H(8A)-C(8)-H(8B)	109.5
C(7)-C(8)-H(8C)	109.5
H(8A)-C(8)-H(8C)	109.5
H(8B)-C(8)-H(8C)	109.5
C(7)-C(9)-H(9A)	109.5
C(7)-C(9)-H(9B)	109.5
H(9A)-C(9)-H(9B)	109.5
C(7)-C(9)-H(9C)	109.5
H(9A)-C(9)-H(9C)	109.5
H(9B)-C(9)-H(9C)	109.5
C(7)-C(10)-H(10A)	109.5
C(7)-C(10)-H(10B)	109.5
H(10A)-C(10)-H(10B)	109.5
C(7)-C(10)-H(10C)	109.5
H(10A)-C(10)-H(10C)	109.5
H(10B)-C(10)-H(10C)	109.5
O(2)-C(11)-C(3)	59.53(12)
O(2)-C(11)-H(11A)	117.8
C(3)-C(11)-H(11A)	117.8
O(2)-C(11)-H(11B)	117.8
C(3)-C(11)-H(11B)	117.8
H(11A)-C(11)-H(11B)	115.0
C(4)-C(12)-H(12A)	109.5
C(4)-C(12)-H(12B)	109.5
H(12A)-C(12)-H(12B)	109.5
C(4)-C(12)-H(12C)	109.5
H(12A)-C(12)-H(12C)	109.5
H(12B)-C(12)-H(12C)	109.5
C(2)-O(1)-H(1)	109.5
C(11)-O(2)-C(3)	61.02(12)
C(5)-O(3)-C(4)	60.66(11)
C(6)-O(4)-C(1)	60.82(11)

Symmetry transformations used to generate equivalent atoms:

Table 50. Anisotropic displacement parameters ($\text{\AA}^2 \times 10^3$) for GB625s. The anisotropic displacement factor exponent takes the form: $-2\pi^2 [h^2 a^{*2} U^{11} + \dots + 2 h k a^* b^* U^{12}]$

	U11	U22	U33	U23	U13	U12
C(1)	31(1)	15(1)	27(1)	2(1)	6(1)	1(1)
C(2)	34(1)	21(1)	26(1)	-1(1)	8(1)	0(1)
C(3)	32(1)	23(1)	28(1)	-1(1)	12(1)	-2(1)
C(4)	31(1)	23(1)	32(1)	-2(1)	9(1)	-1(1)
C(5)	35(1)	25(1)	27(1)	-2(1)	9(1)	-2(1)
C(6)	32(1)	22(1)	29(1)	1(1)	10(1)	1(1)
C(7)	30(1)	24(1)	33(1)	3(1)	6(1)	2(1)
C(8)	35(1)	33(1)	45(1)	-4(1)	1(1)	-1(1)
C(9)	31(1)	40(1)	45(1)	2(1)	11(1)	2(1)
C(10)	36(1)	35(1)	50(1)	14(1)	7(1)	7(1)
C(11)	37(1)	33(1)	39(1)	-5(1)	11(1)	6(1)
C(12)	32(1)	44(1)	40(1)	-4(1)	6(1)	-3(1)
O(1)	47(1)	37(1)	27(1)	-1(1)	10(1)	-3(1)
O(2)	37(1)	43(1)	38(1)	-4(1)	19(1)	-1(1)
O(3)	38(1)	21(1)	38(1)	-4(1)	14(1)	-4(1)
O(4)	33(1)	19(1)	29(1)	4(1)	6(1)	0(1)

Table 51. Hydrogen coordinates ($\times 10^4$) and isotropic displacement parameters ($\text{\AA}^2 \times 10^3$) for GB625s.

	x	y	z	U(eq)
H(2)	275	681	4995	32
H(5)	-1027	920	-1475	34

H(6)	1511	944	308	32
H(8A)	3188	1825	7064	59
H(8B)	3220	2274	4992	59
H(8C)	4565	1805	6209	59
H(9A)	4807	1048	3555	57
H(9B)	3634	1494	1852	57
H(9C)	3514	627	1997	57
H(10A)	2676	60	4905	62
H(10B)	2661	543	6924	62
H(10C)	4123	375	6385	62
H(11A)	-1227	2442	4760	44
H(11B)	-2554	2319	2589	44
H(12A)	-3435	865	-1280	58
H(12B)	-3549	1608	-67	58
H(12C)	-3841	846	919	58
H(1)	846	2024	6354	55

Table 52. Torsion angles [$^{\circ}$] for GB625s.

O(4)-C(1)-C(2)-O(1)	-92.32(18)
C(6)-C(1)-C(2)-O(1)	-158.52(15)
C(7)-C(1)-C(2)-O(1)	46.3(2)
O(4)-C(1)-C(2)-C(3)	36.1(2)
C(6)-C(1)-C(2)-C(3)	-30.1(2)
C(7)-C(1)-C(2)-C(3)	174.68(15)
O(1)-C(2)-C(3)-O(2)	-43.8(2)
C(1)-C(2)-C(3)-O(2)	-173.39(14)
O(1)-C(2)-C(3)-C(11)	23.6(2)
C(1)-C(2)-C(3)-C(11)	-106.07(19)
O(1)-C(2)-C(3)-C(4)	179.25(14)
C(1)-C(2)-C(3)-C(4)	49.6(2)
O(2)-C(3)-C(4)-O(3)	-105.08(17)
C(11)-C(3)-C(4)-O(3)	-172.79(15)
C(2)-C(3)-C(4)-O(3)	31.4(2)

O(2)-C(3)-C(4)-C(5)	-171.47(15)
C(11)-C(3)-C(4)-C(5)	120.82(19)
C(2)-C(3)-C(4)-C(5)	-35.0(2)
O(2)-C(3)-C(4)-C(12)	33.0(2)
C(11)-C(3)-C(4)-C(12)	-34.7(2)
C(2)-C(3)-C(4)-C(12)	169.49(16)
C(3)-C(4)-C(5)-O(3)	103.27(17)
C(12)-C(4)-C(5)-O(3)	-101.38(19)
O(3)-C(4)-C(5)-C(6)	-102.25(18)
C(3)-C(4)-C(5)-C(6)	1.0(2)
C(12)-C(4)-C(5)-C(6)	156.38(18)
C(2)-C(1)-C(6)-O(4)	102.58(16)
C(7)-C(1)-C(6)-O(4)	-102.68(17)
O(4)-C(1)-C(6)-C(5)	-105.01(17)
C(2)-C(1)-C(6)-C(5)	-2.4(2)
C(7)-C(1)-C(6)-C(5)	152.30(16)
O(3)-C(5)-C(6)-O(4)	-118.60(16)
C(4)-C(5)-C(6)-O(4)	-50.9(2)
O(3)-C(5)-C(6)-C(1)	-49.5(2)
C(4)-C(5)-C(6)-C(1)	18.3(3)
O(4)-C(1)-C(7)-C(10)	-174.83(16)
C(6)-C(1)-C(7)-C(10)	-107.13(19)
C(2)-C(1)-C(7)-C(10)	47.1(2)
O(4)-C(1)-C(7)-C(9)	-55.0(2)
C(6)-C(1)-C(7)-C(9)	12.7(2)
C(2)-C(1)-C(7)-C(9)	166.95(15)
O(4)-C(1)-C(7)-C(8)	63.8(2)
C(6)-C(1)-C(7)-C(8)	131.49(17)
C(2)-C(1)-C(7)-C(8)	-74.3(2)
C(4)-C(3)-C(11)-O(2)	103.42(17)
C(2)-C(3)-C(11)-O(2)	-101.79(18)
C(4)-C(3)-O(2)-C(11)	-110.86(18)
C(2)-C(3)-O(2)-C(11)	111.87(18)
C(6)-C(5)-O(3)-C(4)	111.87(17)
C(3)-C(4)-O(3)-C(5)	-107.39(17)

C(12)-C(4)-O(3)-C(5)	112.08(18)
C(5)-C(6)-O(4)-C(1)	111.82(18)
C(2)-C(1)-O(4)-C(6)	-108.11(16)
C(7)-C(1)-O(4)-C(6)	111.67(17)

Symmetry transformations used to generate equivalent atoms:

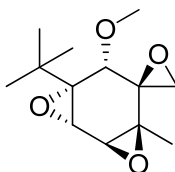
Table 53. Hydrogen bonds for GB625s [\AA and $^\circ$].

D-H...A	d(D-H)	d(H...A)	d(D...A)	$\angle(\text{DHA})$
O(1)-H(1)...O(4)#1	0.84	2.04	2.8403(19)	159.7

Symmetry transformations used to generate equivalent atoms:

#1 $x, -y+1/2, z+1/2$

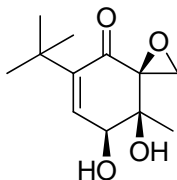
(\pm)-7'-(*tert*-Butyl)-6'-methoxy-4'-methyl-3',8'-dioxaspiro[oxirane-2,5'-tricyclo[5.1.0.0^{2,4}]octane] (84)



To a dry round bottomed flask under argon was added compound **83** (0.10 g, 0.44 mmol, 1.0 eq) and dry THF (2 mL). The flask was cooled to 0°C and then 60% NaH dispersion in mineral oil (0.021 g, 0.53 mmol, 1.2 eq) was added. After stirring for 30 minutes at 0°C MeI (0.033 mL, 0.53 mmol, 1.2 eq) was added. The reaction was quenched with water, and the reaction mixture was transferred to a separatory funnel. The product was extracted with ethyl acetate. The organic layer was dried over MgSO_4 , filtered, and concentrated. The desired product (0.090 g) was isolated in 85% yield as a white solid. (Rf: 0.67; 3:1 hexanes/ethyl acetate). mp: $78\text{-}79^\circ\text{C}$. $^1\text{H NMR}$ (CDCl_3 , 300 MHz): δ :

1.01 (s, 9H), 1.19 (s, 3H), 2.71 (d, 1H, $J = 4.8$ Hz), 3.09 (d, 1H, $J = 4.8$ Hz), 3.35 (d, 1H, $J = 3.0$ Hz), 3.44 (s, 3H), 3.51 (d, 1H, $J = 3.0$ Hz), 4.06 (s, 1H). ^{13}C NMR (CDCl_3 , 100 MHz): δ : 15.3, 27.2, 34.0, 46.3, 55.9, 58.4, 60.0, 60.4, 61.0, 67.8, 76.7. HRMS (APCI): expected for $\text{C}_{13}\text{H}_{21}\text{O}_4$ ($\text{M}+\text{H}$) $^+$ 241.14344. Found 241.14360. IR (neat): ν_{max} 2982, 2958, 2913, 2872, 1115, 1090 cm^{-1} . Elemental Analysis for $\text{C}_{13}\text{H}_{20}\text{O}_4$: Found: C, 64.96; H, 8.51. Calculated: C, 64.98; H, 8.39.

(±)-5-*tert*-Butyl-7,8-dihydroxy-8-methyl-1-oxaspiro[2.5]oct-5-en-4-one (85)



To a round bottomed flask was added **56d** (5.0 g, 26 mmol, 1.0 eq) followed by acetone (50 mL) and water (50 mL). The flask was cooled to 0°C and then OsO_4 (0.33 g, 1.3 mmol, 0.05 eq) was added. Next a 50% 4-methylmorpholine *N*-oxide solution (6.8 mL, 28 mmol, 1.1 eq) was added dropwise over a period of one hour. The reaction was allowed to stir for 16 hours slowly warming to room temperature. The reaction mixture was transferred to a separatory funnel and diluted with water (100 mL). The product was extracted with ethyl acetate. The organic layer was washed with brine, dried over MgSO_4 , filtered, and concentrated. The resulting dark residue was purified on silica eluting with 2:1 hexanes/ethyl acetate to give 3.1 g of the desired product in 53% yield as a white solid. A portion of compound **85** was recrystallized from ethyl acetate for x-ray crystallography. (Rf: 0.06; 3:1 hexanes/ethyl acetate). mp: 148-150 °C. ^1H NMR (CDCl_3 , 300 MHz): δ : 1.21 (s, 9H), 1.30 (s, 3H), 2.56 (s, 1H), 2.59 (d, 1H, $J = 10.2$ Hz),

2.98 (s, 2H), 4.31 (dd, 1H, $J = 10.2$ Hz, 3.3 Hz), 6.75 (d, 1H, $J = 3.3$ Hz). ^{13}C NMR (CDCl_3 , 100 MHz): δ : 20.3, 29.1, 34.8, 49.9, 63.0, 72.3, 73.6, 142.7, 147.3, 192.3. HRMS (APCI): expected for $\text{C}_{12}\text{H}_{19}\text{O}_4$ ($\text{M}+\text{H}$) $^+$ 227.12779. Found 227.12782. IR (neat): ν_{max} 3407, 3354, 2995, 2958, 2913, 2859, 1687 cm^{-1} . Elemental Analysis for $\text{C}_{12}\text{H}_{18}\text{O}_4$: Found: C, 63.83; H, 8.08. Calculated: C, 63.70; H, 8.02. The relative stereochemistry was established by X-ray crystallographic analysis.

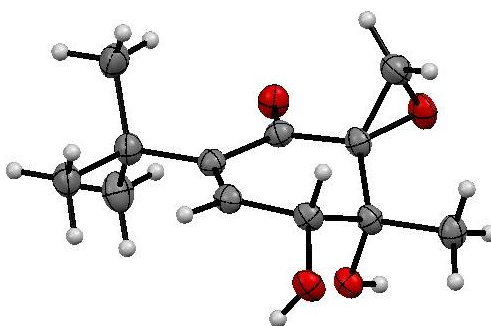


Table 54. Crystal data and structure refinement for gb630bs.

Identification code	gb630bs	
Empirical formula	$\text{C}_{12}\text{H}_{18}\text{O}_4$	
Formula weight	226.26	
Temperature	173(2) K	
Wavelength	1.54178 Å	
Crystal system	Triclinic	
Space group	P-1	
Unit cell dimensions	$a = 7.8826(4)$ Å	$\alpha = 88.124(3)^\circ$.
	$b = 8.1695(4)$ Å	$\beta = 72.201(4)^\circ$.
	$c = 9.6900(6)$ Å	$\gamma = 82.054(3)^\circ$.
Volume	$588.40(6)$ Å 3	
Z	2	
Density (calculated)	1.277 Mg/m^3	
Absorption coefficient	0.784 mm^{-1}	
F(000)	244	
Crystal size	0.49 x 0.12 x 0.06 mm^3	
Theta range for data collection	4.79 to 65.61°.	

Index ranges	-9<=h<=8, -9<=k<=9, -9<=l<=10
Reflections collected	3304
Independent reflections	1704 [R(int) = 0.0133]
Completeness to theta = 65.61°	83.7 %
Absorption correction	Semi-empirical from equivalents
Max. and min. transmission	0.9545 and 0.6999
Refinement method	Full-matrix least-squares on F ²
Data / restraints / parameters	1704 / 0 / 151
Goodness-of-fit on F ²	1.048
Final R indices [I>2sigma(I)]	R1 = 0.0383, wR2 = 0.1067
R indices (all data)	R1 = 0.0403, wR2 = 0.1090
Largest diff. peak and hole	0.211 and -0.240 e.Å ⁻³

Table 55. Atomic coordinates ($\times 10^4$) and equivalent isotropic displacement parameters ($\text{\AA}^2 \times 10^3$) for gb630bs. $U(\text{eq})$ is defined as one third of the trace of the orthogonalized U_{ij} tensor.

	x	y	z	$U(\text{eq})$
C(1)	5022(2)	3699(2)	7060(2)	24(1)
C(2)	6814(2)	3592(2)	5904(2)	24(1)
C(3)	8234(2)	4281(2)	6287(2)	33(1)
C(4)	7212(2)	2134(2)	4868(2)	24(1)
C(5)	8915(2)	2142(2)	3602(2)	29(1)
C(6)	7277(2)	624(2)	5850(2)	24(1)
C(7)	5617(2)	723(2)	7145(2)	25(1)
C(8)	4513(2)	2100(2)	7723(2)	24(1)
C(9)	2803(2)	2109(2)	9013(2)	29(1)
C(10)	1158(2)	2819(2)	8533(2)	38(1)
C(11)	2921(3)	3160(2)	10261(2)	37(1)
C(12)	2539(2)	358(2)	9577(2)	34(1)
O(1)	4127(2)	5045(1)	7447(1)	30(1)
O(2)	7335(2)	5141(1)	5323(1)	33(1)
O(3)	5707(1)	2093(1)	4340(1)	26(1)
O(4)	7601(1)	-889(1)	5075(1)	29(1)

Table 56. Bond lengths [\AA] and angles [$^\circ$] for gb630bs.

C(1)-O(1)	1.2238(18)
C(1)-C(8)	1.487(2)
C(1)-C(2)	1.504(2)
C(2)-O(2)	1.4294(19)
C(2)-C(3)	1.466(2)
C(2)-C(4)	1.519(2)
C(3)-O(2)	1.446(2)
C(3)-H(3A)	0.9900
C(3)-H(3B)	0.9900

C(4)-O(3)	1.4329(18)
C(4)-C(5)	1.517(2)
C(4)-C(6)	1.538(2)
C(5)-H(5A)	0.9800
C(5)-H(5B)	0.9800
C(5)-H(5C)	0.9800
C(6)-O(4)	1.4192(18)
C(6)-C(7)	1.505(2)
C(6)-H(6)	1.0000
C(7)-C(8)	1.346(2)
C(7)-H(7)	0.9500
C(8)-C(9)	1.532(2)
C(9)-C(12)	1.533(2)
C(9)-C(11)	1.538(3)
C(9)-C(10)	1.542(2)
C(10)-H(10A)	0.9800
C(10)-H(10B)	0.9800
C(10)-H(10C)	0.9800
C(11)-H(11A)	0.9800
C(11)-H(11B)	0.9800
C(11)-H(11C)	0.9800
C(12)-H(12A)	0.9800
C(12)-H(12B)	0.9800
C(12)-H(12C)	0.9800
O(3)-H(3)	0.8400
O(4)-H(4)	0.8400
O(1)-C(1)-C(8)	124.21(15)
O(1)-C(1)-C(2)	120.24(14)
C(8)-C(1)-C(2)	115.45(13)
O(2)-C(2)-C(3)	59.91(11)
O(2)-C(2)-C(1)	115.13(12)
C(3)-C(2)-C(1)	116.02(15)
O(2)-C(2)-C(4)	118.18(14)
C(3)-C(2)-C(4)	122.42(14)
C(1)-C(2)-C(4)	114.33(13)

O(2)-C(3)-C(2)	58.79(10)
O(2)-C(3)-H(3A)	117.9
C(2)-C(3)-H(3A)	117.9
O(2)-C(3)-H(3B)	117.9
C(2)-C(3)-H(3B)	117.9
H(3A)-C(3)-H(3B)	115.0
O(3)-C(4)-C(5)	109.80(13)
O(3)-C(4)-C(2)	109.10(12)
C(5)-C(4)-C(2)	114.14(13)
O(3)-C(4)-C(6)	106.80(12)
C(5)-C(4)-C(6)	113.08(12)
C(2)-C(4)-C(6)	103.51(13)
C(4)-C(5)-H(5A)	109.5
C(4)-C(5)-H(5B)	109.5
H(5A)-C(5)-H(5B)	109.5
C(4)-C(5)-H(5C)	109.5
H(5A)-C(5)-H(5C)	109.5
H(5B)-C(5)-H(5C)	109.5
O(4)-C(6)-C(7)	112.10(12)
O(4)-C(6)-C(4)	112.23(13)
C(7)-C(6)-C(4)	111.35(12)
O(4)-C(6)-H(6)	106.9
C(7)-C(6)-H(6)	106.9
C(4)-C(6)-H(6)	106.9
C(8)-C(7)-C(6)	126.63(14)
C(8)-C(7)-H(7)	116.7
C(6)-C(7)-H(7)	116.7
C(7)-C(8)-C(1)	116.92(15)
C(7)-C(8)-C(9)	124.02(14)
C(1)-C(8)-C(9)	119.05(13)
C(8)-C(9)-C(12)	111.40(13)
C(8)-C(9)-C(11)	110.02(14)
C(12)-C(9)-C(11)	108.08(15)
C(8)-C(9)-C(10)	109.26(14)
C(12)-C(9)-C(10)	107.98(14)

C(11)-C(9)-C(10)	110.07(14)
C(9)-C(10)-H(10A)	109.5
C(9)-C(10)-H(10B)	109.5
H(10A)-C(10)-H(10B)	109.5
C(9)-C(10)-H(10C)	109.5
H(10A)-C(10)-H(10C)	109.5
H(10B)-C(10)-H(10C)	109.5
C(9)-C(11)-H(11A)	109.5
C(9)-C(11)-H(11B)	109.5
H(11A)-C(11)-H(11B)	109.5
C(9)-C(11)-H(11C)	109.5
H(11A)-C(11)-H(11C)	109.5
H(11B)-C(11)-H(11C)	109.5
C(9)-C(12)-H(12A)	109.5
C(9)-C(12)-H(12B)	109.5
H(12A)-C(12)-H(12B)	109.5
C(9)-C(12)-H(12C)	109.5
H(12A)-C(12)-H(12C)	109.5
H(12B)-C(12)-H(12C)	109.5
C(2)-O(2)-C(3)	61.30(10)
C(4)-O(3)-H(3)	109.5
C(6)-O(4)-H(4)	109.5

Symmetry transformations used to generate equivalent atoms:

Table 57. Anisotropic displacement parameters ($\text{\AA}^2 \times 10^3$) for gb630bs. The anisotropic displacement factor exponent takes the form: $-2\pi^2 [h^2 a^{*2} U^{11} + \dots + 2 h k a^* b^* U^{12}]$

	U11	U22	U33	U23	U13	U12
C(1)	25(1)	23(1)	24(1)	-1(1)	-8(1)	-2(1)
C(2)	25(1)	18(1)	28(1)	4(1)	-7(1)	-4(1)
C(3)	30(1)	33(1)	38(1)	-3(1)	-9(1)	-8(1)
C(4)	20(1)	22(1)	28(1)	0(1)	-5(1)	-2(1)
C(5)	26(1)	26(1)	31(1)	0(1)	-3(1)	-2(1)

C(6)	24(1)	19(1)	29(1)	-1(1)	-8(1)	-1(1)
C(7)	29(1)	21(1)	26(1)	4(1)	-11(1)	-4(1)
C(8)	25(1)	24(1)	24(1)	1(1)	-8(1)	-4(1)
C(9)	27(1)	29(1)	29(1)	2(1)	-4(1)	-5(1)
C(10)	25(1)	40(1)	45(1)	4(1)	-5(1)	-2(1)
C(11)	40(1)	37(1)	28(1)	-2(1)	0(1)	-8(1)
C(12)	33(1)	34(1)	32(1)	4(1)	-4(1)	-10(1)
O(1)	32(1)	21(1)	32(1)	0(1)	-4(1)	2(1)
O(2)	35(1)	21(1)	39(1)	4(1)	-5(1)	-7(1)
O(3)	26(1)	22(1)	32(1)	4(1)	-11(1)	-4(1)
O(4)	26(1)	20(1)	39(1)	-4(1)	-7(1)	-1(1)

Table 58. Hydrogen coordinates ($\times 10^4$) and isotropic displacement parameters ($\text{\AA}^2 \times 10^3$) for gb630bs.

	x	y	z	U(eq)
H(3A)	7948	4735	7279	40
H(3B)	9489	3753	5861	40
H(5A)	9107	1148	3004	44
H(5B)	9942	2157	3968	44
H(5C)	8796	3126	3015	44
H(6)	8319	657	6227	29
H(7)	5320	-291	7601	30
H(10A)	1276	3956	8200	58
H(10B)	61	2813	9353	58
H(10C)	1093	2140	7740	58
H(11A)	3994	2724	10535	56
H(11B)	1847	3118	11097	56
H(11C)	2995	4307	9947	56
H(12A)	2456	-333	8799	50
H(12B)	1430	402	10392	50

H(12C)	3563	-115	9902	50
H(3)	5594	2931	3834	39
H(4)	6616	-1180	5084	44

Table 59. Torsion angles [°] for gb630bs.

O(1)-C(1)-C(2)-O(2)	-0.5(2)
C(8)-C(1)-C(2)-O(2)	-177.03(13)
O(1)-C(1)-C(2)-C(3)	66.8(2)
C(8)-C(1)-C(2)-C(3)	-109.81(16)
O(1)-C(1)-C(2)-C(4)	-142.14(15)
C(8)-C(1)-C(2)-C(4)	41.28(19)
C(1)-C(2)-C(3)-O(2)	-105.27(14)
C(4)-C(2)-C(3)-O(2)	106.17(17)
O(2)-C(2)-C(4)-O(3)	-90.53(15)
C(3)-C(2)-C(4)-O(3)	-161.05(15)
C(1)-C(2)-C(4)-O(3)	49.92(17)
O(2)-C(2)-C(4)-C(5)	32.71(19)
C(3)-C(2)-C(4)-C(5)	-37.8(2)
C(1)-C(2)-C(4)-C(5)	173.16(13)
O(2)-C(2)-C(4)-C(6)	156.03(13)
C(3)-C(2)-C(4)-C(6)	85.51(18)
C(1)-C(2)-C(4)-C(6)	-63.52(15)
O(3)-C(4)-C(6)-O(4)	63.63(16)
C(5)-C(4)-C(6)-O(4)	-57.25(17)
C(2)-C(4)-C(6)-O(4)	178.72(11)
O(3)-C(4)-C(6)-C(7)	-62.97(16)
C(5)-C(4)-C(6)-C(7)	176.14(13)
C(2)-C(4)-C(6)-C(7)	52.12(15)
O(4)-C(6)-C(7)-C(8)	-149.54(15)
C(4)-C(6)-C(7)-C(8)	-22.9(2)
C(6)-C(7)-C(8)-C(1)	-3.0(2)
C(6)-C(7)-C(8)-C(9)	177.73(14)
O(1)-C(1)-C(8)-C(7)	178.14(15)

C(2)-C(1)-C(8)-C(7)	-5.4(2)
O(1)-C(1)-C(8)-C(9)	-2.6(2)
C(2)-C(1)-C(8)-C(9)	173.85(13)
C(7)-C(8)-C(9)-C(12)	1.2(2)
C(1)-C(8)-C(9)-C(12)	-178.03(14)
C(7)-C(8)-C(9)-C(11)	121.04(17)
C(1)-C(8)-C(9)-C(11)	-58.19(19)
C(7)-C(8)-C(9)-C(10)	-118.02(17)
C(1)-C(8)-C(9)-C(10)	62.75(18)
C(1)-C(2)-O(2)-C(3)	106.74(16)
C(4)-C(2)-O(2)-C(3)	-113.11(16)

Symmetry transformations used to generate equivalent atoms:

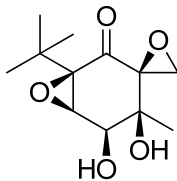
Table 60. Hydrogen bonds for gb630bs [\AA and $^\circ$].

D-H...A	d(D-H)	d(H...A)	d(D...A)	$\angle(\text{DHA})$
O(3)-H(3)...O(1)#1	0.84	2.03	2.8575(15)	168.1
O(3)-H(3)...O(2)#1	0.84	2.53	3.0060(15)	116.9
O(4)-H(4)...O(3)#2	0.84	1.99	2.8026(15)	163.7

Symmetry transformations used to generate equivalent atoms:

#1 -x+1,-y+1,-z+1 #2 -x+1,-y,-z+1

(±)-1-*tert*-Butyl-4,5-dihydroxy-4-methyl-7-oxaspiro[bicyclo[4.1.0]heptane-3,2'-oxiran]-2-one (86)



Following the general procedure for the synthesis of triepoxides compound **85** (0.10 g, 0.44 mmol) was converted into the 0.091 g of the desired product **86** in 85 % yield as a white solid. A portion of compound **86** was recrystallized from ethyl acetate for x-ray crystallography. (Rf: 0.61; ethyl acetate). mp: 113-115 °C. ^1H NMR (CDCl_3 , 300 MHz): δ : 1.11 (s, 9H), 1.20 (d, 3H, $J = 0.9$ Hz), 2.74 (d, 1H, $J = 11.1$ Hz), 2.91 (d, 1H, $J = 6.9$ Hz), 2.96 (d, 1H, $J = 6.0$ Hz), 3.33 (d, 1H, $J = 1.2$ Hz), 3.91 (d, 1H, $J = 3.3$ Hz), 3.96 (dd, 1H, $J = 10.8$ Hz, 3.3 Hz). ^{13}C NMR (CDCl_3 , 100 MHz): δ : 20.7, 25.9, 32.4, 48.0, 61.1, 62.8, 68.5, 70.6, 71.2, 198.2. HRMS (APCI): expected for $\text{C}_{12}\text{H}_{19}\text{O}_5$ ($\text{M}+\text{H}$) $^+$ 243.12270. Found 243.12289. IR (neat): ν_{max} 3469, 2958, 2917, 2876, 1732, 915 cm^{-1} . Elemental Analysis for $\text{C}_{12}\text{H}_{18}\text{O}_5$: Found: C, 59.28; H, 7.44. Calculated: C, 59.49; H, 7.49. The relative stereochemistry was established by X-ray crystallographic analysis.

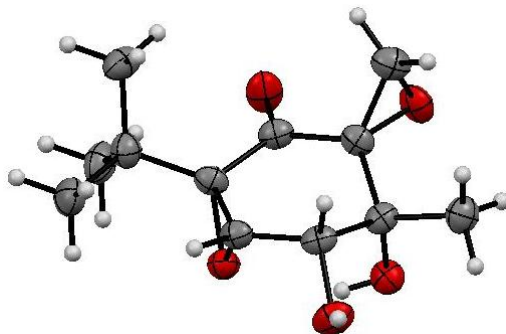


Table 61. Crystal data and structure refinement for GB760.

Identification code	GB760	
Empirical formula	C ₁₂ H ₁₈ O ₅	
Formula weight	242.26	
Temperature	173(2) K	
Wavelength	1.54178 Å	
Crystal system	Orthorhombic	
Space group	Pna2(1)	
Unit cell dimensions	a = 18.301(3) Å	α = 90°.
	b = 7.0310(12) Å	β = 90°.
	c = 9.3902(18) Å	γ = 90°.
Volume	1208.3(4) Å ³	
Z	4	
Density (calculated)	1.332 Mg/m ³	
Absorption coefficient	0.864 mm ⁻¹	
F(000)	520	
Crystal size	0.37 x 0.29 x 0.14 mm ³	
Theta range for data collection	4.83 to 66.52°.	
Index ranges	-19 ≤ h ≤ 21, -8 ≤ k ≤ 8, -11 ≤ l ≤ 10	
Reflections collected	8275	
Independent reflections	1862 [R(int) = 0.0514]	
Completeness to theta = 66.52°	95.3 %	
Absorption correction	Semi-empirical from equivalents	
Max. and min. transmission	0.8886 and 0.7404	
Refinement method	Full-matrix least-squares on F ²	
Data / restraints / parameters	1862 / 1 / 154	
Goodness-of-fit on F ²	1.127	
Final R indices [I > 2σ(I)]	R1 = 0.0398, wR2 = 0.1164	
R indices (all data)	R1 = 0.0432, wR2 = 0.1221	
Absolute structure parameter	0.0(3)	
Largest diff. peak and hole	0.216 and -0.299 e.Å ⁻³	

Table 62. Atomic coordinates ($\times 10^4$) and equivalent isotropic displacement parameters ($\text{\AA}^2 \times 10^3$) for GB760. $U(\text{eq})$ is defined as one third of the trace of the orthogonalized U_{ij} tensor.

	x	y	z	$U(\text{eq})$
C(1)	-3911(2)	-3761(4)	-7981(3)	29(1)
C(2)	-4668(2)	-3288(4)	-8520(3)	29(1)
C(3)	-4757(2)	-1586(4)	-9519(3)	29(1)
C(4)	-4414(2)	154(3)	-8794(3)	28(1)
C(5)	-3661(2)	-217(4)	-8224(3)	28(1)
C(6)	-3394(2)	-2108(3)	-7742(3)	29(1)
C(7)	-2777(2)	-2358(4)	-6642(3)	33(1)
C(8)	-2382(2)	-468(5)	-6381(4)	44(1)
C(9)	-3092(2)	-3064(4)	-5234(4)	40(1)
C(10)	-2222(2)	-3791(5)	-7239(4)	44(1)
C(11)	-5255(2)	-4000(4)	-7587(4)	38(1)
C(12)	-5547(2)	-1197(4)	-9899(4)	38(1)
O(1)	-3746(1)	-5381(3)	-7721(3)	43(1)
O(2)	-5080(1)	-4941(3)	-8904(3)	38(1)
O(3)	-4400(1)	-2029(2)	-10844(2)	34(1)
O(4)	-4380(1)	1658(3)	-9804(2)	39(1)
O(5)	-3179(1)	-1335(2)	-9126(2)	32(1)

Table 63. Bond lengths [\AA] and angles [$^\circ$] for GB760.

C(1)-O(1)	1.204(3)
C(1)-C(2)	1.512(4)
C(1)-C(6)	1.516(4)
C(2)-O(2)	1.432(3)
C(2)-C(11)	1.474(4)
C(2)-C(3)	1.529(4)
C(3)-O(3)	1.439(4)
C(3)-C(12)	1.515(4)

C(3)-C(4)	1.534(4)
C(4)-O(4)	1.422(3)
C(4)-C(5)	1.502(4)
C(4)-H(4A)	1.0000
C(5)-O(5)	1.454(3)
C(5)-C(6)	1.487(3)
C(5)-H(5A)	1.0000
C(6)-O(5)	1.463(3)
C(6)-C(7)	1.540(4)
C(7)-C(9)	1.525(5)
C(7)-C(8)	1.533(4)
C(7)-C(10)	1.537(4)
C(8)-H(8A)	0.9800
C(8)-H(8B)	0.9800
C(8)-H(8C)	0.9800
C(9)-H(9A)	0.9800
C(9)-H(9B)	0.9800
C(9)-H(9C)	0.9800
C(10)-H(10A)	0.9800
C(10)-H(10B)	0.9800
C(10)-H(10C)	0.9800
C(11)-O(2)	1.439(4)
C(11)-H(11A)	0.9900
C(11)-H(11B)	0.9900
C(12)-H(12A)	0.9800
C(12)-H(12B)	0.9800
C(12)-H(12C)	0.9800
O(3)-H(3A)	0.8400
O(4)-H(4B)	0.8400
O(1)-C(1)-C(2)	120.4(2)
O(1)-C(1)-C(6)	122.6(3)
C(2)-C(1)-C(6)	117.0(2)
O(2)-C(2)-C(11)	59.34(19)
O(2)-C(2)-C(1)	112.9(2)
C(11)-C(2)-C(1)	113.2(3)

O(2)-C(2)-C(3)	115.2(2)
C(11)-C(2)-C(3)	123.6(2)
C(1)-C(2)-C(3)	118.4(2)
O(3)-C(3)-C(12)	105.5(2)
O(3)-C(3)-C(2)	108.2(2)
C(12)-C(3)-C(2)	112.8(2)
O(3)-C(3)-C(4)	111.8(2)
C(12)-C(3)-C(4)	110.5(2)
C(2)-C(3)-C(4)	108.0(2)
O(4)-C(4)-C(5)	109.0(2)
O(4)-C(4)-C(3)	108.4(2)
C(5)-C(4)-C(3)	113.2(2)
O(4)-C(4)-H(4A)	108.7
C(5)-C(4)-H(4A)	108.7
C(3)-C(4)-H(4A)	108.7
O(5)-C(5)-C(6)	59.63(17)
O(5)-C(5)-C(4)	116.3(2)
C(6)-C(5)-C(4)	124.4(2)
O(5)-C(5)-H(5A)	114.9
C(6)-C(5)-H(5A)	114.9
C(4)-C(5)-H(5A)	114.9
O(5)-C(6)-C(5)	59.03(17)
O(5)-C(6)-C(1)	108.8(2)
C(5)-C(6)-C(1)	115.8(2)
O(5)-C(6)-C(7)	116.2(2)
C(5)-C(6)-C(7)	123.2(2)
C(1)-C(6)-C(7)	118.0(2)
C(9)-C(7)-C(8)	108.8(3)
C(9)-C(7)-C(10)	110.7(2)
C(8)-C(7)-C(10)	108.3(3)
C(9)-C(7)-C(6)	110.0(2)
C(8)-C(7)-C(6)	110.7(2)
C(10)-C(7)-C(6)	108.3(2)
C(7)-C(8)-H(8A)	109.5
C(7)-C(8)-H(8B)	109.5

H(8A)-C(8)-H(8B)	109.5
C(7)-C(8)-H(8C)	109.5
H(8A)-C(8)-H(8C)	109.5
H(8B)-C(8)-H(8C)	109.5
C(7)-C(9)-H(9A)	109.5
C(7)-C(9)-H(9B)	109.5
H(9A)-C(9)-H(9B)	109.5
C(7)-C(9)-H(9C)	109.5
H(9A)-C(9)-H(9C)	109.5
H(9B)-C(9)-H(9C)	109.5
C(7)-C(10)-H(10A)	109.5
C(7)-C(10)-H(10B)	109.5
H(10A)-C(10)-H(10B)	109.5
C(7)-C(10)-H(10C)	109.5
H(10A)-C(10)-H(10C)	109.5
H(10B)-C(10)-H(10C)	109.5
O(2)-C(11)-C(2)	58.89(18)
O(2)-C(11)-H(11A)	117.9
C(2)-C(11)-H(11A)	117.9
O(2)-C(11)-H(11B)	117.9
C(2)-C(11)-H(11B)	117.9
H(11A)-C(11)-H(11B)	115.0
C(3)-C(12)-H(12A)	109.5
C(3)-C(12)-H(12B)	109.5
H(12A)-C(12)-H(12B)	109.5
C(3)-C(12)-H(12C)	109.5
H(12A)-C(12)-H(12C)	109.5
H(12B)-C(12)-H(12C)	109.5
C(2)-O(2)-C(11)	61.77(19)
C(3)-O(3)-H(3A)	109.5
C(4)-O(4)-H(4B)	109.5
C(5)-O(5)-C(6)	61.33(17)

Symmetry transformations used to generate equivalent atoms:

Table 64. Anisotropic displacement parameters ($\text{\AA}^2 \times 10^3$) for GB760. The anisotropic displacement factor exponent takes the form: $-2\pi^2 [h^2 a^{*2} U^{11} + \dots + 2 h k a^* b^* U^{12}]$

	U11	U22	U33	U23	U13	U12
C(1)	37(2)	22(1)	28(2)	-1(1)	3(1)	4(1)
C(2)	32(1)	20(1)	34(2)	-3(1)	3(1)	0(1)
C(3)	33(1)	27(1)	26(2)	-2(1)	1(1)	6(1)
C(4)	39(2)	22(1)	24(2)	-1(1)	4(1)	4(1)
C(5)	37(2)	22(1)	26(2)	-1(1)	1(1)	-3(1)
C(6)	32(2)	22(1)	35(2)	1(1)	4(1)	0(1)
C(7)	30(1)	32(1)	38(2)	-2(1)	-3(1)	2(1)
C(8)	45(2)	47(2)	40(2)	0(2)	-12(2)	-7(2)
C(9)	43(2)	44(2)	32(2)	5(1)	0(1)	10(1)
C(10)	33(2)	56(2)	42(2)	-4(2)	-5(2)	11(1)
C(11)	39(2)	31(1)	44(2)	3(1)	8(1)	4(1)
C(12)	35(2)	37(2)	40(2)	0(1)	-3(1)	6(1)
O(1)	44(1)	22(1)	64(2)	4(1)	-11(1)	5(1)
O(2)	36(1)	23(1)	54(1)	-3(1)	-2(1)	-4(1)
O(3)	35(1)	32(1)	33(1)	-5(1)	2(1)	1(1)
O(4)	57(1)	21(1)	39(1)	3(1)	-2(1)	6(1)
O(5)	33(1)	31(1)	31(1)	3(1)	1(1)	-1(1)

Table 65. Hydrogen coordinates ($\times 10^4$) and isotropic displacement parameters ($\text{\AA}^2 \times 10^3$) for GB760.

	x	y	z	U(eq)
H(4A)	-4737	557	-7989	34
H(5A)	-3424	896	-7747	34
H(8A)	-2177	-1	-7280	66
H(8B)	-1987	-661	-5692	66
H(8C)	-2729	468	-6006	66
H(9A)	-3346	-4274	-5388	59
H(9B)	-3437	-2122	-4861	59
H(9C)	-2695	-3249	-4548	59
H(10A)	-2465	-5012	-7409	65
H(10B)	-1825	-3968	-6551	65
H(10C)	-2022	-3307	-8136	65
H(11A)	-5112	-4634	-6687	45
H(11B)	-5715	-3262	-7540	45
H(12A)	-5757	-2319	-10364	56
H(12B)	-5572	-108	-10549	56
H(12C)	-5823	-911	-9031	56
H(3A)	-3945	-1960	-10738	50
H(4B)	-4595	2618	-9479	58

Table 66. Torsion angles [$^\circ$] for GB760.

O(1)-C(1)-C(2)-O(2)	-10.4(4)
C(6)-C(1)-C(2)-O(2)	171.7(3)
O(1)-C(1)-C(2)-C(11)	54.7(4)
C(6)-C(1)-C(2)-C(11)	-123.3(3)
O(1)-C(1)-C(2)-C(3)	-149.1(3)
C(6)-C(1)-C(2)-C(3)	32.9(4)
O(2)-C(2)-C(3)-O(3)	-70.4(3)

C(11)-C(2)-C(3)-O(3)	-139.1(3)
C(1)-C(2)-C(3)-O(3)	67.4(3)
O(2)-C(2)-C(3)-C(12)	45.9(3)
C(11)-C(2)-C(3)-C(12)	-22.7(4)
C(1)-C(2)-C(3)-C(12)	-176.3(3)
O(2)-C(2)-C(3)-C(4)	168.3(2)
C(11)-C(2)-C(3)-C(4)	99.7(3)
C(1)-C(2)-C(3)-C(4)	-53.8(3)
O(3)-C(3)-C(4)-O(4)	51.1(3)
C(12)-C(3)-C(4)-O(4)	-66.1(3)
C(2)-C(3)-C(4)-O(4)	170.0(2)
O(3)-C(3)-C(4)-C(5)	-70.0(3)
C(12)-C(3)-C(4)-C(5)	172.8(2)
C(2)-C(3)-C(4)-C(5)	49.0(3)
O(4)-C(4)-C(5)-O(5)	-79.2(3)
C(3)-C(4)-C(5)-O(5)	41.5(3)
O(4)-C(4)-C(5)-C(6)	-149.0(3)
C(3)-C(4)-C(5)-C(6)	-28.3(4)
C(4)-C(5)-C(6)-O(5)	102.8(3)
O(5)-C(5)-C(6)-C(1)	-97.3(3)
C(4)-C(5)-C(6)-C(1)	5.5(4)
O(5)-C(5)-C(6)-C(7)	102.9(3)
C(4)-C(5)-C(6)-C(7)	-154.3(3)
O(1)-C(1)-C(6)-O(5)	111.4(3)
C(2)-C(1)-C(6)-O(5)	-70.7(3)
O(1)-C(1)-C(6)-C(5)	175.3(3)
C(2)-C(1)-C(6)-C(5)	-6.7(4)
O(1)-C(1)-C(6)-C(7)	-23.8(4)
C(2)-C(1)-C(6)-C(7)	154.1(3)
O(5)-C(6)-C(7)-C(9)	176.7(2)
C(5)-C(6)-C(7)-C(9)	108.0(3)
C(1)-C(6)-C(7)-C(9)	-51.4(3)
O(5)-C(6)-C(7)-C(8)	56.4(3)
C(5)-C(6)-C(7)-C(8)	-12.3(4)
C(1)-C(6)-C(7)-C(8)	-171.7(3)

O(5)-C(6)-C(7)-C(10)	-62.2(3)
C(5)-C(6)-C(7)-C(10)	-130.9(3)
C(1)-C(6)-C(7)-C(10)	69.7(3)
C(1)-C(2)-C(11)-O(2)	-103.7(2)
C(3)-C(2)-C(11)-O(2)	101.5(3)
C(1)-C(2)-O(2)-C(11)	104.3(3)
C(3)-C(2)-O(2)-C(11)	-115.6(3)
C(4)-C(5)-O(5)-C(6)	-116.2(3)
C(1)-C(6)-O(5)-C(5)	109.4(2)
C(7)-C(6)-O(5)-C(5)	-114.5(3)

Symmetry transformations used to generate equivalent atoms:

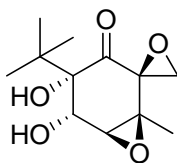
Table 67. Hydrogen bonds for GB760 [\AA and $^\circ$].

D-H...A	d(D-H)	d(H...A)	d(D...A)	\angle (DHA)
O(3)-H(3A)...O(5)	0.84	2.11	2.800(3)	139.1
O(4)-H(4B)...O(2)#1	0.84	2.01	2.842(3)	173.6

Symmetry transformations used to generate equivalent atoms:

#1 x,y+1,z

(\pm)-4-*tert*-Butyl-4,5-dihydroxy-1-methyl-7-oxaspiro[bicyclo[4.1.0]heptane-2,2'-oxiran]-3-one (87)



To a round bottomed flask was added **58d** (2.0 g, 9.6 mmol, 1.0 eq) followed by acetone (1 mL) and water (1 mL). The flask was cooled to 0°C and then OsO_4 (0.12 g, 0.48 mmol, 0.05 eq) was added. Next a 50% 4-methylmorpholine *N*-oxide solution in water

(5.6 mL, 24 mmol, 2.5 eq) was added dropwise over a period of one hour. The reaction was allowed to stir for 16 hours slowly warming to room temperature. The reaction mixture was transferred to a separatory funnel and diluted with water (100 mL). The product was extracted with ethyl acetate. The organic layer was washed with brine, dried over MgSO_4 , filtered, and concentrated. The resulting dark residue was purified on silica eluting with 3:1 hexanes/ethyl acetate. 1.7 g of the desired product was isolated in 76% yield as a white solid. A portion of compound **87** was recrystallized from hexanes and ethyl acetate for x-ray crystallography. (Rf: 0.71; ethyl acetate). mp: 148-150 °C. ^1H NMR (DMSO, 300 MHz): δ : 0.96 (s, 9H), 1.15 (s, 3H), 2.70 (d, 1H, $J = 4.8$ Hz), 3.14 (d, 1H, $J = 4.5$ Hz), 4.13 (d, 1H, $J = 7.5$ Hz), 5.24 (s, 1H), 6.07 (d, 1H, $J = 7.5$ Hz). ^{13}C NMR (CDCl_3 , 100 MHz): δ : 15.0, 25.8, 37.3, 51.2, 61.7, 61.8, 62.7, 68.5, 80.2, 201.0. HRMS (ESI): expected for $\text{C}_{12}\text{H}_{19}\text{O}_5$ ($\text{M}+\text{H}$) $^+$ 243.12270. Found 243.12247. IR (neat): ν_{max} 3407, 2987, 2954, 2921, 2868, 1728 cm^{-1} . Elemental Analysis for $\text{C}_{12}\text{H}_{18}\text{O}_5$: Found: C, 59.55; H, 7.51. Calculated: C, 59.49; H, 7.49. The relative stereochemistry was established by X-ray crystallographic analysis.

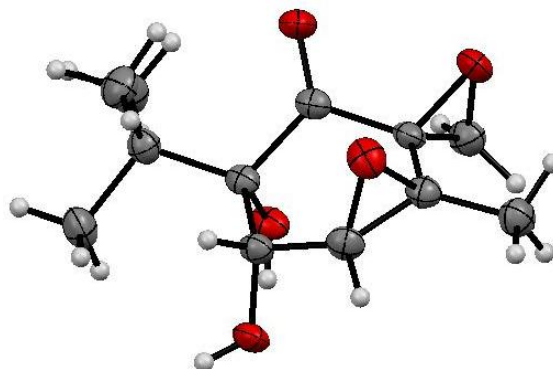


Table 68. Crystal data and structure refinement for gb594_0m.

Identification code	gb594_0m	
Empirical formula	C ₁₂ H ₁₈ O ₅	
Formula weight	242.26	
Temperature	173(2) K	
Wavelength	1.54178 Å	
Crystal system	Monoclinic	
Space group	P2(1)/n	
Unit cell dimensions	a = 8.7273(7) Å	α = 90°.
	b = 11.0261(9) Å	β = 100.211(4)°.
	c = 12.9088(10) Å	γ = 90°.
Volume	1222.51(17) Å ³	
Z	4	
Density (calculated)	1.316 Mg/m ³	
Absorption coefficient	0.854 mm ⁻¹	
F(000)	520	
Crystal size	0.45 x 0.18 x 0.18 mm ³	
Theta range for data collection	5.31 to 65.91°.	
Index ranges	-10 ≤ h ≤ 8, -12 ≤ k ≤ 12, -14 ≤ l ≤ 14	
Reflections collected	7128	
Independent reflections	1920 [R(int) = 0.0191]	
Completeness to theta = 65.91°	90.2 %	
Absorption correction	Semi-empirical from equivalents	
Max. and min. transmission	0.8614 and 0.6998	
Refinement method	Full-matrix least-squares on F ²	
Data / restraints / parameters	1920 / 0 / 160	
Goodness-of-fit on F ²	1.030	
Final R indices [I > 2σ(I)]	R1 = 0.0324, wR2 = 0.0883	
R indices (all data)	R1 = 0.0337, wR2 = 0.0897	
Largest diff. peak and hole	0.154 and -0.187 e.Å ⁻³	

Table 69. Atomic coordinates ($\times 10^4$) and equivalent isotropic displacement parameters ($\text{\AA}^2 \times 10^3$) for gb594_0m. $U(\text{eq})$ is defined as one third of the trace of the orthogonalized U_{ij} tensor.

	x	y	z	$U(\text{eq})$
O(5)	11630(1)	8615(1)	3589(1)	31(1)
O(2)	7142(1)	8637(1)	2107(1)	34(1)
O(1)	9316(1)	6889(1)	2057(1)	34(1)
O(4)	11475(1)	8236(1)	5507(1)	33(1)
O(3)	7679(1)	6994(1)	4272(1)	34(1)
C(2)	8334(1)	8440(1)	3018(1)	25(1)
C(9)	12809(2)	6644(2)	2549(1)	38(1)
C(1)	9519(1)	7488(1)	2855(1)	24(1)
C(5)	10521(1)	7394(1)	4843(1)	26(1)
C(3)	7769(2)	8292(1)	4035(1)	27(1)
C(7)	12163(2)	6427(1)	3567(1)	28(1)
C(6)	10984(1)	7441(1)	3722(1)	24(1)
C(4)	8864(2)	7725(1)	4895(1)	29(1)
C(10)	13550(2)	6451(1)	4490(1)	36(1)
C(11)	8271(2)	9586(1)	2434(1)	33(1)
C(8)	11405(2)	5166(1)	3532(1)	38(1)
C(12)	6429(2)	9048(1)	4245(1)	34(1)

Table 70. Bond lengths [\AA] and angles [$^\circ$] for gb594_0m.

O(5)-C(6)	1.4340(15)
O(5)-H(5)	0.8400
O(2)-C(2)	1.4417(14)
O(2)-C(11)	1.4480(17)
O(1)-C(1)	1.2107(15)
O(4)-C(5)	1.4268(15)
O(4)-H(4)	0.8400

O(3)-C(4)	1.4393(16)
O(3)-C(3)	1.4683(15)
C(2)-C(11)	1.4673(18)
C(2)-C(3)	1.4907(19)
C(2)-C(1)	1.5138(18)
C(9)-C(7)	1.5373(19)
C(9)-H(9A)	0.9800
C(9)-H(9B)	0.9800
C(9)-H(9C)	0.9800
C(1)-C(6)	1.5440(17)
C(5)-C(4)	1.5043(19)
C(5)-C(6)	1.5714(18)
C(5)-H(5A)	1.0000
C(3)-C(4)	1.4703(18)
C(3)-C(12)	1.4995(19)
C(7)-C(8)	1.5368(19)
C(7)-C(10)	1.5410(18)
C(7)-C(6)	1.5570(18)
C(4)-H(4A)	1.0000
C(10)-H(10A)	0.9800
C(10)-H(10B)	0.9800
C(10)-H(10C)	0.9800
C(11)-H(11A)	0.9900
C(11)-H(11B)	0.9900
C(8)-H(8A)	0.9800
C(8)-H(8B)	0.9800
C(8)-H(8C)	0.9800
C(12)-H(12A)	0.9800
C(12)-H(12B)	0.9800
C(12)-H(12C)	0.9800
C(6)-O(5)-H(5)	109.5
C(2)-O(2)-C(11)	61.03(8)
C(5)-O(4)-H(4)	109.5
C(4)-O(3)-C(3)	60.74(8)
O(2)-C(2)-C(11)	59.70(8)

O(2)-C(2)-C(3)	115.58(10)
C(11)-C(2)-C(3)	123.98(12)
O(2)-C(2)-C(1)	113.73(10)
C(11)-C(2)-C(1)	119.32(11)
C(3)-C(2)-C(1)	112.77(10)
C(7)-C(9)-H(9A)	109.5
C(7)-C(9)-H(9B)	109.5
H(9A)-C(9)-H(9B)	109.5
C(7)-C(9)-H(9C)	109.5
H(9A)-C(9)-H(9C)	109.5
H(9B)-C(9)-H(9C)	109.5
O(1)-C(1)-C(2)	119.77(11)
O(1)-C(1)-C(6)	125.16(11)
C(2)-C(1)-C(6)	114.91(10)
O(4)-C(5)-C(4)	106.17(10)
O(4)-C(5)-C(6)	108.28(10)
C(4)-C(5)-C(6)	116.03(10)
O(4)-C(5)-H(5A)	108.7
C(4)-C(5)-H(5A)	108.7
C(6)-C(5)-H(5A)	108.7
O(3)-C(3)-C(4)	58.65(8)
O(3)-C(3)-C(2)	109.20(10)
C(4)-C(3)-C(2)	116.07(11)
O(3)-C(3)-C(12)	115.60(11)
C(4)-C(3)-C(12)	121.57(12)
C(2)-C(3)-C(12)	119.22(11)
C(8)-C(7)-C(9)	109.74(12)
C(8)-C(7)-C(10)	108.28(11)
C(9)-C(7)-C(10)	107.54(11)
C(8)-C(7)-C(6)	111.25(10)
C(9)-C(7)-C(6)	110.43(10)
C(10)-C(7)-C(6)	109.51(11)
O(5)-C(6)-C(1)	100.14(9)
O(5)-C(6)-C(7)	110.52(10)
C(1)-C(6)-C(7)	114.34(10)

O(5)-C(6)-C(5)	108.10(10)
C(1)-C(6)-C(5)	110.71(10)
C(7)-C(6)-C(5)	112.24(10)
O(3)-C(4)-C(3)	60.61(8)
O(3)-C(4)-C(5)	116.17(11)
C(3)-C(4)-C(5)	124.84(11)
O(3)-C(4)-H(4A)	114.7
C(3)-C(4)-H(4A)	114.7
C(5)-C(4)-H(4A)	114.7
C(7)-C(10)-H(10A)	109.5
C(7)-C(10)-H(10B)	109.5
H(10A)-C(10)-H(10B)	109.5
C(7)-C(10)-H(10C)	109.5
H(10A)-C(10)-H(10C)	109.5
H(10B)-C(10)-H(10C)	109.5
O(2)-C(11)-C(2)	59.27(8)
O(2)-C(11)-H(11A)	117.8
C(2)-C(11)-H(11A)	117.8
O(2)-C(11)-H(11B)	117.8
C(2)-C(11)-H(11B)	117.8
H(11A)-C(11)-H(11B)	115.0
C(7)-C(8)-H(8A)	109.5
C(7)-C(8)-H(8B)	109.5
H(8A)-C(8)-H(8B)	109.5
C(7)-C(8)-H(8C)	109.5
H(8A)-C(8)-H(8C)	109.5
H(8B)-C(8)-H(8C)	109.5
C(3)-C(12)-H(12A)	109.5
C(3)-C(12)-H(12B)	109.5
H(12A)-C(12)-H(12B)	109.5
C(3)-C(12)-H(12C)	109.5
H(12A)-C(12)-H(12C)	109.5
H(12B)-C(12)-H(12C)	109.5

Symmetry transformations used to generate equivalent atoms:

Table 71. Anisotropic displacement parameters ($\text{\AA}^2 \times 10^3$) for gb594_0m. The anisotropic displacement factor exponent takes the form: $-2\pi^2 [h^2 a^{*2} U^{11} + \dots + 2 h k a^* b^* U^{12}]$

	U11	U22	U33	U23	U13	U12
O(5)	35(1)	24(1)	30(1)	3(1)	-1(1)	-9(1)
O(2)	32(1)	39(1)	25(1)	-2(1)	-6(1)	5(1)
O(1)	36(1)	36(1)	26(1)	-9(1)	-3(1)	2(1)
O(4)	37(1)	34(1)	23(1)	-4(1)	-8(1)	2(1)
O(3)	32(1)	30(1)	40(1)	6(1)	5(1)	-5(1)
C(2)	26(1)	27(1)	20(1)	-2(1)	-3(1)	-2(1)
C(9)	37(1)	49(1)	31(1)	4(1)	10(1)	8(1)
C(1)	28(1)	23(1)	21(1)	1(1)	3(1)	-5(1)
C(5)	31(1)	25(1)	21(1)	2(1)	0(1)	-1(1)
C(3)	28(1)	26(1)	26(1)	-1(1)	3(1)	-3(1)
C(7)	28(1)	29(1)	26(1)	3(1)	4(1)	1(1)
C(6)	26(1)	21(1)	23(1)	2(1)	2(1)	-4(1)
C(4)	33(1)	33(1)	22(1)	2(1)	6(1)	-2(1)
C(10)	29(1)	45(1)	34(1)	6(1)	2(1)	6(1)
C(11)	40(1)	30(1)	27(1)	3(1)	2(1)	2(1)
C(8)	45(1)	26(1)	45(1)	-1(1)	8(1)	3(1)
C(12)	31(1)	40(1)	33(1)	0(1)	7(1)	2(1)

Table 72. Hydrogen coordinates ($\times 10^4$) and isotropic displacement parameters ($\text{\AA}^2 \times 10^3$) for gb594_0m.

	x	y	z	U(eq)
H(5)	11947	8927	4182	46
H(4)	12098	7857	5964	50
H(9A)	13521	5983	2449	57
H(9B)	13371	7417	2600	57

H(9C)	11947	6669	1949	57
H(5A)	10734	6560	5138	31
H(4A)	8669	7920	5617	35
H(10A)	14370	5908	4335	55
H(10B)	13205	6183	5134	55
H(10C)	13959	7279	4586	55
H(11A)	7915	10319	2765	39
H(11B)	9078	9732	1997	39
H(8A)	10566	5113	2919	57
H(8B)	10976	5038	4176	57
H(8C)	12188	4543	3480	57
H(12A)	6190	8840	4937	52
H(12B)	5515	8889	3701	52
H(12C)	6706	9909	4233	52

Table 73. Torsion angles [$^{\circ}$] for gb594_0m.

C(11)-O(2)-C(2)-C(3)	115.97(13)
C(11)-O(2)-C(2)-C(1)	-111.26(12)
O(2)-C(2)-C(1)-O(1)	-7.59(16)
C(11)-C(2)-C(1)-O(1)	-74.93(15)
C(3)-C(2)-C(1)-O(1)	126.51(12)
O(2)-C(2)-C(1)-C(6)	167.96(10)
C(11)-C(2)-C(1)-C(6)	100.62(13)
C(3)-C(2)-C(1)-C(6)	-57.93(14)
C(4)-O(3)-C(3)-C(2)	109.43(12)
C(4)-O(3)-C(3)-C(12)	-112.83(13)
O(2)-C(2)-C(3)-O(3)	97.91(12)
C(11)-C(2)-C(3)-O(3)	167.30(11)
C(1)-C(2)-C(3)-O(3)	-35.30(13)
O(2)-C(2)-C(3)-C(4)	161.62(11)
C(11)-C(2)-C(3)-C(4)	-128.98(13)
C(1)-C(2)-C(3)-C(4)	28.41(15)
O(2)-C(2)-C(3)-C(12)	-38.07(16)
C(11)-C(2)-C(3)-C(12)	31.32(18)
C(1)-C(2)-C(3)-C(12)	-171.29(11)
O(1)-C(1)-C(6)-O(5)	111.22(13)
C(2)-C(1)-C(6)-O(5)	-64.07(12)
O(1)-C(1)-C(6)-C(7)	-6.93(17)
C(2)-C(1)-C(6)-C(7)	177.79(10)
O(1)-C(1)-C(6)-C(5)	-134.90(13)
C(2)-C(1)-C(6)-C(5)	49.82(13)
C(8)-C(7)-C(6)-O(5)	-171.07(10)
C(9)-C(7)-C(6)-O(5)	-48.97(14)
C(10)-C(7)-C(6)-O(5)	69.27(13)
C(8)-C(7)-C(6)-C(1)	-59.01(14)
C(9)-C(7)-C(6)-C(1)	63.09(14)
C(10)-C(7)-C(6)-C(1)	-178.67(10)
C(8)-C(7)-C(6)-C(5)	68.17(13)
C(9)-C(7)-C(6)-C(5)	-169.72(11)

C(10)-C(7)-C(6)-C(5)	-51.48(13)
O(4)-C(5)-C(6)-O(5)	-25.74(13)
C(4)-C(5)-C(6)-O(5)	93.46(12)
O(4)-C(5)-C(6)-C(1)	-134.49(10)
C(4)-C(5)-C(6)-C(1)	-15.30(15)
O(4)-C(5)-C(6)-C(7)	96.40(11)
C(4)-C(5)-C(6)-C(7)	-144.40(11)
C(3)-O(3)-C(4)-C(5)	-116.98(13)
C(2)-C(3)-C(4)-O(3)	-97.52(12)
C(12)-C(3)-C(4)-O(3)	102.68(13)
O(3)-C(3)-C(4)-C(5)	102.99(14)
C(2)-C(3)-C(4)-C(5)	5.47(19)
C(12)-C(3)-C(4)-C(5)	-154.34(13)
O(4)-C(5)-C(4)-O(3)	179.54(10)
C(6)-C(5)-C(4)-O(3)	59.20(15)
O(4)-C(5)-C(4)-C(3)	108.46(14)
C(6)-C(5)-C(4)-C(3)	-11.88(18)
C(3)-C(2)-C(11)-O(2)	-102.07(13)
C(1)-C(2)-C(11)-O(2)	101.91(12)

Symmetry transformations used to generate equivalent atoms:

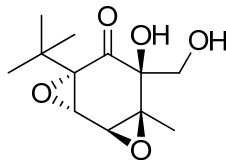
Table 74. Hydrogen bonds for gb594_0m [\AA and $^\circ$].

D-H...A	d(D-H)	d(H...A)	d(D...A)	$\angle(\text{DHA})$
O(5)-H(5)...O(4)	0.84	1.98	2.5377(13)	123.0
O(4)-H(4)...O(1)#1	0.84	2.20	2.9001(12)	140.6
O(4)-H(4)...O(2)#1	0.84	2.21	2.9053(13)	140.7

Symmetry transformations used to generate equivalent atoms:

#1 $x+1/2, -y+3/2, z+1/2$

(±)-4-(*tert*-Butyl)-6-hydroxy-6-(hydroxymethyl)-7-methyl-3,8-dioxatricyclo[5.1.0.0^{2,4}]octan-5-one (**88**)



To a dry round bottomed flask under argon was added compound **60d** (0.10 g, 0.45 mmol) followed by a 0.5 M solution of CsOAc in AcOH (10 mL). The reaction was heated to reflux and allowed to stir for 2 hours. The reaction was cooled and then the acetic acid was removed under vacuum. The resulting residue was dissolved in methanol (10 mL) followed by treatment with K₂CO₃ (0.93 g, 6.8 mmol). The reaction mixture was transferred to a separatory funnel and diluted with water (25 mL). The product was extracted with several portions of ethyl acetate. The organic layers were pooled and washed with brine. The organic layer was then dried over MgSO₄, filtered, and concentrated. The resulting residue was purified on silica eluting with 3:1 hexanes/ethyl acetate. 0.69 g of the desired product was isolated 63% yield as a white solid. A portion of compound **88** was recrystallized from ethyl acetate for x-ray crystallography. (Rf: 0.14; 3:1 hexanes/ethyl acetate). mp: 106-107 °C. ¹H NMR (CDCl₃, 300 MHz): δ: 1.08 (s, 9H), 1.45 (s, 3H), 2.26 dd, 1H, J = 8.7 Hz, 4.5 Hz), 3.55 (d, 1H, J = 2.4 Hz), 3.79 (dd, 1H, J = 11.4 Hz, 4.8 Hz), 3.91 (d, 1H, J = 3.0 Hz), 4.06-4.13 (m, 1H). ¹³C NMR (CDCl₃, 100 MHz): δ: 16.7, 25.8, 32.9, 58.5, 60.4, 62.7, 66.0, 68.9, 81.8, 203.3. HRMS (APCI): expected for C₁₂H₁₉O₅ (M+H)⁺ 243.12270. Found 243.12282. IR (neat): ν_{max} 3461, 2966, 2933, 2909, 2872, 1720 cm⁻¹. Elemental Analysis for C₁₂H₁₈O₅: Found: C, 59.73; H, 7.60. Calculated: C, 59.49; H, 7.49. The relative stereochemistry was

established by X-ray crystallographic analysis.

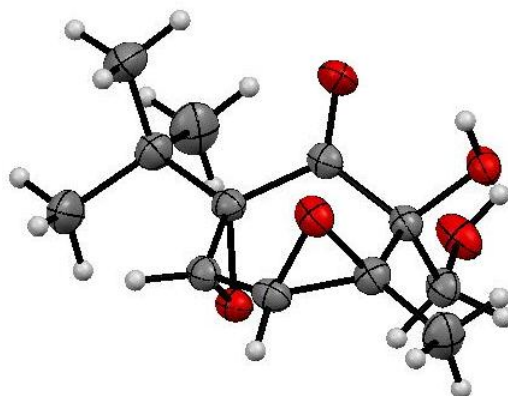


Table 75. Crystal data and structure refinement for GB813s.

Identification code	gb813s	
Empirical formula	C ₁₂ H ₁₈ O ₅	
Formula weight	242.26	
Temperature	173(2) K	
Wavelength	1.54178 Å	
Crystal system	Monoclinic	
Space group	P2(1)/c	
Unit cell dimensions	a = 9.6231(9) Å	α = 90°.
	b = 10.9874(9) Å	β = 108.095(4)°.
	c = 12.3017(10) Å	γ = 90°.
Volume	1236.36(18) Å ³	
Z	4	
Density (calculated)	1.302 Mg/m ³	
Absorption coefficient	0.845 mm ⁻¹	
F(000)	520	
Crystal size	0.48 x 0.21 x 0.10 mm ³	
Theta range for data collection	4.83 to 66.29°.	
Index ranges	-10 ≤ h ≤ 10, -12 ≤ k ≤ 12, -14 ≤ l ≤ 12	
Reflections collected	7467	
Independent reflections	1969 [R(int) = 0.0254]	
Completeness to theta = 66.29°	90.4 %	
Absorption correction	Semi-empirical from equivalents	
Max. and min. transmission	0.9203 and 0.6873	

Refinement method	Full-matrix least-squares on F^2
Data / restraints / parameters	1969 / 0 / 161
Goodness-of-fit on F^2	1.078
Final R indices [$I > 2\sigma(I)$]	R1 = 0.0336, wR2 = 0.0945
R indices (all data)	R1 = 0.0382, wR2 = 0.1017
Extinction coefficient	0.0057(6)
Largest diff. peak and hole	0.220 and -0.162 e. \AA^{-3}

Table 76. Atomic coordinates ($\times 10^4$) and equivalent isotropic displacement parameters ($\text{\AA}^2 \times 10^3$) for GB813s. $U(\text{eq})$ is defined as one third of the trace of the orthogonalized U_{ij} tensor.

	x	y	z	$U(\text{eq})$
C(1)	4322(2)	9605(1)	6841(1)	25(1)
C(2)	5991(2)	9396(1)	7172(1)	26(1)
C(3)	6654(2)	9464(1)	8464(1)	28(1)
C(4)	5747(2)	9182(1)	9189(1)	29(1)
C(5)	4244(2)	8698(1)	8683(1)	26(1)
C(6)	3458(2)	8871(1)	7454(1)	25(1)
C(7)	1782(2)	8857(2)	6973(1)	33(1)
C(8)	1180(2)	10135(2)	7060(2)	45(1)
C(9)	1339(2)	8411(2)	5735(2)	50(1)
C(10)	1139(2)	7981(2)	7661(2)	45(1)
C(11)	6318(2)	8197(2)	6664(1)	30(1)
C(12)	8290(2)	9368(2)	8948(2)	43(1)
O(1)	3745(1)	10378(1)	6152(1)	35(1)
O(2)	6619(1)	10304(1)	6655(1)	31(1)
O(3)	5492(2)	8102(1)	5500(1)	40(1)
O(4)	6002(1)	10442(1)	8944(1)	32(1)
O(5)	4144(1)	7722(1)	7883(1)	27(1)

Table 77. Bond lengths [Å] and angles [°] for GB813s.

C(1)-O(1)	1.2070(19)
C(1)-C(6)	1.517(2)
C(1)-C(2)	1.546(2)
C(2)-O(2)	1.4156(18)
C(2)-C(3)	1.519(2)
C(2)-C(11)	1.531(2)
C(3)-O(4)	1.4586(18)
C(3)-C(4)	1.462(2)
C(3)-C(12)	1.504(2)
C(4)-O(4)	1.4534(19)
C(4)-C(5)	1.484(2)
C(4)-H(4)	1.0000
C(5)-O(5)	1.4393(18)
C(5)-C(6)	1.478(2)
C(5)-H(5)	1.0000
C(6)-O(5)	1.4468(18)
C(6)-C(7)	1.536(2)
C(7)-C(9)	1.529(3)
C(7)-C(10)	1.533(2)
C(7)-C(8)	1.535(3)
C(8)-H(8A)	0.9800
C(8)-H(8B)	0.9800
C(8)-H(8C)	0.9800
C(9)-H(9A)	0.9800
C(9)-H(9B)	0.9800
C(9)-H(9C)	0.9800
C(10)-H(10A)	0.9800
C(10)-H(10B)	0.9800
C(10)-H(10C)	0.9800
C(11)-O(3)	1.409(2)
C(11)-H(11A)	0.9900
C(11)-H(11B)	0.9900
C(12)-H(12A)	0.9800

C(12)-H(12B)	0.9800
C(12)-H(12C)	0.9800
O(2)-H(2)	0.8400
O(3)-H(3)	0.8400
O(1)-C(1)-C(6)	121.30(14)
O(1)-C(1)-C(2)	120.23(14)
C(6)-C(1)-C(2)	118.37(13)
O(2)-C(2)-C(3)	109.61(12)
O(2)-C(2)-C(11)	104.62(12)
C(3)-C(2)-C(11)	113.36(13)
O(2)-C(2)-C(1)	109.28(12)
C(3)-C(2)-C(1)	109.41(12)
C(11)-C(2)-C(1)	110.42(13)
O(4)-C(3)-C(4)	59.70(10)
O(4)-C(3)-C(12)	114.86(13)
C(4)-C(3)-C(12)	119.55(14)
O(4)-C(3)-C(2)	111.49(12)
C(4)-C(3)-C(2)	119.44(14)
C(12)-C(3)-C(2)	117.31(14)
O(4)-C(4)-C(3)	60.05(10)
O(4)-C(4)-C(5)	117.35(13)
C(3)-C(4)-C(5)	120.60(13)
O(4)-C(4)-H(4)	115.8
C(3)-C(4)-H(4)	115.8
C(5)-C(4)-H(4)	115.8
O(5)-C(5)-C(6)	59.45(9)
O(5)-C(5)-C(4)	113.79(12)
C(6)-C(5)-C(4)	120.35(13)
O(5)-C(5)-H(5)	116.8
C(6)-C(5)-H(5)	116.8
C(4)-C(5)-H(5)	116.8
O(5)-C(6)-C(5)	58.94(9)
O(5)-C(6)-C(1)	112.75(12)
C(5)-C(6)-C(1)	113.03(13)
O(5)-C(6)-C(7)	115.93(13)

C(5)-C(6)-C(7)	122.37(13)
C(1)-C(6)-C(7)	119.12(13)
C(9)-C(7)-C(10)	108.24(16)
C(9)-C(7)-C(8)	111.59(16)
C(10)-C(7)-C(8)	108.09(15)
C(9)-C(7)-C(6)	108.72(14)
C(10)-C(7)-C(6)	110.45(13)
C(8)-C(7)-C(6)	109.74(14)
C(7)-C(8)-H(8A)	109.5
C(7)-C(8)-H(8B)	109.5
H(8A)-C(8)-H(8B)	109.5
C(7)-C(8)-H(8C)	109.5
H(8A)-C(8)-H(8C)	109.5
H(8B)-C(8)-H(8C)	109.5
C(7)-C(9)-H(9A)	109.5
C(7)-C(9)-H(9B)	109.5
H(9A)-C(9)-H(9B)	109.5
C(7)-C(9)-H(9C)	109.5
H(9A)-C(9)-H(9C)	109.5
H(9B)-C(9)-H(9C)	109.5
C(7)-C(10)-H(10A)	109.5
C(7)-C(10)-H(10B)	109.5
H(10A)-C(10)-H(10B)	109.5
C(7)-C(10)-H(10C)	109.5
H(10A)-C(10)-H(10C)	109.5
H(10B)-C(10)-H(10C)	109.5
O(3)-C(11)-C(2)	110.82(13)
O(3)-C(11)-H(11A)	109.5
C(2)-C(11)-H(11A)	109.5
O(3)-C(11)-H(11B)	109.5
C(2)-C(11)-H(11B)	109.5
H(11A)-C(11)-H(11B)	108.1
C(3)-C(12)-H(12A)	109.5
C(3)-C(12)-H(12B)	109.5
H(12A)-C(12)-H(12B)	109.5

C(3)-C(12)-H(12C)	109.5
H(12A)-C(12)-H(12C)	109.5
H(12B)-C(12)-H(12C)	109.5
C(2)-O(2)-H(2)	109.5
C(11)-O(3)-H(3)	109.5
C(4)-O(4)-C(3)	60.26(10)
C(5)-O(5)-C(6)	61.61(10)

Symmetry transformations used to generate equivalent atoms:

Table 78. Anisotropic displacement parameters ($\text{\AA}^2 \times 10^3$) for GB813s. The anisotropic displacement factor exponent takes the form: $-2\pi^2 [h^2 a^{*2} U^{11} + \dots + 2 h k a^* b^* U^{12}]$

	U11	U22	U33	U23	U13	U12
C(1)	33(1)	24(1)	20(1)	-3(1)	9(1)	1(1)
C(2)	31(1)	24(1)	26(1)	0(1)	12(1)	-2(1)
C(3)	31(1)	27(1)	28(1)	-3(1)	9(1)	-1(1)
C(4)	35(1)	26(1)	24(1)	2(1)	8(1)	1(1)
C(5)	31(1)	25(1)	25(1)	1(1)	12(1)	2(1)
C(6)	29(1)	23(1)	25(1)	1(1)	10(1)	3(1)
C(7)	27(1)	38(1)	35(1)	4(1)	8(1)	2(1)
C(8)	35(1)	45(1)	56(1)	9(1)	16(1)	12(1)
C(9)	37(1)	65(1)	40(1)	-4(1)	2(1)	-8(1)
C(10)	29(1)	48(1)	60(1)	12(1)	17(1)	1(1)
C(11)	35(1)	29(1)	28(1)	-2(1)	15(1)	1(1)
C(12)	32(1)	58(1)	36(1)	0(1)	6(1)	-3(1)
O(1)	38(1)	37(1)	31(1)	11(1)	12(1)	6(1)
O(2)	39(1)	26(1)	34(1)	0(1)	19(1)	-3(1)
O(3)	64(1)	30(1)	28(1)	-5(1)	18(1)	-8(1)
O(4)	43(1)	26(1)	28(1)	-5(1)	15(1)	-4(1)
O(5)	31(1)	24(1)	26(1)	2(1)	9(1)	2(1)

Table 79. Hydrogen coordinates ($\times 10^4$) and isotropic displacement parameters ($\text{\AA}^2 \times 10^3$) for GB813s.

	x	y	z	U(eq)
H(4)	6283	8893	9979	34
H(5)	3633	8625	9205	32
H(8A)	1524	10409	7858	68
H(8B)	109	10112	6796	68
H(8C)	1524	10700	6583	68
H(9A)	1697	8984	5273	75
H(9B)	272	8358	5432	75
H(9C)	1766	7606	5708	75
H(10A)	1540	7164	7642	67
H(10B)	73	7957	7325	67
H(10C)	1393	8262	8455	67
H(11A)	7373	8156	6742	36
H(11B)	6083	7505	7092	36
H(12A)	8746	9960	8569	64
H(12B)	8599	8545	8820	64
H(12C)	8592	9537	9771	64
H(2)	6326	10992	6786	47
H(3)	5704	8681	5135	59

Table 80. Torsion angles [$^\circ$] for GB813s.

O(1)-C(1)-C(2)-O(2)	6.49(19)
C(6)-C(1)-C(2)-O(2)	-169.92(12)
O(1)-C(1)-C(2)-C(3)	126.50(15)
C(6)-C(1)-C(2)-C(3)	-49.91(17)
O(1)-C(1)-C(2)-C(11)	-108.06(16)
C(6)-C(1)-C(2)-C(11)	75.52(16)
O(2)-C(2)-C(3)-O(4)	79.29(15)

C(11)-C(2)-C(3)-O(4)	-164.24(12)
C(1)-C(2)-C(3)-O(4)	-40.52(16)
O(2)-C(2)-C(3)-C(4)	145.68(14)
C(11)-C(2)-C(3)-C(4)	-97.85(17)
C(1)-C(2)-C(3)-C(4)	25.87(19)
O(2)-C(2)-C(3)-C(12)	-56.09(18)
C(11)-C(2)-C(3)-C(12)	60.38(19)
C(1)-C(2)-C(3)-C(12)	-175.90(15)
C(12)-C(3)-C(4)-O(4)	103.21(16)
C(2)-C(3)-C(4)-O(4)	-99.05(15)
O(4)-C(3)-C(4)-C(5)	105.97(16)
C(12)-C(3)-C(4)-C(5)	-150.82(16)
C(2)-C(3)-C(4)-C(5)	6.9(2)
O(4)-C(4)-C(5)-O(5)	116.50(14)
C(3)-C(4)-C(5)-O(5)	46.8(2)
O(4)-C(4)-C(5)-C(6)	49.2(2)
C(3)-C(4)-C(5)-C(6)	-20.5(2)
C(4)-C(5)-C(6)-O(5)	101.38(15)
O(5)-C(5)-C(6)-C(1)	-103.56(13)
C(4)-C(5)-C(6)-C(1)	-2.2(2)
O(5)-C(5)-C(6)-C(7)	102.86(16)
C(4)-C(5)-C(6)-C(7)	-155.77(15)
O(1)-C(1)-C(6)-O(5)	157.51(13)
C(2)-C(1)-C(6)-O(5)	-26.11(18)
O(1)-C(1)-C(6)-C(5)	-137.93(15)
C(2)-C(1)-C(6)-C(5)	38.45(18)
O(1)-C(1)-C(6)-C(7)	16.6(2)
C(2)-C(1)-C(6)-C(7)	-167.03(13)
O(5)-C(6)-C(7)-C(9)	-83.08(17)
C(5)-C(6)-C(7)-C(9)	-151.31(16)
C(1)-C(6)-C(7)-C(9)	56.64(19)
O(5)-C(6)-C(7)-C(10)	35.54(19)
C(5)-C(6)-C(7)-C(10)	-32.7(2)
C(1)-C(6)-C(7)-C(10)	175.26(14)
O(5)-C(6)-C(7)-C(8)	154.61(14)

C(5)-C(6)-C(7)-C(8)	86.39(18)
C(1)-C(6)-C(7)-C(8)	-65.66(18)
O(2)-C(2)-C(11)-O(3)	-70.03(15)
C(3)-C(2)-C(11)-O(3)	170.60(13)
C(1)-C(2)-C(11)-O(3)	47.44(16)
C(5)-C(4)-O(4)-C(3)	-111.31(15)
C(12)-C(3)-O(4)-C(4)	-111.03(16)
C(2)-C(3)-O(4)-C(4)	112.44(15)
C(4)-C(5)-O(5)-C(6)	-112.39(15)
C(1)-C(6)-O(5)-C(5)	104.04(14)
C(7)-C(6)-O(5)-C(5)	-113.72(15)

Symmetry transformations used to generate equivalent atoms:

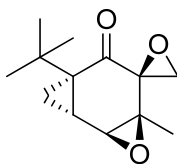
Table 81. Hydrogen bonds for GB813s [\AA and $^\circ$].

D-H...A	d(D-H)	d(H...A)	d(D...A)	\angle (DHA)
O(2)-H(2)...O(5)#1	0.84	2.02	2.8599(15)	173.3
O(3)-H(3)...O(1)#2	0.84	2.09	2.8958(16)	160.1

Symmetry transformations used to generate equivalent atoms:

#1 -x+1,y+1/2,-z+3/2 #2 -x+1,-y+2,-z+1

(±)-7'-(*tert*-Butyl)-4'-methyl-3'-oxaspiro[oxirane-2,5'-tricyclo[5.1.0.0^{2,4}]octan]-6'-one
(90)



To a dry round bottomed flask under argon was added MeI (18 mL) and DMSO (8.7 mL). The solution was heated to reflux and stirred for 3 days. The salt that formed was

collected by vacuum filtration and was washed with CH_2Cl_2 . The Corey-Chaykovsky reagent **89** was dried under vacuum overnight and stored in a desiccator. To a dry round bottomed flask under argon at 0°C was added the Corey-Chaykovsky reagent (0.11 g, 0.50 mmol, 1.05 eq) and DMSO (0.8 mL). While stirring at 0°C 60% NaH dispersion in mineral oil (0.02 g, 0.50 mmol, 1.05 eq) was added. Next compound **58d** (0.10 g, 0.48 mmol, 1.0 eq) in DMSO (0.8 mL) was added dropwise. The flask was then heated to 50°C for 2 hours. After cooling to room temperature water was added to the reaction. The reaction was then transferred to a separatory funnel and the product was extracted with diethyl ether. The organic layer was washed with brine, dried over MgSO_4 , filtered, and concentrated. The resulting residue was purified on silica eluting with 3:1 hexanes/ethyl acetate. The desired product (0.75 g) was isolated 70% yield as a white solid. A portion of compound **90** was recrystallized from hexanes and ethyl acetate for x-ray crystallography. (Rf: 0.16; 3:1 hexanes/ethyl acetate). mp: 100°C . ^1H NMR (CDCl_3 , 400 MHz): δ : 1.00 (s, 9H), 1.19 (s, 3H), 1.28 (t, 1H, $J = 5.2$ Hz), 1.49 (dd, 1H, $J = 8.4$ Hz, 5.6 Hz), 2.30 (m, 1H), 2.68 (d, 1H, $J = 5.6$ Hz), 2.87 (d, 1H, $J = 5.6$ Hz), 3.62 (d, 1H, $J = 3.6$ Hz). ^{13}C NMR (CDCl_3 , 100 MHz): δ : 15.1, 20.0, 24.8, 27.0, 32.0, 42.1, 50.5, 58.6, 59.3, 60.3, 199.1. HRMS (ESI): expected for $\text{C}_{13}\text{H}_{19}\text{O}_3$ ($\text{M}+\text{H}$) $^+$ 223.13287. Found 223.13257. IR (neat): ν_{max} 2995, 2954, 2917, 2872, 1712 cm^{-1} . Elemental Analysis for $\text{C}_{13}\text{H}_{18}\text{O}_3$: Found: C, 70.24; H, 8.18. Calculated: C, 70.25; H, 8.16. The relative stereochemistry was established by X-ray crystallographic analysis.

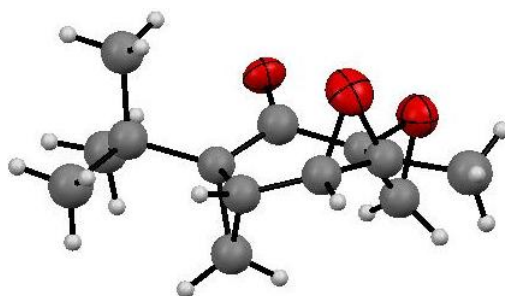


Table 82. Crystal data and structure refinement for GB595m.

Identification code	gb595m	
Empirical formula	C ₁₃ H ₁₈ O ₃	
Formula weight	222.27	
Temperature	173(2) K	
Wavelength	1.54178 Å	
Crystal system	Orthorhombic	
Space group	Pca2(1)	
Unit cell dimensions	a = 12.898(4) Å	α = 90°.
	b = 9.768(4) Å	β = 90°.
	c = 37.958(13) Å	γ = 90°.
Volume	4782(3) Å ³	
Z	16	
Density (calculated)	1.235 Mg/m ³	
Absorption coefficient	0.700 mm ⁻¹	
F(000)	1920	
Crystal size	0.25 x 0.13 x 0.02 mm ³	
Theta range for data collection	8.24 to 66.85°.	
Index ranges	-13 ≤ h ≤ 14, -9 ≤ k ≤ 10, -40 ≤ l ≤ 38	
Reflections collected	13168	
Independent reflections	5737 [R(int) = 0.1383]	
Completeness to theta = 66.85°	82.4 %	
Absorption correction	None	
Refinement method	Full-matrix least-squares on F ²	
Data / restraints / parameters	5737 / 1 / 334	
Goodness-of-fit on F ²	1.048	
Final R indices [I > 2σ(I)]	R1 = 0.0754, wR2 = 0.1186	
R indices (all data)	R1 = 0.2089, wR2 = 0.1514	

Absolute structure parameter	-0.1(7)
Extinction coefficient	0.00079(6)
Largest diff. peak and hole	0.279 and -0.279 e.Å ⁻³

Table 83. Atomic coordinates ($\times 10^4$) and equivalent isotropic displacement parameters ($\text{Å}^2 \times 10^3$) for GB595m. $U(\text{eq})$ is defined as one third of the trace of the orthogonalized U_{ij} tensor.

	x	y	z	$U(\text{eq})$
C(1)	-5438(14)	-10223(15)	-2135(6)	53(5)
C(2)	-5031(10)	-9750(13)	-1780(4)	41(4)
C(3)	-3921(8)	-9318(13)	-1764(4)	48(3)
C(4)	-3479(9)	-8852(14)	-2086(4)	50(4)
C(5)	-4110(8)	-8611(12)	-2406(3)	48(3)
C(6)	-5131(8)	-9373(14)	-2442(4)	44(3)
C(7)	-5532(12)	-9850(13)	-2818(5)	51(5)
C(8)	-6690(14)	-9914(12)	-2830(6)	59(6)
C(9)	-5010(9)	-11251(14)	-2886(3)	58(4)
C(10)	-5110(9)	-8867(13)	-3113(3)	63(4)
C(11)	-5838(10)	-9135(15)	-1542(4)	51(5)
C(12)	-3459(8)	-9017(14)	-1406(3)	64(4)
C(13)	-5110(7)	-7803(12)	-2371(3)	53(4)
C(1B)	-7082(13)	-10115(12)	-9805(5)	42(6)
C(2B)	-7343(10)	-9677(14)	-9415(4)	42(4)
C(3B)	-6468(10)	-9423(14)	-9187(4)	43(3)
C(4B)	-5473(10)	-9037(15)	-9331(4)	49(4)
C(5B)	-5389(8)	-8850(12)	-9715(3)	46(3)
C(6B)	-6157(7)	-7901(12)	-9895(3)	50(3)
C(7B)	-6217(8)	-9446(14)	-9969(3)	42(3)
C(8B)	-5869(14)	-9928(11)	-10328(6)	49(6)
C(9B)	-6747(11)	-9887(11)	-10611(5)	49(5)
C(10B)	-5542(8)	-11449(11)	-10312(3)	61(4)
C(11B)	-4952(8)	-9202(12)	-10500(3)	56(4)
C(12B)	-8346(8)	-8985(14)	-9371(4)	43(4)

C(13B)	-6715(8)	-9048(13)	-8799(3)	57(4)
C(1C)	-4622(13)	-5149(13)	-1203(5)	43(6)
C(2C)	-4897(10)	-4722(13)	-1557(4)	39(4)
C(3C)	-4011(9)	-4434(13)	-1796(4)	43(3)
C(4C)	-3048(9)	-3991(15)	-1628(4)	51(4)
C(5C)	-2963(8)	-3772(11)	-1236(3)	44(3)
C(6C)	-3767(8)	-4428(14)	-1004(3)	42(3)
C(7C)	-3437(13)	-4944(11)	-625(6)	39(5)
C(8C)	-4412(13)	-4981(10)	-397(5)	67(6)
C(9C)	-2993(8)	-6421(12)	-680(3)	60(4)
C(10C)	-2589(8)	-4064(13)	-471(3)	63(4)
C(11C)	-5932(10)	-4045(16)	-1604(4)	63(5)
C(12C)	-4223(8)	-4021(14)	-2166(3)	64(4)
C(13C)	-3765(7)	-2863(12)	-1072(3)	48(3)
C(1D)	-2906(11)	-4865(12)	-8851(5)	33(4)
C(2D)	-2553(11)	-5315(15)	-9200(4)	44(4)
C(3D)	-1452(9)	-5608(13)	-9232(4)	48(3)
C(4D)	-946(10)	-6151(15)	-8901(4)	59(4)
C(5D)	-1550(8)	-6394(12)	-8572(4)	54(3)
C(6D)	-2601(8)	-5667(14)	-8539(4)	40(3)
C(7D)	-2875(11)	-5175(12)	-8170(4)	40(4)
C(8D)	-4091(14)	-5098(11)	-8139(5)	55(6)
C(9D)	-2419(9)	-3782(13)	-8095(3)	57(4)
C(10D)	-2511(9)	-6121(13)	-7872(3)	65(4)
C(11D)	-3310(11)	-5900(16)	-9441(4)	60(5)
C(12D)	-979(8)	-5993(14)	-9579(3)	67(4)
C(13D)	-2547(7)	-7191(12)	-8608(3)	53(4)
O(1)	-5967(5)	-11220(8)	-2158(2)	46(2)
O(2)	-5450(7)	-10502(13)	-1492(3)	57(3)
O(3)	-3297(10)	-10299(12)	-1975(4)	61(4)
O(1B)	-7587(5)	-11046(8)	-9927(2)	56(3)
O(2B)	-8218(7)	-10417(11)	-9277(3)	52(3)
O(3B)	-5650(7)	-10425(12)	-9214(3)	53(3)
O(1C)	-5114(5)	-6118(8)	-1064(2)	52(2)
O(2C)	-5757(7)	-5410(11)	-1716(3)	46(3)

O(3C)	-3175(7)	-5386(12)	-1746(3)	57(3)
O(1D)	-3441(5)	-3799(8)	-8818(2)	51(2)
O(2D)	-2980(7)	-4515(13)	-9491(3)	58(3)
O(3D)	-801(10)	-4759(10)	-9004(4)	49(4)

Table 84. Bond lengths [Å] and angles [°] for GB595m.

C(1)-O(1)	1.192(15)
C(1)-C(6)	1.49(2)
C(1)-C(2)	1.52(3)
C(2)-O(2)	1.423(17)
C(2)-C(3)	1.494(16)
C(2)-C(11)	1.50(2)
C(3)-C(4)	1.423(17)
C(3)-O(3)	1.488(17)
C(3)-C(12)	1.513(15)
C(4)-C(5)	1.481(15)
C(4)-O(3)	1.494(15)
C(5)-C(13)	1.517(13)
C(5)-C(6)	1.519(14)
C(6)-C(13)	1.557(15)
C(6)-C(7)	1.59(2)
C(7)-C(8)	1.50(2)
C(7)-C(9)	1.547(17)
C(7)-C(10)	1.573(18)
C(11)-O(2)	1.439(18)
C(1B)-O(1B)	1.210(16)
C(1B)-C(7B)	1.434(19)
C(1B)-C(2B)	1.58(2)
C(2B)-O(2B)	1.440(15)
C(2B)-C(3B)	1.443(17)
C(2B)-C(12B)	1.470(17)

C(3B)-O(3B)	1.443(15)
C(3B)-C(4B)	1.444(17)
C(3B)-C(13B)	1.550(16)
C(4B)-O(3B)	1.444(17)
C(4B)-C(5B)	1.476(16)
C(5B)-C(6B)	1.519(13)
C(5B)-C(7B)	1.552(14)
C(6B)-C(7B)	1.537(15)
C(7B)-C(8B)	1.51(2)
C(8B)-C(11B)	1.53(2)
C(8B)-C(10B)	1.545(14)
C(8B)-C(9B)	1.56(2)
C(12B)-O(2B)	1.454(16)
C(1C)-O(1C)	1.257(16)
C(1C)-C(2C)	1.45(2)
C(1C)-C(6C)	1.51(2)
C(2C)-O(2C)	1.430(15)
C(2C)-C(3C)	1.485(17)
C(2C)-C(11C)	1.500(18)
C(3C)-O(3C)	1.436(14)
C(3C)-C(4C)	1.461(17)
C(3C)-C(12C)	1.487(16)
C(4C)-O(3C)	1.444(17)
C(4C)-C(5C)	1.506(16)
C(5C)-C(13C)	1.498(13)
C(5C)-C(6C)	1.505(14)
C(6C)-C(13C)	1.550(15)
C(6C)-C(7C)	1.58(2)
C(7C)-C(10C)	1.508(19)
C(7C)-C(8C)	1.53(2)
C(7C)-C(9C)	1.566(15)
C(11C)-O(2C)	1.418(17)
C(1D)-O(1D)	1.255(12)
C(1D)-C(2D)	1.47(2)
C(1D)-C(6D)	1.47(2)

C(2D)-C(11D)	1.45(2)
C(2D)-C(3D)	1.454(16)
C(2D)-O(2D)	1.461(18)
C(3D)-O(3D)	1.462(18)
C(3D)-C(12D)	1.499(14)
C(3D)-C(4D)	1.510(17)
C(4D)-O(3D)	1.427(15)
C(4D)-C(5D)	1.492(16)
C(5D)-C(13D)	1.510(14)
C(5D)-C(6D)	1.535(14)
C(6D)-C(13D)	1.514(14)
C(6D)-C(7D)	1.52(2)
C(7D)-C(9D)	1.509(15)
C(7D)-C(10D)	1.532(17)
C(7D)-C(8D)	1.57(2)
C(11D)-O(2D)	1.431(19)
O(1)-C(1)-C(6)	123.3(18)
O(1)-C(1)-C(2)	120.9(17)
C(6)-C(1)-C(2)	115.8(13)
O(2)-C(2)-C(3)	118.6(12)
O(2)-C(2)-C(11)	58.9(10)
C(3)-C(2)-C(11)	121.8(14)
O(2)-C(2)-C(1)	113.2(12)
C(3)-C(2)-C(1)	116.9(14)
C(11)-C(2)-C(1)	114.5(12)
C(4)-C(3)-O(3)	61.7(9)
C(4)-C(3)-C(2)	116.1(12)
O(3)-C(3)-C(2)	108.4(11)
C(4)-C(3)-C(12)	123.5(11)
O(3)-C(3)-C(12)	113.3(11)
C(2)-C(3)-C(12)	117.9(12)
C(3)-C(4)-C(5)	122.3(11)
C(3)-C(4)-O(3)	61.3(9)
C(5)-C(4)-O(3)	117.9(12)
C(4)-C(5)-C(13)	118.6(11)

C(4)-C(5)-C(6)	118.2(11)
C(13)-C(5)-C(6)	61.7(7)
C(1)-C(6)-C(5)	115.7(12)
C(1)-C(6)-C(13)	114.8(13)
C(5)-C(6)-C(13)	59.1(7)
C(1)-C(6)-C(7)	117.1(12)
C(5)-C(6)-C(7)	120.5(11)
C(13)-C(6)-C(7)	116.7(11)
C(8)-C(7)-C(9)	113.1(11)
C(8)-C(7)-C(10)	110.4(13)
C(9)-C(7)-C(10)	105.7(12)
C(8)-C(7)-C(6)	111.4(14)
C(9)-C(7)-C(6)	105.6(11)
C(10)-C(7)-C(6)	110.4(11)
O(2)-C(11)-C(2)	57.8(8)
C(5)-C(13)-C(6)	59.2(7)
O(1B)-C(1B)-C(7B)	126.6(18)
O(1B)-C(1B)-C(2B)	116.5(15)
C(7B)-C(1B)-C(2B)	116.7(13)
O(2B)-C(2B)-C(3B)	118.8(13)
O(2B)-C(2B)-C(12B)	60.0(8)
C(3B)-C(2B)-C(12B)	122.8(14)
O(2B)-C(2B)-C(1B)	111.9(12)
C(3B)-C(2B)-C(1B)	116.3(12)
C(12B)-C(2B)-C(1B)	114.7(13)
O(3B)-C(3B)-C(2B)	114.3(12)
O(3B)-C(3B)-C(4B)	60.0(9)
C(2B)-C(3B)-C(4B)	120.9(13)
O(3B)-C(3B)-C(13B)	112.2(11)
C(2B)-C(3B)-C(13B)	116.7(11)
C(4B)-C(3B)-C(13B)	118.7(12)
O(3B)-C(4B)-C(3B)	60.0(9)
O(3B)-C(4B)-C(5B)	115.5(12)
C(3B)-C(4B)-C(5B)	118.1(11)
C(4B)-C(5B)-C(6B)	118.2(11)

C(4B)-C(5B)-C(7B)	121.1(10)
C(6B)-C(5B)-C(7B)	60.1(7)
C(5B)-C(6B)-C(7B)	61.0(7)
C(1B)-C(7B)-C(8B)	118.7(13)
C(1B)-C(7B)-C(6B)	114.1(11)
C(8B)-C(7B)-C(6B)	117.1(11)
C(1B)-C(7B)-C(5B)	115.9(13)
C(8B)-C(7B)-C(5B)	118.2(11)
C(6B)-C(7B)-C(5B)	58.9(7)
C(7B)-C(8B)-C(11B)	118.2(13)
C(7B)-C(8B)-C(10B)	110.3(14)
C(11B)-C(8B)-C(10B)	104.6(12)
C(7B)-C(8B)-C(9B)	113.4(14)
C(11B)-C(8B)-C(9B)	104.8(15)
C(10B)-C(8B)-C(9B)	104.4(11)
O(2B)-C(12B)-C(2B)	59.0(8)
O(1C)-C(1C)-C(2C)	118.9(15)
O(1C)-C(1C)-C(6C)	120.6(16)
C(2C)-C(1C)-C(6C)	120.5(13)
O(2C)-C(2C)-C(1C)	116.5(12)
O(2C)-C(2C)-C(3C)	115.4(12)
C(1C)-C(2C)-C(3C)	115.5(13)
O(2C)-C(2C)-C(11C)	57.8(8)
C(1C)-C(2C)-C(11C)	116.9(13)
C(3C)-C(2C)-C(11C)	122.0(13)
O(3C)-C(3C)-C(4C)	59.8(9)
O(3C)-C(3C)-C(2C)	112.0(11)
C(4C)-C(3C)-C(2C)	116.4(12)
O(3C)-C(3C)-C(12C)	116.0(11)
C(4C)-C(3C)-C(12C)	119.2(12)
C(2C)-C(3C)-C(12C)	119.1(11)
O(3C)-C(4C)-C(3C)	59.3(8)
O(3C)-C(4C)-C(5C)	116.6(13)
C(3C)-C(4C)-C(5C)	122.4(11)
C(13C)-C(5C)-C(6C)	62.2(7)

C(13C)-C(5C)-C(4C)	116.4(10)
C(6C)-C(5C)-C(4C)	117.8(10)
C(5C)-C(6C)-C(1C)	114.1(12)
C(5C)-C(6C)-C(13C)	58.7(7)
C(1C)-C(6C)-C(13C)	112.2(10)
C(5C)-C(6C)-C(7C)	118.8(10)
C(1C)-C(6C)-C(7C)	120.2(12)
C(13C)-C(6C)-C(7C)	117.7(10)
C(10C)-C(7C)-C(8C)	113.0(15)
C(10C)-C(7C)-C(9C)	108.2(11)
C(8C)-C(7C)-C(9C)	110.8(10)
C(10C)-C(7C)-C(6C)	111.4(12)
C(8C)-C(7C)-C(6C)	107.5(12)
C(9C)-C(7C)-C(6C)	105.7(13)
O(2C)-C(11C)-C(2C)	58.6(8)
C(5C)-C(13C)-C(6C)	59.1(7)
O(1D)-C(1D)-C(2D)	120.5(15)
O(1D)-C(1D)-C(6D)	120.6(15)
C(2D)-C(1D)-C(6D)	118.9(11)
C(11D)-C(2D)-C(3D)	121.8(14)
C(11D)-C(2D)-O(2D)	58.8(10)
C(3D)-C(2D)-O(2D)	114.3(12)
C(11D)-C(2D)-C(1D)	118.4(13)
C(3D)-C(2D)-C(1D)	115.8(13)
O(2D)-C(2D)-C(1D)	113.9(12)
C(2D)-C(3D)-O(3D)	113.6(12)
C(2D)-C(3D)-C(12D)	121.3(12)
O(3D)-C(3D)-C(12D)	115.3(11)
C(2D)-C(3D)-C(4D)	115.0(12)
O(3D)-C(3D)-C(4D)	57.4(8)
C(12D)-C(3D)-C(4D)	117.8(11)
O(3D)-C(4D)-C(5D)	116.7(13)
O(3D)-C(4D)-C(3D)	59.6(10)
C(5D)-C(4D)-C(3D)	121.8(11)
C(4D)-C(5D)-C(13D)	116.7(12)

C(4D)-C(5D)-C(6D)	117.1(11)
C(13D)-C(5D)-C(6D)	59.6(7)
C(1D)-C(6D)-C(13D)	113.3(12)
C(1D)-C(6D)-C(7D)	120.6(12)
C(13D)-C(6D)-C(7D)	118.8(11)
C(1D)-C(6D)-C(5D)	114.7(11)
C(13D)-C(6D)-C(5D)	59.3(7)
C(7D)-C(6D)-C(5D)	115.2(11)
C(9D)-C(7D)-C(6D)	111.5(11)
C(9D)-C(7D)-C(10D)	106.6(12)
C(6D)-C(7D)-C(10D)	114.6(12)
C(9D)-C(7D)-C(8D)	109.4(11)
C(6D)-C(7D)-C(8D)	108.3(13)
C(10D)-C(7D)-C(8D)	106.3(12)
O(2D)-C(11D)-C(2D)	60.9(8)
C(5D)-C(13D)-C(6D)	61.0(7)
C(2)-O(2)-C(11)	63.3(9)
C(3)-O(3)-C(4)	57.0(8)
C(2B)-O(2B)-C(12B)	61.1(8)
C(3B)-O(3B)-C(4B)	60.0(9)
C(11C)-O(2C)-C(2C)	63.6(9)
C(3C)-O(3C)-C(4C)	61.0(9)
C(11D)-O(2D)-C(2D)	60.3(9)
C(4D)-O(3D)-C(3D)	63.0(9)

Symmetry transformations used to generate equivalent atoms:

Table 85. Anisotropic displacement parameters ($\text{\AA}^2 \times 10^3$) for GB595m. The anisotropic displacement factor exponent takes the form: $-2\pi^2 [h^2 a^{*2} U^{11} + \dots + 2 h k a^* b^* U^{12}]$

	U ¹¹	U ²²	U ³³	U ²³	U ¹³	U ¹²
O(1)	43(5)	38(6)	57(6)	-7(5)	-1(4)	-6(4)
O(2)	63(7)	57(7)	51(8)	4(8)	6(6)	3(6)
O(3)	40(6)	75(9)	68(11)	5(8)	6(6)	10(6)

O(1B)	62(6)	51(7)	55(6)	-11(5)	9(4)	-20(4)
O(2B)	40(6)	55(7)	60(9)	9(8)	11(5)	-12(6)
O(3B)	53(7)	57(8)	49(9)	7(8)	5(5)	11(6)
O(1C)	45(5)	42(6)	69(7)	2(5)	-8(4)	-11(4)
O(2C)	44(5)	46(6)	47(8)	4(7)	-17(5)	-5(6)
O(3C)	26(6)	74(8)	72(9)	-9(9)	7(5)	16(6)
O(1D)	52(5)	49(6)	50(6)	3(5)	-2(4)	-4(4)
O(2D)	60(6)	71(8)	43(8)	15(8)	-3(6)	6(6)
O(3D)	47(6)	44(8)	56(10)	-8(6)	6(6)	-2(5)

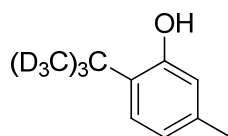
Table 86. Hydrogen coordinates ($\times 10^4$) and isotropic displacement parameters ($\text{\AA}^2 \times 10^3$) for GB595m.

	x	y	z	U(eq)
H(4)	-2868	-8230	-2059	60
H(5)	-3714	-8468	-2629	57
H(8A)	-6979	-9034	-2754	89
H(8B)	-6936	-10640	-2673	89
H(8C)	-6915	-10110	-3072	89
H(9A)	-5176	-11560	-3125	87
H(9B)	-5268	-11922	-2715	87
H(9C)	-4257	-11159	-2861	87
H(10A)	-5401	-7950	-3080	94
H(10B)	-5315	-9218	-3345	94
H(10C)	-4352	-8822	-3099	94
H(11A)	-5616	-8418	-1374	62
H(11B)	-6550	-9028	-1636	62
H(12A)	-3538	-9821	-1254	96
H(12B)	-3818	-8235	-1300	96
H(12C)	-2721	-8802	-1432	96
H(13A)	-5304	-7185	-2567	63
H(13B)	-5311	-7480	-2134	63

H(4B)	-5018	-8452	-9179	58
H(5B)	-4666	-8821	-9810	55
H(6B1)	-5893	-7302	-10086	59
H(6B2)	-6709	-7490	-9748	59
H(9B1)	-6980	-8941	-10643	73
H(9B2)	-7331	-10451	-10532	73
H(9B3)	-6481	-10245	-10834	73
H(10D)	-5355	-11763	-10549	92
H(10E)	-6119	-12000	-10223	92
H(10F)	-4943	-11547	-10155	92
H(11C)	-5119	-8230	-10532	84
H(11D)	-4811	-9619	-10730	84
H(11E)	-4339	-9289	-10350	84
H(12D)	-8415	-8310	-9178	52
H(12E)	-8750	-8770	-9586	52
H(13C)	-6070	-9012	-8663	86
H(13D)	-7176	-9743	-8698	86
H(13E)	-7057	-8152	-8791	86
H(4C)	-2585	-3407	-1776	61
H(5C)	-2245	-3707	-1138	53
H(8C1)	-4807	-4134	-431	101
H(8C2)	-4215	-5065	-149	101
H(8C3)	-4839	-5767	-465	101
H(9C1)	-2919	-6874	-451	90
H(9C2)	-2314	-6363	-795	90
H(9C3)	-3468	-6949	-829	90
H(10G)	-1998	-4044	-633	94
H(10H)	-2370	-4445	-244	94
H(10I)	-2850	-3131	-436	94
H(11F)	-6364	-3902	-1391	76
H(11G)	-5995	-3327	-1786	76
H(12F)	-3570	-3986	-2297	96
H(12G)	-4549	-3115	-2168	96
H(12H)	-4689	-4689	-2276	96
H(13F)	-4311	-2483	-1227	57

H(13G)	-3544	-2255	-877	57
H(4D)	-338	-6769	-8939	71
H(5D)	-1145	-6530	-8350	65
H(8D1)	-4359	-4440	-8312	83
H(8D2)	-4284	-4802	-7902	83
H(8D3)	-4388	-6004	-8186	83
H(9D1)	-1662	-3825	-8117	86
H(9D2)	-2602	-3501	-7855	86
H(9D3)	-2695	-3117	-8264	86
H(10J)	-2702	-5722	-7645	97
H(10K)	-1756	-6227	-7885	97
H(10L)	-2842	-7018	-7898	97
H(11H)	-3064	-6594	-9611	73
H(11I)	-4021	-6053	-9350	73
H(12I)	-233	-6141	-9548	101
H(12J)	-1093	-5254	-9749	101
H(12K)	-1302	-6837	-9665	101
H(13H)	-2741	-7816	-8414	64
H(13I)	-2739	-7517	-8847	64

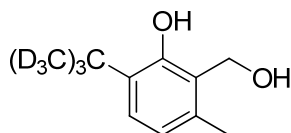
2-*tert*-Butyl-5-methylphenol- d_9 (92)



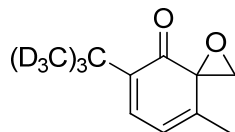
To a dry round bottomed flask under argon was added *m*-cresol (5.3 g, 49.2 mmol, 1.0 eq) followed by dry 1,2-dichloroethane (40 mL). Next was added 2-chloro-2-methylpropane- d_9 (5.0 g, 49.2 mmol, 1.0 eq) and bromopentacarbonylrhenium (I) (0.20 g, 0.49 mmol, 1.0 eq). The reaction mixture was heated to 84°C and stirring was allowed to continue for 3 hours. The reaction mixture was then concentrated and purified on silica eluting with 15:1 hexanes/ethyl acetate. The desired compound (7.0 g) was isolated in

82% yield as a colorless oil. (Rf: 0.45; 8:1 hexanes/ethyl acetate). ^1H NMR (CDCl_3 , 300 MHz): δ : 2.31 (s, 3H), 4.78 (s, 1H), 6.52 (s, 1H), 6.74 (d, 1H, $J = 7.5$ Hz), 7.19 (t, 1H, $J = 4.2$ Hz). ^{13}C NMR (CDCl_3 , 100 MHz): δ : 20.7, 29.1, 33.9, 117.5, 121.1, 127.0, 133.4, 136.9, 154.4. HRMS (APCI): expected for $\text{C}_{11}\text{H}_8\text{D}_9\text{O}$ ($\text{M}+\text{H}$) $^+$ 174.18388. Found 174.18372. IR (neat): ν_{max} 3526, 2925, 2868, 2214, 1405, 1168 cm^{-1} . Elemental Analysis for $\text{C}_{11}\text{H}_7\text{D}_9\text{O}$: Found: C, 76.39; H + D, 9.45. Calculated: C, 76.29; H + D, 9.31.

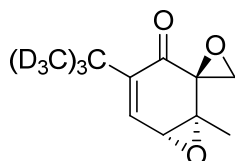
6-*tert*-Butyl-2-(hydroxymethyl)-3-methylphenol- d_9 (93)



Following the general procedure for the synthesis of salicylic alcohols, compound **92** (5.0 g, 29 mmol) was converted into 4.8 g of compound **93** in 81% yield as a white solid. (Rf: 0.17; 8:1 hexanes/ethyl acetate). mp: 50-52 $^{\circ}\text{C}$. ^1H NMR (CDCl_3 , 300 MHz): δ : 1.99 (t, 1H, $J = 5.7$ Hz), 2.26 (s, 3H), 4.97 (d, 2H, $J = 5.4$ Hz), 6.65 (d, 1H, $J = 7.8$ Hz), 7.12 (t, 1H, $J = 3.9$ Hz), 8.05 (s, 1H). ^{13}C NMR (CDCl_3 , 100 MHz): δ : 19.1, 29.0, 34.1, 61.0, 121.6, 123.0, 126.2, 133.5, 135.3, 156.0. HRMS (APCI): expected for $\text{C}_{12}\text{H}_9\text{D}_9\text{O}_2$ (M) $^+$ 203.18662. Found 203.18658. IR (neat): ν_{max} 3338, 2974, 2917, 2876, 2210, 1409, 1230, 972 cm^{-1} . Elemental Analysis for $\text{C}_{12}\text{H}_9\text{D}_9\text{O}_2$: Found: C, 71.16; H + D, 9.09. Calculated: C, 70.93; H + D, 8.93.

(±)-5-*tert*-Butyl-8-methyl-1-oxaspiro[2.5]octa-5,7-dien-4-one-d₉ (94)

Following the general procedure for the synthesis of monoepoxides, compound **93** (3.2 g, 16 mmol) was converted into 2.4 g of the desired compound in 74% yield as an orange oil. (Rf: 0.34; 8:1 hexanes/ethyl acetate). ¹H NMR (CDCl₃, 400 MHz): δ: 1.79 (s, 3H), 3.10 (d, 1H, J = 8.4 Hz), 3.15 (d, 1H, J = 8.4 Hz), 6.26 (dd, 1H, J = 6.8 Hz, 1.6 Hz), 6.93 (t, 1H, J = 3.2 Hz). ¹³C NMR (CDCl₃, 100 MHz): δ: 16.3, 28.4, 33.8, 58.4, 59.8, 123.7, 136.4, 143.0, 145.1, 195.1. HRMS (APCI): expected for C₁₂H₈D₉O₂ (M+H)⁺ 202.17880. Found 202.17867. IR (neat): ν_{max} 2979, 2919, 2212, 1664, 1640 cm⁻¹. Elemental Analysis for C₁₂H₁₆O₂: Found: C, 71.99; H, 8.21. Calculated: C, 71.64; H, 8.02.

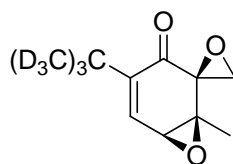
(±)-4-*tert*-Butyl-1-methyl-7-oxaspiro[bicyclo[4.1.0]hept[4]ene-2,2'-oxiran]-3-one-d₉ (95)

Following the general procedure for the synthesis of diepoxides, compound **94** (2.0 g, 9.9 mmol) was converted into 0.55 g of compound **95** in a 28% yield as a white solid. (Rf: 0.14; 8:1 hexanes/ethyl acetate). mp: 61-63 °C. ¹H NMR (CDCl₃, 300 MHz): δ: 1.34 (s, 3H), 3.09 (d, 1H, J = 6.0 Hz), 3.46 (d, 1H, J = 6.0 Hz), 3.47 (d, 1H, J = 4.5 Hz), 7.01 (t, 1H, J = 2.1 Hz). ¹³C NMR (CDCl₃, 100 MHz): δ: 15.4, 28.0, 34.4, 48.7, 54.2, 56.4, 60.3, 137.5, 150.4, 190.4. HRMS (APCI): expected for C₁₂H₈D₉O₃ (M+H)⁺ 218.17371.

Found 218.17378. IR (neat): ν_{\max} 3068, 2995, 2933, 2210, 2137, 2063, 1679 cm^{-1} .
 Elemental Analysis for $\text{C}_{12}\text{H}_7\text{D}_9\text{O}_3$: Found: C, 66.57; H + D, 7.42. Calculated: C, 66.36;
 H + D, 7.43.

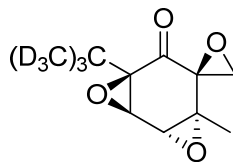
(±)-4-*tert*-Butyl-1-methyl-7-oxaspiro[bicyclo[4.1.0]hept[4]ene-2,2'-oxiran]-3-one-d₉

(96)



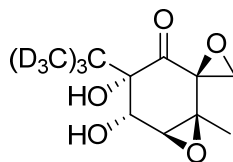
In the formation of diepoxides, 1.1 g of compound **96** was produced in 55% yield along with compound **95** as a white solid. (Rf: 0.06; 8:1 hexanes/ethyl acetate). mp: 89-90 °C.
 ^1H NMR (CDCl_3 , 400 MHz): δ : 1.30 (s, 3H), 2.77 (d, 1H, $J = 6.0$ Hz), 2.90 (d, 1H, $J = 5.2$ Hz), 3.51 (d, 1H, $J = 4.0$ Hz), 6.93 (s, 1H). ^{13}C NMR (CDCl_3 , 100 MHz): δ : 15.0, 28.2, 34.6, 51.7, 54.5, 57.4, 60.8, 136.8, 151.6, 191.2. HRMS (APCI): expected for $\text{C}_{12}\text{H}_8\text{D}_9\text{O}_3$ ($\text{M}+\text{H}$) $^+$ 218.17371. Found 218.17380. IR (neat): ν_{\max} 3081, 2991, 2933, 2210, 1679 cm^{-1} . Elemental Analysis for $\text{C}_{12}\text{H}_7\text{D}_9\text{O}_3$: Found: C, 66.32; H + D, 7.44. Calculated: C, 66.36; H + D, 7.43.

(±)-7'-(*tert*-Butyl)-4'-methyl-3',8'-dioxaspiro[oxirane-2,5'-tricyclo[5.1.0.0^{2,4}]octan]-6'-one -d₉ (**97**)



Following the general procedure for the synthesis of triepoxides, compound **95** (0.20 g, 0.92 mmol) was converted into the 0.17 g of the desired product in 78% yield as a white solid. (Rf: 0.48; 3:1 hexanes/ethyl acetate). mp: 92-94 °C. ¹H NMR (CDCl₃, 300 MHz): δ: 1.25 (s, 3H), 2.97 (d, 1H, J = 5.1 Hz), 3.34 (d, 1H, J = 4.8 Hz), 3.61 (d, 1H, J = 2.7 Hz), 3.93 (s, 1H). ¹³C NMR (CDCl₃, 100 MHz): δ: 15.4, 24.9, 31.8, 47.1, 57.9, 58.2, 58.5, 59.1, 67.4, 197.3. HRMS (APCI): expected for C₁₂H₈D₉O₄ (M+H)⁺ 234.16863. Found 234.16873. IR (neat): ν_{max} 3011, 2958, 2987, 2933, 2222, 1724 cm⁻¹. Elemental Analysis for C₁₂H₇D₉O₄: Found: C, 62.10; H + D, 6.64. Calculated: C, 61.81; H + D, 6.92.

(±)-4-*tert*-Butyl-4,5-dihydroxy-1-methyl-7-oxaspiro[bicycle[4.1.0]heptane-2,2'-oxiran]-3-one-d₉ (**98**)



Compound **98** was synthesized according to the procedure used to synthesize compound **87**. Compound **96** (0.40 g, 1.84 mmol) was converted into 0.31 g of the desired product in 68% yield as a white solid. (Rf: 0.06; 3:1 hexanes/ethyl acetate). mp: 119-121 °C. ¹H

NMR (CDCl₃, 300 MHz): δ : 1.29 (s, 3H), 2.75 (d, 1H, J = 6.9 Hz), 2.92 (d, 1H, J = 5.4 Hz), 3.06 (d, 1H, J = 5.1 Hz), 3.33 (s, 1H), 4.50 (d, 1H, J = 6.6 Hz). ¹³C NMR (CDCl₃, 100 MHz): δ : 14.9, 24.8, 36.5, 51.2, 61.9, 62.3, 62.9, 68.3, 80.2, 201.7. HRMS (APCI): expected for C₁₂H₁₀D₉O₅ (M+H)⁺ 252.17919. Found 252.17932. IR (neat): ν_{\max} 3452, 2991, 2942, 2214, 1740 cm⁻¹. Elemental Analysis for C₁₂H₉D₉O₅: Found: C, 57.37; H + D, 7.20. Calculated: C, 57.38; H + D, 7.22.

Procedure for carrageenan edema model: Acute inflammation was induced by i.p. injection of 50 μ L of λ -carrageenan (1% w/v in saline) or saline into the right or left hind paw of female C57BL/6J mice (Jackson Laboratories). Triptolide analogs were all administered i.p. at 30 mg/kg 30 minutes following carrageenan challenge and continued daily. All triptolide analogs were dissolved in 10% DMSO and 90% 45% β -cyclodextrin (CD). Control animals received corresponding i.p. injections of vehicle. The volume of the carrageenan injected hind paw was measured by a caliper and compared to the volume of the untreated contralateral paw to obtain the edema volume. To get a baseline paw measurement, paw width is measured from the “palm” to the back of the paw on both the right and left hind paws. The volume of the contralateral paw was subtracted from the volume of the injected paw to obtain the edema volume. The animals were sacrificed 74 hours after induction of inflammation, 2 hours after the last injection of triptolide analogs. Following the final paw measurements and photographs of the paws, the paws were removed with scissors and placed into formaldehyde solution for paraffin embedding and histological analysis using H&E staining. Livers were also removed, immediately frozen in liquid nitrogen, and kept at -80°C for RNase protection assay. The

livers of mice from the various groups were processed by Trizol-based method to generate total RNAs. These total RNAs were used to test the levels of inflammation-related cytokines by a RNase protection assay, which simultaneously detected cytokine mRNAs (TNF- α , IL-1 α , IL-1 β , IFN- α , and IL-6) via a RiboQuant custom probe set from PharMingen (San Diego, CA). The liver tissue samples were immediately homogenized with Trizol reagent (1 mL per 100 mg of tissue) using an Eberbach Con-torque power unit (Ann Arbor, MI) to yield total RNA and were centrifuged to remove cellular debris. RNA pellets for each liver section were obtained from three to five mice and were resuspended in nuclease-free water for group/batch processing. ³²P-uridine triphosphate-labeled cRNA probes were hybridized overnight with 20 mg of total sample RNA at 56°C, digested with RNase A/T1 mixtures, extracted with phenol/chloroform, ethanol precipitated, and then separated on 5% polyacrylamide/8M urea gels. The gels were dried and then subjected to autoradiography to observe protected bands. Specific bands were identified based on their individual migration patterns in comparison with the undigested probes. The bands were quantitated by densitometric analysis (NIH Image, Bethesda, MD) and were expressed as arbitrary pixel units normalized according to glyceraldehydes-3-phosphate dehydrogenase (GAPDH) density measures in each sample.

TNF- α release from stimulated Jurkat cells assay: Jurkat cells were grown in RPMI-1640 medium supplemented with 10% fetal bovine serum in 6 x 25 cm² flasks at 37°C. The cell concentration was not allowed to exceed 3 x 10⁶ cells/mL. The cells were spun down and the medium discarded. The cell pellet was resuspended in medium to a concentration of 2 x 10⁶ cells/mL. Stock solutions of each triptolide analog were

prepared by dissolving the analog in DMSO to a final concentration of 20 mM. The stock solution was then diluted in cell culture medium to obtain 2000 nM, 200 nM, and 2 nM working solutions of each analog. Each well of a 96-well plate received 200 μ L of cells. Wells receiving test article received 200 μ L of the appropriate working solution of each test article. Wells not receiving test article received 200 μ L of DMSO vehicle. This experiment was done in triplicate. The plates were incubated at 37°C for 75 minutes in a 5% CO₂ atmosphere while gently rocking. While the cells were incubating, PMA and ionomycin stock solutions were prepared. PMA stock solution was prepared by dissolving PMA into DMSO to a final concentration of 1 mg/mL. This solution was further diluted by transferring 5 μ L of PMA stock to 45 μ L of cell growth medium. Ionomycin was diluted in DMSO to a final concentration of 3 mM. 5 μ L of this solution was then diluted with 45 μ L of cell growth media to form an ionomycin working solution. 10 μ L of the PMA working solution and 25 μ L of the ionomycin working solution were diluted with 5 mL of cell growth media to form the PMA/I working solution. Once the cells had incubated for 75 minutes, 44 μ L of cell growth media was added to all cells not being stimulated and 44 μ L of PMA/I working solution was added to all cells being stimulated. The cells were then incubated for 6 hours at 37°C in a 5% CO₂ atmosphere while gently rocking. Wells containing cells treated in the same manner were pooled and centrifuged at 5000 x g for 10 minutes at 4°C. The supernatants were transferred to new tubes and stored at -20°C until they were analyzed. The supernatants were analyzed in duplicate using Quantikine[®] ELISA (R&DSystems) following the manufacturer's protocol.

2.7 References

- (1) http://www.aarda.org/autoimmune_statistics.php **2009**.
- (2) <http://www.gene.com/gene/products/education/immunology/ad-factsheet.html>
2005.
- (3) <http://www.womenshealthresearch.org> **2004**.
- (4) <http://www.the-scientist.com/2007/05/01/s27/1/>.
- (5) <http://www.labtestsonline.org/understanding/conditions/autoimmune.html> **2009**.
- (6) <http://arthritis.about.com/cs/betterliving/fr/maryshomon.htm> **2006**.
- (7) <http://www.bio-medicine.org> **2009**.
- (8) <http://www.wrongdiagnosis.com/a/ai/treatments.htm>.
- (9) <http://www.webmd.com/rheumatoid-arthritis/guide/biologics>.
- (10) http://www.hopkins-arthritis.org/arthritis-info/rheumatoid-arthritis/rheum_treat.html.
- (11) <http://arthritis.ygoy.com/history-of-arthritis/> **2007**.
- (12) Janeway Jr., C. A.; Travers, P.; Walport, M.; Shlomchik, M. J. *Immuno Biology: The Immune System in Health and Disease*, 6th Edition; Lawrence, E., Editor; Garland Science Publishing: New York, 2005; 557-608.
- (13) Janeway Jr., C. A.; Travers, P.; Walport, M.; Shlomchik, M. J. *Immuno Biology: The Immune System in Health and Disease*, 6th Edition; Lawrence, E., Editor; Garland Science Publishing: New York, 2005; 37-96. ©2005 From *Immunobiology 6E* by Janeway et al. Reproduced by permission of Garland Science/Taylor and Francis LLC.
- (14) <http://www.cdc.gov/ncidod/EID/vol10no11/04-0367.htm> **2004**.

- (15) <http://emedicine.medscape.com/article/172940-overview> **2009**.
- (16) http://www.cureresearch.com/g/graves_disease/prevalence.htm **2003**.
- (17) <http://www.thyroidmanager.org/Chapter8/8-frame.htm> **2008**.
- (18) <http://www.cdc.gov/arthritis/arthritis/lupus.htm> **2008**.
- (19) http://www.wrongdiagnosis.com/m/multiple_sclerosis/prevalence.htm.
- (20) <http://www.psoriasis.org/NetCommunity/Page.aspx?pid=798>.
- (21) <http://www.cdc.gov/arthritis/arthritis/rheumatoid.htm> **2008**.
- (22) http://www.cerebel.com/lupus/sjogrens_syndrome.php.
- (23) http://www.cdc.gov/diabetes/projects/diab_children.htm **2008**.
- (24) Janeway Jr., C. A.; Travers, P.; Walport, M.; Shlomchik, M. J. *Immuno Biology: The Immune System in Health and Disease*, 6th Edition; Lawrence, E., Editor; Garland Science Publishing: New York, 2005; 1-34. ©2005 From Immunobiology 6E by Janeway et al. Reproduced by permission of Garland Science/Taylor and Francis LLC.
- (25) Janeway Jr., C. A.; Travers, P.; Walport, M.; Shlomchik, M. J. *Immuno Biology: The Immune System in Health and Disease*, 6th Edition; Lawrence, E., Editor; Garland Science Publishing: New York, 2005; 338-339.
- (26) Llewelyn, M.; Cohen, J. *The Lancet Infectious Diseases* **2002**, 2, 156-162.
- (27) Srinivasan, R.; Houghton, A. N.; Wolchok, J. D. *Cancer Immunity* **2002**, 2, 8-17.
- (28) Ferrero-Miliani, L.; Nielsen, O. H.; Andersen, P. S.; Girardin, S. E. *Clinical and Experimental Immunology* **2006**, 147, 227-235.
- (29) Perkins, N. D. *Nature Reviews* **2007**, 8, 49-62.
- (30) <http://people.bu.edu/gilmore/nf-kb/>.

- (31) Bertoline, A.; Ferrari, A.; Ottani, A.; Guerzoni, S.; Tacchi, R.; Leone, S. *CNS Drug Reviews* **2006**, 12, 250-275.
- (32) Botting, R. *Thrombosis Research* **2003**, 110, 269-272.
- (33) Chandrasekharan, N. V.; Dai, H.; Roos, K. L. T.; Evanson, N. K.; Tomsik, J.; Elton, T. S.; Simmons, D. L. *Proceedings of the National Academy of Science* **2002**, 99, 13926-13931.
- (34) Scherrer, G.; Imamachi, N.; Cao, Y.; Contet, C.; Mennicken, F.; O'Donnell, D.; Kieffer, B. L.; Basbaum, A. I. *Cell* **2009**, 137, 1148-1159.
- (35) <http://www.webmd.com/rheumatoid-arthritis/guide/nsaids-rheumatoid-arthritis>.
- (36) Barnes, P. J. *British Journal of Pharmacology* **2006**, 148, 245-254.
- (37) Newton, R. *Thorax* **2000**, 55, 603-613.
- (38) Maltzman, J. S.; Koretzky, G. A. *The Journal of Clinical Investigation* **2003**, 111, 1122-1124.
- (39) Fox, R. I.; Herrmann, M. L.; Frangou, C. G.; Wahl, G. M.; Morris, R. E.; Strand, V.; Kirschbaum, B. J. *Clinical Immunology* **1999**, 93, 198-208.
- (40) Wenger, R. M. *Angewandte Chemie International Edition in English* **1985**, 24, 77-138.
- (41) Sullivan, P. G.; Thompson, M.; Scheff, S. W. *Experimental Neurology* **2000**, 161, 631-637.
- (42) Takahata, M.; Hasino, S.; Izumiyama, K.; Chiba, K.; Suzuki, S.; Asaka, M. *Bone Marrow Transplantation* **2001**, 28, 713-715.
- (43) Ho, S.; Clipstone, N.; Timmermann, L.; Northrop, J.; Graef, I.; Fiorentino, D.; Nourse, J.; Crabtree, G. R. *Clinical Immunology and Immunopathology* **1996**, 80,

S40-S45.

- (44) McCarroll, N.; Keshava, N.; Cimino, M.; Chu, M.; Dearfield, K.; Keshava, C.; Kligerman, A.; Owen, R.; Protzel, A.; Putzrath, R.; Schoeny, R. *Environmental and Molecular Mutagenesis* **2008**, 49, 117-131.
- (45) Kyburz, D.; Brentano, F.; Gay, S. *Nature* **2006**, 2, 458-459.
- (46) Andersson, S. E.; Johansson, L.; Lexmüller, K.; Ekström, G. M. *European Journal of Pharmaceutical Sciences* **2000**, 9, 333-343.
- (47) Nestorov, I. *Seminars in Arthritis and Rheumatism* **2004**, 34, 12-18.
- (48) Fleischmann, R. M.; Tesser, J.; Schiff, M. H.; Schechtman, J.; Burmester, G.; Bennett, R.; Modafferi, D.; Zhou, L.; Bell, D.; Appleton, B. *Annals of the Rheumatic Diseases* **2006**, 65, 1006-1012.
- (49) Ruderman, E. M.; Pope, R. M. *Nature* **2006**, 2, 654-660.
- (50) Shaw, T.; Quan, J.; Totoritis, M. C. *Annals of the Rheumatic Diseases* **2003**, 62, ii55-ii59.
- (51) <http://www.arthritis.ca/> **2009**.
- (52) <http://www.law.duke.edu/journals/dltr/articles/2008dltr0009.html> **2008**.
- (53) Kupchan, S. M.; Court, W. A.; Dailey, R. G.; Gilmore, C. J.; Bryan, R. F. *Journal of the American Chemical Society* **1972**, 94, 7194-7195.
- (54) Westerheide, S. D.; Kawahara, T. L. A.; Orton, K.; Morimoto, R. I. *The Journal of Biological Chemistry* **2006**, 281, 9616-9622.
- (55) Qiu, D.; Zhao, G.; Aoki, Y.; Shi, L.; Uyei, A.; Nazarian, S.; Ng, J. C. H.; Kao, P. N. *The Journal of Biological Chemistry* **1999**, 274, 13443-13450.
- (56) Yang, D.; Ye, X.; Xu, M. *Journal of Organic Chemistry* **2000**, 65, 2208-2217.

- (57) Gassman, P. G.; Amick, D. R. *Tetrahedron Letters* **1974**, 38, 3463-3466.
- (58) Casiraghi, G.; Casnati, G.; Puglia, G.; Sartori, G.; Terenghi, G. *Journal of the Chemical Society, Perkin Transactions 1* **1980**, 1862-1865.
- (59) Anwar, H. F.; Skattebøl, L.; Skramstad, J.; Hansen, T. V. *Tetrahedron Letters* **2005**, 46, 5285-5287.
- (60) Leese, M. P.; Hejaz, H. A. M.; Mahon, M. F.; Newman, S. P.; Purohit, A.; Reed, M. J.; Potter, B. V. L. *Journal of Medicinal Chemistry* **2005**, 48, 5243-5256.
- (61) Auksi, H.; Yates, P. *Canadian Journal of Chemistry* **1981**, 59, 2510-2517.
- (62) Singh, V.; Sahu, P. K.; Singh, R. B.; Mobin, S. M. *Journal of Organic Chemistry* **2007**, 72, 10155-10165.
- (63) Cox, C.; Danishefsky, S. J. *Organic Letters* **2000**, 2, 3493-3496.
- (64) Yang, D.; Wong, M.; Cheung, K. *Tetrahedron Letters* **1997**, 38, 6865-6868.
- (65) Hinch, M.; Jacques, O.; Drago, C.; Caggiano, L.; Jackson, R. F. *Journal of Molecular Catalyst A: Chemical* **2006**, 251, 123-128.
- (66) Chan, E. W.; Cheng, S. C.; Sin, F. W.; Xie, Y. *Toxicology Letters* **2001**, 122, 81-87.
- (67) Zhou, R.; Zhang, F.; He, P.; Zhou, W.; Wu, Q.; Xu, J.; Zhou, Y.; Tang, W.; Li, X.; Yang, Y.; Li, Y.; Zuo, J. *International Immunopharmacology* **2005**, 5, 1895-1903.
- (68) Harrowven, D. C.; Lucas, M. C.; Howes, P. D. *Tetrahedron* **2001**, 57, 791-804.
- (69) Bai, L.; Wang, J. *Current Organic Chemistry* **2005**, 9, 535-553.
- (70) Badone, D.; Cardamone, M. B. R.; Ielmini, A.; Guzzi, U. *Journal of Organic Chemistry* **1997**, 62, 7170-7173.

- (71) Oi, S.; Watanabe, S.; Fukita, S.; Inoue, Y. *Tetrahedron Letters* **2003**, 44, 8665-8668.
- (72) Ito, N.; Esaki, H.; Maesawa, T.; Imamiya, E.; Maegawa, T.; Sajiki, H. *Bulletin of the Chemical Society of Japan* **2008**, 81, 278-286.
- (73) Arcadi, A.; Attanasi, O. A.; Berretta, S. Bianchi, G.; Filippone, P. *Synthesis* **2006**, 15, 2523-2530.
- (74) Weinert, E. E.; Dondi, R.; Colloredo-Melz, S.; Frankenfield, K. N.; Mitchell, C. H.; Freccero, M.; Rokita, S. E. *Journal of the American Chemical Society* **2006**, 128, 11940-11947.
- (75) Danishefsky, S. J.; Masters, J. J.; Young, W. B.; Link, J. T.; Snyder, L. B.; Magee, T. V.; Jung, D. K.; Isaacs, R. C.; Bornmann, W. G.; Alaimo, C. A.; Coburn, C. A.; Di Grandi, M. J. *Journal of the American Chemical Society* **1996**, 118, 2843-2859.
- (76) Li, C.; Pace, E. A.; Liang, M.; Lobkovsky, E.; Gilmore, T. D.; Porco, J. A. *Journal of the American Chemical Society* **2001**, 123, 11308-11309.
- (77) Pal, M.; Veermaneni, V. R.; Padakanti, S.; Nagabelli, M.; Vanguri, A.; Mamnoor, P.; Castur, S. R.; Misra, P.; Mullangi, R.; Yeleswarapu, K. R. *Indian Journal of Chemistry* **2003**, 42B, 593-601.
- (78) Griffith, R. C.; Napier, J. J. (Fisons Corp., USA). Application: US 88-207839, **1988**, 25pp.
- (79) Hamze, A.; Rubi, E.; Arnal, P.; Boisburn, M.; Carcel, C.; Salom-Roig, X.; Maynadier, M.; Wein, S.; Vial, H.; Calas, M. *Journal of Medicinal Chemistry* **2005**, 48, 3639-3643.

- (80) Chackal-Cateon, S.; Miao, Y.; Wilson, W. D.; Wenzler, T.; Brun, R.; Boykin, D. W. *Bioorganic and Medicinal Chemistry* **2006**, 14, 7434-7445.
- (81) Nguyen, P.; Corpuz, E.; Heidelbaugh, T. M.; Chow, K.; Garst, M. E. *Journal of Organic Chemistry* **2003**, 68, 10195-10198.
- (82) Ple, P. A.; Green, T. P.; Hennequin, L. F.; Curwen, J.; Fennell, M.; Allen, J.; Brempt, C. L.; Costello, G. *Journal of Medicinal Chemistry* **2004**, 47, 871-887.
- (83) Nishiyama, Y.; Kakushou, F.; Sonoda, N. *Bulletin of the Chemical Society of Japan* **2000**, 73, 2779-2782.
- (84) Barros, M. T.; Maycock, C. D.; Ventura, M. R. *Journal of the Chemical Society, Perkin Transactions 1* **2001**, 166-173.
- (85) Trost, B. M.; Tang, W.; Toste, F. D. *Journal of the American Chemical Society* **2005**, 127, 14785-14803.
- (86) Kobayashi, S.; Ishii, A.; Toyota, M. *Synlett* **2008**, 7, 1086-1090.
- (87) Brandt, G. E. L.; Schmidt, M. D.; Prisinzano, T. E.; Blagg, B. S. J. *Journal of Medicinal Chemistry* **2008**, 51, 6495-6502.
- (88) Garcia-Granados, A.; Lopez, P. E.; Melguizo, E.; Parra, A.; Simeo, Y. *Synthetic Communications* **2006**, 36, 3001-3018.
- (89) Leiva de Faria, M.; Magalhaes, R. de A.; Silva, F. C.; Matias, L. G. de O.; Ceschi, M. A.; Brocksom, U.; Brocksom, T. J. *Tetrahedron: Asymmetry* **2000**, 11, 4093-4103.
- (90) Corey, E. J.; Chaykovsky, M. *Journal of the American Chemical Society* **1965**, 87, 1353-1364.
- (91) Lay, L. *Synthetic Communications* **2006**, 36, 2203-2209.

- (92) Sorrell, T. N.; Ellis, D. J. *Journal of Organic Chemistry* **1985**, 50, 5765-5769.
- (93) Chattopadhyay, S. K.; Biswas, T.; Maity, S. *Synlett* **2006**, 14, 2211-2214.
- (94) Sarkar, D.; Venkateswaran, R. V. *Synlett* **2008**, 5, 653-654.
- (95) Richter, J. M.; Ishihara, Y.; Masuda, T.; Whitefield, B. W.; Llamas, T.; Pohjakallio, A.; Baran, P. S. *Journal of the American Chemical Society* **2008**, 130, 17938-17954.
- (96) Chen, B. J. *Leukemia and Lymphoma* **2001**, 42, 253-265.
- (97) Gu, W., Brandwein, S. R. *International Journal of Immunopharmacology* **1998**, 20, 389-400.
- (98) Tobe, M.; Isobe, Y.; Tomizawa, H.; Nagasaki, T.; Takahashi, H.; Hayashi, H. *Bioorganic and Medicinal Chemistry* **2003**, 11, 3869-3878.
- (99) http://www.emdchemicals.com/life-science-research/pathways-nf-kb-interactive-pathway/c_zIeb.s1Oud8AAAEjEkh6cXJA?back=true. NF- κ B pathway image used with permission by EMD Chemicals Inc.

3.1 Appendix